Universidad de Valladolid

INSTITUTO DE OFTALMOBIOLOGÍA APLICADA

TESIS DOCTORAL:

CORRECTION AND CONTROL OF OCULAR ABERRATIONS WITH ADAPTIVE OPTICS: EFFECTS ON HUMAN VISION

Presentada por LUCIE SAWIDES
para optar al grado de doctora por la Universidad de Valladolid

Dirigida por:
SUSANA MARCOS CELESTINO

Instituto de Óptica "Daza de Valdés" 2013
Cover illustrated by Maïe.

Universidad de Valladolid

Impreso 2T

AUTORIZACIÓN DEL DIRECTOR DE TESIS

(Art. 2.1. c de la Normativa para la presentación y defensa de la Tesis Doctoral en la UVa)

Dª. SUSANA MARCOS CELESTINO, con D.N.I. nº07954600G
profesor de Investigación del Instituto de Óptica "Daza de Valdés" del Consejo Superior de Investigaciones Científicas (CSIC), como Director de la Tesis Doctoral titulada :

"CORRECTION AND CONTROL OF OCULAR ABERRATIONS WITH ADAPTIVE OPTICS: EFFECTS ON HUMAN VISION"

presentada por Da. LUCIE SAWIDES
alumna del programa DOCTORADO EN CIENCIAS DE LA VISION
impartido por el departamento INSTITUTO UNIVERSITARIO DE OFTALMOLOGÍA APLICADA

autoriza la presentación de la misma, considerando que es un trabajo original, de gran relevancia en la óptica visual, y cuyos resultados han sido de elevado impacto en las comunidades de óptica, oftalmología y visión. Por tanto es APTA para su defensa.

Valladolid, 21 de Mayo de 2013

El Director de la Tesis,

Fdo.: Dra Susana Marcos Celestino

SR. PRESIDENTE DE LA COMISIÓN DE DOCTORADO

Contents

Índice

1

Introduction

The quality of images of the outside world projected on the retina is limited by imperfections of the ocular optics, known as optical aberrations. Optical aberrations arise primarily from the cornea and the crystalline lens and their relative alignment, and they which degrade the contrast and limit the spatial frequency content of the images.

In the last years, multiple technologies have been developed for the measurement of ocular aberrations and important knowledge has been gained on the contribution of the different components of the eye to the degradation of image quality. However, the effects of the ocular aberrations on vision are not yet well understood. This information is essential to understand the limits of human spatial vision and to design and optimize new alternatives of correction of presbyopia/myopia and more complex individualized refractive corrections.

Investigating the role of aberrations on visual performance including visual acuity or other visual tasks will allow not only to further advance the understanding of the limits of spatial vision but also contribute to the development of refractive surgery ablation algorithms, intraocular lenses, contact lenses and ophthalmic lenses to go beyond the correction of conventional refractive errors. As customized wavefront guided correction appears more feasible in the form of laser ablation patterns, customized contact or intraocular lenses, the question whether correction of high order aberrations produces indeed a relevant improvement in vision becomes critical.

Quoting Von Helmholtz [1855] "we never perceived the objects of the external world directly. On the contrary, we only perceive effects of these objects on our nervous apparatuses, and it has always been like that from the first moment of our life". Studies of adaptation aftereffects have shown that changes on the state of adaptation largely impact how the world looks. So one question still remains: how can the visual system take full advantage of the higher spatial detailed information reaching the retina when the brain has never been used to process so perfect retinal images? Or alternatively, if the optical quality deteriorates as a consequence of treatment or disease, will the visual system be able to adapt to the new optical

blur?

In this thesis, we present a series of psychophysical experiments to study the effect on high order aberrations on vision, to test neural adaptation to ocular aberrations and directly assess the correlation between the internal code of blur and the optical blur produced by the ocular aberrations in terms of level and orientations. For these purposes, we used a custom adaptive optics system combined with psychophysical channels specifically developed for these studies.

1.1 Motivation

In the last years, wavefront sensing techniques to measure and correct the aberrations of the eye have improved dramatically, and have made their way into the clinic.

These advances have been expanded with the development of Adaptive Optics (AO) technique in the eye, allowing not only the measurement, but also the correction and manipulation of the aberrations. In the 1990's, wavefront sensing has been applied to the understanding of the optical quality of the eye, and its change with refractive error, accommodation, aging in the normal eye, disease (i.e. Keratoconus) and treatment (refractive surgery, cataract surgery, contact lenses, intraestromal rings, etc...)

Since the first AO deformable mirror, capable of correcting defocus and astigmatism [Dreher et al., 1989; Liang et al., 1994] and phase plate custom corrections [Navarro et al., 2000; Burns et al., 2002] techniques have improved dramatically, allowing retinal imaging with extraordinary resolution, upon dynamic correction of the ocular aberrations. Although technical developments in AO retinal imaging have been spectacular in the last years, the first reports on AO in vision science already acknowledged the great potential of the technique in psychophysics.

Ocular aberrations vary largely between subjects, in distribution and in magnitude, and an increase of ocular aberrations is associated to some ocular conditions (high myopia, aging, corneal refractive surgery, corneal pathology like Keratoconus). Ocular aberrations also determine some properties of the eye such as depth of focus, essential in the eye without any capacity of accommodation. Correcting ocular high order aberrations opens the possibility for "super-vision", beyond the limits imposed by standard refractive correction. The possibility of measuring visual function under fully corrected optics provided by with Adaptive Optics allows exploring the limits of visual performance in different conditions of luminance, contrast polarities and daily-life visual tasks. Besides, each subject is chronically exposed to different pattern of aberrations. The questions arise whether subjects are specifically adapted to their own aberrations, to which extent perception changes when the aberrations change, and whether subjects can adapt to a new pattern of aberrations.

In this chapter we present a brief review of the optical quality of the eye and its measurement. We also review the Adaptive Optics technology and its application to the eye and we finally review the state of the art of the psychophysical measurement of visual performance and visual adaptation.

1.2 The human visual system: a very brief summary

Visual perception results from a series of transformations that can be classified in three stages: optical, retinal, and cortical. The light arriving into the eye from a scene is first focused by the eye's optics to form an image on the retina. This image is then transformed into neural signals by the photoreceptors. These signals

exit the eye via the optic nerve and are transformed into cortical representations in the brain. The following sections describe the optics of the eye, the retina and the neural process onto the brain.

1.2.1 The optics of the human eye

The optical system of the eye is mainly formed by the cornea and the crystalline lens, which project the images on the retina thought a limiting aperture, the pupil defined by the iris. The iris contracts or expands in response to the ambient illumination controlling the amount of light entering the eye and impacting on the retinal image quality through the influence of diffraction.

The axial length of the human eye is approximately 24 mm. The relaxed eye achieves its refractive power (60 diopters) with the two refractive elements, the cornea (with the greatest refraction around 40 D) and the crystalline lens (responsible for the remaining refraction) [Atchison and Smith, 2000]. The cornea is an inhomogeneous cellular and fibrilar structure composed of 5 layers, the Epithelium, the Bowman's Membrane, the Stroma, the Decemet's membrane and the Endothelium [Barbero, 2006]. The crystalline lens has the shape of a biconvex lens. The lens capsule (transparent membrane) is attached to the ciliary body by the zonules. Contraction of the ciliary body decreases the tension of the supporting zonules fibres and bulges the lens into a more curved shaped lens increasing its axial thickness, its curvature and thus its optical power, which is called accommodation providing the eye with the ability to focus near and far objects.

1.2.2 The neurosensory retina

The retina is the neural structure located at the eye fundus and is the sensitive tissue of the eye. The retina and its light-sensitive photoreceptors (cones and rods) are directly connected to the brain.

Histologically, the retina is a seven-layered structure of alternating cells, pigmented and nerve fibres involved in the signal transduction, conversion of the light into neural signal. The nuclear or cells layers contain cell bodies of the neurons while plexiform layers contain axons and dendrites (the synapses). The ganglion cells provide the only retinal output signal. Their terminals converge at the optic nerve and they exit the retina at a single location called the optic disk. The light reaches the retina at the inner limiting membrane and the image projected on the retina is sampled by the two kinds of photoreceptors, the rods and cones, organized roughly in a hexagonal mosaics. The rods are sensitive to dim light and the cones are wavelength sensitive. Three kind of cones, can be distinguished, the short-wavelength (S) cones with a sensitivity peak at 420 nm (blue), the medium-wavelength (M) cones with a peak at 531 nm (green), and the long-wavelength (L) cones with a peak at 588 nm (red). The area of higher resolution in the retina is the fovea (located at about 5^{o} from the optical axis contains only cones at high density). The central fovea contains only cones, peaking at a density of around

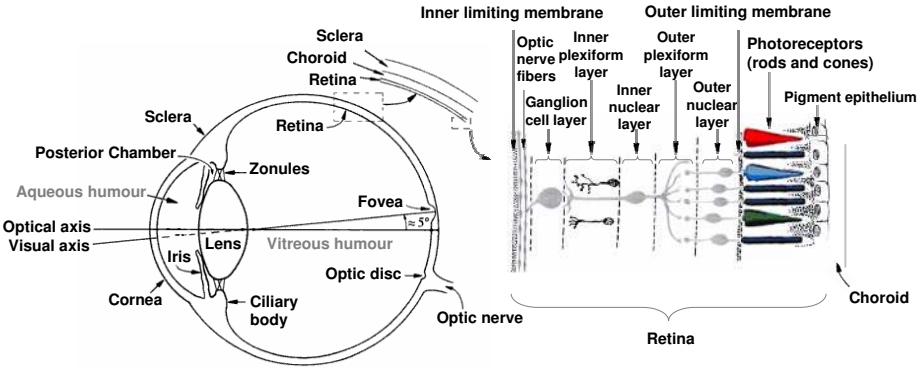

Figure 1.1: Drawing of the section of a human eye and the enlargement of the layered retinal structure involved in signal transduction. (Modified from Atchison and Smith [2000]).

150 000 cones/mm^2 [Ostergerb, 1935]. A complete scheme of the eye and retinal structure is shown in Figure 1.1

1.2.3 The visual cortex

Neural impulses leave the retina via the optic nerve and travel to the optic chiasm where the nerve fibers from the nasal side of the fovea in each eye cross over to the opposite side of the brain, while the fibers receiving input from temporal retina remain on the same side of the brain. From the lateral geniculate nucleus of the thalamus the signals are led, via the optic radiation, to a large area in the occipital cortex called primary visual cortex (area V1) that consists of around 150 millions neurons. The visual area constitutes about 25 % of the cortex in humans with approximately 5 billion neurons. The study of the visual cortex has revealed more than 20 other cortical regions (such as V2, V3, V4 and MT) that play a significant role in processing information such as shapes, orientations, color, movement, size, noise reduction, edge filtering, color separation, image compression, motion analysis, pattern and object recognition and other processing that occur in the brain.

1.2.4 The optical quality of the eye

It is well known that the human eye is not a perfect optical system, and particularly for large pupils it greatly differs from diffraction limit. The images projected on the retina are blurred by ocular aberrations which vary widely in the population, in range and in distribution [Castejón-Mochón et al., 2002; Porter et al., 2001; Thibos et al., 2002; Hartwig and Atchison, 2012; Plainis and Pallikaris, 2008]. The most important refractive anomalies are defocus and astigmatism (known as low order aberrations). However, the eye suffers from other high order aberrations. The existence of higher-order ocular aberrations was first reported by Von Helmholtz

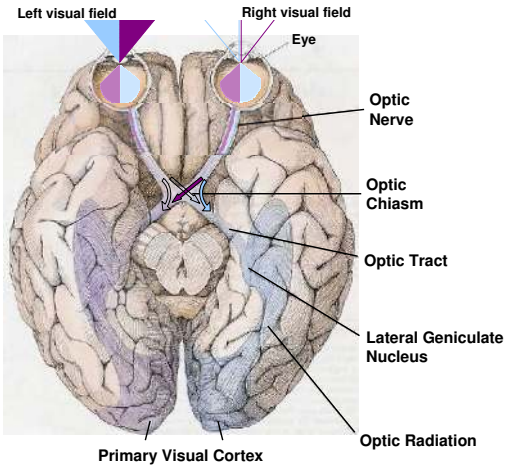

Figure 1.2: Visual pathway from the retina to the primary visual cortex via the lateral geniculate nucleus for a human brain. Adapted from Hubel [1963].

[1881]. Ocular aberrations contribute to the spread in the image projected on the retina, reducing image contrast, limiting spatial frequencies available for further stages of the visual processing. In the last decades, with the development of rapid and reliable aberrometers and the implementation of novel techniques, the accurate measurement of ocular aberrations has become easier.

Wave aberrations

The optical performance of the eye is usually described in terms of wave aberration. The wave aberration represents the distortions of the wavefront (surface containing points with the same phase and orthogonal to the propagation axis) in the pupil plane as it goes through the optical system. In a perfect aberration-free system, the wavefront would be perfectly spherical-shaped and the image of a point source through a circular pupil would be only limited by diffraction. The presence of aberrations induces deviations in the wavefront from the ideal spherical shape. The wave aberration map W(x,y), represents therefore the difference between a perfect spherical wave (reference sphere) and the aberrated wavefront at the exit pupil [Charman, 1991]. An example of wave aberration map is shown in Figure 1.3, where the color indicates the distance between the aberrated wavefront and the reference sphere.

Zernike polynomials

The wave aberration is normally described mathematically by a series of polynomials, orthogonal in a circular region: The Zernike polynomials (Z_n^m, corresponding to the radial order n and the meridional frequency m), originally described by Frits Zernike in 1934 [Zernike, 1934].

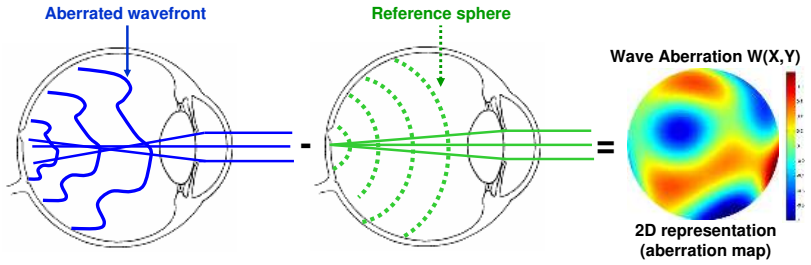

Figure 1.3: schematic representation of the wave aberrations (adapted from Marcos [2005]).

Zernike polynomial expansion has become the standard to represent the ocular wave aberration, for their advantages with respect to other representations. They are orthonormal in a unit circle and the low order terms relate to common refractive errors measured clinically, such as defocus and astigmatism. Wave aberrations are therefore described by a weighted sum of Zernike polynomials. The weights of polynomials are called the Zernike coefficients (c_n^m, corresponding to the radial order n and the meridional frequency m) and represent the magnitude of each particular ocular aberration present in the wave aberration. Thus we can express the wave aberration following equation 1.1.

$$W(x,y) = \sum_{n,m} c_n^m Z_n^m(x,y) \tag{1.1}$$

where W(x,y) is the wave aberration expressed in Cartesian coordinates, Z_n^m (x,y) the Zernike polynomial expressed in Cartesian coordinates, and c_n^m are the corresponding Zernike coefficients for radial order n and meridional frequency m.

Figure 1.4 (left panel) shows the Zernike polynomials from 2^{nd} order to 6^{th} order (the zeroth and 1^{st} order are not used in this thesis).

The Root Mean Square (RMS) wavefront error is typically used as a global metric for optical quality. RMS is computed directly from the Zernike coefficients, using the equation 1.2.

$$RMS = \sqrt{\sum_{n,m} c_n^{m2}} \tag{1.2}$$

where c_n^m is the Zernike coefficient corresponding to the order n and frequency m. Moreover, the Zernike terms are normalized so that the coefficient of a particular term or mode is the RMS contribution of that term.

Retinal Image quality metrics

Several optical quality functions can be obtained from the wave aberration using Fourier optics computations. Retinal image quality metrics computed from the wave aberration will include the combined effects of diffraction and aberrations

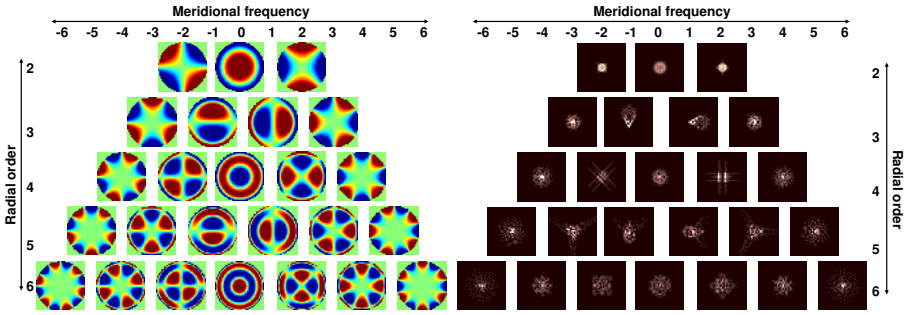

Figure 1.4: Representation of the Zernike polynomials from 2^{nd} order to 6^{th} order and the PSF corresponding to 0.5 μm Zernike coefficient over 5 mm pupil.

(but not scattering). In this thesis we typically described the optical quality using retinal image quality based metrics, including the Point Spread Function, the Optical Transfer Function, the Strehl Ratio and Visual Strehl Ratio.

The Point Spread Function (PSF) is the image of a point object through the optical system. It is calculated as the squared magnitude of the inverse Fourier transform of the pupil function. The pupil function, $P(x, y)$, defines how light is transmitted by the eye optics.

$$P(x,y) = A(x,y)\ \exp(i\frac{2\pi}{\lambda}W(x,y)) \tag{1.3}$$

$$\begin{aligned} PSF(x,y) &= K\ \left| FT\left[A(x,y)\ \exp(i\frac{2\pi}{\lambda}W(x,y))\right]_{fx=\frac{x}{z},fy=\frac{y}{z}}\right|^2 \\ &= K\ \left|FT\big[P(x,y)\big]_{fx=\frac{x}{z},fy=\frac{y}{z}}\right|^2 \end{aligned} \tag{1.4}$$

where K is a constant, $P(x, y)$ is the pupil function, $A(x, y)$ is an apodization function (when the waveguide nature of cones is considered) and $W(x, y)$ is the wave aberration. $P(x, y)$ is zero outside the pupil. FT is the Fourier Transform operator, z is the distance from the pupil to the image (eye length).

The point spread function for a perfect optical system (only limited by diffraction) is the Airy disk. The presence of ocular aberrations causes the light to spread out over an area and the corresponding PSFs is considerably broader than the aberration-free PSF for the same pupil size, particularly for pupils higher than 3 mm. Figure 1.4 (right panel) shows the PSFs corresponding to individual Zernike terms (with 0.5 μm zernike coefficients over 5 mm pupil). Figure 1.5 illustrates how the PSF changes with pupil diameter for a perfect eye only limited by diffraction and for a normal human eye. In the normal eye, aberrations dominate at larger pupil sizes

The Optical Transfer Function (OTF) is the autocorrelation of the pupil function, or equivalently, the Fourier Transform of the PSF. The OTF is a complex

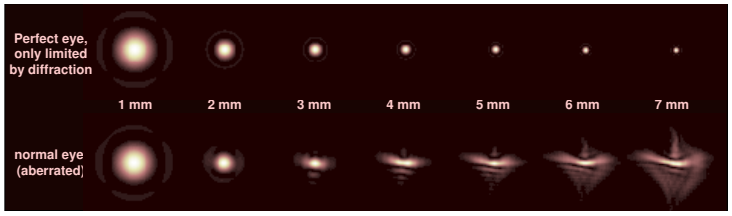

Figure 1.5: The dependence of the PSF on pupil diameter for a perfect eye only limited by diffraction (top row) and for a normal aberrated human eye (lower row) for which at small pupil sizes, diffraction dominates and for larger pupils, aberrations blur the PSF.

function that measures the loss in contrast in the image of a sinusoidal target, as well as any phase shifts. The modulus of the OTF is the Modulation Transfer Function (MTF), which represents the decrease in the contrast as a function of the spatial frequency. The phase of the OTF is the Phase Transfer Function (PTF). The PTF produces phase shifts, and it is associated with the presence of asymmetrical aberrations, such as coma and astigmatism.

The Strehl Ratio (SR) is a scalar metric used to describe the quality of the PSF in an eye. It was introduced by K. Strehl at the end of 19^{th} century. In the spatial domain, it can be calculated directly from the PSF. It is the maximum value of the PSF in the presence of aberrations, normalized to the maximum of the diffraction limited PSF for the same pupil size. The Strehl Ratio ranges from 0 to 1, with 1 defining a perfect optical system. The Marechal criterion states that a system is regarded as diffraction limited if the Strehl Ratio is 0.8 or greater. In the frequency domain, the Strehl Ratio is computed as the volume under the OTF of an aberrated system normalized by the diffraction-limited OTF, for the same pupil diameter. As the strehl ratio includes in the calculation regions of the OTF with spatial frequencies beyond those relevant to the visual system, a new metric was introduced [Iskander, 2006] to adapt the definition to visual optics (visual Strehl). The visual OTF is computed by multiplying the OTF by the inverse of the neural contrast sensitivity function -from a general population, and assuming meridional symmetry)- Visual Strehl is computed as the volume under the OTF.

1.2.5 The cone mosaic sampling and factors limiting eye resolution

The image of the outside world is projected onto the retina and is first degraded by the aberrations of the eye that blur the image followed by the cone mosaic sampling and neural factors that limit the finest resolvable detail. Neural factors affecting spatial visual perception include neural sampling by the photoreceptors, both spatial and spectral due to their size, spacing and directionality, and spatial and temporal summation of quanta [Hecht et al., 1942] due to the quantum nature of light.

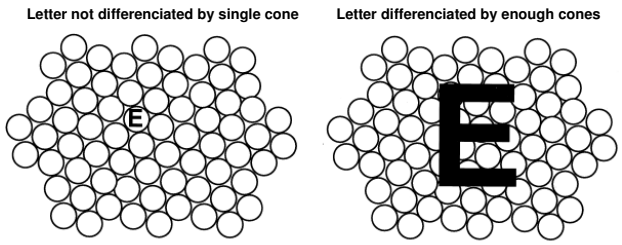

Figure 1.6: The sampling problem. To be seen, the letter must be sampled by sufficient photoreceptors to resolve the letter traits. (adapted from Applegate et al. [2001]).

Stiles and Crawford [1933] found that human observers are considerably more sensitive to light coming through the center of the pupil than they are to the off-center rays. The Stiles-Crawford effect is due to the directionality of the human cones that acts like waveguides and are tuned typically towards the center of the pupil becoming more sensitive to light entering near the centre of the pupil than in peripheral regions [Marcos et al., 1999].

The photoreceptor mosaic samples discretely the continuous distribution of light in the retinal image. Therefore, the visual system is susceptible to sampling artifacts, or aliasing. The problem of sampling induced by photoreceptor size and packing is illustrated in Figure 1.6. If the eye's optics could image a letter "E" within the entrance aperture of a single cone, the letter "E" could not be differentiated into its components parts. To be seen as a letter "E", it must cover a sufficient number of cones [Applegate et al., 2001]. Young [1802] observed that jointly sampling spatial and spectral signals with a single array of photoreceptors presents a problem, because "there cannot be an "infinite number" of detectors for different frequencies of light at each point on the retina". Ostergerb [1935] estimated that the highest density of human fovea1 cones was around $150\,000\,\mathrm{mm}^2$. The Nyquist limit (critical frequency expressed in c/deg) is estimated at around 60 c/deg. When the spatial frequency of a retinal image is above the Nyquist limit, under-sampling occurs that yields to a misrepresentation of the signal projected onto the retina, and is called aliasing.

There are additional factors that might preclude aliasing in the fovea such as irregularities in the mosaic [Yellott, 1982], low pass filtering by individual photoreceptors [Miller and Bernard, 1983] and fixation instability might produce high temporal frequencies that effectively blur the high spatial frequencies.

1.2.6 Representing retinal image by means of PSF convolution

It is possible to simulate the retinal image as the convolution of the original image with the PSF of the eye [Goodman, 1996]. The use of convolved images to represent the retinal image quality has been largely used in visual optics, although there are recent reports showing systematic differences in the visual acuity measured using

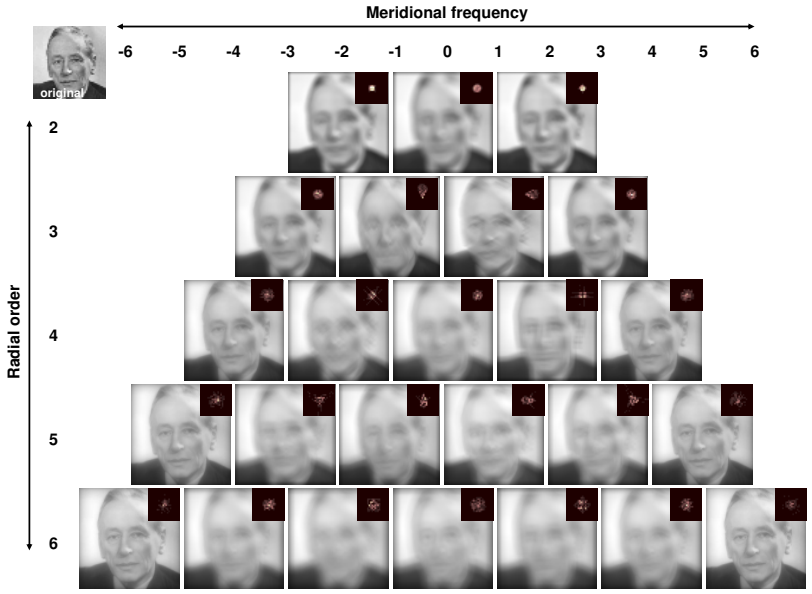

Figure 1.7: Zernike polynomials and the effect on a simulated image (Zernike face) by convolution with the corresponding PSF, from 2^{nd} to 6^{th} order.

simulated versus real aberrated targets [de Gracia et al., 2009; Ohlendorf et al., 2011]. Flamant [1955] pioneered the application of the Fourier theory of optics with convolution of a slit target with the eye's line-spread function. Westheimer and Campbell [1962] studied light distribution in the image formed by the living human eye. Later, Burton and Haig [1984] simulated and studied the effects of Seidel aberrations (primary defocus, spherical aberration, astigmatism, and coma) and Artal [1990] computed the Foveal point-spread functions from experimental wave-aberration data for individual emmetropic subjects. Thibos and Bradley [1995] studied how post-receptoral neural processing of the retinal image affects the processing of blurred retinal images in a manner that can be modelled as a mathematical convolution of the optical PSF with a neural point-spread function. Peli and Lang [2001] presented filtered images to bilaterally implanted patients with monofocal/multifocal intraocular lenses (IOLs), to simulate the appearance of images through the multifocal IOL. Applegate et al. [2003b] used an image-convolution based approach to evaluate the effects of individual aberration terms on visual acuity. Legras et al. [2004] used convolved images to simulate the degradation produced by defocus, astigmatism and spherical aberration to evaluate the minimum amounts of these aberrations that produced just-noticeable differences to subjects.

Figure 1.7 shows the simulated image (Fritz Zernike's face) aberrated by convolution with the corresponding PSF of the specific aberrations (pupil=5 mm; viewing angle 2^{o} ; 0.5 microns of RMS aberrations).

1.3 Visual perception and adaptation

By computing the retinal image by convolution with the PSF of an individual's eye, we illustrate the retinal images projected on the retina of each particular eye. However, the subjective image quality of the human eye is affected by both optical blur and neural factors that limit the eye resolution as well as by the observer's visual experience. Thanks to the theory of Psychophysics, developed by Fechner [1851, Vol.1 tranlated to English in 1966] visual perception can be measured in a variety of ways.

To examinate the neural plasticity after that perception has been modified experimentally, Stratton [1896, 1897] first studied the effect of presenting to the retina an inverted image. He reported that after removing the reversing lenses at day eight, it took several hours for his vision to return to normal. This experiment has originated a long series of further experiments on retinal inversion (Theodor Erismann (1883-1961), Ivo Kohler (1915-1985), Harris [1965], Gregory [1998], Linden et al. [1999]). Two fundamental mechanisms can occur when examining the neural plasticity: The perceptual learning that refers to the performance after a training task. The other mechanism is the adaptation process that recalibrates the internal norm to maintain a match between visual coding and visual environment.

In this section we will present psychophysical methods to measure visual function and refer briefly to the mechanism of perceptual learning and the neural adaptation process studied in this thesis.

1.3.1 Psychophysical methods to measure visual function

Psychophysics is used to measure an observer's performance of a visual task. This section will review various decision tasks that may be used to measure visual performance and visual perception (visual acuity, contrast sensitivity, detection, identification and recognition task, judgment of blur). In vision science, the classical methods in psychophysics are those that measure a threshold such as visual acuity threshold, quantified in terms of the finest size of detail in a scene that can just be resolved by the eye measured with different targets such as lines, bars, grating, letters (Snellen E, Landolt C, charts Bailey and Lovie [1976]) and contrast sensitivity threshold at which one observer can detect a sinusoidal grating of different spatial frequencies. Fundamentally, there are two kinds of decision tasks: adjustments – where the observers have to adjust the stimulus accordingly to the task asked for- and judgments – where the observers have to classify the stimulus of percept [Pelli and Farell, 1995, Chapter 29].

Among adjustment tasks, contrast sensitivity threshold is the most common form. The observer is asked to adjust the stimulus contrast up and down to the point where it is just barely detectable. Another example is the nulling task where a stimulus is distorted by some experimental manipulation, and the observer is given control over the stimulus and asked to adjust it so as to cancel the distortion, for example luminance motion can be nulled by chromatic motion in the

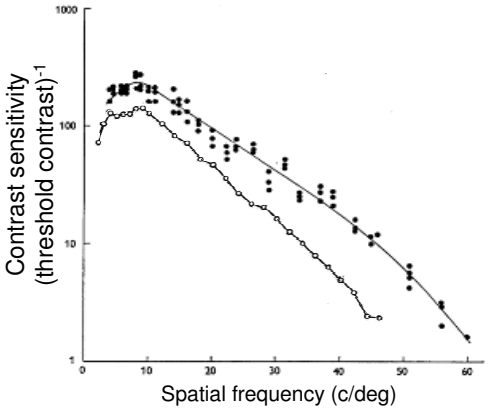

Figure 1.8: Contrast threshold functions for whole eye of one subject combining neural and optical system (open-circle) measured with sinusoidal gratings presented to the subject on a television monitor with a green phosphor through 2 mm artificial pupil through emmetropic correction; and contrast sensitivity of the retina alone (neural system alone) (black circle) obtained by means of interference fringes using monochromatic light (633 nm) (adapted from Campbell and Green [1965]).

opposite direction [Cavanagh and Anstis, 1991]. In matching tasks, two stimuli are presented and the observer is asked to adjust one to match the other. For example, the observer might be shown two grating patches, one fine and one coarse, and asked to adjust the contrast of one to match the contrast of the other [Georgeson and Sullivan, 1975].

The judgment decision tasks differ from the adjustment decision tasks primarily in the number of alternative stimuli that may be presented on a given trial and the number of alternative responses that the observer is allowed. Among them, the alternative forced choice procedure, and the rating scale were used in this thesis. In the two-alternative forced choice procedure (2AFC), two separate stimuli (blank/nonblank) are presented in random order, sequentially or side by side and the observer is forced to choose between alternative choices, whether the nonblank stimulus was first or second (or on the left or right). In a 2AFC, there is already a 50 % chance of a correct response and the starting threshold is commonly considered as 75 % (half way between 50 and 100 %). For a 4AFC, threshold is considered to be at the 62.5 % seen level (half way between 25 % and 100 %).

In the rating scale task, the observer is asked to rate the likelihood that a nonblank stimulus was presented. There must be blank and nonblank stimulus alternatives, and there may be any number of alternative ratings. The end points of the rating scale are "stimulus definitely blank" and "stimulus definitely nonblank" with intermediate degrees of confidence in between. The results are illustrated as a receiver operating characteristic (ROC) curves that represent the probability of a yes when a nonblank stimulus was present (True positive) against the probability

of a yes when a blank stimulus was present (False positive) [Metz, 1978, 1986; Metz et al., 1984]. Generally, the ROC curve is quantified by the area under the curve, where a perfect performance corresponds to an area of 1, and a total arbitrary response produce an area of 0.5.

Most judgment experiments usually require many trials. An uninterrupted sequence of trials is called a run. A powerful method of sequencing the trials within a run to measure threshold in a limited number of trials is the use of the observer's previous responses to calculate the next stimulus size and estimate the threshold with algorithm such as QUEST (Quick Estimate by Sequential Testing) [Watson and Pelli, 1983]. At the end of the procedure, the trial size is considered the best estimate of the subject's threshold.

The limitations in the use of psychophysical experiment reside in that they require a conscious cooperating subject and a full understanding of the task. So the question has to be formulated precisely and sufficiently simple to obtain a convincing answer to reliably report the sensed events. In this thesis we used different psychophysical paradigms. We will describe each psychophysical method in the Methods Chapter and the corresponding chapters describing each particular study.

1.3.2 Perceptual learning

J.J. Gibson [1950] pointed out that "the correspondence of perception to the information available in stimulation does not have to be a wholly innate and unchanging correspondence. Psychophysical correspondence can be refined with practice and effort". [Owen, 1978, Chapter 18]

Perceptual learning refers to the phenomenon where practice or training in perceptual tasks often substantially improves perceptual performance. [Lu et al., 2011]. The hallmark of perceptual learning is its specificity in what is learned is highly specific to the stimulus and the task factors, such as retinal location, spatial frequency, orientation, background texture or visual field position. Karni and Sagi [1991] reported long-term learning in a simple texture discrimination task where learning is specific for retinal input and demonstrated that learning was local, orientation specific, and strongly monocular, reporting little interocular transfer of learning from a trained to an untrained eye. Fiorentini and Berardi [1980] showed that perceptual learning was specific to orientation and spatial frequency by measuring, in a forced choice procedure, the effects of practice in the discrimination of briefly flashed gratings, either complex gratings of different waveforms or of simple (sinusoidal) gratings of slightly different spatial frequency. Ahissar and Hochstein [1996, 1997] in a series of experiments demonstrated that learning is specific to the stimuli used in the training and reported that the degree of specificities depends on the difficulty of the training conditions. Poggio et al. [1992] investigated fast improvement of visual performance in several hyperacuity tasks (vernier acuity and stereoscopic depth perception) and found that the fast phase of perceptual learning (within less than 1 hour training) is specific for the visual field position and

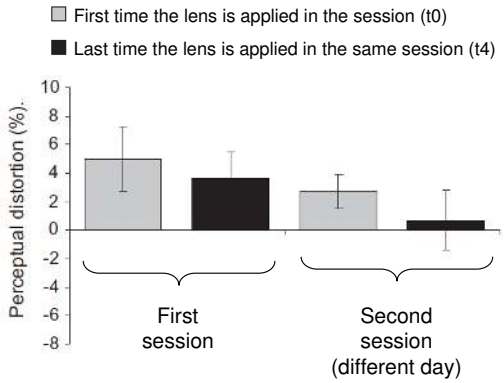

Figure 1.9: The learning effect: Comparison of the first two sessions shows a continuous decrease in distortion, from 5±2 % at time t0 of the first session to 0.68±2 % at time t4 of the second session. Adapted from Yehezkel et al. [2010].

for the particular hyperacuity task. Fahle and Morgan [1996] reported no transfer of perceptual learning between similar tasks. On the contrary, McGovern et al. [2012b] suggested that sensory improvements derived from perceptual learning can transfer between very different visual tasks (orientation discrimination, curvature discrimination and contrast discrimination task). They also reported [McGovern et al., 2012a] that, although conventionally treated as distinct forms of experience-dependent plasticity, the limits of neural adaptation mechanisms and perceptual learning have become increasingly blurred, raising the possibility that they might interact. Perceptual learning operates in a very specific manner, which depends on stimulus and task, whereas adaptation is thought to reflect a recalibration of the visual system to handle a change in the visual world.

Yehezkel et al. [2010] investigated whether adaptation is affected by previous experience with the adapting stimulus to examinate whether adaptation becomes more effective with experience. Efficient adaptation processes may reduce biases in perception, both when the adapting stimulus is applied and removed, the latter by reducing the duration of after-effects. In their study, they induced an artificial one-dimensional visual blur by using a cylindrical lens of 1 D mounted in front of one eye of the observers for an adaptation period of 4 h in two sessions, (in two different days) and probed the underlying mechanism and the time course of the adaptation effect. The obtained learning effect suggested learning of adaptation to the induced blur rather than learning of the task per se.

1.3.3 Neural adaptation

The visual system continuously adjusts to changes in the environment such as color, contrast, luminance and blur, as well as to changes within the observer (aging, diseases, treatments, spectacles) to maintain a match between visual coding and visual

environment, which is called the perceptual constancy such as contrast constancy [Georgeson and Sullivan, 1975] and color constancy [Werner and Schefrin, 1993; Webster and Mollon, 1995; Webster et al., 2010]. "The term visual adaptation describes the processes by which the visual system alters its operating properties in response to changes in the environment. These continual adjustments in sensory processing are diagnostic as to the computational principles underlying the neural coding of information and can have profound consequences for our perceptual experience." [Clifford et al., 2007]. Adaptation constantly recalibrates visual coding so that our vision is normalized according to the stimuli that observers are currently exposed to. These normalizations can occur over very a wide range of time-scales going from only milliseconds to life-spans [Webster, 2011]. Short-term adaptation adjusts the visual system to temporary changes. For example changes in light illumination levels (as exit into the outdoor sunlight for example), or in the blur perceived in natural scenes. Brief periods of exposure to stimulus blur can strongly affect the subsequent perception of focus [Webster et al., 2002; Vera-Diaz et al., 2010; Elliott et al., 2011]. These aftereffects occur and can be selective for different types of stimuli, for luminance or chromatic blur [Webster et al., 2006], spatial or temporal blur [Bilson et al., 2005], and different depth planes [Battaglia et al., 2004], whereas long-term adaptation adjusts the visual system to changes in the environment or within the observer.

In this section we will give some examples of adaptation that occur to changes in the environment, adaptation to changes within the observer, and possible adaptation of the visual system to ocular aberrations.

Examples of Visual Adaptation

One intensively studied form of adaptation is adaptation to contrast. Prolonged viewing of a high contrast vertical pattern reduces the perceived contrast of a similar pattern in a subsequently viewed test stimulus [Blakemore and Campbell, 1969a]. Blakemore and Campbell [1969b] studied the adaptation to a grating by determining the contrast threshold before and after adaptation. They found a temporary rise in contrast threshold after exposure to a high contrast grating of the same orientation and spatial frequency. The reduction in perceived contrast is strongest for test stimuli that have the same orientation as the adapter. The contrast images in Figure 1.10 illustrate perceptual reduction in apparent contrast. Adapting to the image A results in a low-contrast portion of the test image B that briefly appears invisible. Adaptation to the pattern in C does not reduce sensitivity to the test pattern, demonstrating the orientation specificity of the effect.

If observers are exposed to and thus adapted by different environments, their vision will be normalized in different ways and their subjective visual experience may differ. On the contrary, if observers are exposed and adapted to common properties in the environment, their vision will be adjusted toward common states, and may develop common features in their visual response. How the world looks depends on the recent and long-term visual experience. Different environments can

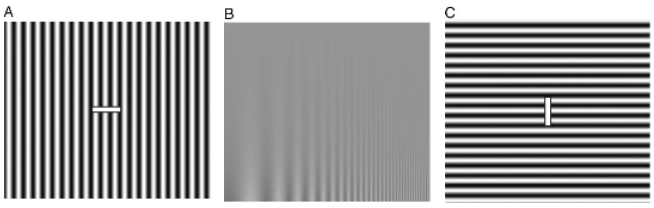

Figure 1.10: Perceptual reduction in apparent contrast. A and C are the adapting images, B is the test image.

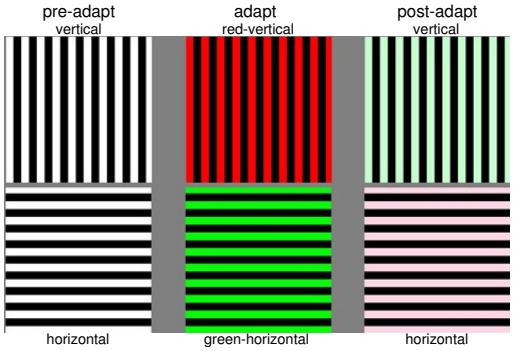

Figure 1.11: Illustration of the McCollough Effect. (From McCollough-Howard and Webster [2011].

vary widely in their color properties and it has been shown that "color differences across scenes are in principle sufficient to hold observers under different adaptation states" [Webster and Mollon, 1997; Mizokami et al., 2004]. Someone living in an aride environment will not perceive the palette color the same as someone living in a tropical country. Sensitivity is normalized to the brightness and color of the environment or adapting stimuli. As the stimulus changes, our color perception is shifted accordingly. Long-term adjustments have been described for color vision. A classic example is the McCollough effect, in which the color aftereffect is contingent on the spatial orientation of the patterns [McCollough-Howard and Webster, 2011]. Figure 1.11 shows an illustration of the basic McCollough Effect. After viewing red/vertical and green/horizontal stripes, white/vertical stripes appear slightly greenish and white/horizontal stripes appear slightly reddish.

Appearance of the visual degradation produced by an ocular disorder (myopia, keratoconous, cataract) constrains the observer to continuously adapt to their vision as well as treatment. It is well known that the visual system changes over time. Werner and Schefrin [1993] studied how the visual system is calibrated for some longer term estimate of the environment by measuring the locus of the achromatic point. They found no significant changes as a function of age in subjects who did not suffer from ocular disease, suggesting that partial compensation for age-related changes in visual mechanisms occurs in a way that preserves constancy

Figure 1.12: Left : Monet's Japanese Bridge at Giverny, 1900, Monet did not suffer at this time from cataract. Right: Monet's The Japanese Footbridge at Giverny, around 1923, Paris. Monet suffered from cataract. Adapted from Ravin [1985]

of the achromatic locus across the life-span. On the other hand, an example of aged-related change is the brunescence of the crystalline lens. The visual system adapts to the changes in the retinal stimulus with the yellowing of the lens to maintain constancy of color appearance across the life span. An example of age related change adaptation is the case of the impressionist Claude Monet (1840-1926) who suffered from cataract that affected his late style. Figure 1.12 shows the same scene painted in different moment in Monet's life, in around 1900, when he did not suffer yet from cataract (left image) where blue tone is dominating the painting and around 1923 (right image) when he suffered from cataract. The painting in this case showed a dominance of red colors [Ravin, 1985; Werner, 1997].

Delahunt et al. [2004] examined the changes in color appearance following lens replacement in cataract patients as the cataractous lens strongly filters short wavelength light, and thus immediately after the operation many patients report that the world appears bluish. They tracked the changes in this perception by measuring the achromatic point at different times after surgery. Figure 1.13 shows the changes in the white point following cataract surgery for 4 observers, as distance in the standard CIE chromaticity diagram D65) the smaller the Euclidean distance the closer to the theoretical white point D65. They reported that the visual system gradually adapts so that achromatic settings shift toward a typical white point over a 3-month period.

Fine et al. [2002] addressed the question of how the visual system adjusts to limited and distorted visual input and examined blur perception in an individual who had bilateral congenital cataract removed after 43 years. Besides the color effect noticed by the subject, blur adaptation also occur and it was reported that "after their removal, edges appeared to be too sharp, and this aftereffect showed little sign of diminishing even after months".

Understanding adaptation to spatial blur

As ocular aberrations produce a spatial blur of the retinal images, we will refer in more extent to blur adaptation. Blur is an important factor of image quality

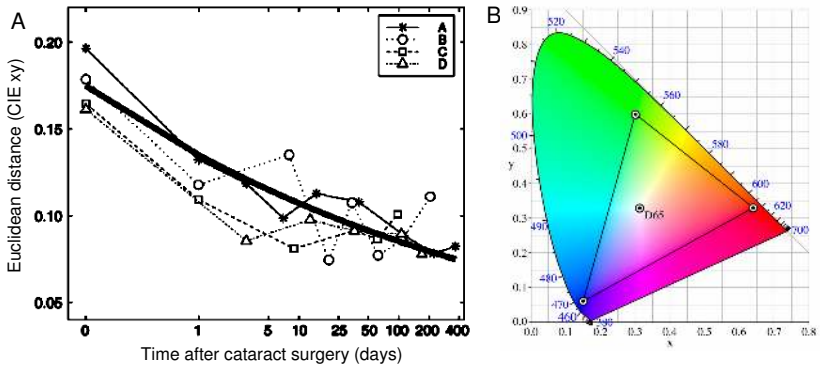

Figure 1.13: A) Shift in the achromatic settings over time following cataract surgery for 4 observers. The y-axis shows the Euclidean distance in CIE xy chromaticity space from the presurgical white point (D65). The x-axis shows the days from surgery (in log units). Each observer's data were well fitted by a scaled decaying exponential function of time (bold curve) (adapted from Delahunt et al. [2004]). B) The CIE 1931 color space chromaticity diagram; with the White point D65 (coordinates: 0.3127; 0.3290)

and the visual system makes intuitive blur judgments. Large intrinsic differences between observers are known to continuously occur in the perception of blurred images. The role of prior visual experience on visual experience was realized in an early report by D. Owen [1978, Chapter 18] "one of the major problems with which theorists have been confronted themselves since the beginning of attempts to explain perception is how and at what locus prior experience comes to have an influence on subsequent perceiving. One observer may see something that another does not, or the one may see something in a way that the other does not".

Short-term adaptation to blur was first reported by Webster et al. [2002]. This seminal studied showed that subjects can adapt to blur produced by computed generated Gaussian blur. After viewing a blurry or sharpened image, a physically focused image appeared too sharp or too blurry, respectively (Figure 1.14). Thus the point of subjective focus shifted toward the adapting image. These effects are consistent with a re-normalization of perception, so that the currently viewed stimulus becomes the new prototype for proper image focus.

Instead of using artificial blur (computed generated Gaussian blur), several studies have reported adaptation to optical blur produced by real low order aberrations (defocus or astigmatism) by showing improvements in visual acuity following adaptation to optical defocus induced by wearing positive lenses, after a period of spectacle removal or after a period of adaptation to simulated or trial lenses-induced blur.

Mon-Williams et al. [1998] assessed Visual Acuity (VA) before and after exposure to induced myopia (optical defocus with +1.00 D ophthalmic lenses) in 15 emmetropic subjects. They found that an improvement in visual acuity following exposure to optical defocus (as illustrated in Figure 1.15 where the majority of

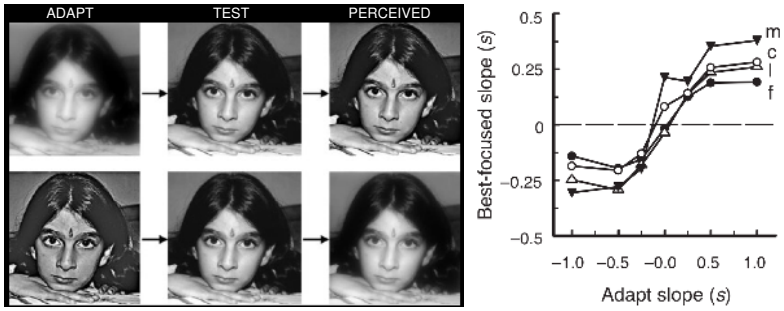

Figure 1.14: A) Blur adaptation process: Viewing a blurred image (positive slope) causes the correctly focused image to appear too sharp and viewing a sharpened image (negative slope) leads to the opposite after-effect B) Slope of the image amplitude spectrum that appeared best-focused after adapting to images with different spectral slopes, testing 4 different images: face (f), leaves (l), check board (c) and meadow (m). (adapted from Webster et al. [2002, 2005]).

points for VA fall below the line of equal acuity). As an ophthalmic change did not occur, they attributed the changes to a neural compensation for the defocus condition.

Following up on the observation that "myopes of low degree commonly report that their vision seems poorer upon removal of their spectacles compared to that after a period without spectacle wear", adaptation to optical defocus was tested after a period of spectacle removal, maintaining distance fixation throughout the uncorrected trial period to obtain the maximum blur effect. Pesudovs and Brennan [1993] measured visual acuity after a television viewing with and without their spectacle correction and found that visual acuity underwent a slight but significant increase after the session without spectacle wear. Similarly, Rosenfield et al. [2004] found significant improvements in the unaided VA during the period of sustained blur whereas subjects keeping their spectacle correction throughout the session did not showed changes in their visual acuity. They considered that this improvement in visual resolution was not produced by any significant change in refractive error, nor can it be explained by a learning effect produced during the repeated acuity measures. Several other studies have investigated the lower visual acuity reduction in myopes after short term adaptation to myopic defocus than in emmetropes [George and Rosenfield, 2004; Poulere et al., 2013] due to prior-experience to blur in myopes, suggesting an adaptation to blur.

Pesudovs [2005] studied the effect of neural adaptation to surgically induced high order aberrations and measured unaided logMAR visual acuity at presentation, while they were adapted to their habitual unaided vision (blur adapted) and after 1 min of adaptation to their newly prescribed refractive correction (correction adapted) in 26 patients after LASIK surgery, to study the dominance of learning effect or blur adaptation. The results of this study suggested that adaptation to surgically induced blur occurred in patients 10 weeks after LASIK surgery, as shown in Figure 1.17, following a learning effect period.

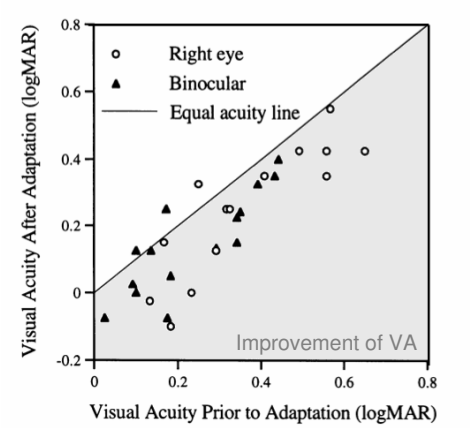

Figure 1.15: Visual Acuity (VA) prior to adaptation is plotted against visual acuity (VA) following 30 minutes exposure to optical defocus, for right eye and binocular condition. The solid line indicates equal acuity. It may be seen that the majority of points fall below the line illustrating the improvement in VA following exposure to optical defocus. Adapted Mon-Williams et al. [1998].

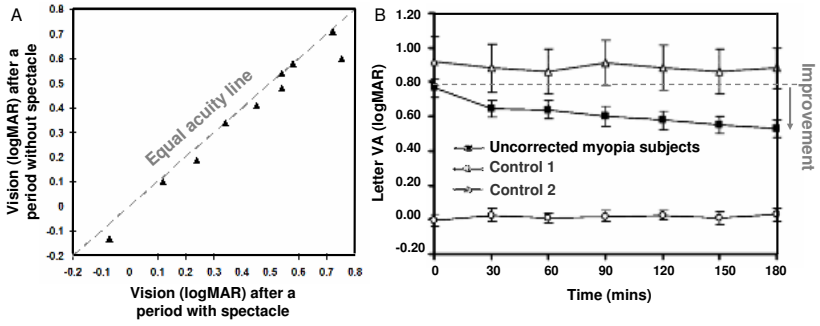

Figure 1.16: A. Visual Acuity (logMAR) after a period without spectacle wear vs. vision after a period with spectacle wear.(Adapted from Pesudovs and Brennan [1993]). B. Mean visual acuity (VA logMAR) as a function of time during the 3-h trial period for 22 subjects with uncorrected myopia as well as for two control studies (8 myopic subjects with their spectacle including (control 1) or except (control 2) for VA measurement)(Adapted from Rosenfield et al. [2004]).

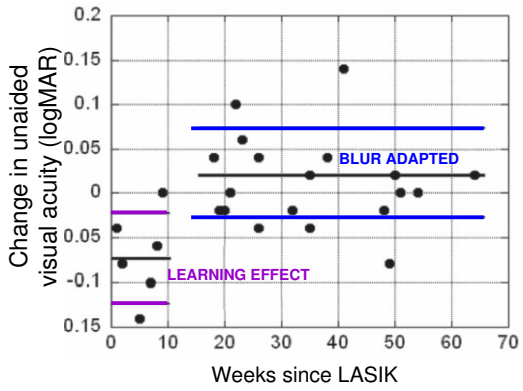

Figure 1.17: Blur adaptation represented by the difference in unaided VA (correction adapted-blur adapted) as a function of weeks since LASIK surgery. Adapted from Pesudovs [2005].

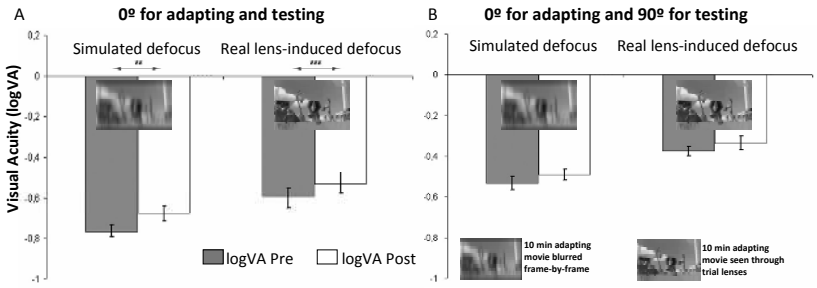

Figure 1.18: Logarithm of visual acuity with simulated and real astigmatic defocus of +3 D at 0 º (A) or 90 º (B) before (log VA pre) and after (log VA post) adaptation to the astigmatically (0º) defocused movie over a period of 10 minutes. Error bars denote the standard errors of the paired differences in visual acuity (**p<0.01; *** p<0.001). (Adapted from Ohlendorf et al. [2011]).

Ohlendorf et al. [2011] studied short term (10 min) adaptation to "simulated" (by convolution with astigmatic PSF) and optically-induced "real" astigmatic defocus (astigmatic trial lenses), to investigate how much subjects adapt and how selective adaptation was for the axis of astigmatism and found that adaptation to either simulated or real astigmatic defocus increased visual acuity and when rotating the axis of astigmatism to 90 º for testing images, no significant changes occurred in visual acuity, suggesting that adaptation involves a re-adjustment of the spatial filters selectively for astigmatic meridians.

While low order aberrations (defocus and astigmatism) are normally corrected by conventional correction, high order aberrations (HOA) (i. e. coma, trefoil, spherical aberration) remain uncorrected leaving the eye chronically exposed to blurred image. High order aberrations induce a decrease in the resolution and contrast of the images projected on the retina. However, observers do not have the

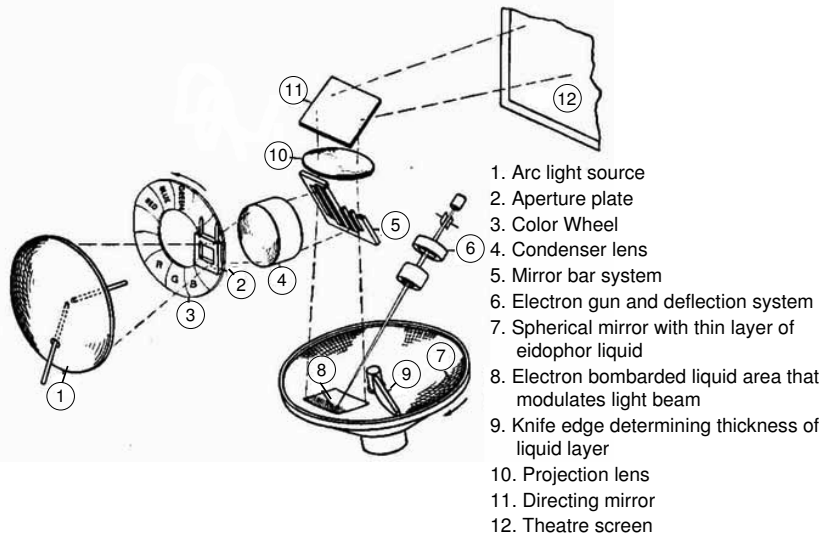

Figure 1.19: The mechanical layout of the swiss inspired "Eidophor" theater projection system published in Radio and Television News, August 1952, [Fischer, 1952].

impression of image degradation, perhaps due to the presence of a mechanism such that the visual system may be compensated for the eye's imperfections. These prior studies suggest that the state of adaptation may therefore play a fundamental role in determining the way that the world look to the different observers. Quoting Webster et al. [2005, Chapter 9], we would like to address the question "What might the world look like if we could see it through the eyes of another?"

Adaptive Optics places itself as an ideal tool to investigate the limits of neural adaptation to ocular optics by allowing simulation of any ocular wavefront and therefore manipulating the retinal image.

1.4 Adaptive Optics

Adaptive optics has its origins in astronomy specifically in Horace W. Babcock who proposed, in 1953, a solution to the problem of imaging objects in space through the atmospheric turbulence by introducing the idea of an adaptive optical element capable of correcting the time-varying aberrations caused by the atmospheric turbulence. In 1952, Babcock saw an article on the Eidophor, an electronic device developed by Dr Fritz Fischer in 1939, that explained the mechanical layout of the swiss inspired "Eidophor" theater projection system (depicted in Figure 1.19) published in radio and television news [Fischer, 1952].

The Eidophor employs a mirror covered with a thick film of oil scanned by a modulated electron beam that allows the deposition of electric charge onto the oil film which induced local slopes changes that modified the wavefront reflected

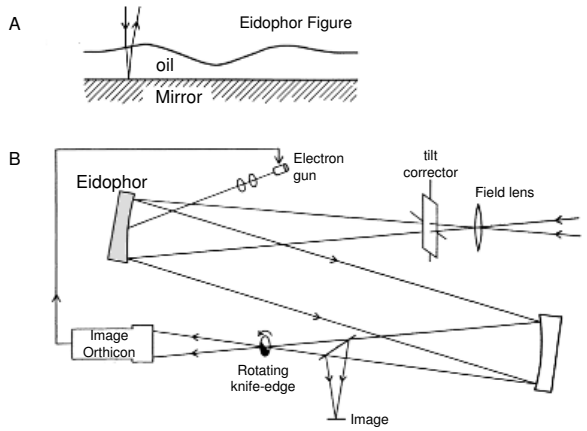

Figure 1.20: Resulting deformation of eidophor figure, showing correction of deviated ray. B: Schematic diagram of seeing compensator proposed by Babcock (1953 for compensation in real time of wavefront disturbances by means of an electronically deformed oil film on the Eidophor mirror). Adapted from [Babcock, 1953, p. 232-233].

from the mirror (see Figure 1.20A). Babcock noted that this principle could be used for correcting optical wavefronts distorted by the atmospheric turbulence and suggested the use of a close-loop feedback system to measure and correct the wavefront distorsions in real time [Babcock, 1953]. Figure 1.20B, depicts a copy of the original illustration of the system in Babcock's publication, which combined a seeing sensor and a wavefront corrector the first account of what is now known as adaptive optics.

Due to the technical complexity of measuring atmospheric aberrations and fabricating and controlling wavefront correctors, the first successful adaptive optics system in astronomy was only developed in 1977 by Hardy et al. [1977]. Today, the major ground-based telescopes worldwide are provided with Adaptive Optics systems, which can collect high resolution images comparable to those obtained with space telescopes (Hubble launched in 1990 and Spitzer in 2003 [Waldrop, 1990; Dalcanton, 2009; Gehrz et al., 2007]).

In the 1990's, an Adaptive Optics system was first applied to the eye. These advances were paralleled by the development of a new ocular aberrometer based on Hartman-Shack wavefront sensing, by Liang et al. [1994] (first applied in astronomy in 1971 [Shack and Platt, 1971]), which largely exceeded in spatial resolution and temporal acquisition prior ocular aberroscopes [Walsh et al., 1984; Charman, 1991]. The first adaptive optics device used to correct the aberrations of the eye was a segmented mirror, which proved capable of correcting astigmatism and of increasing the quality of retinal images [Liang et al., 1994]. Liang et al. [1997] presented the first closed-loop adaptive optics system that could correct higher order aberrations in the eye in a high-resolution retinal imaging AO system and provide "normal eye with supernormal optical quality". They reported an improvement of

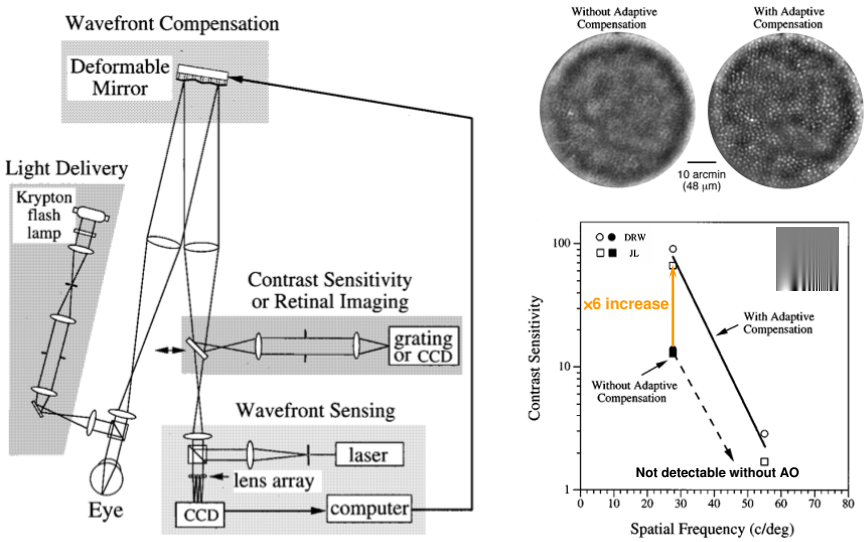

Figure 1.21: Wavefront sensing and adaptive compensation system developed in 1997, with an improvement in contrast sensitivity (for two eyes for horizontal grating of 27.5 and 55 c/deg) and higher contrast images of the cones mosaic (image of the retina at 4-deg eccentricity for one subject) with adaptive compensation, adapted from Liang et al. [1997].

contrast sensitivity of the eye in monochromatic light, better than that obtained with the best conventional spectacle correction and obtained higher contrast images of the cones mosaic.

While the benefit of correcting higher order aberrations has been also shown using phase plates, customized to correct the subjects aberrations measured in a prior session [Navarro et al., 2000; Burns et al., 2002], this method can only provide a static correction, preventing from correcting changes in the aberration pattern associated to movements or dynamic fluctuations of the optics. Real time correction of the wave aberration became possible with the development of automated wavefront sensing by Hofer et al. [2001] which allowed dynamic measurement of the ocular aberrations and closed-loop correction with a bandwidth of 1-2 Hz. The use of an Adaptive Optics system to measure, correct or induce low and high order aberrations is increasing with applications both in high-resolution retinal imaging and psychophysical testing under controlled optics.

1.4.1 Basic principles of an adaptive optics system applied to the eye

The extent to which AO can effectively improve resolution depends on its ability to accurately measure, track and correct the ocular aberrations. Even if there is a wide range of different adaptive optics systems worldwide, they share common principles.

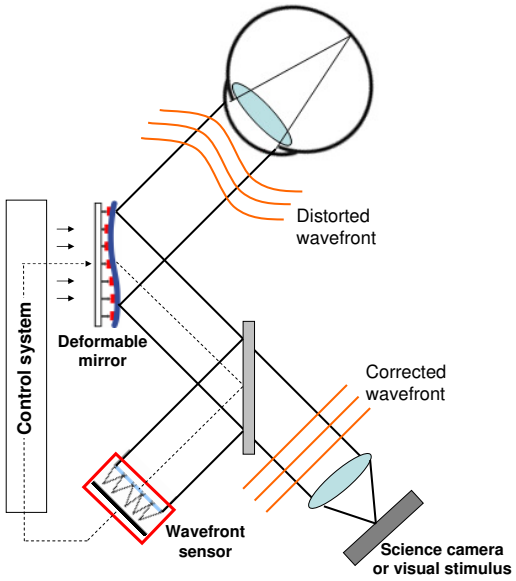

Figure 1.22: Basic scheme of an Adaptive Optics system in vision.

Adaptive Optics corrections in the eye comprise three steps: the light from the retina is reflected by a deformable optical component that corrects the wave distortions (wavefront correction). The reflected light is divided into two paths, by a beam-splitter which directs the light into the wavefront sensor that measures any residual distortion in the wavefront (wavefront sensing). Centroid positions are obtained form the wavefront sensor data and processed by a calculator (adaptive optics control) to determine the appropriate voltages applied to the wavefront corrector to modify its shape. The three steps are repeated in a loop that compensates in real time the aberrations of visual optics and micro-fluctuations of accommodation. Both the wavefront sensor and the wavefront corrector are placed in pupil conjugated planes and communicate by means of an adaptive optics control computer.

Wavefront sensing and principle of the Hartmann-Shack

The wavefront sensors in an adaptive optics system measures the optical aberrations in the pupil plane of the eye. The most suitable wavefront sensor is the Hartmann-Shack wavefront sensor. A typical Hartmann-Shack (HS) wavefront sensor consists of matrix of microlenses (lenslet array) of the same focal length, and a CDD camera at the focal of the lenslet. When an ideal perfect spherical wavefront passes through the HS wavefront sensor, each microlens focusses at the focal on the CCD camera, forming a regular array of spots (reference spots). Then, when a distorted wavefront passes through the HS, the corresponding lenslet focuses a

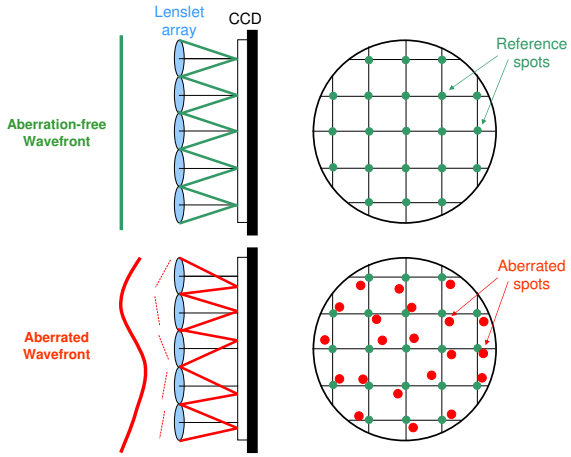

Figure 1.23: Illustration of an aberration-free wavefront and an aberrated wavefront reaching the Hartmann Shack wavefront sensor.

spot in a position laterally shifted with respect to the reference (see Figure 1.23). The local slope of the wavefront at the corresponding lenslet position is obtained from the shift of each spot with respect to the reference spot. Wave aberrations are calculated from the local slopes acquisition.

Phase modulators and wavefront correctors

Wavefront correctors alter the phase profile of the incident wavefront by either changing the refractive index of the medium through which the wavefront propagates (principle of the liquid crystal) or by changing the physical length over which the wavefront propagates. The latter are mostly based on mirror technology and produce phase changes by adjusting their surface shape. In what follows, we will describe deformable mirror based systems, as this was the one used in the thesis.

The common principle of deformable mirror is the use of multiple actuators located at the rear of the reflective surface. Depending on the voltage applied to each actuator, it pushes or pulls the surface, allowing to control the exact shape of the mirror by computer.

Several active mirror technologies coexist in this field and can be classified in two groups: the segmented correctors and the continuous surface correctors, mostly used in vision science. Segmented deformable mirrors consist of individual plane mirrors each attached to a separate actuator independently controlled (Piston-only and piston/tip/tilt segmented correctors). As opposed to segmented mirrors, in the continuous surface correctors the actuators are coupled, so that when an actuator moves, the deflection is not restricted to the area above that given actuator and extends to adjacent actuators. Continuous surface correctors include: Discrete actuator deformable mirror, bimorph mirrors and membrane mirrors. These last ones consist of a flexible reflective membrane, sandwiched between transparent top

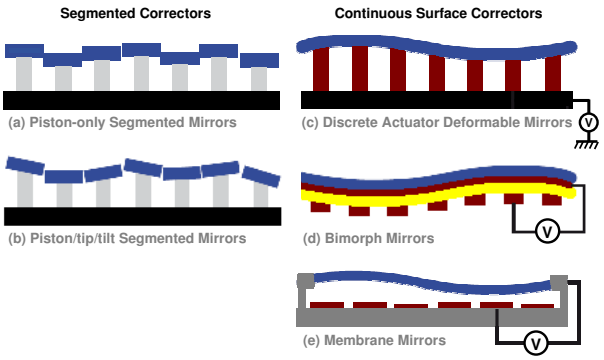

Figure 1.24: Segmented and continuous surface correctors (a) Piston-only Segmented corrector (1 degree of freedom), (b) piston/tip/tilt segmented correctors (3 degrees of freedom, (c) Mirror actuated by actuators that expand or contract, (d) Bimorph mirror and (e) Membrane mirror. Adapted from Hampson [2008].

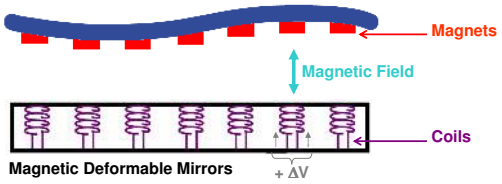

Figure 1.25: Electromagnetic deformable mirror. Adapted from Hampson [2008].

electrode and an underlying array of patterned electrodes. Applying voltage to one electrode induces an attraction that deflects the entire membrane (Figure 1.24). Because the edges of the membrane are clamped and cannot move, only a central effective diameter is useful for correction.

In this work, we used a magnetic deformable membrane mirror (by Imagine Eyes) that is used in all the studies presented in the thesis. The actuators of the magnetic deformable mirror are composed by a magnet, located behind the reflective membrane, and a coil. When applying a voltage to the coils, an electromagnetic field is created pushing or pulling the magnets and so the surface changes locally allowing the control of the mirror shape. A scheme of the electromagnetic mirror is shown in Figure 1.25.

Computer control

The control algorithm is the crucial link between the wavefront sensor and the wavefront corrector in an adaptive optic system for vision science.

Its function is to convert the wave aberrations measurement made by the wavefront sensor into a set of actuators commands that are applied to the wavefront

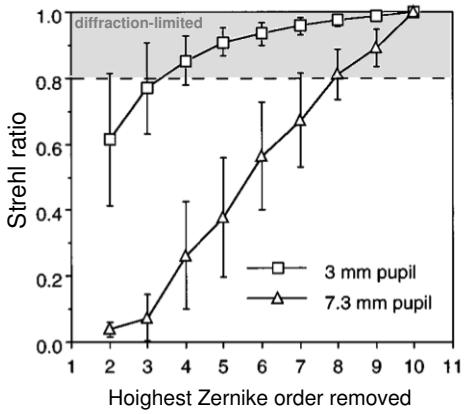

Figure 1.26: Strehl ratio of the eye's PSF for 3 mm (squares) and 7.3 mm pupil diameter (triangles). (on average of the 12 subjects tested for 3-mm and 14 subjects for 7.3-mm pupil diameter) The abscissa indicates the highest lower order removed in each case. To achieve a diffraction limited performance, correction up to the fourth order for 3 mm pupil diameter and up to eighth order for 7.3 mm pupil diameter is needed. adapted from Liang et al. [1997].

corrector to satisfy a suitable system performance criterion, such as minimizing the residual wave aberrations or presenting other wave aberrations to the eye.

When a unit voltage is applied to one actuator on the deformable mirror the surface deformation produced by this activated actuator is called the actuator's influence function. In order to calibrate the deformable mirror and to know the influence of each actuator over the entire deformable membrane, a voltage (typically ± 0.2 V) is applied to each actuator and its effect on the membrane is saved in the Influence Matrix that records all the individual actuator's influence functions. From this interaction matrix the command control matrix is calculated, which defines the corresponding voltage to apply to each actuator to correct (or induce) a given pattern of aberrations.

Image quality in the eye can be significantly improved by dilating the pupil to minimize diffraction and subsequently by correcting ocular aberrations across a large pupil using an AO system. The extent to which AO produces optical quality approaching diffraction limit thus depends on the eye's pupil diameter and the number of Zernike orders that are taken into account in the closed-loop correction. Liang et al. [1997] estimated the increase of Strehl Ratio as a function of the numbers of higher Zernike orders removed from the wave aberrations. For a 3 mm pupil diameter, correcting up to the fourth- order aberrations produced a diffraction limited Strehl Ratio whereas for a pupil of 7.3 mm, orders up to eighth-order had to be corrected to achieve diffraction limited performance (see Figure 1.26). In this thesis, we considered correction up to seventh-order corresponding to 36 Zernike coefficients.

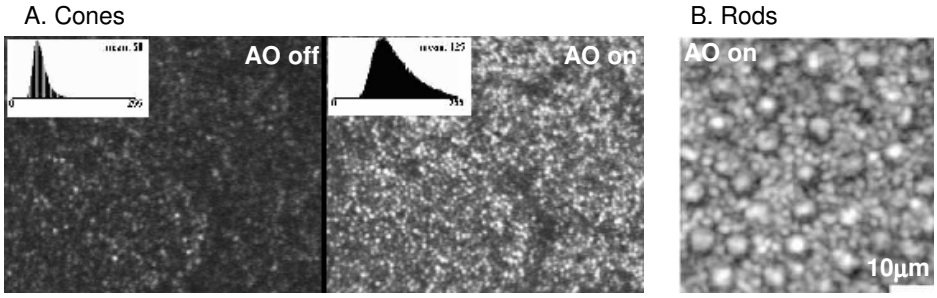

Figure 1.27: A. Images of the same area of retina with the cone photoreceptors, with and without AO correction. The insets shows histograms of gray scales in the image (from Roorda et al. [2002]). B. Human peripheral rod photoreceptor mosaic (10° temporal) imaged with a confocal Adaptive Optics scanning ophthalmoscope (using 680 nm light and 0.4 Airy disk pinhole size). The image is shown with logarithmic scales to facilitate rods visualization (adapted from Dubra et al. [2011])

1.4.2 Ophthalmic applications of Adaptive Optics

Adaptive optics has been used in the last year to image the retina with unprecedented resolution, and to perform psychophysics under manipulated optics. As the studies of this thesis fall within the psychophysical applications of adaptive optics, this section will focus on the application of Adaptive optics for visual function and neural adaptation testing, after a brief review on advances in retinal imaging with adaptive optics.

Retinal Imaging

Retinal Imaging is one of the broad lines of research where the application of adaptive optics has spread. The increase in contrast and resolution limit permits observation of retinal structure at the single cell level, which could not otherwise be possible in the living eye. Since the first work imaging cone photoreceptors by Liang et al. [1997] (see Figure 1.27), adaptive optics has been combined with different retinal imaging instruments. AO combined with a confocal scanning laser ophthalmoscope has been widely spread since its first use in 2002 by Roorda et al. [2002].

A variety of modifications have been made possible to improve these instruments: These include using two different deformable mirrors to increase aberrations correction ability of the system [Chen et al., 2007a; Hammer et al., 2006], using multiple imaging wavelengths [Grieve et al., 2006] as the chromatic aberrations of the eye cause the different wavelength to focus in different retinal planes, using eye tracking compensation of saccadic movement and a wide-field imaging system to guide the imaging and give a feedback to the operator [Burns et al., 2007], and using a simultaneous imaging and stimulus delivery by modulating the scanning laser, line-by-line to ensure that the stimulus is focused in the cone mosaic and to

determine which cones interact with the stimulus [Poonja et al., 2005].

In 2003, adaptive optics was combined with Optical Coherence Tomography (OCT) by Miller et al. [2003] to provide increase lateral resolution, lower speckle, and enhanced sensitivity from conventional flood illumination Ophthalmoscopes and Scanning Laser Ophthalmoscopes. There are 2 different categories of operation based on how the depth-resolved image is formed in an OCT system: Time Domain (TD) and Spectral Domain (SD) OCT. In the TDOCT, the reference mirror moves axially and a retinal image is acquired for each position of the reference mirror. Depth-resolved images are collected over time. Whereas, in the SDOCT, the reference mirror remains fixed and a spectrometer- diffraction grating- is used in conjunction with a linear array. Recently, swept source OCT has been developed where the wavelength of the light source is rapidly swept to obtain the necessary spectral information to compute the depth profile at each retinal location [Drexler and Fujimoto, 2008; Williams, 2011]. Figure 1.29 illustrates the first depth-resolved images obtained from a time domain OCT in 2004 [Hermann et al., 2004] with and without AO-correction, where an axial resolution of 3 microns with AO was achieved and from a spectral domain OCT in 2005 [Zhang et al., 2005], combined with an Adaptive Optics system to image inner and outer segments of individual photoreceptors. AO combined with OCT system has undergone significant advances and provided ultrahigh 3 D resolution to capture images of retinal structures previously only visible with histology, as shown in Figure 1.29C [Zawadzki et al., 2007; Miller et al., 2011].

Since its first use, retinal imaging AO system have been widely used for imaging the cone mosaic, to investigate their nature - acting like waveguides, their brightness depends upon the angle of the incident light relative to their axis [Roorda and Williams, 2002], their reflectance properties- reflectance of individual cones varied over the course of minutes [Pallikaris et al., 2003], the arrangement of the three cone classes – combined with retinal densitometry [Roorda and Williams, 1999], and more recently, AO has allowed to image the rod photoreceptors [Dubra et al., 2011] with a confocal Adaptive Optics scanning ophthalmoscope, allowing to detect diseases such as cone/rod dystrophy, age related macular degeneration, retinitis pigmentosa, color dystrophy. Moreover, Adaptive optics have allowed to image the flow of single blood cells through the vasculature of the retina and determine their velocity [Zhong et al., 2008] for detection of disease that causes changes in the retinal vasculature such as diabetic retinopathy.

Visual performance and eye quality

The question of whether inducing changes in the optics of the eye has an impact on visual performance [Applegate et al., 2003a, 2006; Levy et al., 2005; Jimenez et al., 2008; Marsack et al., 2004; Atchison et al., 2003a; Sabesan et al., 2007; Marcos, 2001] is more relevant when considering the possibility of altering high-order aberrations (with lenses or surgery) of individual subjects [Barbero and Marcos, 2007; MacRae, 2000; MacRae et al., 2000; Schwiegerling and Snyder, 2000; Yoon

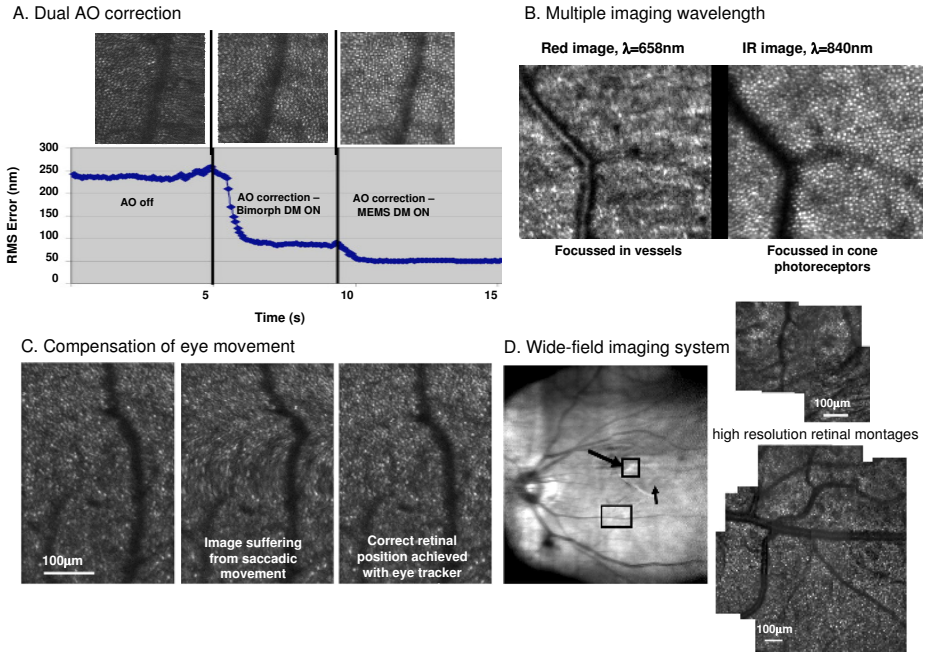

Figure 1.28: A. Use of dual deformable mirror (bimorph and MEMS) to increase the correction ability of the system. Measured wavefront aberration over a 6 mm before and after AO compensation. The retinal images are from a healthy subject taken at 3 ° nasal/3 ° superior retina, 1.1 ° scanning angle, wavelength of 843 nm; (modified from Chen et al. [2007a]). B. Use of multiple wavelength (red, 658 nm; and IR, 840 nm) for different focussing retinal planes. The red image (left) is focused in vessels while IR image (right) is focused in the cone photoreceptors (adapted from Grieve et al. [2006]). C. Eye tracker compensation of small saccadic movements. In the middle frame a saccade was initiated, the eye tracker compensated with a slight delay, and in the third frame the correct retinal position is again achieved and is well aligned to the first frame, and D. Use of a Wide field imaging system to guide the imaging and provide feedback to the operator. Left: Near IR (920 nm) view of the retina, obtained from the wide-field imaging system. The boxes show the approximate locations of high-resolution retinal montage (center and right). The short arrow shows the location of the fovea. (adapted from Burns et al. [2007]).

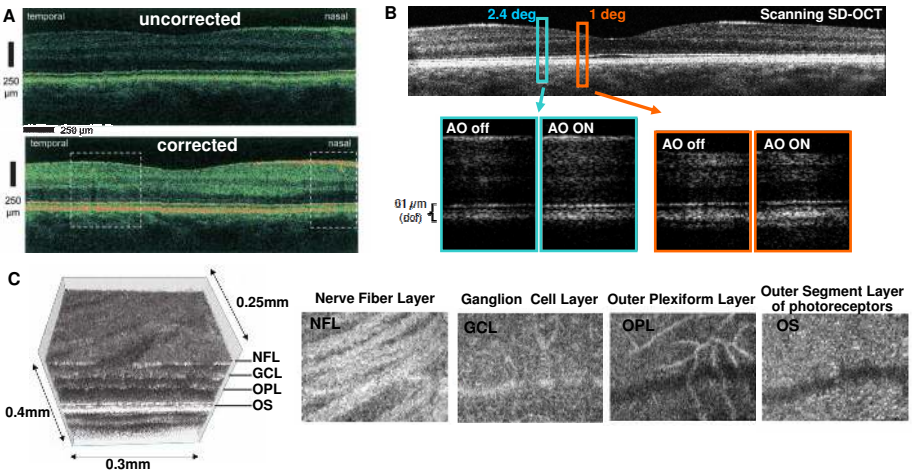

Figure 1.29: A. Ultrahigh resolution OCT (UHR) (Time Domain) with and without AO-correction (upper images) of a normal human eye in the foveal region (adapted from Hermann et al. [2004]). B. AO combined with a Spectral Domain OCT to image inner and outer segments of individual photoreceptors. Status OCT3 and SD-OCT B-scans collected in the same subjects. blue and orange rectangles depict deep subsections centered at 1° and 2.4° eccentricity with their respctive magnified view, imaged with and without AO (adapted from Zhang et al. [2005]). C. AO–OCT volume acquired over a 1° retinal region located temporal of the fovea, and face views of particular retinal layers (adapted from Zawadzki et al. [2007]).

et al., 2004].

In combination with a psychophysical channel, adaptive optics has become a useful tool to simulate visual experience, for example with new lens designs, before the lens is implanted or even manufactured [Manzanera et al., 2007; Piers et al., 2007]. Several studies investigate to which extent visual performance increases at correcting higher order aberrations.

Applegate [2000] asked "Will "ideal" corrections lead to better vision? If so, how much better?" He explored the limits imposed by the optical and neural properties of the eye and reported that optical theory, when combined with knowledge of the anatomy and physiology of the eye's neural system, enables us to define the limits to improvement of vision and to predict the visual consequences of optical interventions and/or non-intervention and reported that correcting the higher order aberrations will provide images with higher contrast and crisper edges. The impact of optical aberrations on visual performance or, alternatively, the benefits of correcting ocular aberrations on vision are important questions in visual optics to investigate whether such corrections will have a positive impact on daily life activities.

In this section, we will present a brief review of studies that investigated visual performance under AO manipulated optics.

Few studies have addressed the changes in visual performance with correction of high-order aberrations with different luminance conditions. Yoon and Williams [2002] found a significant improvement in logMAR Visual Acuity, by a factor of 1.2 for high luminance ($\sim 20\,\mathrm{cd/m^2}$) and by a factor of 1.4 for dim luminance when correcting monochromatic aberrations, and by a factor of 1.6 for dim luminance ($\sim 2\,\mathrm{cd/m^2}$) (using an interference filter) when correcting both monochromatic and chromatic aberrations in a group of 7 subjects. The benefits of correcting aberrations (with adaptive optics) on visual performance as a function of light level was addressed by Dalimier et al. [2008]. However, they measured contrast thresholds using a relatively large target (15 arcmin Landolt C) but not for targets in the spatial resolution limit. For their experimental conditions they found that for lower luminances, the drop in neural sensitivity limits the impact that increased optical degradation has on vision. In their study, visual benefits ranged between 1 and 1.7, across three subjects and 0.35 to 40 $\mathrm{cd/m^2}$ luminances.

The differences in the benefit of correcting high order aberrations on visual acuity in myopes and emmetropes has been studied by Rossi et al. [2007]. In their study, they used targets directly projected on the retina using an Adaptive Optics Scanning Laser Ophthalmoscope on a group of emmetropes (n=9) and low myopes (n=10). They found a lower benefit in the myopic group, despite the fact that both groups were left with negligible residual aberrations. Legras and Rouger [2008a] measured the visual benefit, in terms of contrast sensitivity and visual acuity, of correcting only defocus and astigmatism and when correcting high order aberrations (with AO, up to 5^{th} order) in myopes and emmetropes and examined the accuracy of wave aberrations based metrics to predict the impact of monochromatic aberrations on visual performance. They found an increase in both

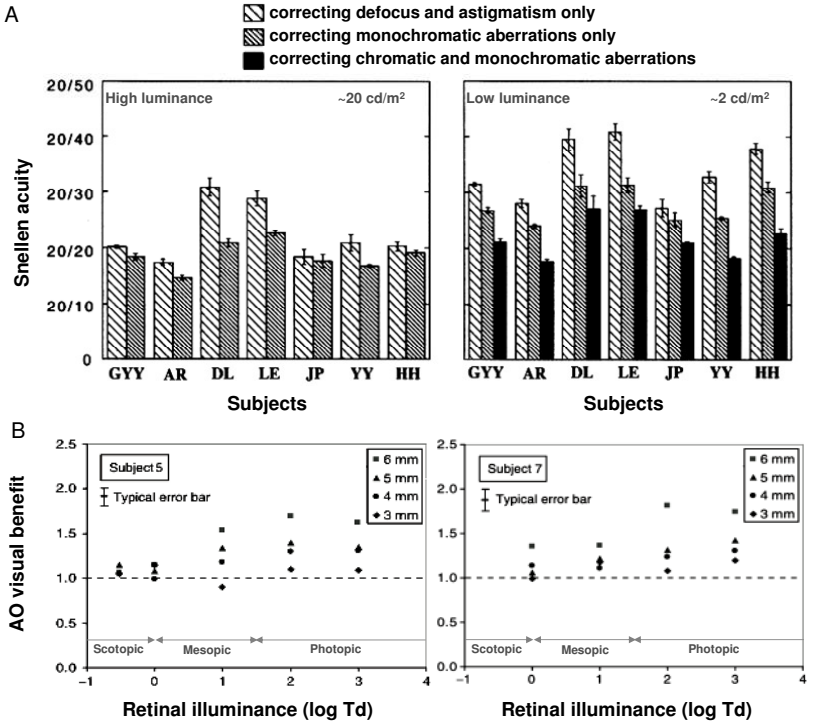

Figure 1.30: A. Visual acuity measurements at two retinal illuminance levels (575 Td corresponding to 20 cd/m^2 and 57 Td corresponding to 2 cd/m^2) when various aberrations were corrected. Dilated (cyclopegia) pupil size=6 mm diameter. (adapted from Yoon and Williams [2002]) B. Adaptive optics benefit measured as a function of retinal illuminance and pupil size (3-, 4-, 5- and 6-mm pupil diameter) for 2 subjects (Adapted from Dalimier et al. [2008]).

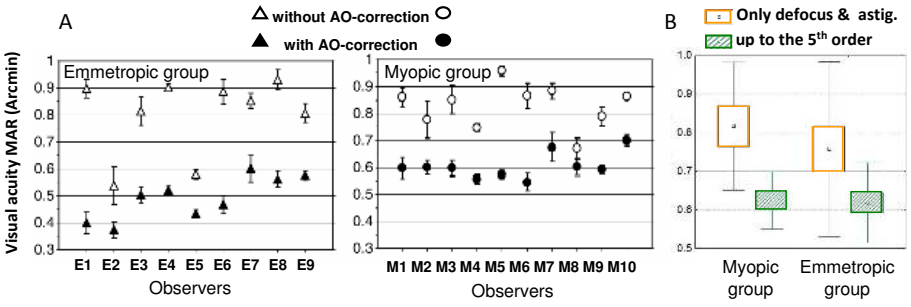

Figure 1.31: A. Visual acuity (raw MAR) for the emmetropic and myopic group with (filled) and without (open) Adaptive optics correction. (Adapted from Rossi et al. [2007]). B. Averaged measured visual acuity (MAR, arcmin) for the myopic group and the emmetropic group when correcting only defocus and astigmatism versus correcting aberrations up to the 5^{th} order. The box and the error bars represent respectively the standard error and the standard deviation of the mean (adapted from Legras and Rouger [2008a]).

visual acuity and contrast sensitivity when correcting higher order aberrations.

Elliott et al. [2009] used a closed-loop Adaptive Optics to test the contributions of optical and neural factors to age-related losses in spatial vision. They estimated the visual benefit of correcting monochromatic high-order aberrations (HOA) on contrast sensitivity in a group of young and older observers (18 to 81 years old). With AO compensation, there is a clear improvement in contrast sensitivity for both age groups. Below 4.5 c/deg, both groups show the same benefit at correcting HOA. Young observers showed a large benefit of correcting monochromatic high order aberrations at high spatial frequencies (with a 2.5-fold increase at 18 c/deg.), whereas older observers exhibited the greatest benefit at middle spatial frequencies (4.5 and 9 c/deg). Contrast sensitivity was still reduced for the older age group when compared to the younger age group without AO correction, suggesting neural contribution to the age related loss in spatial vision.

de Gracia et al. [2011b] explored the limits of the visual improvement due to the optical improvements in retinal image quality by measuring the contrast sensitivity function (CSF) in monochromatic and polychromatic conditions under natural aberrations and after AO correction for a wide range of angles and frequencies. They found that CSF increased on average by 1.35 times (only for the mid and high spatial frequencies) and was lower (0.93 times) for polychromatic light. The consistently higher benefit in the MTF in the CSF than in the CSF (factor of 5) of correcting aberrations suggests a significant role for the neural transfer function in the limit of contrast perception.

Instead of focusing on correcting all aberrations with adaptive optics, Applegate et al. [2003b] studied the interaction of aberrations that could increase visual performance specifically of combinations of defocus and spherical aberrations as well as astigmatism and secondary astigmatism. They found that although these combinations decrease Visual Acuity compared to unaberrated conditions, some particular combinations produced significantly better performance than one of the aberration alone (as shown in Figure 1.32). These results can be of significant importance when considering that aberrations are being induced or not entirely eliminated by wavefront-guided corrections.

de Gracia et al. [2010] found that the combination of coma with astigmatism improved decimal Visual Acuity by a factor of 1.28 (28 %) and 1.47 (47 %) in two subjects, over VA with astigmatism alone when all the rest of aberrations were corrected. Although, in the presence of typical normal levels of HOA the effect of the coma/astigmatism interaction is considerably diminished. Legras and Rouger [2008b] showed the subjective effect of blur with side-by-side comparison of images blurred with high order aberrations or partially corrected spherical aberrations (SA), coma and trefoil and reported that the subjective quality of vision of a subject with typical aberrations could be improved by either a partial (50%) or a full correction of both SA and coma, this gain being comparable to 1/8 D of defocus blur. Atchison and colleagues [Atchison et al., 2009a,b; Atchison and Guo, 2010] investigated, in a series of studies, the aberration magnitudes when blur becomes noticeable, troublesome or objectionable. They tested blur produced by defocus,

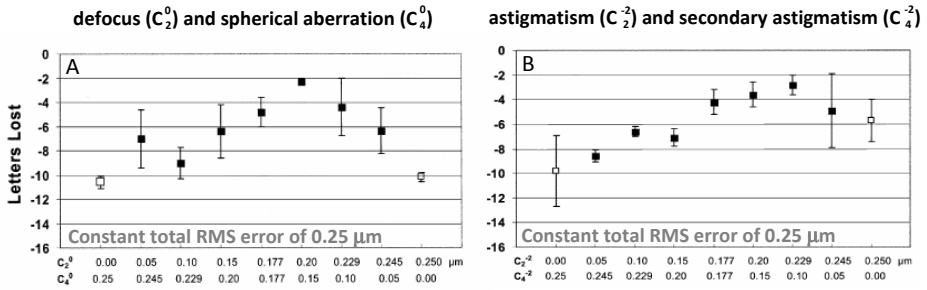

Figure 1.32: Average letters lost across subjects as a function of various combinations that results in a constant RMS error of 0.25 µm for A. Combination of defocus and spherical aberrations and B. Combinations of astigmatism and secondary astigmatism. (adapted from Applegate et al. [2003b]).

crossed-cylinder astigmatism, and higher order aberrations suches trefoil, coma and spherical aberrations induced by means of an adaptive optics deformable mirror. They found that overall mean blur limits for defocus (5 mm pupils) ranged from 0.185±0.08 D (just noticeable) to 1.01±20.27 D (objectionable). They reported that subjective tolerance to blur produced by an oriented aberration (astigmatism) was greater (30 to 50 %) than the tolerance to defocus, although the amounts varied with the experimental conditions, with the overall influence of cylinder axis being 20 %, and blur limits increased more quickly for the higher order aberrations as the criterion changed from just noticeable to just troublesome and then to just objectionable.

Adaptive optics can be used to investigate the role of ocular aberrations on the accommodative response [Gambra et al., 2009] as well as to quantify the extent to what reduced depth of focus that arises with corrected aberrations may compromise vision out of focus in subjects without accommodation capabilities. Guo et al. [2008] found that full correction of HOA may worsen spatial visual performance in the presence of some defocus.

Neural adaptation and visual perception

The possibility of undertaking psychophysical experiments without the retinal blur produced by optical aberrations allows exploring neural adaptation.

Artal et al. [2004a] showed that the stimuli seen through an individual's natural aberrations always appear sharper than when seen through a rotated version of the same aberrations. In their experiment, besides removing the higher order aberrations, the deformable mirror also generated the natural subject's blur as well as a wave aberration that in combination with the subject's aberrations produced rotated PSFs. In their experiment (on 5 subjects) the observer was asked to adjust the magnitude (the root mean square, RMS) of the aberrations by multiplying it by a factor (F) in the rotated case to match the subjective blur of the stimulus to that seen when the wave aberration was in the normal orientation. A factor below

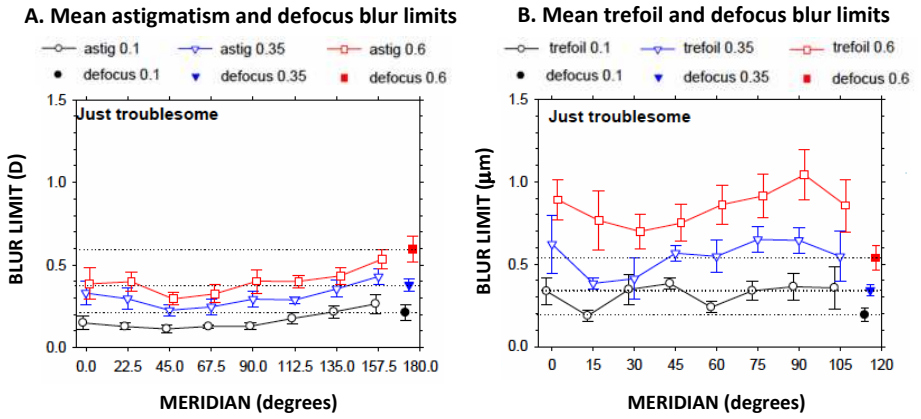

Figure 1.33: Limits for troublesome blur (level of blur for which subjects first start to be troubled by the lack of clarity of the target, but still are able to read the letters.) A. Mean astigmatism and defocus blur limits as a function of astigmatism axis (in diopters). B Mean trefoil and defocus blur limits as a function of trefoil axis (in microns). Data are for one subject (DAA), pupil size of 5 mm; Intrinsic ocular higher-order aberrations corrected with Adaptive optics. In each case results are shown for letter sizes 0.1, 0.35 and 0.6 logMAR. Error bars represent standard deviations of 5 measurements. Adapted from Atchison et al. [2009b,a]; Atchison and Guo [2010].

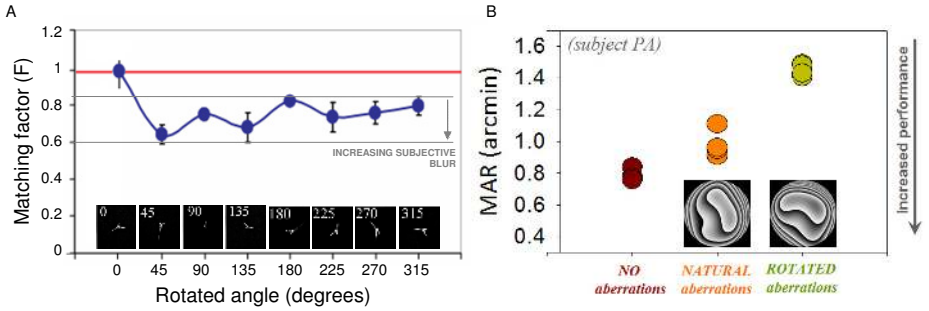

Figure 1.34: A. Blur matching as a function of PSF orientation. The matching factor F is the amount for which the magnitude of natural subject's aberrations had to be changed to generate the same perceived blur as the natural blur produced by the native PSF orientation (Adapted from Artal et al. [2004a]). B. Visual Acuity (Mar arcmin) measured under AO-corrected aberrations, natural aberrations and 45 ° rotated version of subject aberrations (Adapted from [Artal, 2007]).

1 suggested that images blurred with the rotated version of subject's aberrations appeared more blurred than the natural image. They suggested that these results may be a consequence of neural adaptation to the specific degradation produced by someone's HOA. In a subsequent study [Artal et al., 2004b] they found that observers showed higher visual acuities with stimuli viewed through their native ocular higher-order aberrations (average of 1.0 logMAR) to a 45 º rotated versions of their aberrations (average of 1.55 logMAR) which increased to an average of 1.16 logMAR after 15 minutes of continuous viewing through the 45 º rotated aberrations. Chen et al. (2007) also found that subjective image quality was best when the observer's HOA was not fully corrected, though the implied adaptation was only a small fraction (12 %) of the effect predicted by complete adaptation.

Several studies show evidence that eyes are adapted to HOA induced by corneal pathology where long-term experience and adaptation may play a role in adjusting to more extreme higher-order aberrations in keratoconic eyes. Sabesan and Yoon [2010] measured high (100 %) and low (20 %) contrast Visual Acuity (VA) (tumbling letter E) in four moderate keratoconic (KC) eyes in which the subjects were wearing their own prescribed soft toric contact lenses over a 6-mm pupil. In addition, visual acuity was measured in three emmetropic normal eyes where an adaptive optics system was used to correct the natural ocular aberrations and to induce the aberration of the KC eye simultaneously during vision testing. The magnitude of neural compensation was defined by the improvement in VA in each KC eye compared with the normal eyes with KC aberrations. KC eyes showed significantly better high and low contrast VA than normal eyes with KC aberrations, with an average 1.2-line improvement in both high- and low-contrast VA in the KC eyes compared with the normal eyes. In KC eyes, the neural visual system appears to compensate for long-term visual experience with an asymmetrically blurred retinal image, resulting in improved visual performance.

Several studies demonstrated adaptation to astigmatic blur, both in terms of visual performance and in terms of visual perception. de Gracia et al. [2011a] concluded that habitually non-corrected astigmats appeared adapted to astigmatism, as the measured visual acuity was less impaired by the induction of astigmatism than in non-astigmatic subjects with the same amount of induced astigmatism. In that study, astigmatism was induced at a fixed 45 º, regardless of the axis of the subject's natural astigmatism. In a recent study, Vinas et al. [2013] tested the impact on VA of astigmatism induction, at different axis of astigmatism (including the natural axis of astigmatism) in corrected and un-corrected astigmatic subjects and found that both habitually-corrected and initially non-corrected astigmats after correction of astigmatism showed a bias towards better performance with astigmatism induced at their natural axis. Furthermore, they studied the influence of astigmatism (and its correction) on perceptual judgment of oriented blur and reported that habitually non-corrected astigmats showed significant shifts of the perceived neutral point away from isotropy prior to correction, which shifted towards isotropy immediately after correction of astigmatism [Vinas et al., 2012].

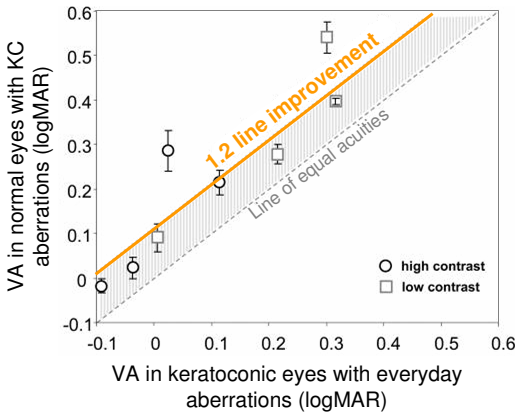

Figure 1.35: Comparison of visual performance between KC eyes and normal eyes with KC aberrations. Each data point represents the average of three normal eyes for each KC eye. Dashed line: equal acuity line; shaded region: average 1.2-line improvement in VA in KC eyes. Adapted from Sabesan and Yoon [2010].

1.5 Open questions

Understanding the role of aberrations on visual performance will not only increase knowledge on the spatial limits of vision, but will also have an impact on the development of corneal laser ablation algorithms, intraocular lenses, contact lenses, aiming at customized corrections or at increasing depth of focus by manipulating aberrations. Adaptive optics has been used in the last years to image the retina with unprecedented resolution, and to perform psychophysics under manipulated optics. Moreover, the possibility of undertaking psychophysical experiments without the retinal blur produced by optical aberrations allows exploring neural adaptation.

The studies of this thesis fall within the psychophysical applications of adaptive optics and address the following questions:

1. Does correction of high order aberrations produce a relevant improvement in vision? In particular, does correction of high order aberrations produce a relevant improvement in in visual acuity and does the benefit vary with luminance and contrast polarities? Do subjects have the impression that natural images look sharper with AO correction? Are familiar face recognition and facial expression recognition tasks improved by correction of high order aberrations?

2. Does the perception of natural images changes after short-term adaptation to blur? In particular, is short-term adaptation selective to orientation? Can subjects adapt to the degradation induced by High Order Aberrations? Are adaptation aftereffects different while adapting to someone else's aberrations?

3. How sensitive is the adaptation to specific pattern of blur resulting from the observer's HOA? In particular, to what extent are subjects naturally adapted to their own aberrations? To what extent judgments of perceived blur depend on the magnitude versus the specific orientation of individual's HOA?

1.6 Goals of this thesis

The main purpose of the thesis is the understanding of the relationships between the optical quality of the retinal image degraded by the natural aberrations of the eye and the visual quality, as well as the understanding of the role of neural adaptation to the ocular aberrations in visual perception.

The specific goals are:

- To develop an adaptive optics system – to measure, correct/induce aberrations - combined with psychophysical paradigms to study visual performance and visual perception. To calibrate and validate the system and to design new psychophysical paradigms.

- To explore the effects of the aberrations on visual performance, in particular visual acuity in a range of luminances and contrast polarities, subjective impression of sharpness and face recognition tasks.

- To understand short and long-term adaptation to blur produced by ocular aberrations: the extent to which subjects are adapted to their own aberrations (amount and orientation) and the capability to adapt to new patterns of astigmatism and high order aberrations.

1.7 Hypothesis

The hypotheses of this thesis are:

- Visual performance increases with the correction of high order aberrations.
- Correcting aberrations has a positive impact on the subjective impression of sharpness of natural images.
- Correcting aberrations also improves performance of daily visual tasks such as face recognition.
- Adaptation to astigmatic images changes the perception of oriented blur.
- Short-term adaptation to images with scaled aberrations (more or less blurred) or other subject's aberrations induces a shift in the perceived best-focus.

- The natural state of adaptation is related to the individual aberrations, both in magnitude and orientation.

1.8 Structure of this thesis

The body of this thesis is structured as follows:

The current introductory chapter (**chapter 1**) presents the background and motivation of the thesis.

Chapter 2 presents a description of the common methods used throughout this thesis and common to the different studies. In particular, it includes a description of the Adaptive Optics system to measure and correct subject's aberrations, including its calibrations, validation and developped control software.

In **chapter 3**, we investigate whether high contrast visual acuity improves with the correction of high order aberrations and whether it varies with luminance and high contrast target. We performed visual acuity tasks (snellen E) in seven conditions of luminance (varying from 0.8 to 50 cd/m^2) and with different contrast polarities (white letter on black background and black letter on white background), with and without full Adaptive Optics correction.

In **chapter 4** we address whether subjects have the impression that natural images look sharper with AO correction and whether familiar face and facial expression recognition improve by correcting HOA. For this purpose, psychophysical experiments were performed involving 34 natural images, viewed under natural or full AO correction, presented sequentially, 33 familiar and unfamiliar faces as well as 52 happy and angry faces presented to the subjects randomly with and without AO-correction.

In **chapter 5**, we investigate short-term adaptation to astigmatic blur (produced by a combination of defocus and astigmatism, under constant blur strength) and its aftereffects. In particular, we investigate whether adaptation effects could arise from actual sphero-cylindrical refractive errors and whether they can be selective for different axis of astigmatism. Shifts of the perceived isotropic point were measured before and after adapting to images blurred by different amounts of astigmatism and defocus, from strongly vertically oriented blur to strongly horizontally oriented blur.

In **chapter 6** we explore short-term adaptation to blur produced by individual's high order aberrations and scaled versions of them to fully understand how the visual system adapts to changes that can happen within the observer. Subject's natural aberrations were measured and natural images blurred by convolution with scaled version of subject's PSF (factor varying from 0 (diffraction limited)

to 2 (double amount of subject's aberrations)) were generated. Shifts in the best perceived focus point were measured after adapting to different levels of blur.

In **chapter 7**, we examinate long term adaptation to the blur produced by the eye's optic. In particular, we study whether subjects are naturally adapted to the level of blur produced by their high order aberrations. The natural best perceived focus point, from a series of images blurred with natural aberrations from real subjects, was measured and compared to the natural level of blur produced by subject's high order aberrations.

In **chapter 8**, we explore the dependence of the perceived best-focus on the blur level and the blur orientation of the natural adaptation to the individual's HOA. For this purpose, we isolated the effect of blur level (with stimulus blurred by different amounts of defocus only) and orientation (with stimulus blurred with the same blur magnitude, but different real orientation).

In **chapter 9**, we used a "Classification Image" based method to extract the orientation features of the Point Spread Function internally coded as producing the best perceived image quality.

Finally the major findings of this work, and their implications, are summarized in the **Conclusions**.

2 Methods

In the current chapter, the experimental techniques used in this thesis are described, specifically the development of the Adaptive Optics (AO) system, its calibration and validation for measurement, correction and induction of aberrations in human eye. The system was built to perform psychophysical experiment aiming at investigating the impact of aberrations on vision, and neural adaptation to aberrations.

In this chapter we describe the implementation of the optical system, control routines, software development, calibration and validation of the system. We also describe general protocols shared by all the studies of the thesis. Particular implementations and developments for each specific study will be presented in the corresponding chapter.

The author of this thesis designed and implemented the AO system, calibrated and validated the system, in collaboration with Enrique Gambra, Carlos Dorronsoro, Daniel Pascual and Susana Marcos. She also participated in the development of the routines to control the AO system, as well as of the psychophysical routines for visual acuity measurements, perception of natural images, face recognition and perception of best focus.

A description of the experimental system was first presented at the "II Reunión Red Temática Española de Óptica Visual" (march 2007), in Murcia, Spain and at the 6^{th} Workshop, Adaptive Optics for industry and medicine (june 2007) in Galways, Ireland.

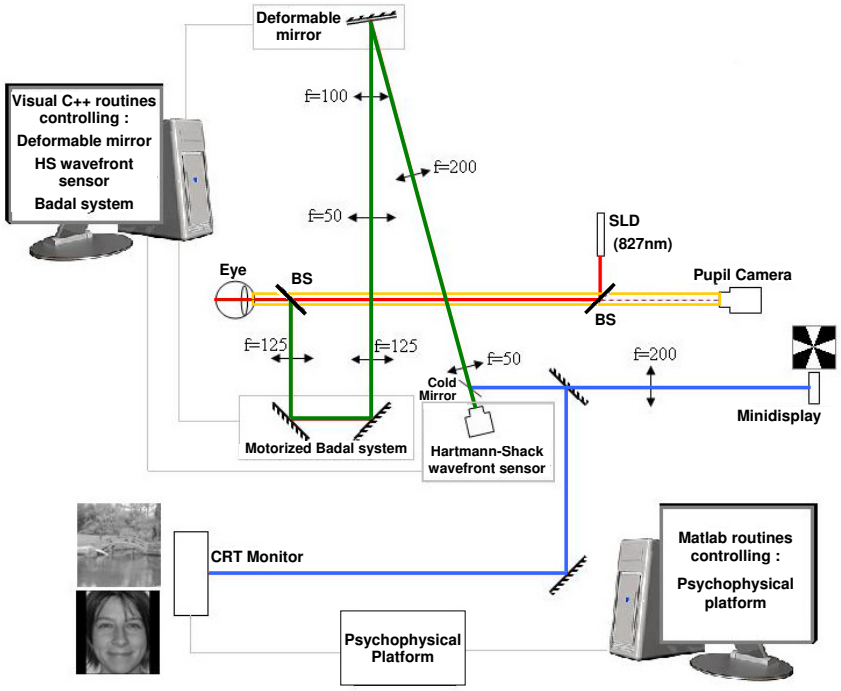

Figure 2.1: Schematic diagram of the system with its five channels: illumination channel with a 827 nm SLD source (red); AO-control channel with the Hartmann-Shack wavefront sensor and the deformable mirror (green); Psychophysical channels, one provided with a minidisplay, the other with a CRT monitor (blue); Pupil monitoring channel (yellow).

2.1 Custom development of an Adaptive Optic system for visual psychophysics

2.1.1 General description of the Adaptive Optic system

We developed an Adaptive Optics system to study the visual performance of the eyes in the presence /absence of aberrations. The system (depicted in a schematic diagram in Figure 2.1) comprises five different channels: the Illumination channel (red line in the figure); the AO- control channel (green line) mainly composed of the Hartmann-Shack wavefront sensor and the deformable mirror, the two psychophysical channels (blue lines) - one provided with a minidisplay, the other with a CRT monitor - and the pupil monitoring channel (yellow line). The system is mounted on an optic table (except for the CRT monitor) and the physical dimensions of the optical set-up are 60x90 cm.

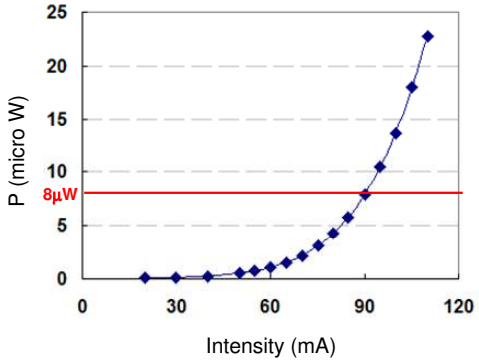

Figure 2.2: Measurement of the SLD power in the subject's pupil plane as a function of the SLD intensity

The illumination channel

The illumination comes from a Super Luminescent Diode (SLD) coupled to an optical fiber (Superlum, Ireland) emitting at 827 nm. The beam is collimated, and enters the eye with a diameter of around 1 mm. The beam is slightly (1 mm) off-centered with respect to the pupil center to avoid a corneal reflection in the Hartmann-Shack images. An SLD module driving current and temperature set, allowed light intensity adjustment. Figure 2.2 shows the curve of SLD power at the pupil plane (entering the eye) as a function of light intensity. According to the maximum permissible exposure (ANSI, Z136.1-2007; Delori et al. [2007]) we set an irradiance of 8 µW on the cornea, for which we set the current limit to 90 mA when measuring human eyes.

The Adaptive Optics control channel

The primary components of the AO-control channel are the Hartmann Shack wavefront sensor and the electromagnetic deformable mirror. Their effective diameters are 3.65 mm (Hartmann-Shack) and 15 mm (deformable mirror). In order to measure a 7 mm subject's pupil diameter we set the focal lenghts of the lenses in the opitcal relay system so that a x2 magnification was achieved from subject's pupil to MIRAO and a x0.5 magnification from subject's pupil to HASO plane. The deformable mirror is conjugated to the pupil by a pair of relay lenses of focal lengths of 50 mm and 100 mm and the microlens matrix of the Hartmann-Shack wavefront sensor is conjugated to the pupil with another pairs of relay lenses of focal lengths of 200 mm and 50 mm. The light comes directly from the SLD (without further beam focusing) and enters the eye. The reflected light off the retina passes through a Badal system, the deformable mirror and is focused on the CCD camera of the Hartmann-Shack wavefront sensor.

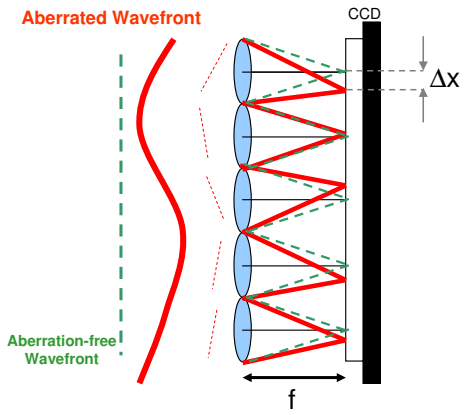

Figure 2.3: Illustration of the Hartmann-Shack wavefront sensor centroid calculus

The Hartmann-Shack wavefront sensor The Hartmann-Shack wavefront sensor used in this thesis is composed by a matrix of 32x32 microlenses of the same focal and a CDD camera at the focal of the lenslet. (HASO 32 OEM, Imagine Eyes, France). The microlens matrix is conjugated to the pupil with a x0.5 magnification factor from the pupil to the microlens array. The effective diameter of the sensor is 3.65 mm. The size of microlenses is 160 microns (i.e. the microlenses work in a configuration limited by diffraction). In order to keep the sensor's optimal performance, the size of the angle from the source must be less than λ/d=0.3 degrees (with λ=827 nm). When an aberration-free wavefront (of flat wavefront) passes through the HS wavefront sensor, each microlens focuses a portion of the incident wavefront at its focal on the CCD camera, forming an array of spots equidistant from each other. Such array serves to set the origin of coordinates for each subapertures on the focus plane (reference spots). If the incident wavefront is not flat the local tilt at each subapertutre will determine the position of each spot centroid at the focus plane. The array of spots is casted on the detector and finally computer software calculates the centroid of each spot and its position with respect to the calibration array spots (from the reference). Geometric rays are perpendicular to the wavefront. Therefore, if the wavefront is locally approximated by a tilted plane, the displacement of each aberrated spot with respect to the reference spot is proportional to the local slope of the wavefront. Figure 2.3 illustrates the displacement calculus. The wavefront error can be reconstructed from the first derivatives of the wave aberration by equations 2.1.

$$\begin{aligned} \left.\frac{\partial W(x,y)}{\partial x}\right|_{x=xi,y=yi} &= \frac{\Delta xi}{f} \\ \left.\frac{\partial W(x,y)}{\partial y}\right|_{x=xi,y=yi} &= \frac{\Delta yi}{f} \end{aligned} \tag{2.1}$$

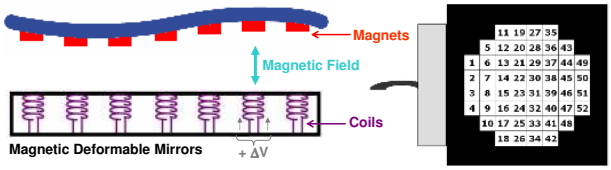

Figure 2.4: Magnetic deformable mirror (Adapted from Hampson [2008]) and the schematic representation of the MIRAO52 (imagine eyes, France)

where i is the lenslet considered, f the focal length of the lenslet, Δxi and Δyi the displacements of the aberrated spots measured behind the considered lenslet on the CCD camera, $\frac{\partial W(x,y)}{\partial x}\Big|_{x=xi,y=yi}$ and $\frac{\partial W(x,y)}{\partial y}\Big|_{x=xi,y=yi}$ the averaged partial derivatives of the wavefront aberration over the lenslet area.

The Magnetic deformable mirror The magnetic deformable mirror (MIRAO52, Imagine Eyes, France) is an optical component that includes a high quality reflecting membrane (>98 % for 830 nm wavelength) and 52 miniature actuators assembled in a rigid aluminium housing. The actuators of the magnetic deformable mirror are composed by a magnet, located behind the reflective membrane, and a coil. When applying a voltage to the coils, an electromagnetic field is created pushing or pulling the magnets so that the surface changes locally allowing the control of the mirror shape. A scheme of the deformable mirror is shown in Figure 2.4.

The stroke (maximum generated wavefront amplitude) of the mirror is 50 microns. Interactuators distance is 2 mm and the mirror effective diameter is 15 mm. In the optical system, the deformable mirror is conjugated to the pupil with a x2 magnification factor from the pupil to the mirror. The angle of the incident and reflected beam is 15 degrees. The stability of the system was checked with an artificial eye and fluctuations of the total RMS was less than 0.3 % over a three-hour measurement. The performance of this mirror had been extensively evaluated by Fernandez et al. [2006].

The Badal system

The Badal system compensates for spherical error of the subjects. It is mounted on a motorized stage and is composed of two mirrors and 2 lenses (focal length=125 mm). The zero position was achieved when the distance between the lenses is equal to the sum of their focal lengths (an afocal configuration is obtained and therefore no correction is induced). When the distance is longer that the sum of their focal lenses, rays converge towards the eye to compensate hyperopic refractive error, when the distance is shorter, rays diverge towards the eye to compensate for myopic refractive error. A displacement of 7.8 mm is equivalent to 1 D. The resolution of the Badal system was 0.125 D. The calibration of the Badal system was achieved by

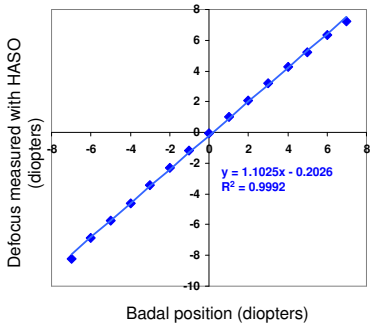

Figure 2.5: Calibration of the Badal system. Defocus measured by the HS, as a function of the estimated dioptric changes produced by the Badal displacement from -7 D to 7 D in a 1 D step.

measuring defocus with the HS system for different positions in the Badal system (Figure 2.5), using an artificial eye consisting of a 35 mm focal length achromat doublet and a rotating diffuser as an artificial retina. The deformable mirror was set as to produce a flat wavefront.

The psychophysical channels

A cold mirror behind the wavefront sensor allows inserting visual stimulus channel in the deformable mirror path, so that the subject can perform psychophysical tasks under controlled optical aberrations. The flip mount mirror allows selecting between two different psychophysical channels, one with a minidisplay and the other with a CRT monitor controlled by a programmable computer graphics system for psychophysical visual stimulus generation (ViSaGe, Cambridge research system). The psychophysical channels were implemented to display visual stimuli during measurement and experiments.

The minidisplay channel The first psychophysical channel is composed of a 12 x 9 mm SVGA OLED minidisplay (LiteEye 400) placed at the at the focal length of a 200 mm achromatic lens, i.e. at optical infinity to the observer, and subtended 2.58 degrees on the retina. The minidisplay was also used for fixation during measurement and correction of the subject's aberration, typically displaying a white and black Maltese cross. The high contrast E letters used in the visual acuity measurements through luminance and contrast polarity (chapter 3) were also presented in the minidisplay. The minidisplay has 800 x 600 pixels SVGA resolution (pixel size 15 µm × 15 µm), i.e. a total subtend of 2.58 deg (0.0043 deg/pixel), then a 20/20 VA letter spanning 38.8 pixels considering the 0.5 magnification introduced in the system from the pupil. The minidisplay has a nominal luminance of 100 cd/m^2, with a black level < 0.5 cd/m^2 (as calibrated using a ColorCal luminance-meter/colorimeter, Cambridge Research Systems). The effective luminance of the minidisplay at the pupil plane was 50 cd/m^2. This value was estimated

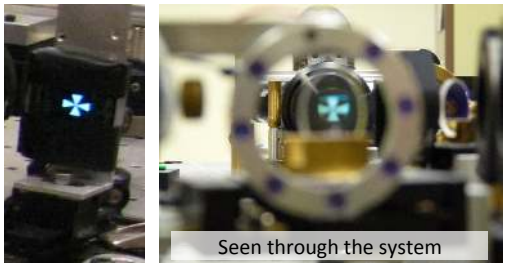

Figure 2.6: Photographies of the Maltese cross projected on the minidisplay and seen through the AO system.

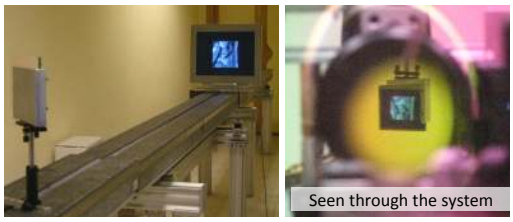

Figure 2.7: Photographies of a natural image (Lena) projected on the CRT monitor and seen through the AO system.

taking into account the light losses in the system.

The CRT monitor channel The second psychophysical channel was specifically developed to allow the presentation of gray-scale images on a 12 x 16 inches CRT Monitor. This channel was introduced in the system by means of a flip-mount mirror before the 200 mm achromatic lens. Its active area is 406 x 304 mm. The resolution used in this thesis was 1064 x 768 pixels at 100 Hz. A 400-pixel image projected on the CRT monitor measured 150 mm. The distance of the monitor to the lens ranged from 2.60 meters to 3.65 meters, i.e. producing an angular subtend ranging from 1.98 ^{o} to 1.4 ^{o} for a 480 pixels image, depending on the experiment. The monitor was calibrated to provide linear luminance levels and has an effective luminance of 100 cd/m^2, with a black level < 0.5 cd/m^2 (as calibrated using a ColorCal luminance-meter/colorimeter, Cambridge Research Systems). The calibration of the gamma correction was performed using the ViSaGe platform and the ColorCAL colorimeter of Cambridge Research System (64 tones, linear, 64 readings, was validated following a procedure similar to that implemented in Psychtoolbox's VisualGammaDemo; [Brainard, 1997; Pelli, 1997]) and then applied to the monitor.

Pupil monitoring channel and motorized Badal system software

A pupil monitoring channel consisting of a CCD camera (TELI, Toshiba) conjugated to the pupil, is inserted in the system by means of a plate beam-splitter, and is collinear with the optical axis of the imaging channel. The camera allowed

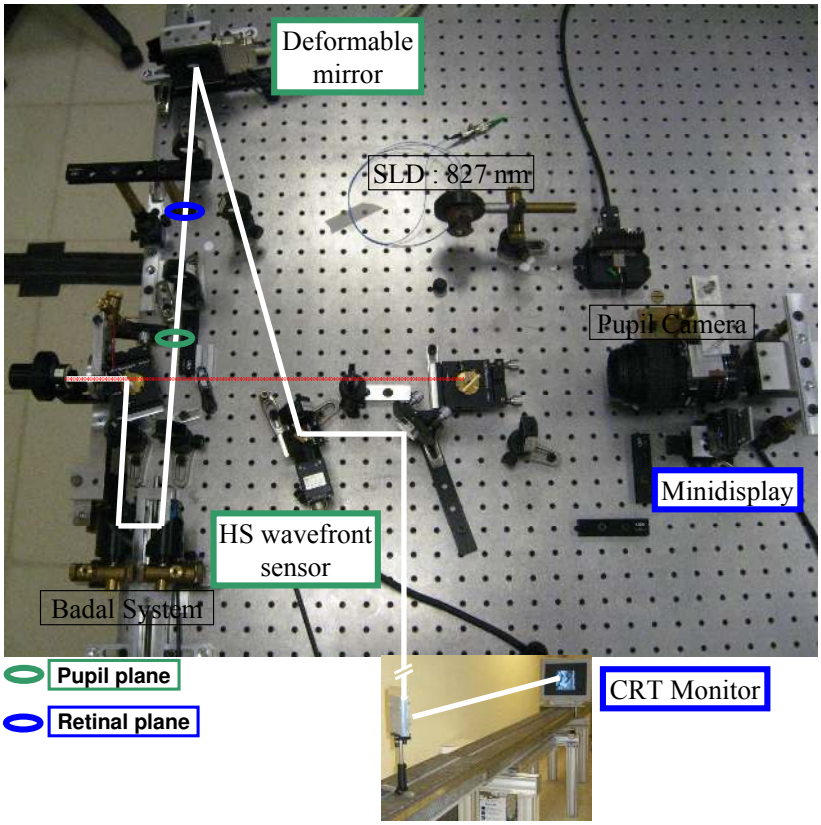

Figure 2.8: Photography of the system and location of the pupil planes (green) and retinal planes (blue) used for the proper alignment.

continuous viewing of the pupil and was used to perform proper centration of the eye aligned to the system (using a x-y-z stage) using the line of sight as a reference. A ring of infrared diodes (λ=900 nm) placed facing the eye provided illumination for pupil monitoring.

Pupils and retinal planes

Alignment was performed to ensure proper centration and accurate location of pupil (green elements in Figure 2.8) and retinal (blue elements in the figure) conjugated planes.

In the first pupil plane (green circle in Figure 2.8), a pinhole was placed that acted as an artificial pupil. The magnification from subject's pupil to the artificial pupil was $x1$ so that we ensured a constant pupil diameter during the measurement and psychophysical experiments regardless the position of the Badal system. As previously indicated, the Hartmann-Shack sensor and the deformable mirror have to be placed in pupil-conjugated planes. An iris was also placed in a retinal plane in front of the mirror (blue cirlce in Figure 2.8) in order to remove the undesired

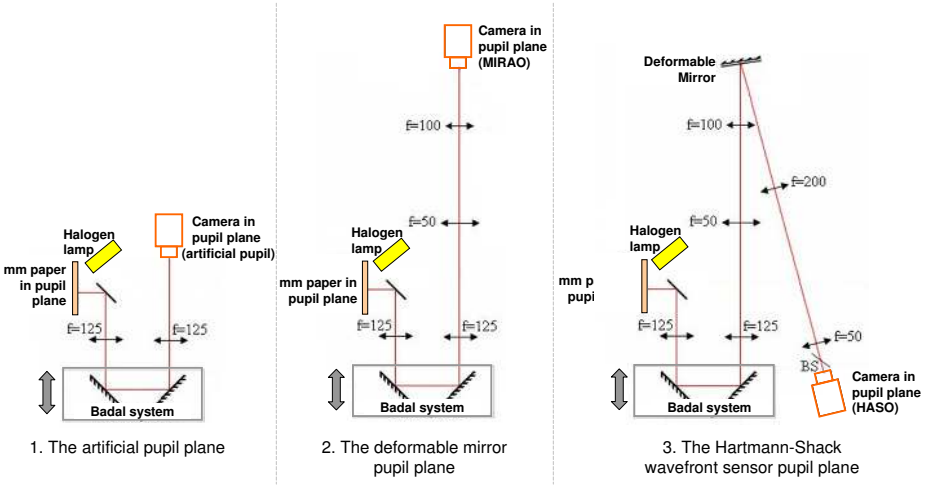

Figure 2.9: Illustration of the schematic configuration of the camera in each pupil plane used to check the constant magnification (artificial pupil (x 1); MIRAO deformable mirror (x 2) and HASO HS sensor (x 0.5)) regardless the Badal system position.

reflection from the cornea and to also check the projection of the images presented on the CRT monitor and minidisplay.

2.1.2 Configuration and validation of the Adaptive Optics system

Validation of the pupils planes for different positions of the Badal system

In the building phase of the system, the different pupil planes of interest (artificial pupil, deformable mirror (MIRAO) and Hartmann Shack sensor (HASO)) were identified. To ensure proper centration, locations and magnifications (artificial pupil (x 1), deformable mirror (x 2) and HS sensor (x 0.5))) of the different conjugated pupil planes regardless the Badal position, we placed a camera (TELI, without any objective) in each pupil plane and recorded images of a millimetric paper placed at the exit pupil of the eye – or the artificial eye- when moving the Badal System from -7 D to 7 D (1 D step) as illustrated in Figure 2.9.

The intensity profile of each recorded image was processed to calculate the magnification in each plane. A direct image of the millimetric paper establishes a scale of 41.5 pixels/mm. Figure 2.10B shows the intensity profiles for millimetric paper images from direct imaging and different positions of the Badal system, revealing constant magnification.

Goodman [1996] said "Two planes within an optical system are said to be conjugate planes if the intensity distribution across one plane is an image (generally magnified or demagnified) of the intensity distribution across the other plane. Likewise, two points are said to be conjugate points if one is the image of the

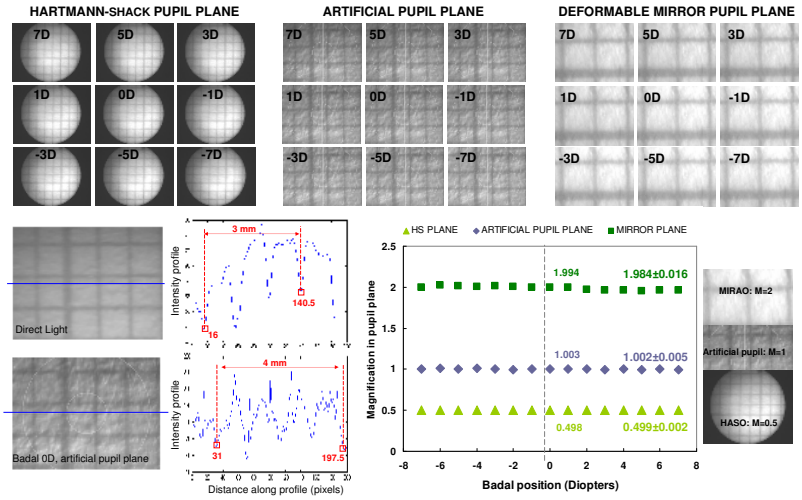

Figure 2.10: A. Recorded images of the millimetre paper for the different conjugated pupil planes (artificial pupil, deformable mirror plane and wavefront sensor plane) through Badal position. B. Images of a millimetre-paper and the corresponding intensity profile with direct light (upper raw, 41.5|,pixels/mm) and through the 0 D Badal position in the artificial pupil plane (lower raw, 41.625 pixels/mm; magnification from the exit pupil to artificial pupil=1.003). C. Magnification in the different pupil planes for different positions of the Badal system.

other." Therefore, applying a deformation on the deformable mirror will introduce changes in the shape of the wavefront but not in the intensity profile. By pushing the central actuators (number 22 and 31) of the deformable mirrors, the wavefront is deformed while the intensity profile recorded in the HS does not change, as illustrated in Figure 2.11.

Measurement and correction configurations

The measurement of wave aberrations and a closed-loop correction operation are performed in a few steps which consisted in Local Slopes Acquisition, Interaction Matrix Acquisition, Command Matrix Construction and finally the Closed-Loop Correction (or induction) of wave aberrations. These steps are performed using an artificial eye consisting of a doublet (focal length=35 mm) and a rotating diffuser acting as an artificial retina. When measuring this artificial eye, we set the current of the SLD to 63 mA in order to not saturate the Hartmann Shack sensor.

Local Slopes Acquisition Local slope acquisition was performed with the Hartmann-Shack wavefront sensor, with a 32 x 32 microlens matrix. Image of the Hartmann-Shack spots are illustrated in Figure 2.12 (left panel). For each acquisition, the system automatically detects all the calculable supaperture and infers the largest possible pupil, according to the phase reconstruction mode chosen. Typ-

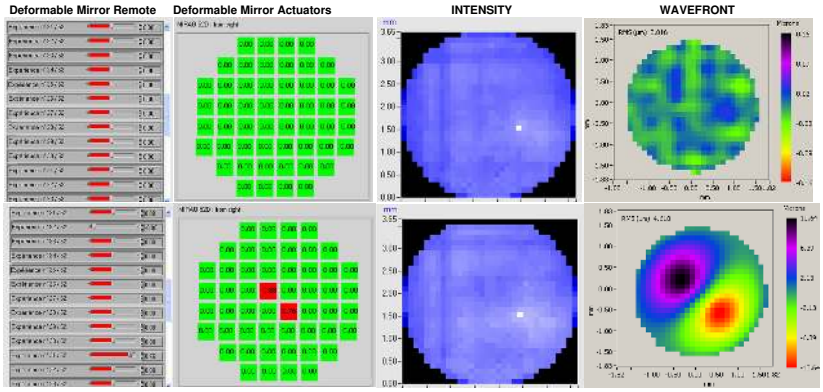

Figure 2.11: Checking the pupil conjugation. The actuator control remote, the representation of the deformable mirror with each actuator and the corresponding voltage applied, the Intensity profile and the wavefront (performed onto a closed-loop).

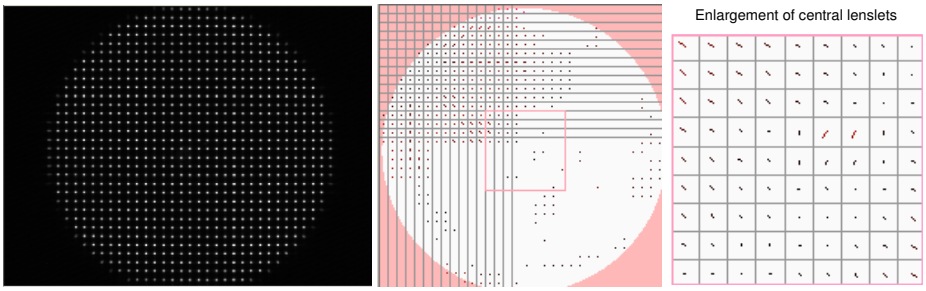

Figure 2.12: Hartmann-Shack sensor spots and the corresponding local slopes in the supapertures.

ically, a 6.5 mm pupil diameter uses 655 subpupils. The slopes are estimated to calculate the wavefront aberrations and expressed as vectors (shown in Figure 2.12 (right panel)). The amplitude of the vectors corresponds to the amplitude of the slope, while the orientation of the vector designates the angle of the largest slope of the wavefront. A light grey grid enables the microlenses to be located, the center of the each square representing the center of the microlenses. When measuring the wavefront aberrations, the software interpolates the slope from the adjacent subapertures.

Interaction Matrix Acquisition When a unit voltage is applied to one actuator of the deformable mirror, the surface deformation produced by this activated actuator is called the actuator's influence function. The interaction matrix accounts for the influence of each actuator – i.e. for the deformation of the entire membrane when pushing and pulling each actuators. Typically, a ± 0.2 V is applied to each actuator, and its effect on the membrane is saved in the Influence Matrix that records all the individual actuator's influence functions. The Interaction ma-

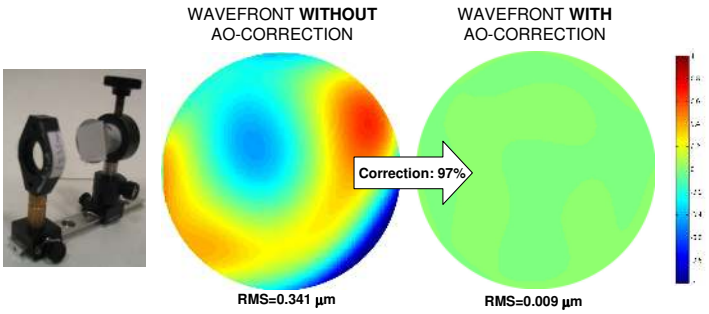

Figure 2.13: Photograph of the artificial eye used for calibrations (left panel) and wave aberration before and after closed-loop correction (right panels).

trix is constructed using the full pupil diameter (7.2 mm diameter).

Command Matrix Construction The command matrix accounts for the voltage that should be applied to each actuator to generate different patterns of aberrations. The command matrix is constructed from the Interaction Matrix. Mathematically, it is the pseudoinverse matrix of the Interaction Matrix. A modal reconstruction algorithm projects the measured phase (or slopes) onto a polynomial perpendicular base. Forty-eight modes are used and Zernike polynomials up to 7^{th} for circular pupils.

Closed-Loop Correction After having the calibration of the deformable mirror by acquiring the Interaction Matrix and building the Command Matrix, the pupil diameter was selected by closing the artificial pupil iris in the first pupil plane and the pupil diameter was estimated by software. A closed-loop operation could then be performed to correct the wave aberrations. A closed-loop operation consists on the acquisition of the local slopes, calculation of the voltages needed to apply to the actuators of the deformable mirror to change its shape and a subsequent acquisition of the residual slopes. These steps are repeated in N loops, N being the number of iterations required to obtain the desired wavefront pattern. With the artificial eye we measured the aberrations inherent to the system (RMS=0.341 microns for 6.5 mm pupil, excluding tilt and defocus), and corrected them in a closed-loop operation. The wave aberrations before and after the closed-loop operation are illustrated in Figure 2.13. We checked that the residual wavefront error decreases below 0.02 microns, stabilizes and no longer decreases. We deeemed the correction as good when it reached $\sim$95% of correction. The state of the mirror that correct for the system's aberration is saved and kept as a reference file named "flat mirror", used when measuring natural subject's aberrations (tilt and defocus are measured but kept free).

The effect of the gain on the correction mainly affected the time necessary to reach the correction level and the stability of the corrected optics. Figure 2.14 shows that the system begins to be unstable at a gain above 0.6 where oscillations

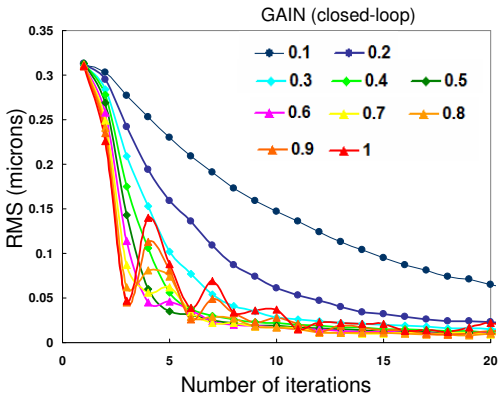

Figure 2.14: Correction of aberrations as a function of the gain (in the closed-loop).

can be seen. We typically used a gain between 0.3 and 0.5, the integration time was set at 45 ms (but can be adjusted for each wavefront measurement) and a stable closed-loop correction was obtained in 15 iterations.

Daily Calibration The 4 steps described above – wavefront measurement, Interaction Matrix acquisition, Command Matrix construction, Closed-Loop Correction of the system aberration – are performed daily with the artificial eye before each experimental session. The interaction matrix is constructed for the full pupil diameter, and the correction performed for a given pupil diameter (depending on the psychophysical experiment, typically 5 or 6 mm pupil diameter are used). The corrected state of the mirror named "flat mirror" is saved for a future use in order to ensure an adequate measurement of natural aberrations.

Validation of the AO system with an artificial eye

The performance of the system was validated using an artificial eye with known aberrations (artificial eye, provided by Alcon, Spain). We compared the values of the known aberrations (astigmatisms, defocus, coma and spherical aberration) as well as the value of the RMS of High Order Aberrations (HOA), with the values measured with our custom Adaptive Optics system (6.5 mm pupil diameter). Measurement were performed for the SLD current set at 47.7 mA; integration time 60 ms. As shown in Figure 2.15, there was a good correspondence between the nominal and the measured aberrations with the AO system of the different aberrations present in this artificial eye.

2.2 Automatic control interface

The system is controlled using custom routines written in Visual Basic ,Visual C++ (with the use of DLL libraries) and Matlab. Two different synchronized

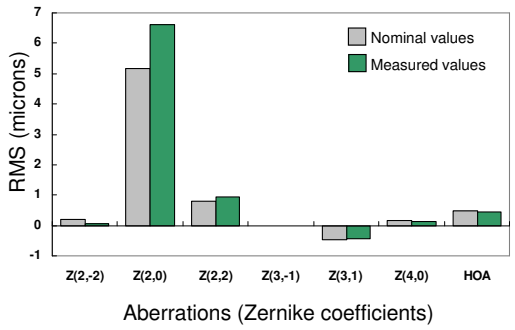

Figure 2.15: Comparison between the nominal and measured aberrations (different Zernike terms) of an artificial eye of known aberrations.

computers were used, one to control the AO system (MIRAO deformable mirror, HASO Hartmann-Shack wavefront sensor) and the motorized Badal system, and the other to control the Visage psychophysical platform and CRT monitor. The computers were synchronized using the User Datagram Protocol (UDP) for a rapid presentation of visual stimuli under controlled aberrations (AO correction/ aberrations induction) and best spherical error correction (Badal System) of the subject when needed.

The Interface program allows measurement, correction induction of ocular aberrations, monitoring the pupil, automatized displacement with the motorized Badal system, communication and synchronization of the control computers and data saving.

2.2.1 Adaptive Optics system control software

A dedicated interface was programmed in Visual C++ to allow the control of the Adaptive Optics and Hartmann-Shack system. We used libraries available in Visual C++ (Software Development Kit, Imagine Eyes). Figure 2.16 shows our custom program, which includes the following modules: Parameter module (gray box), the motorized Badal System module (purple box), Aberrations Measurement module (yellow boxes) to measure subject's aberrations with a specific state of the mirror; Interaction Matrix Selection module (pink box) to select or acquire the interaction matrix necessary for the closed-loop correction of induction of aberrations, Closed-Loop Correction module (green boxes) that allows the correction of the subject's aberrations, Aberrations Induction module (blue box) that allows to create a specific state of the mirror and Communication Module (orange box) implemented for the specific experiments that required communication between computers.

Parameters Module: This module sets the parameters used in the program: Integration Time for the HS acquisition (displayed in micro seconds) and set by default at 45 ms; Modal Mode used along with a Zernike reconstruction under a round pupil (always checked by default); the Gain (0.3 by default) and the number of iterations used in the Closed-loop Correction and Aberrations induction modules (15 iterations by default). The default values can be modified by the user.

Badal System module: This module allows to move the Badal system and therefore change te spherical correcion of the subject. The displacement can be expressed in diopters or in millimetres by the user's interface. If the "manual motor" box is checked the correction can be searched by the subject while viewing a stimulus through the system using the keyboard (2/8 numeric button). The module displays the current Badal position and allows to save the different badal positions (i.e. those corresponding to the best subjective spherical correction for a subject under natural aberrations or under corrected aberrations).

Aberration Measurement module: This module allows measurement of the subject's aberrations and includes three boxes. The Select Experiment box allows to select the experiment to be performed from a series of saved protocols. The MIRAO Select Mirror State box allows to select the state of the mirror before measurement the subject's aberrations. The "Flat mirror" – obtained during the daily calibration - corresponds to the system aberrations correction state and allows to perform measurements under the natural aberrations of the subject's. The "Select Mirror State" button allows to select from different states of the deformable mirror (for example a closed-loop correction or particular aberrations induction states). The Measurement box allows to document the name of the subject and the condition of measurement ("natural", "corrected" or "aberrations induced"). The Capture button is clicked to perform the measurement. The estimated Zernike polynomials from a HS measurement are written in an excel files along with the pupil diameter. The RMS value of the last measurement is calculated and automatically displayed in the dialogue box "RMS". This is particularly useful when measuring aberrations under AO-corrected state of the mirror.

Interaction Matrix Selection: An interaction matrix is obtained prior to a daily experimental calibration session. The corresponding interaction matrix can be selected from a list of saved files. This interaction matrix is necessary to perform a closed-loop correction or induction of aberrations in the corresponding modules.

Closed-Loop Correction module: This module allows to perform a closed-loop correction in N iterations – N being the number of iterations displayed in the Parameters module. An excel file saved all the Zernike coefficients, along with pupil diameter. The sate of the mirror at the end of the closed-loop is saved for a future use and will be available in the "Select Mirror State" of the Aberrations

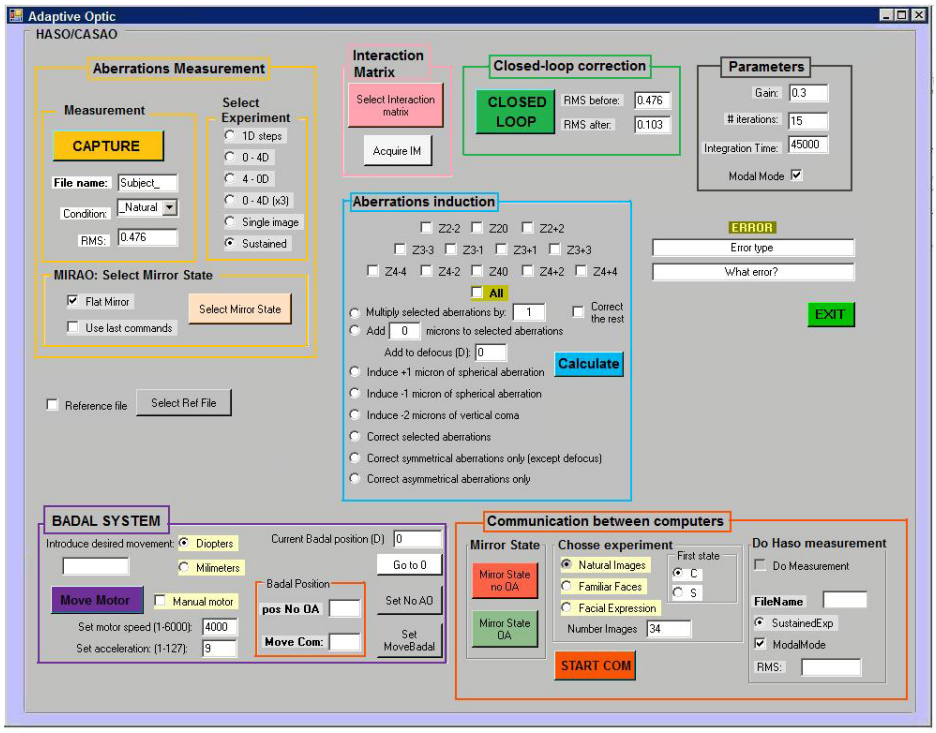

Figure 2.16: Visual C++ interface for the AO control: Parameters module (gray box), Badal System module (purple box), Interaction Matrix module (pink box), Measurement (yellow boxes), Correction (green box) and induction (blue box) of aberrations and the interface for Psychophysical experiments the natural images and face recognition experiment where the communication and synchronization between the two computer (one for the AO system and Badal system, the other for the visage) was needed for a rapid presentation of the stimuli in the adequate mirror state and Badal position.

Measurement module. The RMS of the first measurement (iteration 1) and the RMS at the end of the closed-loop (iterations N) are displayed in the "RMS before" and "RMS after" boxes for a rapid check of the correction.

Aberration Induction module: This module controls the induction of individual selected aberrations required in several experiments conducted with this instrument (i.e. Gambra et al. [2009]; de Gracia et al. [2010]; Vinas et al. [2013]). Aberrations can be induced directly on the subject's natural wave aberration ("correct the rest" unchecked) or on the subject's AO-correction of aberrations ("correct the rest" checked). The button "Calculate" performs the closed-loop induction in N iterations and saves the deformable mirror state for future use (and made available in the "Select Mirror State" of the Aberrations Measurement module). Along with the mirror state, the data (Zernike coefficient and pupil diameter) is saved in an excel file in each iteration.

2.2.2 Communication and synchronization

A complete platform for controlling the system and launching the psychophysical experiments has been developed. The system controls and synchronizes two computers, with programs written in Visual C++ and Matlab. This is particularly important in experiments requiring fast displaying of sequences of images under different states of aberrations (i.e. Natural aberrations and fully corrected optics). One computer controls the AO system (Deformable mirror, Hartmann–Shack wave front sensor) and the Badal system. The second computer controls the ViSaGe psychophysical platform and the CRT Monitor. Computers were synchronized using routines in Matlab, which allows a rapid presentation of visual stimuli under controlled aberrations (with the AO mirror) and best spherical refractive error correction (with a Badal system). The Communication module allows the communication between computers and was necessary in the natural images, face and facial expression recognition experiments (chapter 4). This module comprises The Badal position box (included in the Badal System module where the Badal positions for the natural and AO corrected subject's aberrations are stored), the Mirror state box (where the state of the deformable mirror in the natural and AO-corrected state are selected), the "Choose Experiment" box (which allows to select the experiment to run), the "do Haso measurement" box (which allows, if "do measurement" is checked, to perform an aberrations measurement and to ensure that the state of the deformable mirror is correct). When pushing the "START COM" button, the experiment is automatically run in visual C++ and in Matlab allowing a rapid presentation of psychophysical stimulus under different states of aberrations. Data of the different images displayed on the CRT monitor, state of the mirror and Badal system for each images and subject's responses are automatically saved in excel files

2.2.3 Pupil monitoring software

The pupil camera monitoring and motorized Badal System were controlled using custom-built software programmed in VB.Net 2005 (Microsoft). Figure 2.17 shows a snapshot of the pupil monitoring and motorized Badal system software.

The motorized Badal System software was initially written in Visual Basic but then transfered to Visual C++ for integration with the rest of the software). This module allows automatic control of the motorized Badal system from the user's interface (entering the desired movement manually, in diopters or in millimeters) or by the observers (pushing "Manual Motor" button) to adjust his/her best spherical correction.

The pupil camera allows continuous viewing of the pupil and is used to center the eye during the measurements. A ring of LEDs is used to illuminate the pupil. The interface allows the user to draw circles of different pupil diameters to assist centration, to save snapshot of the pupil or to capture a pupil video. The pupil camera calibration yielded a scale of 12.16 pixels/mm.

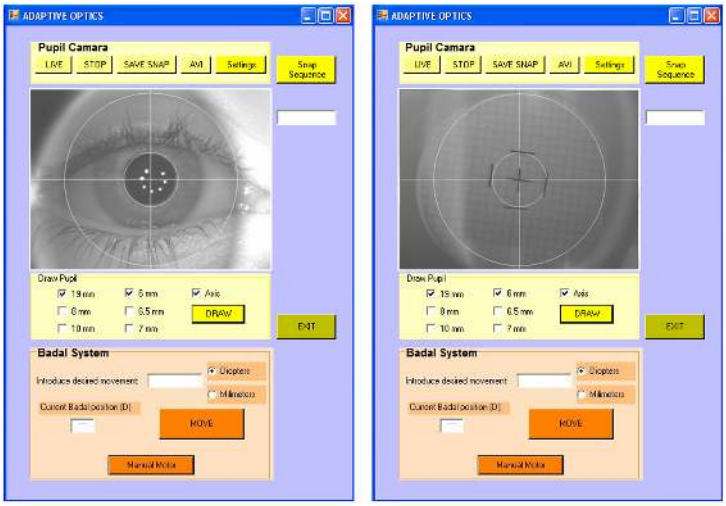

Figure 2.17: The Visual Basic program for pupil monitoring and the first motorized Badal system software. Snapshot during human eye measurement and during the calibration of the pupil camera.

2.3 Measurement and correction of aberrations of human eye

2.3.1 General protocols with human subjects

Ethics Statement

A total of 72 subjects participated in the different experiments described in this thesis. All subjects were normal volunteers (no ocular disease, spherical errors between 1.0 D and -5.5 D, cylinder < 0.75 D). The procedures were reviewed and approved by Institutional Bioethical Committees of the Consejo Superior de Investigaciones Científicas and met the tenets of the Declaration of Helsinki. All patients were fully informed, understood and signed an informed consent before enrolment in the study.

Refraction measurements

Prior to the experiments, the subject's refraction was measured, which allowed an initial setting for defocus correction in the Badal system. Measurements were performed using the Automatic Refractor Model 597, Humphrey-Zeiss.

2.3.2 Measurement with the Adaptive Optics system

Alignment of the eye and pupil selection

Subjects were fixed to the system by means of a dental impression mounted on a xyz linear stage. The subjects were aligned to the system while looking at a

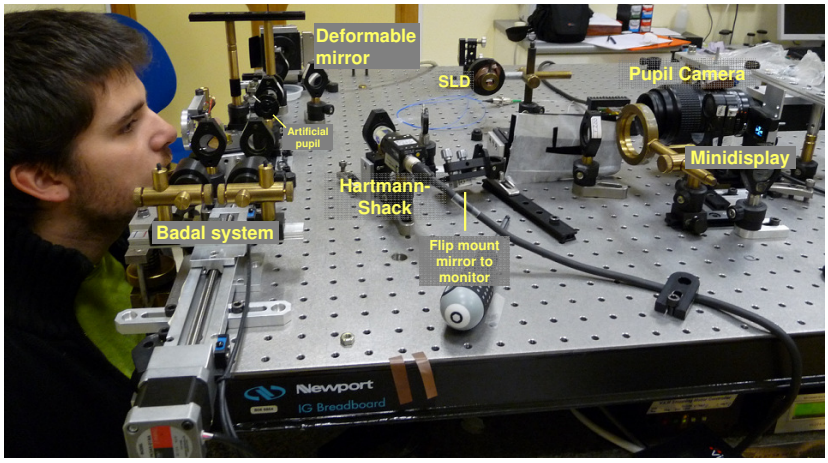

Figure 2.18: Adaptive Optics system and the main components when measuring the eye's aberrations.

Maltese cross presented on the minidisplay, while their pupil was monitored on the pupil monitoring system, focused, and its center aligned with respect to the optical axis of the instrument. In most studies, the measurements were performed under natural viewing conditions. Some experiments (chapters 3) were performed under mydriasis (with 1 drop tropicamide 1%) following a clinical eye exam.

Refractive error correction with the Badal System

The subject was asked to adjust the best subjective focus (starting from a myopic defocus) by controlling the Badal system with a keyboard while looking at a high contrast Maltese cross on the minidisplay, under his/her natural aberrations (noAO; flat state of the mirror). Given the chromatic difference of focus between the infrared aberration-measurement channel and the visible psychophysical channel [Llorente et al., 2003], defocus was left uncorrected with the mirror, and the Badal system was used instead. Best subjective focus was obtained for the different states of aberrations (i.e. Fully corrected or natural aberrations) under test.

Measurement and correction of the eye's aberrations

Once the subject is aligned to the system, a wavefront measurement with the "flat mirror" was perfromed to obtain the natural aberrations of the subjects. A closed-loop correction was then performed and the state of the deformable mirror was saved and applied accordingly to the psychophysical experiment.

An AO-correction was deemed satisfactory if the residual aberration was below 0.2 microns. In most cases the residual was around 0.1 µm. A close-loop correction (at a rate of 13 Hz) was typically achieved in 15 iterations. To check that the correction was stable, we performed a measurement of the wave aberrations with the newly generated mirror state and checked that the residual RMS. Psy-

chophysical measurements were performed under static corrections of aberrations, as continuous dynamic correction would have involved continuous viewing of the spot test and discomfort to the subject (particularly given the relatively long duration of the test. Pupil monitoring and aberration measurements were performed immediately before and after each psychophysical measurement, to ensure proper centration and AO-correction. A new closed-loop AO-correction was performed if the percentage of correction had fallen from the initial values. The length of the experiment varied according to the specific psychophysical tasks, from 2 h to 10 h

2.4 Psychophysical experiments

2.4.1 Selection of visual stimuli

Depending on the psychophysical tasks, different images were used in the experiments, from high contrast Snellen E letter (for visual acuity tests), to gray-scaled complex natural scenes including natural images, faces, textures and noise images (as shown in Figure 2.19). The tumbling E letter was presented on the minidisplay whereas the natural images, faces, noises and textures were presented on the CRT monitor. Images typically subtended between 0.7 and 1.98 degrees, depending on the experiment.

2.4.2 Manipulation of retinal blur

Manipulation of retinal blur was done differently, depending on the study. In the studies presented in chapters 3 and 4, retinal blur was manipulated by controlling the aberrations through which the subject viewed the stimulus with the deformable mirror. In the experiments presented in chapters 5-9, we maintained a full-AO-corrected-state of the subjects aberrations in the deformable mirror and manipulated the retinal blur by projecting stimuli blurred by convolution with known aberrations (low and high order aberrations). Adaptive Optics allow to cancel the natural aberrations of all subjects, exposing observers to identical aberration patterns and ensuring that any difference across subjects would arise from their own neural processing and their prior neural adaptation.

Standard Fourier optics techniques (Goodman, 1996), including the Fast Fourier Transform programmed in Matlab, were used to calculate the corresponding Point Spread Function (PSF). The PSF was scaled to match the pixel size of the original image. All computations were performed for a constant pupil diameter (5 mm pupil). The Stiles–Crawford effect was not considered, as for typical ρ values ($\rho <$ 0.1; Marcos & Burns, 2009) its effect was negligible for the purposes of our study. A double diffraction when viewing the convolved image through a diffraction-limited 5 mm pupil (convolution + artificial pupil aperture) was not corrected by means of inverse filtering, as it was considered negligible. Simulations conducted to assess the impact of these two factors revealed that the effect on the final contrast of convolved E targets with similar levels of blur to those used on the experiment was

Figure 2.19: Examples of images used in the experiments of this thesis.

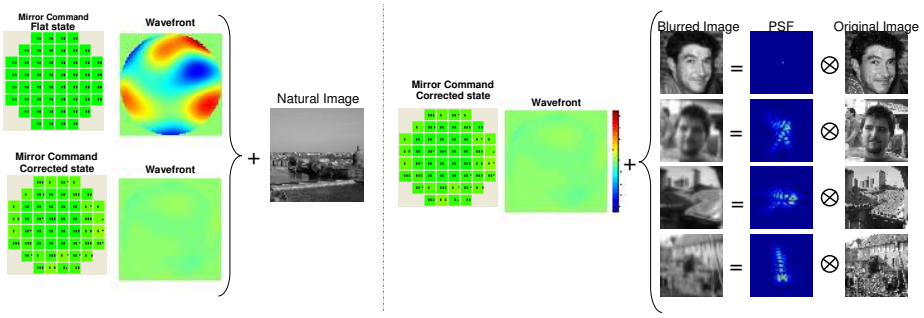

Figure 2.20: Manipulation of retinal blur: by projecting natural images under different mirror states (natural versus corrected) or neither by projecting different images blurred by convolution under full AO correction.

less than 10 % with respect to the contrast obtained without including these two factors.

2.4.3 Visual psychophysical techniques used under Adaptive Optic controlled aberrations

Different psychophysical experiments have been developed throughout the thesis for testing visual performance or neural adaptation to ocular aberrations. Subject's responses were recorded (using a keyboard or a specific response box) and analysed in different ways according to the different psychophysical paradigms (specific details can be found in the corresponding chapter).

Visual Acuity (VA) was measured using a four alternative choice procedure with high contrast tumbling Snellen E letters **[chapter 3]**. The thickness of the lines and gaps of the E letter were $1/5^{th}$ of their total size. Subjects were asked to identify the orientation of the letter E (pointing right, left, up, or down) that was displayed on the minidisplay. Each run consisted on 50 trials presented during 0.5 seconds with no feedback to the subject. A point fixation stimulus was shown between letters. A QUEST (QUick Estimate by Sequential Testing) algorithm was programmed in Matlab with Psychtoolbox [Brainard, 1997; Pelli, 1997] to select the size of each stimuli and optimize the estimation of the spatial resolution threshold.

The face recognition tasks **[chapter 4]** involved presentation of faces (familiar versus unfamiliar or happy versus angry) presented randomly under subject's natural aberrations and/or under AO-correction of subject's aberrations. Each image was presented during 3 s. A rating scale experiment was used in which the subject provided a graded response from 1 to 6 according to their level of confidence in recognizing the face (1/6 for definitely, 2/5 for probably, 3/4 for a lower level of confidence on the face being familiar-happy/unfamiliar-angry). Response Operating Characteristic (ROC) curves were used to analyse the data.

The best perceived focus shift was obtained after adaptation to images blurred by low order aberrations (a combination of defocus and astigmatism) **[chapter 5]**, by scaled versions of subject's High order aberrations **[chapter 6]**. The subjects made a 2-alternative forced-choice response to indicate the axis (vertical or horizontal) of the perceived blur. The level of astigmatic blur in the test images was varied with a staircase to estimate the perceived isotropic point, the point where the image seems to have no orientation **[chapter 5]**. The best perceived focus shift after adaptation to different level of blur produced by subject's scaled high order aberrations **[chapter 6]**, was measured in a two- alternative forced-choice procedure (2AFC), where the subject had to respond whether the image was sharp or blurred.

Natural adaptation to subject's natural level of blur **[chapter 7]** was obtained under neutral adaptation (adapting to gray screen instead of adapting to a blurred image). The psychophysical paradigm consisted of a 2AFC procedure, where the subject responded whether the image was sharp or blurred. Stimulus levels were varied with a QUEST algorithm in order to find the level of best perceived focus point under neutral adaptation and test images blurred by either different complex aberration patterns from real eyes or by pure defocus.

Image pair comparisons were performed in **chapter 4** to assess the subjective image sharpness of natural images and in **chapter 8** to test the natural adaptation to subject's orientation point spread function. The subjective image sharpness assessment experiment consisted on a two-alternative forced-choice test where 34 natural images were presented to the subject under controlled aberrations (natural versus AO-corrected aberrations). On each trial, both an AO-corrected and a natural image were presented in a randomized order. The image was presented during 3 s in both conditions (AO and noAO). The subject's task was to choose the one of two that appeared sharper to him/her.

Judgments of best focus from pairs of images with identical overall blur level (matching the strehl ratio of the subject under test) and different blur orientation were obtained and the psychophysical paradigm consisted of a 2AFC procedure where two images blurred with two different HOA patterns were presented sequentially (1.5 s each) **[chapter 8]**. The subject had to respond whether the first or second image appeared better focused. In a subsequent study, where a paradigm inspired by the "Classification image" was used **[chapter 9]**, the subject responded with a graded response from 1 to 6 - high certainty (1 or 6), moderate certainty (2 or 5) and low certainty (3 or 4) - to the image pairs comparisons.

3

Visual acuity as a function of luminance and contrast polarity

Stimulated by the potential of customized refractive surgery and high-order aberration correcting intraocular, contact or ophthalmic lenses, the debate on the visual benefits of achieving a perfect optics has been reopened. In the current chapter, we evaluated the benefit at correcting high order aberrations on visual acuity at different luminances and contrast polarities to adress whether the correction of high order aberrations produces a relevant improvement in visual quality in a wide range of conditions.

This chapter is based on the paper by Marcos, Sawides et al. "Influence of Adaptive-Optics ocular aberration correction on visual acuity at different luminances and contrast polarities" Journal of Vision, 2008. The co-authors of the study are Enrique Gambra and Carlos Dorronsoro.

The author of this thesis implemented the experimental procedure, performed the measurement on human eye's and data collection, and the data analysis in collaboration with Susana Marcos, Enrique Gambra and Carlos Dorronsoro. This work was also presented at the Association for Research in Vision and Ophthalmology (ARVO) annual meeting (May 2008) in Fort Lauderdale, Florida, USA, as an oral contribution.

3.1 Introduction

Despite the increasing popularity of Adaptive Optics, few studies have addressed the changes in visual performance with correction of high-order aberrations in an extended range of conditions (luminance and contrast polarity).

Yoon and Williams [2002] found a significant decrease in the logMAR by a factor of 1.2 for high luminance ($\sim 20\,\mathrm{cd/m^2}$) polychromatic targets, and of 1.6 for dim ($\sim 2\,\mathrm{cd/m^2}$) monochromatic light (using an interference filter) in a group of 7 subjects.

Most of these studies used relatively high luminances and black targets on a bright background. Relative measurements of the contrast sensitivity function in the same subject after a change in the optics reveal larger effects for higher spatial frequencies and for low-contrast than for high contrast targets, in good agreement with the changes of the optical modulation transfer function [Atchison et al., 1998]. The difference in the benefits of correcting aberrations (with Adaptive Optics) on visual performance as a function of light level has been stressed by Dalimier et al. [2008]. However, they measured contrast thresholds using a relatively large target (15 arcmin Landolt C) rather than targets in the spatial resolution limit. For their experimental conditions they found that for lower luminances, the drop in neural sensitivity limits the impact that increased optical degradations have on vision. In their study, visual benefits ranged between 1 and 1.7, across the three subjects and luminances.

Most studies use black letters on a white background. However, the effects of ocular aberrations are more usually subjectively experienced in night-time conditions (large pupils) and bright targets on dark backgrounds (street lights, the moon, etc.). The intrinsic difference of measuring visual acuity with white targets on a black (WoB) background as opposed to the more standard measurement using black targets on a white background (BoW) has been addressed in very few studies [Pointer, 2001; Westheimer et al., 2003; Westheimer, 2003; Wilcox, 1932].

Westheimer's predictions that WoB targets would produce better visual performance than BoW were supported experimentally by psychophysical measurements using Landolt C on 4 subjects [Westheimer, 2003] and clinical measurements using conventional and reversed Snellen charts on 106 patients of different ages [Westheimer et al., 2003]. He attributed the differences observed in visual resolution by reversing contrast polarity to changes in the effective retinal contrast of the target. Scattering and aberrations cause flattening and broadening of the point-spread function, affecting BoW targets more than WoB targets. If this hypothesis is correct, the relative advantage of WoB targets over BoW targets should decrease when aberrations are corrected, and therefore possibly tested using Adaptive Optics.

The relative impact of optical, pre-neural and neural factors in the change of visual resolution with luminance has been previously discussed on both real and ideal observers [Banks et al., 1987; Campbell and Green, 1965; Losada et al., 1993; Marcos and Navarro, 1997]. Recently, models incorporating optical and neural filtering, neural noise, and decision rules have been even implemented to simulate

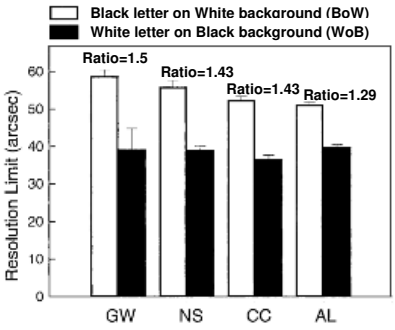

Figure 3.1: Resolution thresholds for normal and reversed contrast polarity Landolt C's for 4 subjects. The threshold ratios are depicted above the bars. Adapted from Westheimer [2003]

a visual acuity task [Watson and Ahumada, 2008]. While these models are able to reproduce measured visual performance for a set of optical aberrations, whether they can be extrapolated to other conditions of luminance or contrast remains to be explored.

This chapter investigates the benefit of correcting high order aberrations at various conditions, by measuring high contrast visual acuity as a function of luminance in the mesopic and photopic range, using standard and reversed-contrast polarity targets, under natural aberrations and Adaptive Optics corrected aberrations. We thus investigate the following questions: Does high contrast visual acuity improve with AO correction and if so, does it vary with luminance and contrast polarity? Is the change in VA correlated with the amount of corrected aberrations? Is the benefit of White letters on Black background (WoB) reduced with the correction of aberrations?

3.2 Methods

3.2.1 Subjects

In this study, seven young subjects aged 25 to 35 years (29.5±4.4) participated in the experiment. Spherical errors ranged between 0 and -5.75 D (-2.21±2.22 D). Cylinder was < 0.5 D in all cases. Astigmatism accounted for less than 26% of the RMS (excluding defocus and tilt). Subjects signed a consent form approved by the Institutional Review Boards after they had been informed on the nature of the study. All protocols met the tenets of the Declaration of Helsinki. The subjects were three of the authors and other four naïve subjects.

3.2.2 Measurement and correction of subject's aberrations

We used our custom Adaptive Optics system described in chapter 2 where the 12 mm x 9 mm SVGA OLED minidisplay (LiteEye 400) is used to project high contrast targets for fixation while measuring and correcting aberrations, and Snellen E letter while measuring Visual Acuities under the wide range of conditions. The Badal system, and pupil camera monitoring were automatically controlled using the custom-built software programmed in VB.Net 2005 (Microsoft) whereas the Hartmann-Shack wavefront sensor, deformable mirror, and closed-loop correction were controlled with the software provided by the manufacturer. Wave aberrations were measured and a closed-loop Adaptive Optic correction was applied. The Badal system was adjusted by the subjects under natural and AO corrected aberrations.

3.2.3 Visual Acuity measurements

VA was measured using a four alternative choice procedure with high contrast tumbling Snellen E letters. The thickness of the lines and gaps of the E letter were 1/5th of their total size. Subjects were asked to identify the orientation of the illiterate letter E (pointing right, left, up, or down) that was displayed on the minidisplay. Each run consisted on 50 trials presented during 0.5 seconds with no feedback to the subject. A QUEST algorithm was programmed in Psychtoolbox [Brainard, 1997] to select the size of each stimuli and optimize the estimation of the spatial resolution threshold. Experiments were done for white E letters on a black background and black E letters on a white background. The effective luminance of the minidisplay at the pupil plane was 50 cd/m^2. This value was estimated taking into account the light losses in the system. Measurements were performed for different luminances (50, 25, 16, 5, 2.5, 1.6 and 0.8) in the photopic and mesopic range, achieved by placing neutral density filters of appropriate optical density in a filter holder in front of the display. Luminances are specified in terms of the white area of the display. This refers to the background in the BoW experiments and the foreground on the WoB experiments.

3.2.4 Experimental Procedure

A total of 42 conditions were tested on each subject, corresponding to seven luminances, two aberration states (natural aberrations and AO-corrected aberrations), two contrast polarities (WoB and BoW), and two pupil dilation states. Measurements with WoB targets were done under undilated and dilated conditions, and measurements with BoW targets were done for dilated conditions only. Experiments were conducted on three sessions on two different days, each typically lasting around three hours.

The first session of measurements was always conducted with undilated pupil and WoB targets. In the undilated condition, the pupil diameter ranged between 5.7±0.8 mm to 4.7±0.7 mm on average, and for the lowest luminance the pupil

diameter was up to 6.6 mm in certain subjects (S1 and S7) and for the highest luminance it was down to 4.1 mm in certain subjects (S3, S4, S5 S6). The second session involved WoB and BoW targets under pupil dilation with 1% tropicamide. An artificial pupil of 6 mm diameter was projected onto the eye's pupil, in the dilated measurements only. All patients dilated up to 6 mm or more, so that the effective pupil diameter was always 6 mm in the dilated condition.

For each condition, VA was measured for ascending level of luminance to minimize the time required for dark adaptation. For the undilated pupil condition this also guaranteed that the aberration measurement and correction were performed for the largest pupil. Subjects were allowed to adapt to the light of each condition by looking at a BoW or WoB square before starting the experiment. For each luminance, VA acuity measurements were performed with natural aberrations and corrected aberrations in random order (with the corresponding defocus correction in each condition). Subjects were allowed to rest whenever required, and they were never informed on the correction-state at which they were performing the test in each moment.

3.2.5 Data analysis

Wave aberrations were fitted by 7^{th} order Zernike polynomial expansions. Optical quality was evaluated in terms of root-mean-square wavefront error (excluding tilt and defocus) and volume under the Modulation Transfer function (MTF), normalized to the diffraction-limited MTF volume, assuming a homogeneous pupil. Modulation for spatial frequencies beyond 100 c/deg was not considered in the computation [Marcos et al., 1999]. This metric (or equivalent as the Strehl ratio) has been shown to be better correlated with visual function than the RMS [Marsack et al., 2004] and to provide good estimates of refractive error [Guirao and Williams, 2003; Thibos et al., 2004]. Through-focus estimates of the MTF (shifting the defocus term between –1 and 1 D) were computed to assess through-focus optical quality (in terms of Strehl ratio), and the best objective focus position.

Visual resolution thresholds were estimated in terms of minimum angle of resolution (MAR), in pixels, converted to arcmin taking into account the focal length of the collimating lens in front of the display (0.026 arcmin/pixels). Visual acuity (VA) will be given in terms of Decimal visual acuity (inverse of MAR). The threshold usually converges to the final value in less than 30 trials. At the end of the 50 trials run, the threshold is checked to be stable over the last 10 trials and the VA is obtained as the average of these 10 last visual thresholds.

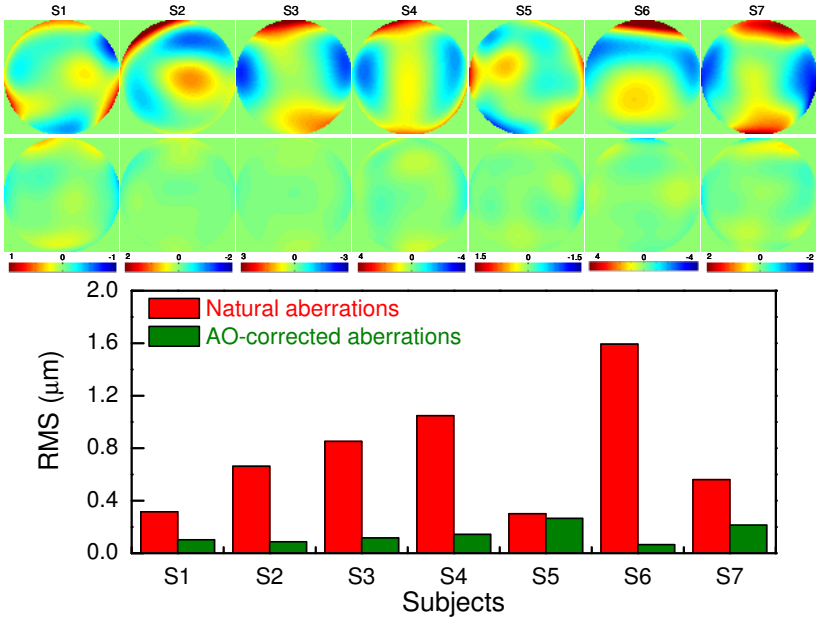

Figure 3.2: Wave aberrations maps before and after closed-loop AO-correction and RMS wave front error (excluding tilt and defocus) for all seven subjects before and after AO correction. Data are for 6 mm-dilated pupil diameters. (Reproduced from Marcos et al. [2008]).

3.3 Results

3.3.1 Best corrected ocular aberrations and defocus

Figure 3.2 illustrates the wave aberrations maps (excluding tilt and defocus) for all seven subjects before and after correction of aberrations with Adaptive Optics (for 6 mm pupil diameters). On average, RMS (excluding tilts and defocus) decreased from 0.76±0.45 to 0.14±0.07 μm, with an average correction of 81 %.

Figure 3.3 shows through-focus Strehl for all subjects with natural and AO-corrected aberrations. Strehl ratios have been computed for a 2-D range around zero defocus (Z_2^0 term). Except for subject S5, there is a dramatic difference in through-focus optical quality between both conditions. In all cases, there is a shift of best objective focus position (more negative in the natural aberration condition). Except for subject S4, this shift is in general agreement with the subjective focus shift performed by the subject between conditions (indicated by a vertical line in the graphs). The focus shift is particularly relevant for the subject with larger amount of aberrations (S6, RMS = 1.59 µm), with a focus shift of 0.75 D (Strehl) or 0.9 D (subjective) between the aberrated and AO-corrected condition, illustrating positive interactions of defocus and high order aberrations [Applegate et al., 2003b; McLellan et al., 2006]. Comparisons of Strehl ratio for natural and AO-corrected aberrations will be performed for the maximum values of the through-focus curves

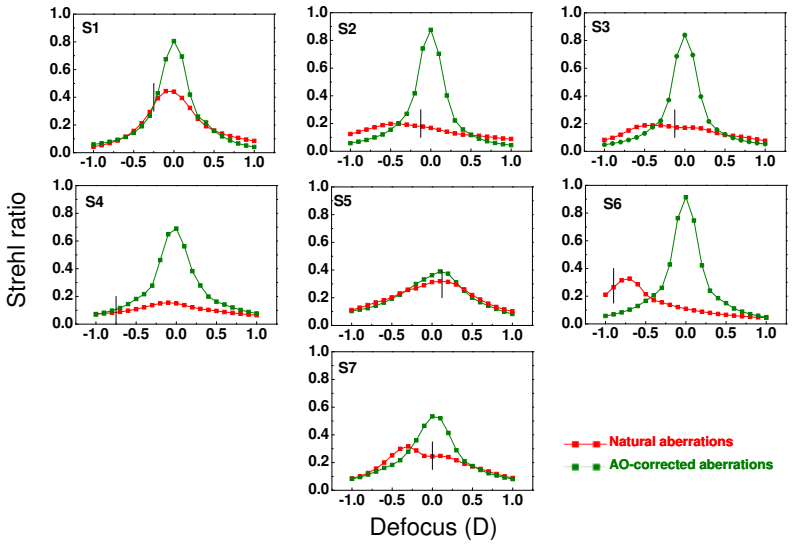

Figure 3.3: Through-focus Strehl ratio computed from natural and AO-corrected wave aberrations in all subjects (6 mm pupils). The vertical line indicates the subjective best focus as chosen by the subject for the natural aberration condition (with respect to the best focus in the AO-condition). Defocus is referred to $Z_2^0 = 0$. Data are for 6 mm pupils. (Reproduced from Marcos et al. [2008]).

in Figure 3.3.

3.3.2 Visual acuity under natural and AO-corrected aberrations as a function of luminance (BoW targets)

There is a consistent average increase of VA with background luminance in both the natural aberrations and AO-correction conditions and a mean improvement of VA at all luminances with AO-correction, as shown in Figure 3.4 (for all individual eyes and for the average across all eyes). The mean increase of VA is fairly constant across luminances, although this varied across individuals. All subjects except for S1 and S5 showed a significant increase of VA with AO-correction. These two subjects showed the lowest RMS before AO correction and the highest VA under natural aberrations.

Figure 3.5 shows data for all subjects plotted in VA vs. logL form. The numbers on the graphs show the slope of linear regressions to the data. In all eyes (except for S1 and S5) there is not only an increase of VA with AO-correction, but an increase in the slope of the VA vs. logL function (by a factor of 1.35 on average).

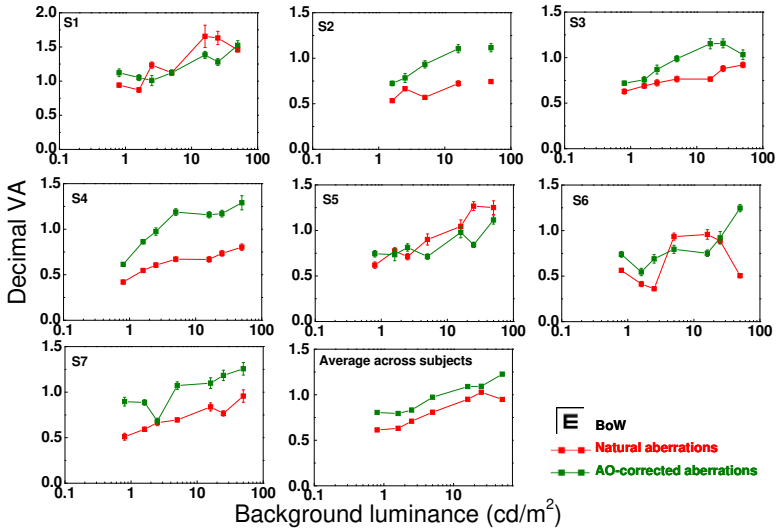

Figure 3.4: Decimal visual acuity as a function of background luminance (in a log-linear scale) for BoW targets, with dilated pupil (6 mm diameter) for all subjects. Error bars stand for standard deviation (of at least ten stabilized threshold estimates). D. Average across 7 eyes. (Reproduced from Marcos et al. [2008]).

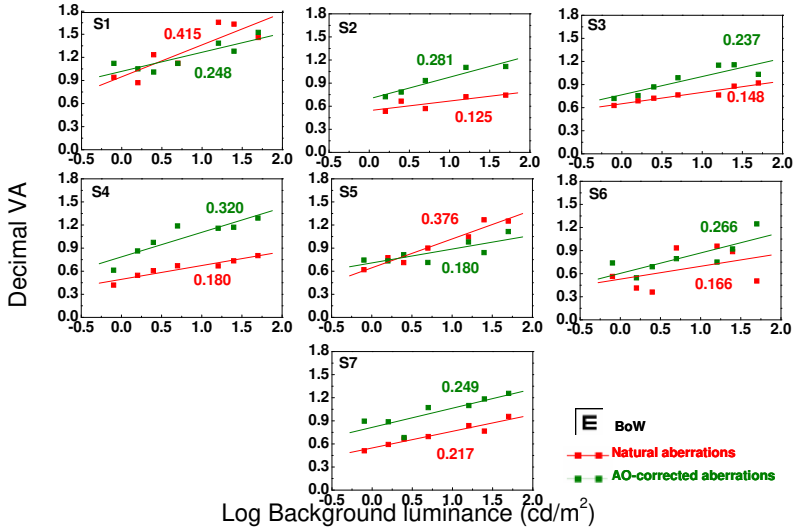

Figure 3.5: Decimal visual acuity as a function of log background luminance for BoW targets for all eyes, with dilated pupil (6 mm diameter). Data have fitted to linear regressions to the Decimal VA vs. logL function (the slope is indicated by the number above each line). Except for in S1 and S5 there is an increase in the slope of the regression with correction. (Reproduced from Marcos et al. [2008]).

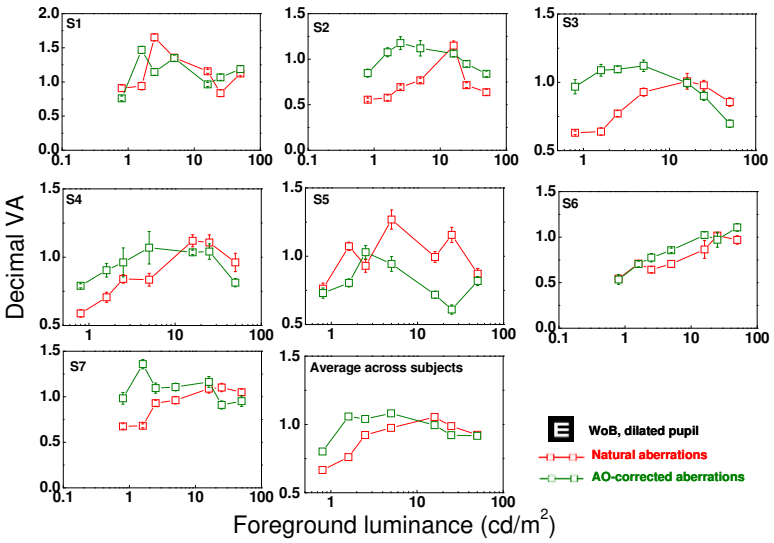

Figure 3.6: Decimal visual acuity as a function of foreground luminance (in a log-linear scale) for WoB targets for all subjects, and on average across the 7 eyes, with dilated pupil (6-mm). Error bars stand for standard deviation (of at least ten stabilized threshold estimates). (Reproduced from Marcos et al. [2008]).

3.3.3 Visual acuity under natural and AO-corrected aberrations as a function of foreground luminance (WoB targets)

Figures 3.6 and 3.7 show Decimal visual acuity as a function of foreground luminance for WoB targets. Figure 3.6 shows the results for dilated pupils and Figure 3.7 for undilated pupil (for all individual eyes and for the average across all eyes). Unlike in 3.4 (BoW targets) where a systematic increase in VA with luminance was found, curves in Figure 3.6 show a systematic inverted U shape (i.e. visual acuities are higher for intermediate luminances than for low and high luminances) (except for S6). AO-correction of aberrations produced a leftward displacement of the curve, and a significant increase of VA for low and intermediate luminances, but not for the highest luminances tested. Those subjects that did not benefit from AO-correction for BoW targets (S1 and S5) did not benefit from correction for WoB targets.

Under undilated condition, pupils varied from 5.7±0.8 mm to 4.7±0.7 mm with increasing foreground luminances (WoB targets). For the natural aberration condition results are similar with dilated and undilated conditions. However AO-correction increases performance less with undilated than with dilated pupils.

3.3.4 Differences between targets polarities BoW and WoB

We have evaluated the visual benefit of the AO correction of astigmatism and high order aberrations for all conditions in terms of VA ratios (AO-corrected /natural

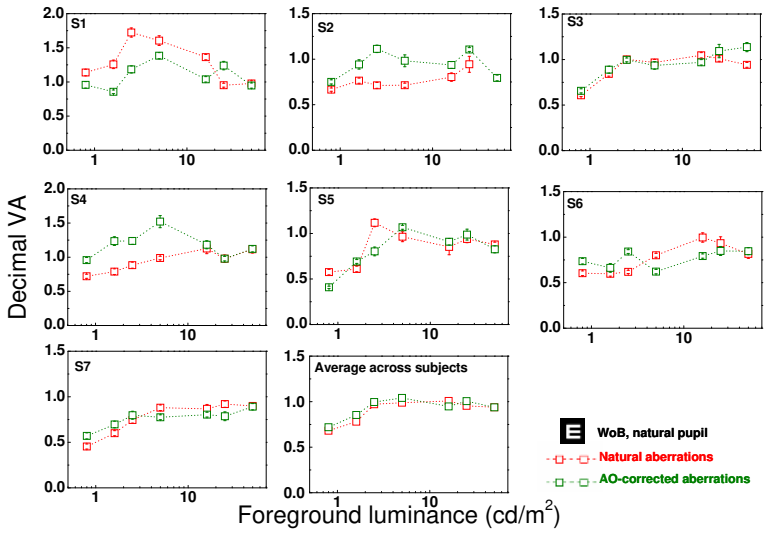

Figure 3.7: Decimal visual acuity as a function of foreground luminance (in a log-linear scale) for WoB targets for all subjects and on average across the 7 eyes, with natural, undilated pupil. Error bars stand for standard deviation (of at least ten stabilized threshold estimates). (Reproduced from Marcos et al. [2008]).

aberrations) as shown in Figure 3.8. The benefit is largest for BoW targets than WoB targets (at all luminances except for 1.6 cd/m^2). There is a significant benefit for WoB targets (dilated condition) for low and intermediate luminances, but the ratio falls below 1 for luminances 16 and 25 cd/m^2. The benefit for WoB targets (undilated condition) is very modest, and the ratio falls below 1 at 16 cd/m^2.

We compared visual performance between standard and reversed contrast polarity targets for the same foreground/background luminances, and both natural and AO-corrected aberrations (Figure 3.9). When the natural aberrations are present, the use of WoB targets produce significantly higher visual performance than BoW targets at least for luminances below 25 cd/m^2. When aberrations are corrected, the relative benefit of using WoB targets is reduced, and except for one luminance (1.6 cd/m^2) WoB/BoW ratio is lower for the AO-correction than natural aberrations conditions, and WoB targets only produced higher visual performance than BoW targets (WoB/BoW >1) for the lowest luminances.

3.3.5 Visual acuity versus optical quality: AO-correction benefit

With natural aberrations, subjects with larger amounts of ocular aberrations tend to have lower VA. Figure 3.10 shows mean VA (across luminances and contrast polarities) as a function of Strehl ratio at best focus, with dilated pupils (6 mm). The correlation is significant (p=0.037) when the Strehl ratio metric is used. Our sample included subjects with a large range of natural aberrations and VAs. When subject S1 (with highest Strehl and VA) was not included, the correlation did not

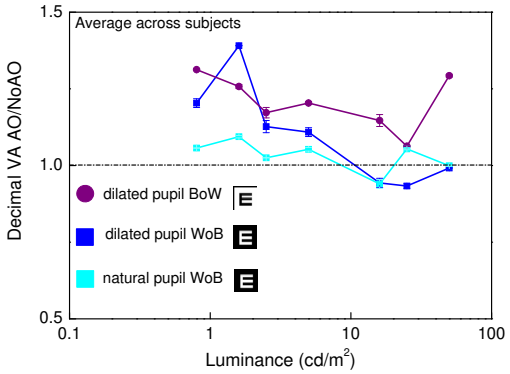

Figure 3.8: Decimal VA ratios (AO-corrected /natural aberrations) as a function of luminance, in a log-linear scale, (background luminance in the BoW condition and foreground luminance in the WoB condition) for all conditions tested: BoW targets (dilated), WoB targets (dilated), WoB targets (undilated), averaged across subjects. Error bars stand for standard deviations. (Reproduced from Marcos et al. [2008]).

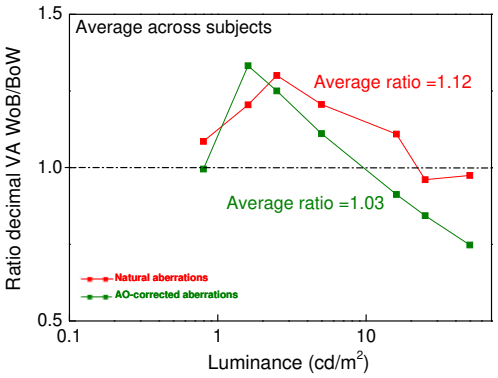

Figure 3.9: Decimal VA ratios (WoB target/BoW target) as a function of luminance (in a linear-log scale), with natural and AO aberration correction, for dilated pupils (6 mm). (Reproduced from Marcos et al. [2008]).

reach statistical significance (p=0.11), when the mean Decimal VA (across conditions) was used. The correlation was also disrupted when aberrations are corrected (p=0.582). With AO correction the functions are displaced toward higher Strehl values and higher VA. Mean Decimal VA (across conditions) was not significantly correlated with RMS, neither for natural aberrations nor for AO-correction. We performed a similar analysis of VA versus optical quality for each luminance and target type individually. We found better correlations for BoW than WoB targets. For natural aberrations, correlations were statistically significant for BoW targets at 25 cd/m^2 (p=0.05), 16 cd/m^2 (p=0.0005) and 5 cd/m^2 (p=0.0038) using Strehl ratio, and at 50 cd/m^2 (p=0.009), 2.5 cd/m^2 (p=0.0046) and 1.6 cd/m^2 (p=0.0186) using RMS. All of these correlations still held when subject S1 was excluded (except at 25 cd/m^2). For WoB targets, correlations were statistically significant only for 5 cd/m^2 (p=0.036 and p=0.045 for Strehl and RMS respectively) and 0.8 cd/m^2 (p=0.034 and p=0.048 for Strehl and RMS respectively). For AO-corrected aberrations, none of the correlations were significant.

We found that subjects that experienced larger amounts of optical corrections also experienced a larger increase in VA at correcting aberrations. This is shown in Figure 3.11 A by correlations of the mean VA AO/noAO ratios (across luminances and contrast polarities) with Strehl AO/no AO ratios at best focus (for dilated pupils). The correlation was significant (p=0.04), but not when RMS AO/noAO ratio was used as a metric (p=0.14). The same analysis was performed individually for each luminance and contrast polarities, using both Strehl AO/noAO and Strehl AO-noAO as metrics. We did not find any systematic trend with luminance for AO benefit in relation to amount of optical correction.

We also found that subjects that experienced a larger amount of optical correction showed a larger increase in the slope VA vs logL (with BoW targets, see Figure 3.5). This is shown in Figure 3.11 B which shows the correlation between the mentioned slope AO/no AO ratio and the Strehl AO/noAO ratio (p=0.0092).

3.4 Discussion

We found that correcting aberrations produced an increase in high contrast visual acuity in normal eyes under a range of conditions of luminance and target contrast polarity. The maximum increase of Decimal VA was by a factor of 2.5 for the subject with the highest amount of ocular aberrations, BoW targets and the highest luminance (50 cd/m^2). In general, the increase in VA was more modest for WoB targets (by a factor of 1.13, averaged across luminances and subjects) than for BoW targets (by a factor of 1.29). For WoB targets there was no improvement in VA at the highest luminances.

Previous studies had shown an increase (of similar order of magnitude) of high contrast visual acuity in normal eyes (typically for high luminance and BoW targets) when aberrations had been corrected with Adaptive Optics [Yoon and

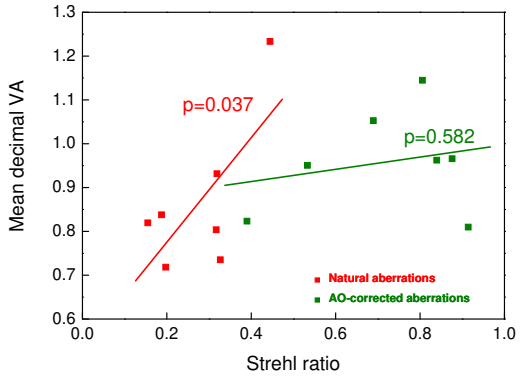

Figure 3.10: Mean Decimal VA versus Strehl ratio for all eyes, for natural aberrations and AO-corrected aberrations. Mean VA is the average across luminances and contrast polarities (for dilated pupils, 6 mm). Strehl ratio is the maximum value of curves of Figure 3 (i.e., Strehl ratio at best focus). (Reproduced from Marcos et al. [2008]).

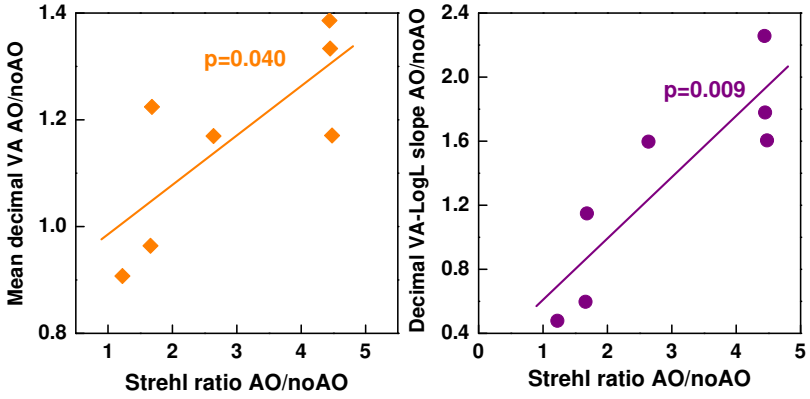

Figure 3.11: A. Ratio of mean VA (corrected /natural aberrations) versus Strehl ratio (corrected/natural aberrations) from data shown in Figure 10. B. Ratio of slope VA vs. LogL functions (corrected/natural aberrations) versus Strehl ratio (corrected/natural aberrations) using data from Figures 3 and 5. Linear regression to the data (and the corresponding p values) IS also shown, indicating a significant correlation between between visual and optical improvement (A) and between increase in the rate of change of VA with log luminance and optical improvement (B). (Reproduced from Marcos et al. [2008]).

Williams, 2002] or phase-plates [Yoon et al., 2004]. Others had shown that increasing the RMS error decreased VA [Applegate et al., 2003b]. We have demonstrated that the improvement of VA is actually correlated with the amount of aberrations corrected in normal eyes. It is also interesting that in the presence of aberrations VA appears correlated with optical quality, indicating that aberrations impose a major limit in spatial resolution. The fact that the correlation gets disrupted when aberrations are corrected agrees with previous literature that found that in eyes with high visual acuity photopic high contrast logMAR acuity is insensitive to variations in retinal image [Applegate et al., 2006], and it is indicative of the limiting effects of other non-optical factors when aberrations are corrected. As the sample was small and most of the subjects were emmetropes we did not attempt to correlate these findings with refractive error, as the study by Rossi et al. [2007] had done.

The change of visual acuity with luminance and target contrast polarity, and how these functions change upon correction of aberrations may give new insights into the physical limits of visual spatial resolution. While it has been shown for more than a century that visual acuity increases with increasing luminance in normal foveal vision [Ferree and Rand, 1932; Riggs and Graham, 1965], the relative contribution to visual resolution of optical aberrations, pre-neural factors (quantal fluctuations in the stimulus, transmittance of the optical media, aperture, quantum efficiency and spatial distribution of foveal photoreceptors) and neural factors for different luminances is not fully established. We have shown that correcting aberrations (for BoW targets) improves VA on average at all luminances, but the increase of VA with luminance also occurs in close to diffraction-limited conditions, indicating that quantum catch properties are a major factor in the effect. The effect of artificial blurring in the retinal image (with trial lenses) on the acuity vs. logL slope had been investigated before [Sloan, 1968]. That study aimed at testing the hypothesis that the increase in acuity with luminance results from a decrease in the size of the retinal area that acts as a single photoreceptor unit. We found that similarly to defocus, the blur produced by high order aberrations also produce a decrease in the slope of the acuity vs. logL.

While the change in visual acuity with luminance has been extensively studied in previous literature for BoW targets, there are scarce data in the literature with WoB targets, and very few have looked at changes with luminance. Wilcox [1932] addressed the changes in threshold resolution and the effect of the variation in intensities of test object and background on visual acuity. He measured the resolution threshold (in arcsec) for bright bars (intensities of bars varied) on Black background and dark bars on bright background (intensities of background varied).

It is interesting that visual acuity with WoB targets does not increase steadily with luminance, but following an initial increase for lower and intermediate luminances, decreases for higher luminances. This "U shape" behaviour agrees with that reported by Wilcox (Figure 3.12). This effect may be related to that described as "irradiation" in old literature [Walls, 1943; Wilcox, 1932], i.e. when

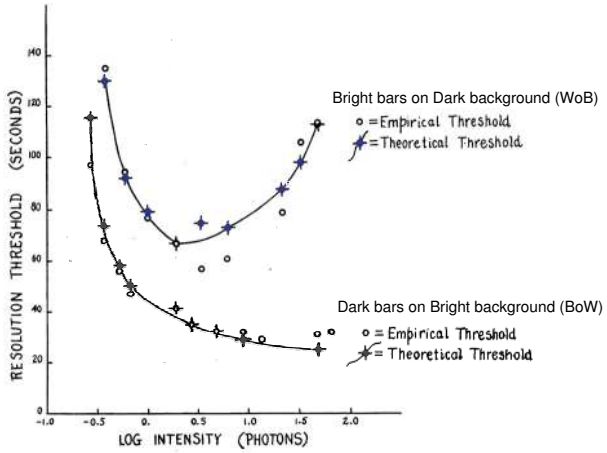

Figure 3.12: Showing the variation of the resolution threshold (arcsec) with intensity of the test objects in the case of bright bars on dark background and with intensity of the background in the case of dark bars on bright background. test object consisted of two narrow parallel vertical bars of constant size but variable separation. The acuity was tested by determining the least interval between the bars which would lead a perception of doubleness. Bars and background were separately illuminated. The average visual angle subtended by the minimum perceptible interval was taken as the resolution threshold. Adapted from [Wilcox, 1932].

the brightness of narrow lines on dark field (as in the WoB letter targets) is increased, angular resolution is compromised as the perceived gap is filled in with light. When aberrations are corrected the function seems to be shifted leftwards, as if this phenomenon started to occur at lower luminances. Whatever the origin, there appears to be a benefit of correcting aberrations at low and intermediate luminances, but not at higher luminances for WoB targets. It should also be noted that the state of dark adaptation is different for the same condition of background or foreground luminance. We found slightly poorer benefit of AO-correction at the lower luminances under undilated pupil compared to the dilated conditions (WoB targets). This may indicate that, at least with natural aberrations, the pupil miosis provides optimal aperture for visual acuity at each luminance [Campbell and Gregory, 1960]. However differences in the pupil diameter between these dilated and undilated conditions (6 vs. 5.17 ± 0.87 mm at $1.6\,\mathrm{cd/m^2}$, for which the largest difference in VA occurs) cannot account for the difference in visual performance. Also a stable correction may be more challenging under free accommodation and dim illumination (dim targets on black background), which may result in lower VA than with dilated conditions.

Previous literature suggests better visual performance for WoB targets than BoW targets, the magnitude of the effect varying across studies, experimental conditions and age of the population [Pointer, 2001; Westheimer et al., 2003; Wes-

theimer, 2003]. Westheimer [2003] argued that even for identical targets but of reversed polarity, contrast is different because the background light level, which is a dividing factor in the contrast calculation, is much less when only the letters are bright. As contrast is the limiting factor in visual acuity, reversed contrast (WoB) would be expected to be better, and more in eyes where aberrations and light scatter widen the point-spread function. We have found (Figure 3.10) that for a wide range of luminances (particularly low and intermediate luminances) performance with WoB targets exceeds BoW under natural aberrations, and that this advantage significantly decreases when aberrations are corrected. The presence of scattering may explain that even with AO-correction visual acuity with WoB targets still exceeds that with BoW targets at low and intermediate luminances.

3.5 Conclusions

Correcting aberrations results in an overall improvement in visual acuity under a range of conditions, particularly in eyes with significant amounts of aberrations. Comparing the effect of correcting aberrations as a function of luminance and contrast polarity has allowed us to test hypothesis on physical limits to spatial vision.

However, it remains to be seen to which extent those benefits are of clinical importance, could the same amounts of corrections (70% on average) be achieved with customized lenses or surgery. Comparisons of results with dilated and undilated pupils show that the benefits are reduced under undilated conditions.

We have used high contrast targets and polychromatic light. It is likely that higher benefits would have been achieved for low contrast targets and monochromatic light. In the next Chapter, we investigated the change in visual performance when aberrations are corrected using natural targets and more complex real-life tasks.

4

Visual performance with natural images and daily tasks, under AO-corrected aberrations

As the correction of high order aberrations is being considered in the clinical practice, it is important to investigate whether such correction will have a positive impact on daily life activities. In the current chapter, we investigate whether correcting high order aberrations produces a relevant improvement in vision for everyday life by testing perception of natural images under AO-corrected optics as well as in familiar face and facial expression recognition tasks.

This chapter is based on the paper by Sawides et al. "Visual performance with real-life tasks under Adaptive-Optics ocular aberration correction" Journal of Vision, 2009. The co-authors of the study are, Enrique Gambra, Daniel Pascual, Carlos Dorronsoro and Susana Marcos.

The author of this thesis implemented the experimental procedure, performed the measurement on human eye's and collected the data,performed the data analysis in collaboration with the rest of authors, and implemented the custom algorithm corresponding to the communication between the two computers in collaboration with Daniel Pascual. This work was also presented at the Association for Research in Vision and Ophthalmology (ARVO) annual meeting (May 2009) in Fort Lauderdale, Florida, USA, as an oral contribution.

4.1 Introduction

To date, most studies that have looked into the effects of aberrations on vision used standard visual tests, primarily contrast sensitivity and visual acuity with high contrast targets (chapter 3).

The importance of using natural images and of assessing visual performance using tasks that are closer to the daily experience of subjects has been widely recognized. Although the physical constraints of the Adaptive Optics equipment does not allow to perform in situ tests in complex environments, as those undertaken in other areas (i.e., assessment of low vision devices [Peli et al., 1991, 1994], at least it is possible to perform visual tests using images of natural scenes (landscapes, buildings, faces, etc.).

An obvious way to evaluate the benefits of optical correction is the subject's subjective image sharpness assessment between the corrected and original image, where the subject has to choose between the two images which one he or she considered of better quality. These methods are widely used in radiology, and other areas where image processing techniques to compress images are used [Gur et al., 1997; Slone et al., 2000]. Alternatively, one can test whether the ability to perform a given visual task is improved upon correction, or change with aging or disease. For example, Owsley and Sloane [1987] used identification of faces and daily objects like lamps, bicycles, or road signs to assess contrast thresholds in patients. Bullimore et al. [1991] tested face and facial expression recognition on healthy and age related macular degeneration (ARMD) patients by determining the equivalent viewing distance required for recognition of identity and expression. They found that in normal patients face and expression recognition was similar but in ARMD patients, the decline in performance was due predominantly to difficulties in identity recognition. The equivalent viewing distance required for recognition of identity and of expression was very similar except in subjects with very poor visual acuity, for whom recognizing expressions became easier than recognizing identity. Peli et al. [1991] used a celebrity face recognition test to evaluate the visual improvement in low vision patients with digitally enhanced images. The data were analysed in terms of the area under the receiver operating characteristic (ROC) curves for the two conditions natural and enhanced. ROC analysis has been shown to be a powerful tool to compare techniques or methods, and the statistical study of the ROC curves is well documented [Metz et al., 1984; Metz, 1978, 2006, 2008; Hanley and McNeil, 1982, 1983; Hanley, 1988].

Face perception is perhaps one of the most highly developed visual skills in humans and it is mediated by high level cognitive process. Face recognition is accomplished since a very early age, while facial expression recognition is essential for social communication. There have been debates on the role of spatial frequency on face and facial expression recognition [Halit et al., 2006; Ruiz-Soler and Beltran, 2006; Peli et al., 1991; Costen et al., 1996; Owsley and Sloane, 1987]. Correction of HOA will likely produce a contrast enhancement of the critical frequency band for face recognition (4–8 cycles/face [Peli et al., 1991]; 8–16 cycles/face [Näsänen,

1999; Gold et al., 1999]). Different spatial frequency sensitivities have been found between face identification and emotional expression recognition tasks [Vuilleumier et al., 2003; Posamentier and Abdi, 2003]. Previous studies have examined the influence of image blur by digital band-pass filtering the images [Costen et al., 1996].

In an effort to understand the parameters (neural and optical) that influence the effect of aberration correction on visual performance and whether correcting aberrations represents a real benefit in real world tasks, we examined the subjective image sharpness assessment (with natural or corrected aberrations) on complex natural scenes and the differences in familiar face recognition and facial expression recognition with and without aberration correction in normal individuals. In particular, the current chapter addresses whether correcting optical aberrations results in a better perceptual quality of natural images and in an improvement of functional visual tasks. In particular, it addresses the following questions: Do subjects have the impression that natural images look sharper with AO correction and if so, is it correlated with the amount of corrected aberrations? Is familiar face and facial expression recognition improved by the correction of High Order Aberrations?

4.2 Methods

4.2.1 Subjects

Seventeen young subjects aged 24 to 38 years (28.1±4.8) participated in the experiment (seventeen participated in the subjective image sharpness assessment and facial expression recognition tests; twelve participated in the facial expression recognition test). Spherical errors ranged between -5 and 4 D (-1.16±1.13 D). Astigmatism ranged between 0 and 0.12 D (0.05±0.03 D on average). HOA accounted for almost 70% of the RMS (excluding defocus and tilt). Subjects signed a consent form approved by the Institutional Review Boards after they had been informed on the nature of the study and possible consequences. All protocols met the tenets of the Declaration of Helsinki. Four of the subjects were trained and the others were naïve subjects.

4.2.2 Improvement of the system for presentation of complex psychophysical stimuli

The 12 mm x 9 mm SVGA OLED minidisplay (LiteEye 400) was used for fixation during measurement and correction of the subject's aberration, where a white and black Maltese cross was projected. The second psychophysical channel was specifically developed for this study and allows the presentation of gray-scale images on the CRT monitor controlled by the psychophysical platform (ViSaGe, Cambridge Research System, UK) and custom routines written in Matlab.

4.2.3 Control of the ocular aberrations

The system was controlled using custom routines written in Visual C++ and Matlab from two different computers, one controlling the AO system (Deformable mirror, Hartmann–Shack wavefront sensor) and the Badal system, the other controlling the ViSaGe psychophysical platform and the CRT Monitor.

Astigmatisms and higher order aberrations were controlled with the deformable mirror, in a closed-loop operation where the static state of the mirror was saved and applied during the measurements when required in the psychophysical protocol. The refractive error correction was achieved with the Badal system, adjusted by the subjects under natural aberrations (noAO) and AO-corrected aberrations. The positions of the Badal system for these two states of the mirror were saved and applied appropriately during the psychophysical experiment.

Computers were synchronized for a rapid presentation of visual stimuli under controlled aberrations (with the AO mirror) and best spherical refractive error correction (with the Badal system).

4.2.4 Natural and face images

The images presented to the subjects were acquired using a photographic digital camera (Canon PowerShot) with an original resolution of 4M pixels. All the photographs were converted to grayscale. Grayscale face photographs were taken of volunteers, showing neutral, angry and happy expressions. The subjects included people that were known to the participating observers (in most cases colleagues from the institute) and people unknown to them. The faces were cropped to remove background and the identification was predominantly dependent on facial features. For the facial expression recognition, the faces that were not sufficiently expressive were discarded.

Some examples of natural scenes (typically landscapes, trees, buildings, street scenes, etc...) and four examples of face images used in the face recognition experiments (familiar/unfamiliar and happy/angry) are shown in Figure 4.1.

Images were presented on the CRT monitor. The natural scene images (640 x 480 pixels) subtended vertically 1.4 deg. The face images (320 x 240 pixels) subtended vertically 0.7 deg and therefore a normal subject would have its maximum contrast sensitivity (CSF) at about 3.5 cycles/face and a theoretical limiting resolution larger than 28 cycles/face.

4.2.5 Experimental procedure and Psychophysical measurements

The measurements were performed with subject's natural pupil (which ranged between 4.3 and 6.0 mm; a 6 mm artificial pupil was placed to avoid effective pupils larger than this diameter) and each experiment was conducted in one session for each subject, lasting around two hours. Experiments involving the three visual tests described below (subjective image sharpness assessment, familiar face recognition and facial expression recognition) were performed in the same session for

Figure 4.1: Examples of natural scenes from the subjective image sharpness assessment experiment and examples of facial images from the familiar face and facial expression recognition experiments.

each subject. Each test was only performed once to avoid learning bias.

Subjective Image Sharpness Assessment Experiment The Subjective Image Sharpness Assessment Experiment consisted on a two Alternative Forced Choice test. Thirty-four natural images were presented to the subject. On each trial, both an AO-corrected and a natural image were presented (with the appropriate best spherical refractive error correction controlled with the Badal system), in a randomized order. There was no adaptation time to gray scale at the beginning. The image was presented during 3 s in both conditions (AO and noAO), without any grayscale screen in between, and then disappeared into a black screen until the subject make his/her choice. The subject's task was to choose the one of two that appeared sharper to him/her.

Familiar face recognition experiment The familiar face recognition involved presentation of 33 faces (15 familiar and 18 unfamiliar faces) to the subjects. The images were presented randomly viewed with the subject's natural aberrations and with the AO correction (with the appropriated best spherical refractive error correction). Each image was presented during 3 s in one condition and each image appeared twice throughout the experiment (for both AO and noAO conditions). There was no adaptation time to gray scale before the test, and between images there was a black screen during which the subject made his/her choice. The subject provided a graded response from 1-6 for their level of confidence in recognizing the face (1/6 for definitely familiar/unfamiliar, 2/5 for probably familiar/unfamiliar, 3/4 for a lower level of confidence on the face being familiar/unfamiliar).

Facial expression recognition experiment Fifty-two different facial expressions (26 happy and 26 angry faces) were randomly presented to the subjects, half of the images viewed under the subject's natural aberrations and the other half with the AO-correction (with the appropriated best spherical refractive error correction in each case). The image presentation lasted 3 s. Each image was presented only in one condition (AO or noAO) during the experiment. There was no adaptation time to gray scale before the test and there was a black screen between two images

during which the subject made his/her choice. The subject's choices were similar to those in the face recognition experiment, providing a graded response from 1-6 (1/6 for definitely happy/angry, 2/5 for probably happy/angry, 3/4 for a lower level of confidence on the face being happy/angry).

4.2.6 Data analysis

Aberrations

Wave aberrations were fitted by 7^{th} order Zernike polynomial expansions. Tilt and residual defocus term in the Zernike polynomial expansion were set to zero. Optical quality was evaluated in terms of RMS wavefront error (excluding tilt and defocus) and Strehl ratio.

Subjective image sharpness assessment experiment

Results of subjective image sharpness assessment were analysed as percentage of images considered sharper with and without AO correction and presented for each subject.

Face and facial expression recognition

Results of face (familiar and expression) recognition were analysed in terms of the area under Receiver Operating Characteristic (ROC) curves, for the two conditions (natural and AO-corrected aberrations) where subjects have to give a score between 1 and 6 depending on their level of confidence (1 if he/she is confident that the face was familiar – or happy - and 6 if he/she is confident that the face was unfamiliar/angry).

ROC curves: Cumulative probabilities. The ROC curves were generated using the subject's confidence ratings to calculate the probabilities of identifying a familiar face as familiar (p(familiar $\|$ familiar)) (True Positive) and an unfamiliar face as familiar (p(unfamiliar $\|$ familiar)) (False Positive). These probabilities were calculated as the fraction of faces identified with a certain confidence rating. For the first point of the ROC curve, the fraction of familiar faces receiving the rating 1 was plotted against the fraction of unfamiliar faces receiving the same rating. The following points of the curve were calculated as the cumulative fraction of the subsequent ratings. Therefore the ROC curves represent the True Positive Fraction versus False Positive Fraction [Metz, 1978, 2006, 2008], i.e. the probability of correctly identifying a face as familiar versus the probability of incorrectly identifying an unfamiliar face as familiar. The same analysis is performed for happy/angry faces.

Area under the ROC curves. The area under the ROC curves (Au_ROC) was measured with a trapezoidal method using the raw data.

Perfect performance corresponds to an Au_ROC=1. Inability to recognize any face or expression, i.e. completely arbitrary responses, will produce Au_ROC=0.5.

For some calculations and illustration purposes we subtract the offset, and defined Au_ROC' =Au_ROC-0.5. The analysis was performed separately for images viewed through natural aberrations and AO-corrected aberrations. The area under ROC curves was taken as a measure of recognition in each condition.

Statistical analysis. The areas under the ROC curves in both conditions, Au_ROC_noAO and Au_ROC_AO, were statistically compared. For both recognition experiments, the statistical analysis was based on the Standard Error (SE) of the difference between Au_ROC_noAO and Au_ROC_AO and follows the procedures of Hanley and McNeil [1982, 1983], which is similar to Wilcoxon (or Mann-Whitney).

As the familiar face recognition experiment was conducted by presenting the images twice throughout the experiment (with both conditions, noAO and AO), the correlation between Au_ROC_noAO and Au_ROC_AO was taking into account, performing a Correlated ROC Analysis as described by Hanley and McNeil [1983]. In the facial expression recognition experiment we presented images only once (with either one or the other condition, noAO or AO). No correlation existed between Au_ROC_noAO and Au_ROC_AO and therefore we applied a standard bivariate statistical analysis to calculate the Standard Error (SE).

To calculate the SE of one ROC curve, we used equation 4.1, from previous literature [Hanley and McNeil, 1982]: For more comprehension of the long equation, we annoted the following notations: A=Au_ROC=Area Under ROC curve

$$SE = \sqrt{\frac{A(1-A) + (n_2 - 1)(Q_1 - A^2) + (n_1 - 1)(Q_2 - A^2)}{n_1 n_2}} \tag{4.1}$$

where n_1 is the number of unfamiliar/angry faces (in the familiar face and facial expression recognition, respectively), n_2 is the number of familiar/happy faces (in the familiar face and facial expression recognition, respectively) Q_1 and Q_2 calculated as equation 4.2 and 4.3(3)

$$Q_1 = \frac{A}{2 - A} \tag{4.2}$$

$$Q_2 = \frac{2A^2}{1 + A} \tag{4.3}$$

We calculated the standard error of the difference (SE (AnoAO – AAO)), annotated SE(diff) in the equations 4.4 for the facial expression recognition experiment (where different set of images were used in the two conditions AO, noAO, standard bivariate statistical analysis) and 4.5 for familiar face recognition where the same sets of images were used in both conditions and where Au_ROC_AO and Au_ROC_noAO are likely to be correlated (Correlated ROC Analysis).

$$SE(diff) = \sqrt{SE^2\left(A_{noAO}\right) + SE^2\left(A_{AO}\right)} \tag{4.4}$$

$$SE(diff) = \sqrt{SE^2\left(A_{noAO}\right) + SE^2\left(A_{AO}\right) - 2rSE\left(A_{noAO}\right)SE\left(A_{AO}\right)} \tag{4.5}$$

where r is a quantity representing the correlation introduced between the two areas by studying the same sample of faces [Hanley and McNeil, 1983].

Once we have the standard error of the difference in areas, we can calculate the statistic z using equation 4.6.

$$z = \frac{A_{noAO} - A_{AO}}{SE(diff)} \tag{4.6}$$

If z is above a critical level, we accept that the difference between the two ROC curves is significant. Typically, for a confidence level of 95% the critical level is set at 1.96, which correspond to a type I error probability (p-value, two tails) of 0.05 as a criterion for a significant difference.

Potential improvements in performance were analysed in terms of ratios and differences of Au_ROC' (AO vs noAO) (annoted A'$_{noAO}$ and A'$_{AO}$), and also in terms of Gain. Gain was defined as the actual improvement normalized to the potential maximum improvement, as expressed by equation 4.7.

$$z = \frac{A'_{noAO} - A'_{AO}}{0.5 - A'_{noAO}} \tag{4.7}$$

4.3 Results

4.3.1 Best corrected ocular aberrations

Figure 4.2 shows RMS wavefront error (excluding tilt and defocus) for all seventeen subjects of the study before and after AO-correction of aberrations. Data are for 5 mm pupil diameters, except for subject S8 that had a 4.3 mm pupil diameter. Subject S1 performed the measurements wearing her soft contact lenses. On average, RMS (excluding tilts and defocus) decreased from 0.366±0.154 to 0.101±0.055 μm, with an average correction of 72±7 %. The estimated RMS excluding tilts, defocus and astigmatism was 0.244±0.113 μm.

4.3.2 Subjective image sharpness assessment Experiment

Figure 4.3 shows the percentage of images considered sharper with and without AO by each subject. On average, subjects considered sharper 84±14% of images viewed with AO.

We explored potential correlations between the subjective image sharpness assessment and the amount of corrected aberrations. Figure 4.5 shows the correlation plots and corresponding regression lines between the percentage of images considered sharper with AO-correction and the optical quality improvement in terms of RMS (Fig. 4.4 A) or Strehl ratio at best focus (Fig. 4.4 B) for a 5 mm pupil (4.3 mm pupil for S8). We found a significant correlation between the percentage of images considered sharper with AO and the amount of corrected aberrations in both cases (R=-0.7, p<0.002 for RMS and R=0.5, p<0.05 for Strehl ratio).

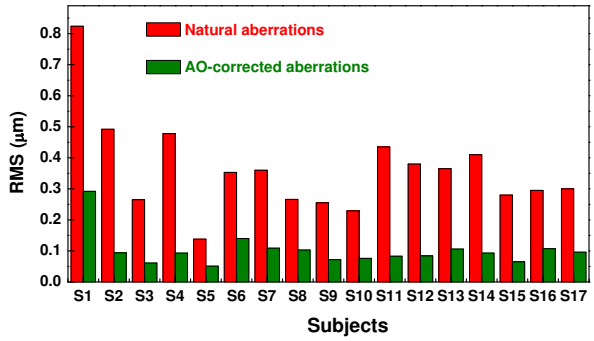

Figure 4.2: RMS wavefront error (excluding tilt and defocus) for all seventeen subjects before and after AO-correction. Data are for 5 mm pupil diameters (except for S8, who had a 4.3 mm pupil diameter). (Reproduced from Sawides et al. [2010a]).

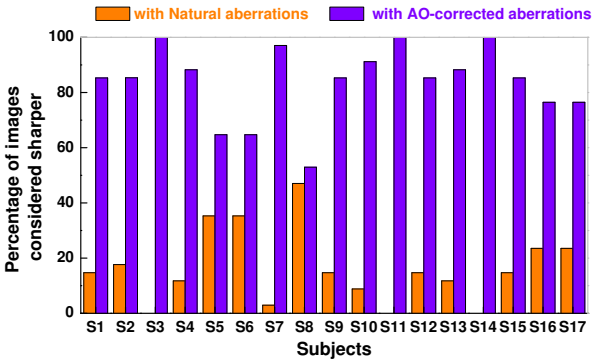

Figure 4.3: Percentage of images considered sharper with or without AO for each subject. (Reproduced from Sawides et al. [2010a]).

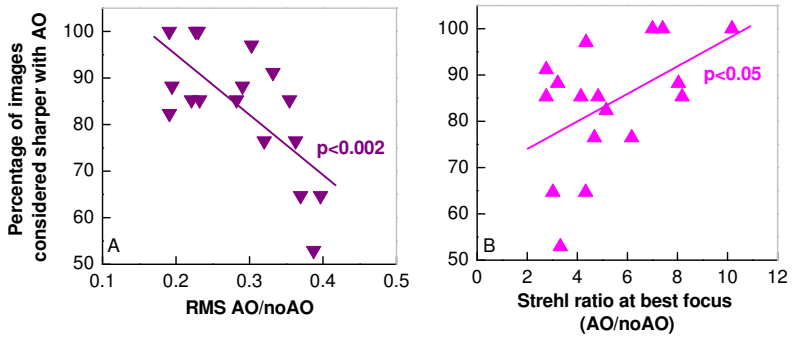

Figure 4.4: Correlation between the percentage of images considered sharper with AO and the optical quality improvement in terms of RMS (A) or Strehl ratio at best focus (B) for a 5 mm pupil (4.3 mm pupil for S8). (Reproduced from Sawides et al. [2010a]).

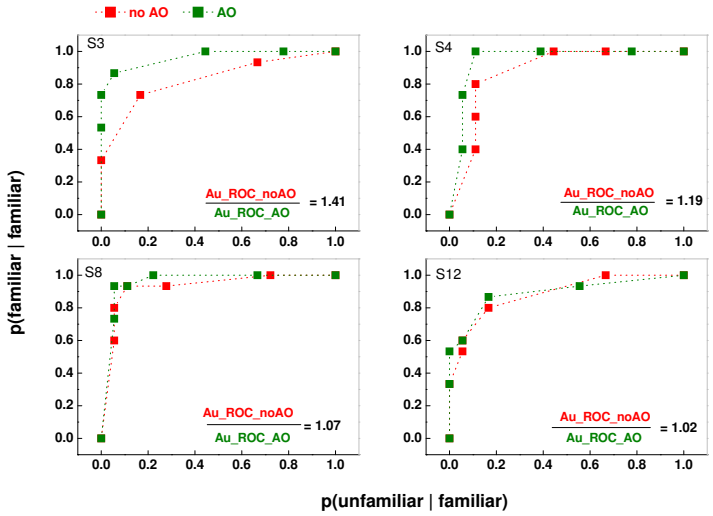

Figure 4.5: Examples of ROC curves, probability of correctly identifying a face as familiar versus the probability of incorrectly identifying an unfamiliar face as familiar, for four subjects. The inset shows the ratio of the area under the curves. (Reproduced from Sawides et al. [2010a]).

This indicates that the subjects who experienced larger improvement in their optics considered sharper a larger number of images viewed under Adaptive-Optics correction than under natural aberrations.

4.3.3 Familiar face recognition

Au_ROC_noAO ranged from 0.69 to 0.98 and Au_ROC_AO from 0.74 to 1.0 across subjects. Figure 4.5 shows an example of Response Operating Characteristic (ROC) curves, for four representative subjects. In terms of area under ROC, although the overall performance is very different, we observe an improvement in familiar face recognition with AO in all four subjects.

As Au_ROC=0.5 corresponds to arbitrary responses, an offset of 0.5 was subtracted from the computed areas. Au_ROC' then correspond to the area under ROC without the 0.5 offset. Figure 4.6 A shows the change in the areas under ROC curves, under natural and AO-corrected aberrations for the twelve subjects that participated in the test (after the 0.5 offset subtraction). Except for one subject (S7, with Au_ROC' ratio of 0.98), there is systematic increase in the area under ROC curve with AO correction. On average, Au_ROC' increased by 1.13±0.12 with correction. A paired t-test showed a statistical significant difference between the ROC curves under natural and AO-corrected aberrations across all subjects (p=0.0027).

Statistical calculation using equation 4.6 showed a statistically significant difference between the two areas under ROC curves (AO-corrected and natural aber-

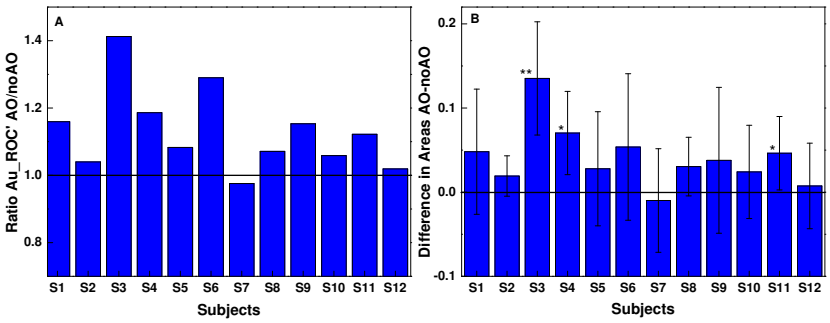

Figure 4.6: A. Ratio of the area under ROC (AO/noAO) for familiar face recognition (after 0.5 offset subtraction). B. Difference in areas under ROC (AO−natural aberrations) for familiar face recognition. Error bars correspond to the Standard Error (SE) calculated with the statistical analysis. Double stars indicate a significant difference with a 95% level of confidence and single stars for a level of confidence higher than 70%. (Reproduced from Sawides et al. [2010a]).

ration), with a level of confidence of 95% in one eye (S3) and two other eyes with a level of confidence more than 70%. Figure 4.6 B shows the difference in the areas under ROC curves for each subject, their standard errors and the cases where the difference is statistically significant.

4.3.4 Facial expression recognition

Figure 4.7 shows examples of ROCs representing the probability to recognize a happy face when it is happy, for four subjects, the same as in the familiar face recognition experiment. We did not see a systematic improvement with the AO-correction. Au_ROC_noAO ranged from 0.85 to 1.0 and Au_ROC_AO ranged from 0.86 to 1.0 across all subjects.

Figure 4.8 A shows the change in the areas under the ROC curves, under natural and AO-corrected aberrations for all subjects (after the 0.5-offset subtraction). In 9 out of 17 subjects AO correction improved facial expression recognition, but in 8 subjects the ratio was below 1. On average, Au_ROC' ratio was 1.01±0.11. A paired t-test did not show a statistically significant difference between the areas under ROC curves, under natural and AO-corrected aberrations across subjects (p-value=0.8315).

Statistical calculation using equation 4.6 did not show any statistically significant difference between the two areas under ROC curves (AO corrected and natural aberration), with a level of confidence of 95% but a statistically significant difference with a level of confidence higher than 70% for three subjects. Figure 4.8 B shows the difference in the areas for each subject, their standard errors and the cases where the difference is statistically significant.

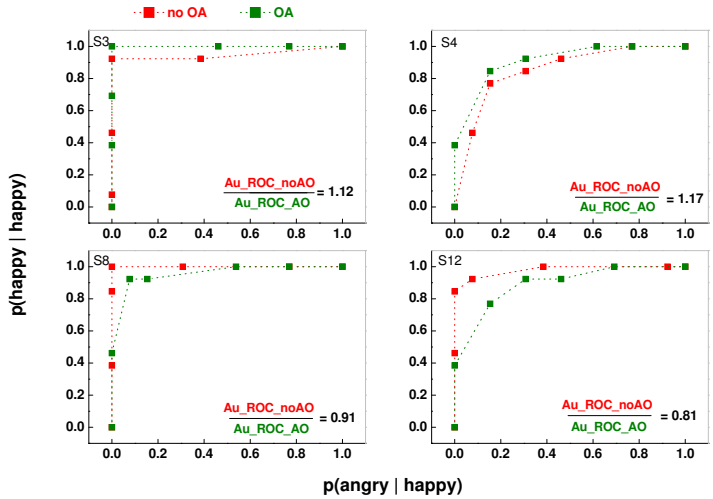

Figure 4.7: Example of ROC curves, probability of correctly identifying a happy facial expression versus the probability of incorrectly identifying an angry expression as a happy one, for four patients. The inset shows the ratio of the area under the curves. (Reproduced from Sawides et al. [2010a]).

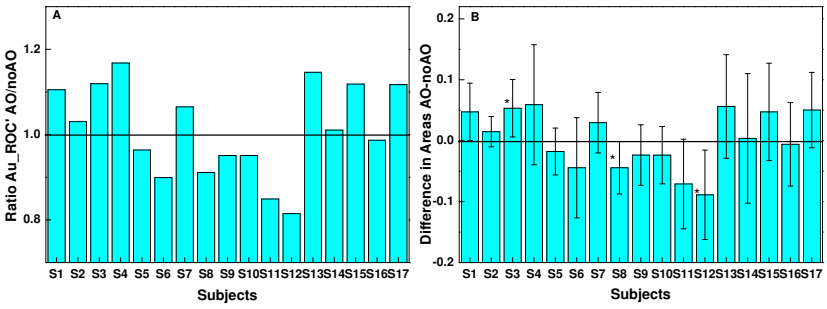

Figure 4.8: A. Ratio of the area under ROC (with AO/natural aberrations) for facial expression recognition (after 0.5 offset subtraction). B. Difference in areas under ROC (AO - natural aberrations) for familiar face recognition and errors bar correspond to the Standard Error (SE) calculated with the statistical analysis. Single stars indicate a significant difference with a level of confidence higher than 70%. (Reproduced from Sawides et al. [2010a]).

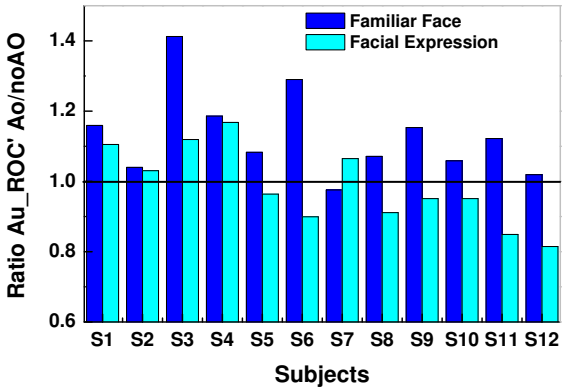

Figure 4.9: Comparing familiar face and facial expression recognition in terms of changes in the area under ROC' with AO correction. (Reproduced from Sawides et al. [2010a]).

4.3.5 Comparison of familiar face and facial expression recognition

Figure 4.9 compares the ratio of the areas under ROCs' for familiar and face expression recognition in all subjects that performed both experiments. Except for subject S7 the improvement in performance for familiar face recognition when the aberrations where corrected was systematically higher than the improvement of facial expression recognition. The difference varied across individuals and the increase in performance in the familiar face recognition task was uncorrelated with the change in performance in the facial expression recognition ($p>0.8$).

We correlated positive gain (equation 4.7) with optical quality improvement in terms of RMS (AO/noAO) (for 5 mm pupil, and 4.3 mm pupil for S8), as shown in Figure 4.10. We found a nearly statistically significant correlation ($p=0.09$) for familiar face recognition. For facial expression recognition, the gain with AO-correction was always lower than 10% and did not show any correlation with the optical quality improvement in terms of RMS (AO/noAO).

4.4 Discussion

We found that correcting aberrations increases dramatically the subjective impression of sharpness in natural images. On average, subjects identified as sharper more than 80% of the images (up to 100% of the images for some subjects) viewed under AO-corrected aberrations. We did not observe that some image category (i.e. artificial environments or natural landscapes) was more consistently identified as sharper with AO-correction than others. The fact that there is a significant correlation between the percentage of images considered sharper with AO- correction and the amount of corrected aberrations (Fig. 4.4) indicates that the correction of aberrations effectively increases contrast and enhances high spatial frequencies

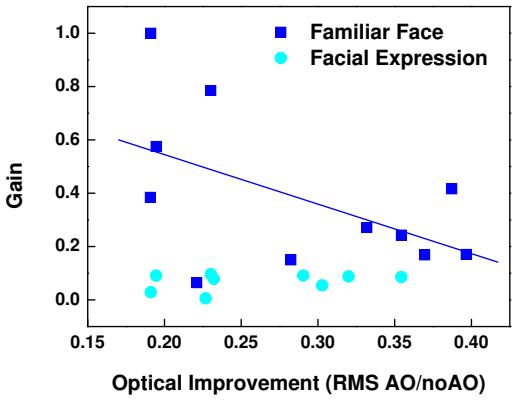

Figure 4.10: Correlation between Gain (defined in equation 4.7) and optical quality improvement (in terms of RMS (AO/noAO) for 5 mm pupil (4.3 mm pupil for S8) for familiar face and facial expression recognition tasks. (Reproduced from Sawides et al. [2010a]).

that may not be visible in the presence of aberrations.

Correcting aberrations improved slightly (but systematically in all subjects but one) visual performance of real-life visual tasks such as familiar face recognition. However, although AO-correction had a positive impact on facial expression recognition in some subjects, on average performance on this task did not improve. Correction of HOA will likely produce a contrast enhancement of the critical frequency band for face recognition (4-8 c/face [Peli et al., 1991]; 8-16 c/face [Näsänen, 1999; Gold et al., 1999]). A frequency band of 4-8 c/face corresponds to a spatial frequency range of 6-11 c/deg in our setting, and 8-16 c/face to 11-23 c/deg. We estimated that the AO-correction resulted in an increase of x 1.9 in the volume under the MTF in the lower frequency band, and an increase by a factor of x 2.7 in the higher frequency band, on average across subjects. The increase in contrast and in the spatial frequency content of the image may have made it easier for the subject to recognize the scene. Moreover, we found that gain in the familiar face recognition were correlated with the optical correction (Fig. 4.10) suggests that subjects use contrast increase and spatial resolution as cues. The differences between the responses to the familiar face and facial expression recognition tasks likely arise from fundamental differences in the neural pathways [Bruce and Young, 1986; Young et al., 1986], as well as the different facial features critical in each task, even if both tasks are accomplished since a very early age [Nelson, 2001; Grossmann and Vaish, 2008; Erickson and Schulkin, 2003]. Familiar face recognition is a more difficult task than facial expression, as indicated by its systematically lower AU_ROCs.

Studies using functional magnetic resonance imaging (fMRI) in humans have shown that neural responses to repeating the same face identity were greater with intact or high-spatial-frequency face stimuli than with low-frequency faces, regard-

less of emotional expression. However, responses to fearful expressions were greater for intact or low-frequency faces than for high-frequency faces [Vuilleumier et al., 2003]. These results are consistent with our finding that correction of HOA has a higher positive impact on recognition of familiar faces than on recognition of emotional expressions, a task that can be successfully undertaken. Very likely, a higher spatial frequency range is used to recognize a familiar face than a facial expression. Debates are open to determine these critical spatial frequencies.

The practical relevance of these improvement remains to be evaluated to deem whether correction of higher order aberrations in normal subjects is sufficiently important from a clinical point of view. However, our results indicate that a static correction of aberrations is very significantly appreciated by the subject and may result in improvements of some daily life activities (such as recognition of faces). While we cannot exclude effects of neural adaptation [Webster et al., 2002; Webster and MacLeod, 2011] to the natural aberrations of the eye, those are potentially secondary in our results, as we did not find a trend toward better performance with the natural aberrations of the eye with respect to the AO-corrected optics.

4.5 Conclusions

Correcting ocular aberrations produced an improvement in visual performance. The subjective impression of sharpness increased significantly when high order aberrations were corrected by means of Adaptive Optics.

The improvement of familiar recognition was systematic in all but one subject. Correcting high order aberrations did not improve systematically facial expression recognition (8 subjects out of 17 show a lower performance in recognizing facial expression at correcting high order aberrations).

the studies presented in chapters 3 and 4 reveal an improvement of visual performance when correcting aberrations. A question that arises is to which extend neural adaptation to the subjects own aberrations, as to the new state of corrected aberrations play a role in visual perception. The possibility of undertaking psychophysical experiments without the retinal blur produced by optical aberrations allows exploring this fundamental question, as the effects will be dominated purely by neural factors.

5

Short-term adaptation to Astigmatic Blur

Visual perception is constantly calibrated by adaptation processes that can alter the perception of blur in natural scenes. Blur is inherent in the retinal image because of low and high order aberrations of the eye. In the Current chapter, we investigate whether adaptation effects could arise from actual sphero-cylindrical refractive errors and can be selective for different axis of astigmatism, by testing aftereffects in images simulating second-order astigmatism.

This chapter is based on the paper by Sawides et al. "Adaptation to astigmatic blur" Journal of Vision, 2010. The co-authors of the study are Susana Marcos, Sowmya Ravikumar, Larry Thibos, Arthur Bradley and Michael A. Webster. All the experiments have been performed at Prof. Michael A. Webster's Lab, in the University of Nevada, Reno, except for the control experiment, which has been done at the Institute of Optics in Madrid with the Adaptive Optics system.

The authors of this thesis generated the set of images for the experimental procedure, analysed the data and implemented the experimental procedure of the control experiment performed at the Institute of Optics in Madrid, performed the measurement on subjects, collected and analysed the data.

This work was also presented at the Vision Science Society (VSS) Annual meeting (May 2009) in Naples, Florida, USA

5.1 Introduction

Clinically it is well known that observers require time to adjust to progressive spectacles that induce significant amounts of astigmatism and field distortions (e.g. Adams et al. [2001]), or to large refractive corrections for astigmatism which are consequently introduced in stages. Long-term adaptation to astigmatism was also suggested by Georgeson and Sullivan [1975] on contrast constancy. The perceived contrast of suprathreshold gratings is relatively invariant with spatial frequency and thus compensated for the sensitivity limits revealed at threshold by the contrast sensitivity function. Perceived contrast moreover showed compensation for the orientation-selective sensitivity losses in astigmatic observers [Georgeson and Sullivan, 1975]. Finally, adjustments to astigmatism have also been described for individuals who wore cylindrical lenses for prolonged periods [Anstis, 2002; Yehezkel et al., 2005].

Orientation and spatial frequency tuning are among the most prominent features of cortical receptive fields, which are reflected in the orientation and spatial frequency selectivity of short-term spatial adaptation [Blakemore and Campbell, 1969b; Bradley et al., 1988]. It is plausible, therefore, that short-term blur adaptation may have an orientation bias if image blur is produced by astigmatism. In the current chapter, we examined whether observers can adapt to astigmatic blur at the rapid timescales characteristic of pattern-selective adaptation.

Optical blurring can change a number of image attributes, including the salience of texture at different spatial scales, a reduced resolution of image features or increasing "fuzziness" of edges, phase shifts and reversals, and the perceived shape of features. For example, Figure 5.2 shows an image of Frits Zernike (from Wikipedia), who developed a mathematical representation for describing optical aberrations. The blurred versions correspond to the lower order aberrations of spherical defocus, and either positive (i.e. horizontal) or negative (i.e. vertical) astigmatism, all with a constant blur strength of 0.76 dioptres [Thibos et al., 1997; Raasch, 1995], (5.3). The blurred images have the characteristic appearance of low pass filtered images, but notably the blurred images also look like different individuals. These apparent shape changes could thus induce aftereffects in the images because of adaptation to the perceived differences in the shapes, just as adaptation to different faces induces aftereffects in face perception [Webster and Maclin, 1999]. Spatial distortions with astigmatism are well known in the El Greco fallacy [Anstis, 2002], as shown in Figure 5.1. In El Greco's paintings the figures often appear stretched vertically, and this has been attributed to distortions in his retinal image from astigmatism. The fallacy is that this distortion would alter the appearance of both the subject and their portrait, and thus could not account for a failure to preserve the same physical dimensions in the paintings. In one sense, however, there is a fallacy to this fallacy. The PSF is a function of visual angle while the visual angle of the subject varies with distance. If El Greco had astigmatism – and was not compensating for it – then a subject farther away than his canvas could in fact appear more distorted because they would subtend a smaller angle.

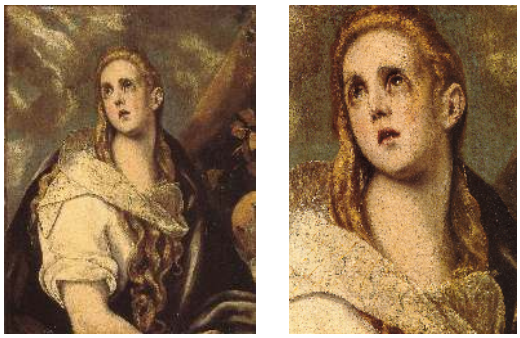

Figure 5.1: El Greco's painting. The Penitent Magdalene (and detail). 1578-Spain.

More generally, equally-blurred large and small images are not scaled versions of each other. In contrast, magnifying a blurred image preserves the same perceived "shape" by rescaling the image luminance profile by a constant, but results in images that appear to have greater blur (because the effective PSF is also magnified). Put another way, blur has an equal effect on the spectrum of differently sized images in retinocentric coordinates (cycles per degree), while magnification has a constant effect across size in object-centric coordinates (cycles per object). This raises the question of whether adaptation to astigmatic blur might reflect response changes at visual levels that are more closely tied to object-centric vs. retinocentric image characteristics.

Figural aftereffects can show strong transfer over a size change. For example, adapting to distortions in a face at one size can strongly affect the appearance of faces viewed at different sizes [Zhao and Chubb, 2001], and in fact this size change is often included as a control to try to reduce the contribution of "low-level" pattern adaptation to face aftereffects. Watson and Clifford [2003] tested how figural aftereffects for faces depend on the relative orientation of the adapting and test images. Consider a face blurred along the axis of the head by vertical blur (negative astigmatism) but tilted at 135 deg (see Figure 5.8, below). The blurring is along the negative diagonal of the image plane, but along the vertical axis of the face. If adaptation is specific to the object orientation, and not retinal orientation, then a test object tilted along the positive diagonal should show a negative aftereffect consistent with the same object axis but now along the orthogonal retinal axis. Conversely, if the blurring biases appearance along the axis of the blur independent of the objects, then the aftereffect should appear reversed. That is, blur along the horizontal axis of the target head should appear increased following adaptation to vertical head axis blur in a 90 degrees rotated adapting head.

Examining the effect of the magnitude of adapting blur can be of interest in order to assess 1) whether there is a range of blur levels that might be compensated completely by short-term adaptation; and 2) whether the perceived neutral point can also be recalibrated for very strong levels of blur. Corresponding measurements for defocus have not been assessed, but Webster et al. [2001] found that for

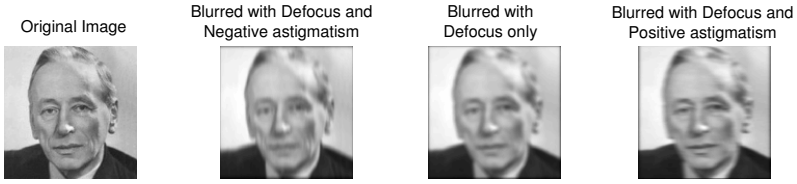

Figure 5.2: Convolution of an image of Frits Zernike with the PSF of wavefronts containing the low order aberrations of astigmatism and defocus. A negative astigmatism at 0/90 deg produces blur with a vertical orientation bias; a positive astigmatism produces a horizontal bias. Equivalent blur from defocus only produces isotropic blurring.

Gaussian blur the aftereffects were non-monotonic with blur magnitude. That is, high levels of Gaussian blur produced weaker aftereffects in subjective focus, possibly because these blur levels strongly reduced the overall contrast of the adapting image or the contrast within the spatial frequency range that might be important for judging image focus.

In this chapter, we conducted 5 experiments to investigate the perceptual consequences of short-term adaptation to simulated astigmatic refractive errors. Specifically, observers were adapted to physically blurred images that were convolved with PSFs corresponding to different axes and magnitudes of astigmatism in order to simulate the effects of optical blur (and differ from previous studies that have instead blurred the image optically). Control experiments, in which the adaptation effects were instead assessed under correction with Adaptive Optics for the observer's natural aberrations where carried out to ensure that the principal effects of the adaptation to image blur were not biased by further degradation in the image imposed by uncorrected high order aberrations of the eye or differences in pupil size.

We investigate how the visual system adjusts after brief exposure to blur produced by low order aberrations (i.e. defocus and astigmatism), in particular, we assessed whether adaptation could be selective for different axes of astigmatism; we determined if the adaptation to astigmatic blur was a simple orientation and spatial-frequency specific contrast aftereffect, or if it reflects a form of figural aftereffect associated with the apparent structural changes seen in the images and finally we examined the effect of the magnitude of adapting blur. For all of the experiments, we used a task that directly measured the perceived orientation bias in the images, rather than measuring perceived sharpness as in previous studies.

5.2 Methods

All experiments were designed to test whether prior adaptation to images blurred with horizontal or vertical astigmatism would induce a change in the image blur that appeared isotropically blurred. In order to evaluate such a bias, we employed

a series of blurred images each with the same level of blur, but with differing levels of orientation bias (e.g. see Figures 5.4 and 5.5). Based upon the observations made with meridionally uniform (isotropic) blur [Webster et al., 2002], we hypothesize that orientation-selective blur adaptation will lead to a relative decrease in perceived blur along the adapting orientation. Thus subsequently viewed spherical defocus will appear to have less blur at the adapting orientation and therefore relatively greater blur along orientations perpendicular to the adapting orientation. In order to test this hypothesis, we developed a method for varying the meridional bias in blur while keeping the overall blur level constant, and thus using these stimuli we can identify any orientation bias in the stimuli that appear to exhibit isotropic blur. The experiments differ in using different sets of adapting and test images to characterize the basis for the aftereffects.

5.2.1 Subjects

We performed five different experiments at the University in Nevada, Reno. The observers included two of the authors and 4 students who were unaware of the aims of the experiment. Two or three subjects were tested in each experiment, with author LS (labelled S1) participating in all conditions and MW (labelled S2) and all but the last experiment confirmed on a naive observer. Experiment 1 was repeated at the Institute of Optics, in Madrid, Spain on 4 subjects, correcting low and high order aberrations with an Adaptive Optics system. Subjects in this experiments included 2 of the authors (LS labelled S1 and SM labelled S7 in test control) and 2 naïve observers (S8 and S9). All subjects had normal vision as assessed by standard tests, low astigmatism and corrected spherical refractive errors.

5.2.2 Apparatus and stimuli

Five different experiments were conducted at the University of Nevada. The images were displayed on a gamma-corrected Sony 500 PS monitor controlled by a Cambridge Research Systems VSG graphics card (Cambridge Research System, UK). The images subtended 4 deg but were displayed through a 3.5 deg window to allow their spatial position to be jittered slightly during adaptation in order to avoid local light adaptation. All images had a mean luminance of 15 cd/m^2 and were shown against a 15 x 10 deg uniform gray background with the same luminance. Observers viewed the display binocularly from a distance of 150 cm in an otherwise dark room. All images were 8-bit grayscale with a size of 256 x 256 pixels. Different sets of images included: 1) 3 samples of filtered noise, with a 1/f amplitude spectrum and rms contrast of 0.35; 2) 4 close-ups of natural textures, taken from relatively homogenous images of foliage (from Webster and Miyahara [1997]); and 3) 4 natural objects or scenes, which included outdoor scenes and Zernike's image. Some of the latter scenes had been used the previous psychophysical experiments of the effect of Adaptive Optics correction of ocular aberrations on

Figure 5.3: Images of noises, textures and natural scenes used in the experiments.

subjective image sharpness assessment (see chapter 4). The images are shown in Figure 5.3.

As a control experiment, an alternative version of Experiment 1 was conducted at the Institute of Optics (CSIC), in Madrid. In this case, we used the Adaptive Optics system to compensate for the subject's astigmatism and high order aberrations. An artificial pupil of 6 mm was placed onto the AO-system. The stimuli were presented on the gamma-corrected CRT monitor through the Badal and AO-mirror correction. Stimulus display was controlled by the psychophysical platform,(ViSaGe, Cambridge Research System, UK). The images (480 x 480 pixels) subtended 1.98 deg and included an image of perlin noise and three natural images (of houses, tulips or a face). The images were again jittered in time during adaptation in order to avoid local light adaptation.

5.2.3 Images blurred with astigmatism and defocus

In all the experiments, custom algorithms written in Matlab were used to obtain simulated images blurred with astigmatism and defocus; Using Fourier Optics, aberrated images were computed as the convolution of the original image (object) and the PSF corresponding to a wave aberration with all Zernike terms set to zero except for C_2^2 (astigmatism at 0/90 deg) and C_2^0 (defocus). In most cases the astigmatic term was varied in the wave aberration from -0.3 to 0.3 microns in 5 nm steps, and defocus was varied from 0.127 to 0.247 μm. For Experiment 5 we instead varied the astigmatism over a larger range, from -0.6 to 0.6 microns (with defocus varied from 0.374 to 0.566 μm) in order to test how the aftereffects varied with blur strength. The image simulations were calculated for a 3 mm pupil, assuming

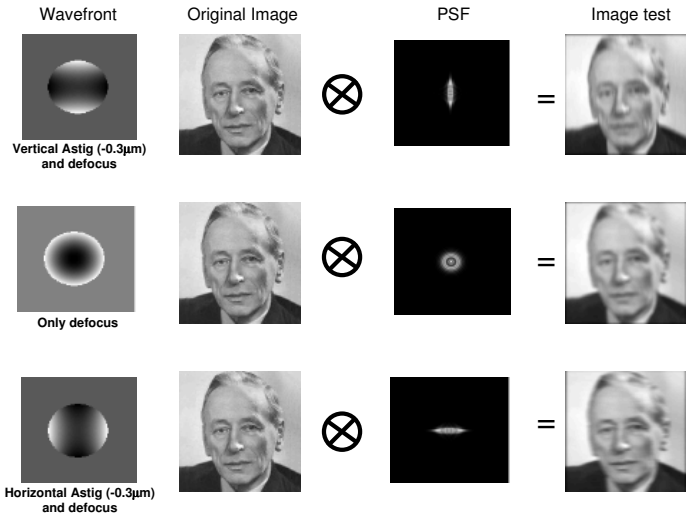

Figure 5.4: Convolution of an original image (Face) and the PSF of the wavefront containing the low order aberrations of astigmatism and defocus.

monochromatic aberrations only and a 500-nm wavelength and a viewing angle of 4 deg. Each combination of astigmatism and defocus produced the same amount of blur strength (B=0.76 D, or B=1.74 D for Experiment 5). We defined blur strength (B) by equation 5.1.

$$B^2 = M^2 + J_0^2 + J_{45}^2 \tag{5.1}$$

where M, J_0 and J_{45}, in dioptres, represent the equivalent defocus (M), the vertical/horizontal astigmatism (J_0) and oblique astigmatism (J_{45}) as defined by Thibos et al. [1997, 2002].

$$M = \frac{-4\sqrt{3}C_2^0}{r^2}; J_0 = \frac{-2\sqrt{6}C_2^2}{r^2}; J_{45} = \frac{-2\sqrt{6}C_2^{-2}}{r^2} \tag{5.2}$$

where r is the pupil radius in mm.

Thus, to keep the blur strength constant (and maintain the same amount of optical degradation in all test conditions, [Raasch, 1995; Schwendeman et al., 1997]), defocus was varied to satisfy the equation 5.3.

$$2(C_0^2)^2 + (C_2^{+2})^2 + (C_2^{-2})^2 = K \tag{5.3}$$

where, for astigmatism at 0/90 deg, C_2^{-2} was set to 0 and C_2^2 varied from -0.3 to 0.3 μm (and from -0.6 to 0.6 μm in Experiment 5).

Figure 5.4 shows an example of the convolution of an original image with the PSF for a wave aberration with vertical astigmatism, defocus and horizontal astigmatism, while Figure 5.5 shows how the appearance of the images varied with the magnitude of astigmatism. Larger amounts of negative astigmatism introduce more vertical blur in the image, while positive astigmatism introduces horizontal

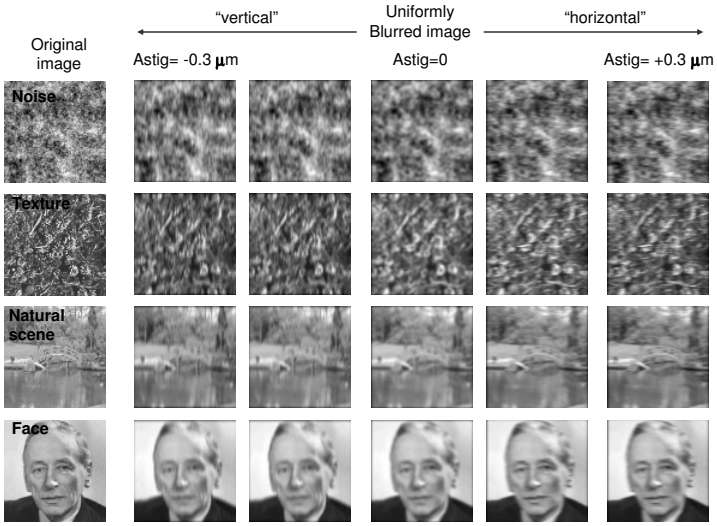

Figure 5.5: Examples of the images from the stimulus arrays formed by varying different combinations of astigmatism and defocus (keeping a constant blur strength B=0.76 D). Astig stands for Zernike coefficient C_2^2.

blur. The image blurred by adding only defocus in the wave aberration instead appears isotropically blurred. It is assumed that the angular subtense of the stimuli in the experiments lies within the isoplanatic area of the eye, and therefore the convolution is performed using a spatially invariant PSF. In the human eye the changes in astigmatism are small across the central 10 degrees [Atchison et al., 2006, 2003b]. However as a result the computationally blurred stimuli did not include the (small) astigmatic distortion produced when principal powers are unequal (i.e. meridional differences in magnification).

For the experiment performed in the AO system, the stimuli were generated using identical procedures. The astigmatism term (at 0/90 deg) varied from -1 to 1 micron in 10 nm steps and the defocus term varied from 0.693 to 0.990 microns, for a 1.98 ^{o} viewing angle and 6 mm pupil. Each combination of astigmatism and defocus produced the same amount of blur strength (B=0.76 D) as in the corresponding experiment under natural viewing.

5.2.4 Experimental procedure

Observers adapted during a 2-min exposure either to the gray field or to strong vertical (negative Zernike coefficient C_2^2) or horizontal (positive Zernike coefficient C_2^2) astigmatic blur. During adaptation the position of the adapting image was randomly varied every 100 msec over a range of 0.25 deg, though as noted the image was displayed within a window with constant borders. A test image was then displayed for 300 msec interleaved with 5 sec top-ups to the gray field or adapting image. The top-up and test intervals were separated by a 100 msec gray fields. The

subjects made a 2-alternative forced choice response to indicate the axis (vertical or horizontal) of the perceived blur. The level of astigmatic blur in the test images was varied with a staircase to estimate the perceived isotropic point, which was based on the mean of the last 12 reversals. Typically 4 repeated settings were made for each adapt and test condition with the order across conditions counterbalanced except for the AO-noAO correction experiment where 1 or 2 measurements were performed in each condition.

Protocols specific to each of 5 experiments were as follows:

Experiment 1: Astigmatic blur and orientation-selective blur aftereffects. We tested for the presence of an aftereffect from exposure to astigmatic blur and whether it was selective to the axis of the astigmatism for a wide range of images (see Figure 5.3). In each run, the adapt and test images were created from the same original stimulus. Subjects adapted to the image blurred with positive (horizontal) or negative (vertical) astigmatism corresponding to $\pm 0.3\,\mu$m, or to the equivalent blur from isotropic (spherical) defocus, and the blur level in the test image was then varied with the 2AFC staircase until the blur in the test image appeared isotropic. When the experiment was performed in the AO-system, the psychophysical paradigm was identical (with the adapting image blurred with positive or horizontal astigmatism corresponding to $\pm 1\,\mu$m) and performed under natural aberrations and under AO-correction of subject's aberrations.

Experiment 2: Selectivity of blur adaptation for the adapting images. In Experiment 2 we determined if the adaptation to astigmatism was specific to the adapting target (e.g. a face), or if its effect would generalize across different post-adaptation targets. This allowed us to test the extent to which observers might adapt to the attribute of blur independent of a specific target. To test how adaptation to blur in one image influences the appearance of a different test image, we compared the aftereffects of adaptation to a single adapting image on the appearance of the same image or 2 different images. An example is illustrated in Figure 5.6 where adaptation to blur in one image (pine needles, 1/f noise, and face) was tested on the same image or on the two images that were not shown during adaptation. For each adapting condition the aftereffects for the three test images were measured simultaneously with 3 randomly interleaved staircases during each adaptation sequence.

Experiment 3: Aftereffects dependent on local blur versus global shape In Experiment 3, we determined if the adaptation to astigmatism transfers across a change in image size. Tests of shape vs. blur aftereffects induced by astigmatic blur were based on a single image of a face (Zernike). A face was chosen because configural changes are particularly salient in face images. Blurred versions of the image were generated with the same amount of astigmatism and defocus as before, but for two different object sizes (2 deg image and 6 deg image in Figure 5.7). Although the blur had the same retinal size, the effect of this blur on small and large images produced differences in perceived shape ("Same blur and different shape"). To produce images with equivalent global shape, we instead magnified the blurred

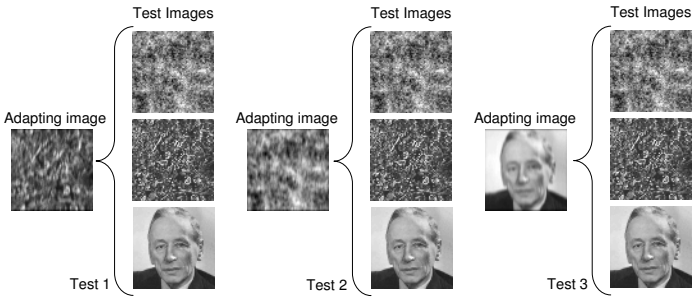

Figure 5.6: Example of conditions for measuring how adaptation to astigmatic blur in a single image affects perceived blur in the same or different images.

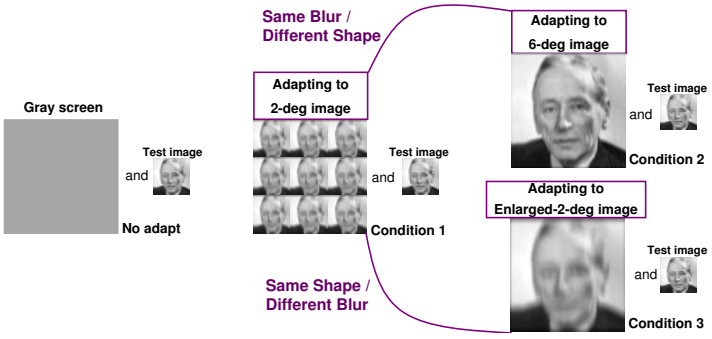

Figure 5.7: Adaptation to blur (here to vertical astigmatism) at different sizes. Test conditions 1 and 2 measure the aftereffects for images with different size but blurred with the same aberration, while conditions 1 and 3 use the same image at different magnification to measure the aftereffects for images that have the same shape but different levels of blur.

2 deg image to 6 deg (Enlarged-2-deg image in Figure 5.7). In this case the shape was preserved but the level of blur was increased 3-fold ("Same shape and different blur"). We then tested how adaptation to either image size affected the isotropic settings in the 2 deg image. Viewing distance was reduced to 106 cm, and the 2 deg images for adaptation were shown in a 3 by 3 matrix in order to stimulate the same retinal area as the 6 deg images (Figure 5.7).

Experiment 4: Blur adaptation and object orientation In Experiment 4, we determined if the adaptation to astigmatic blur was specific to retinocentric orientation or to the orientation of the objects. Adapting images were blurred as described above but were shown rotated 45 deg anticlockwise (adapt images). Aftereffects were then assessed in test images at the same orientation or tilted 45 deg clockwise (Figure 5.8). As in Experiment 3 these tests were conducted with the face image.

Experiment 5: Adaptation and blur strength In Experiment 5, we examined the effect of the magnitude of adapting blur by testing whether the astigmatic blur might also induce stronger shifts at moderate blur levels. In this case the

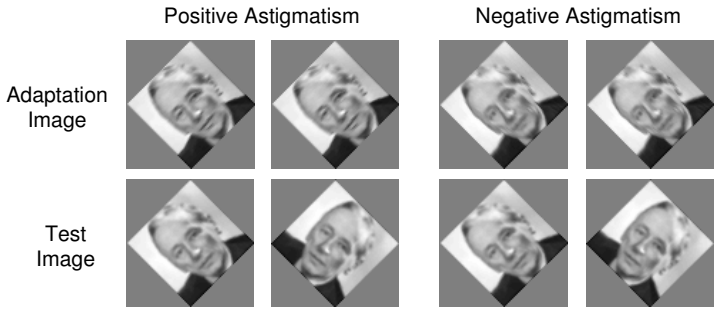

Figure 5.8: Conditions tested in experiment 4: Left: adaptation to positive astigmatism along the axis of the face and then tested at the same image orientation or rotated 90 deg. Right: adaptation to negative astigmatism along the image axis (positive and negative astigmatism correspond to horizontal or vertical astigmatism, respectively).

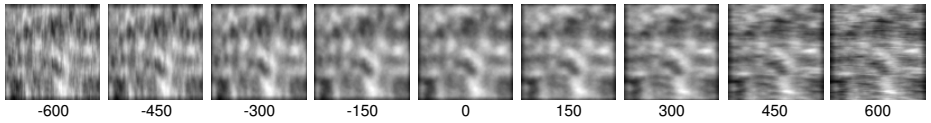

Figure 5.9: A noise image with the 9 different levels of astigmatism (in nm) used as adapting images.

stimulus was a single noise image with the astigmatic term varied over a larger range from -0.6 to 0.6 microns in 10 nm steps, and defocus varied from 0.374 to 0.566 microns. Each combination of astigmatism and defocus now produced a constant blur strength of 1.74 D. Adaptation was measured for a range of 9 different levels spanning the array (Figure 5.9).

5.3 Results

5.3.1 Experiment 1: Astigmatic blur and orientation-selective blur aftereffects

Adaptation to simulated blur through natural optics

As noted, in the first experiment, we tested for the presence of an aftereffect from astigmatic blur and whether it was selective for the axis of the astigmatism. Figure 5.10 shows the results for three observers. In Figure 5.10 A-C, each bar shows the perceived neutral (isotropic) point for a single image before adaptation (gray) or after adaptation to the image with negative (blue) or positive (purple) astigmatism. Adaptation effects were assessed by comparing the mean settings before or after adaptation with t-tests. For all subjects and for most images there are strong and significant shifts in the neutral point following adaptation, with

shifts in opposite directions for the different axes of astigmatism. In particular, consistent with our prediction, negative astigmatism (vertical blurring) caused the original isotropic image to appear horizontally blurred, and thus required a physical shift in the neutral point toward the adapting axis (negative in this case). Similarly, adaptation to the positive astigmatism induced a corresponding shift in the perceived isotropic point toward horizontal blur. To directly characterize the actual aftereffect, we plotted the difference between the pre- and post-adapt settings, on average across subjects (Fig. 5.10 D). For most images there are clear and opposite aftereffects following adaptation to the different axes. This indicates that adaptation to astigmatic blur induces strong and robust aftereffects that are selective for the actual form of the aberration.

Adaptation to simulated blur through corrected optics

Note again that for the conditions of Figure 5.10 observers viewed the images with their natural pupils and native correction, and thus the retinal image was not controlled for any degradation introduced by the individual observer's optics. However, because the effects of astigmatism were simulated directly on the image, these variations do not interact with the subject's pupil size or with their natural astigmatism, residual defocus or accommodation-related changes of focus. While the contribution of the subject's natural aberrations varies across observers, these variations are minor relative to the imposed astigmatism, and the additional blur introduced will be equal (within each individual) across the series of physically blurred images. Thus these uncontrolled observer differences should not affect the basic pattern of the aftereffects, though they might introduce baseline individual differences in the stimulus level that appears isotropic.

Nevertheless, to assess the potential contribution of the observer's own optics to the aftereffects induced by the simulated blur, a similar experiment was conducted using Adaptive Optics to compensate for the subject's aberrations. In this case measurements were performed for either natural or corrected aberrations and controlled pupil size with a 6 mm artificial pupil (to limit the subject's pupil size which ranged between 5.6 and 6.0 mm).

Figure 5.11 shows the shift in the perceived neutral point after adaptation to positive (horizontal, in blue) or negative (vertical, in purple) astigmatism, for the 4 observers (A-D) and on average across subjects (E). The darker bars (left in each pair) represent the data without correction of astigmatism and HOA, and the lighter bars (right in the pair) the data after AO-correction. Data are for the four different image types tested. As in the preceding experiment, for all subjects and for most images, there are strong shifts in the neutral point following adaptation, with shifts in opposite directions for the different axes of astigmatism. Moreover, similar aftereffects occurred whether or not the individual observer's aberrations were corrected and the average magnitude of the aftereffects did not significantly differ between the corrected and uncorrected conditions. Thus the control settings confirm that orientation-selective aftereffects are likely to occur from orientation-

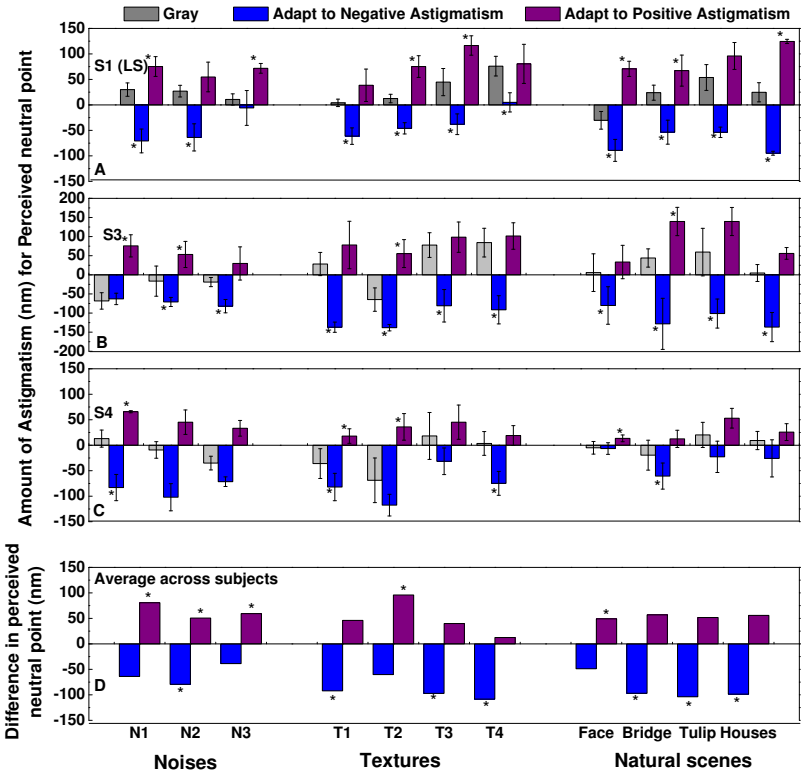

Figure 5.10: A, B, C: Stimulus levels that appeared isotropic before or after adapting to the same image with negative (blue) or positive (purple) astigmatism tested on three subjects for individual images of noise, close-up textures, or natural scenes. The vertical axis represents the amount of astigmatism (in nm) (negative for vertical and positive for horizontal) that makes the image appear isotropically blurred for the observer; D: Difference in the perceived neutral point before and after adaptation to negative astigmatism (blue) or positive astigmatism (purple) shown on average across the three subjects and for each of the 11 tested images. The vertical axis represents the difference in perceived neutral point in terms of the amount of astigmatism (in nm) necessary for the observers to perceive the test images as isotropically blurred. Negative values mean that the observer shifted their neutral point to images more vertically oriented, and vice versa for positive values. Error bars represent standard deviation across measurements. * indicates significant differences ($p<0.05$) before vs. after adaptation. (Reproduced from Sawides et al. [2010b]).

selective blur present in the retinal image.

5.3.2 Experiment 2: Selectivity of blur adaptation for the adapting image

The previous experiment showed that similar aftereffects of astigmatic blur occur for a wide range of images, when the adapting and test image are the same. Experiment 2 tested how adaptation to blur in one image generalizes to affect the perceived isotropic point for a different test image. Figure 5.12 shows the shifts in the perceived neutral point for two observers, when adapting to a positive astigmatism (left panels) and to a negative astigmatism (right panels). The three rows of plots show how adaptation transferred across a) very different stimuli (images of noise, pine needles, or a face); b) very similar stimuli (3 samples of 1/f noise); or c) different natural scenes (images of the face, houses, or tulips). The results again indicate that there is a strong adaptation effect that is selective for the axis of the astigmatism. Aftereffects were generally strongest when assessed with the same test image, though there is also substantial transfer of the blur aftereffect to the other test images. For example, aftereffects did not significantly differ across the same or different test images, and showed only weak selectivity for one observer across the different natural images.

5.3.3 Experiment 3: Aftereffects dependent on local blur versus global shape

The preceding experiment examined the transfer of blur adaptation to different images. We next tested how the adaptation transferred across image size, and specifically, whether the aftereffects were more similar when the adapt and test images had the same blur (but different "shapes") or when the images had the same "shape" (but consequently different levels of blur). Again, these stimuli differed in whether the second image was created by first magnifying and then blurring (for same blur), or by first blurring and then magnifying (for same shape). The aftereffects for the face image are illustrated in Figure 5.13. If observers are adapting directly to the perceived shape (and if these transfer across size), then these aftereffects should be similar for the two sizes when the shapes remain equivalent. This is shown in the left panels for the three observers and for both axes of adaptation. In each case there was no significant difference between the magnitude of the shifts induced by the 2 or 6 deg images. Conversely, when the larger image had the same level of blur but a different shape to the smaller image (right side of Figure 5.13), the larger image induced significantly weaker aftereffects in 5 of the 6 cases (right panel).

5.3.4 Experiment 4: Blur adaptation and object orientation

Experiment 4 further explored the basis for the adaptation by asking how the aftereffects transferred across rotations between the adapt and test images. Figure

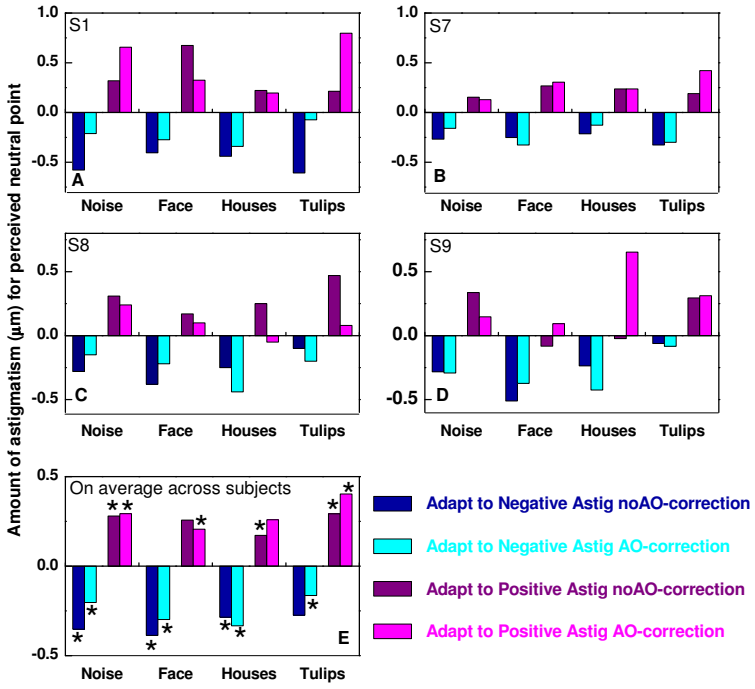

Figure 5.11: Adaptation effect to astigmatic blur with and without AO correction of the subject's aberrations, tested on 4 subjects for individual images of noise, face and natural scenes. A,B,C,D: Difference in the perceived neutral point before and after adaptation to negative astigmatism (blue) or positive astigmatism (purple), for the 4 subjects tested, with and without the AO-correction of the subject aberrations. E: on average across subjects. * indicates significant differences ($p<0.05$) before vs. after adaptation. No significant differences were found in the difference in perceived neutral point between the two conditions with and without AO-correction. The vertical axis represents the difference in perceived neutral point in terms of the amount of astigmatism (in microns) necessary for the observers to perceive the test images as isotropically blurred. (Reproduced from Sawides et al. [2010b]).

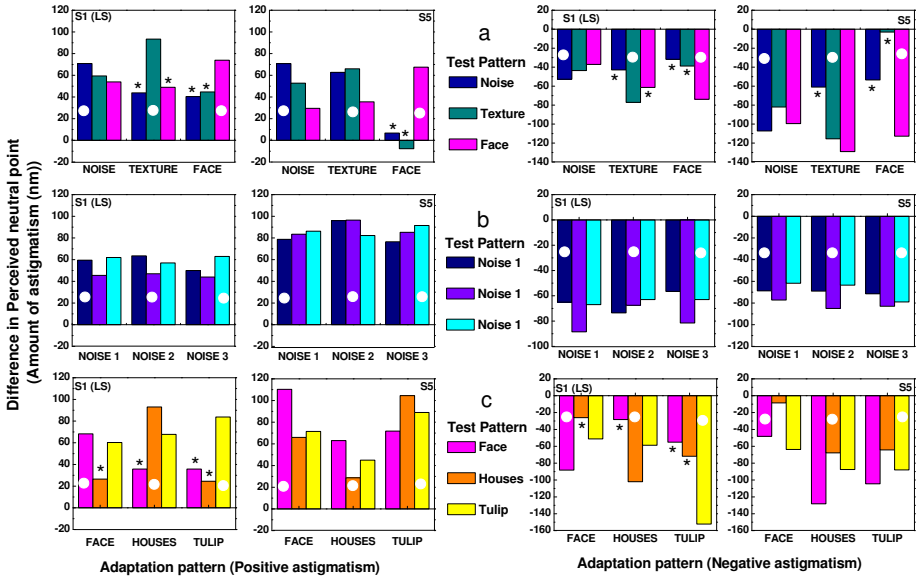

Figure 5.12: Aftereffects of adapting to a positive (left panels) or negative (right panels) astigmatism for a) very different stimuli (images of noise, pine needles, or a face); b) very similar stimuli (3 samples of 1/f noise); or c) different natural scenes (images of the face, houses, or tulips). Bars plot the shift in the perceived neutral point for each image measured for two different observers. The white circle indicates conditions when the adapting and test images were the same. * indicates significantly ($p<0.05$) smaller aftereffects when the test and adapting images were different vs. the same. The vertical axis represents difference in the perceived neutral point in term of amount of astigmatism (in nm) necessary for the observers to perceive the test images as isotropically blurred. (Reproduced from Sawides et al. [2010b]).

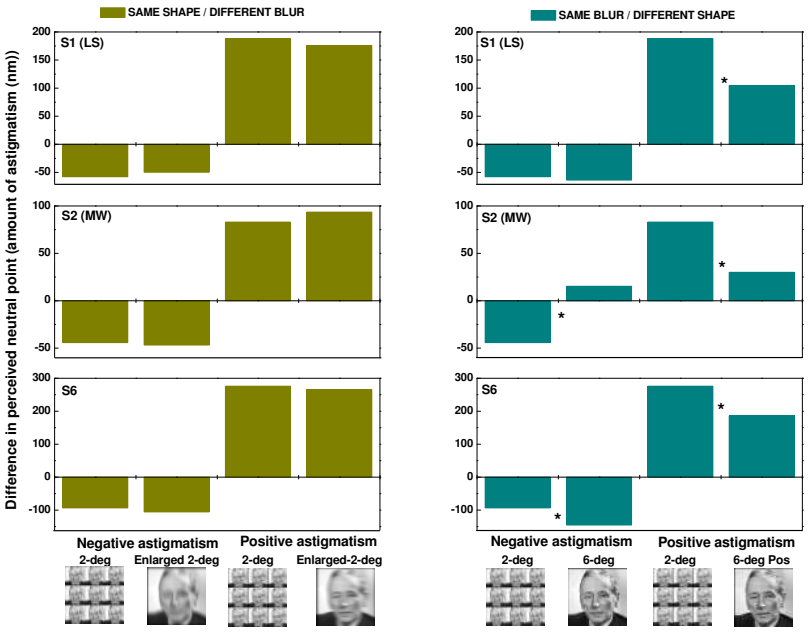

Figure 5.13: Aftereffects for 2-deg and corresponding 6-deg images that had the same shape (blurred then magnified; left panels); or the same blur (magnified then blurred; right panels) for 3 observers. The vertical axis represents the difference in perceived neutral point in term of amount of astigmatism (nm) necessary for the observers to perceive the test images as isotropically blurred. Negative, or positive, values mean the observer shifted their neutral point to images more vertically, or horizontally, oriented, respectively. * indicates a significant difference ($p<0.05$) in the strength of the aftereffect for the two adaptation stimulus sizes. (Reproduced from Sawides et al. [2010b]).

5.14 shows how the adaptation to orientation-selective blurring transferred across a change in the orientation of the face image. Again, if adaptation is adjusting to the face shape, then the aftereffect should be in the same direction at both test orientations; while if the adaptation is instead tied to the retinal orientation of the blur, then it should bias the appearance of the rotated test in the opposite direction. However, results for 3 observers tested were mixed. Both S1 and S2 showed significant aftereffects in the same direction at both test orientations for the face blurred with the negative astigmatism, while the shifts in the rotated test image were not significant following adaptation to positive astigmatism and thus did not discriminate between the two models. (Note that the sign of the effect is relative to the object orientation and not the image plane.) A third subject's settings were consistent with retinotopically referenced adaptation in that the adaptation effect reversed sign with a 90 degree rotation of the test object. However, this subject's data were highly variable and did not reach significance for any of the conditions.

5.3.5 Experiment 5: Adaptation and blur strength

In the final experiment, we asked how the aftereffect varied as a function of the level of adapting blur. Figure 5.15 shows the change in perceived neutral point as a function of the level of astigmatism in the adapting image. Aftereffects tended to saturate at the more extreme levels, but showed little evidence for a diminution at the highest levels. This pattern is roughly similar to the pattern found for blurring images by varying the slope of the amplitude spectrum [Webster et al., 2002]. Thus at least over this range of astigmatic blur there continued to be robust adaptation. Over much of the tested range the aftereffect increases roughly linearly with blur strength, with a slope of 0.45 over the linear range of the curves. Thus no level of blur exhibited complete compensation for the very short-term timescale examined. Note that subject S1 showed an offset in their perceived isotropic point relative to the physically isotropic level. This might be a consequence of the presence of natural vertical astigmatism (as it is also supported by a consistent shift of the neutral focus point toward horizontal astigmatism, which does not occur when astigmatism and high order aberrations are corrected) or a long-term adaptation to her natural astigmatism.

5.4 Discussion

It is clear that if adaptation is important for maintaining image quality then the perceived quality of a refractive correction may depend on how adaptation adjusts to these changes. We explored these adjustments by examining how visual coding adapts to lower order astigmatism. Our results reveal strong orientation-selective aftereffects in the appearance of images after adaptation to images that simulate moderate levels of astigmatism (Experiments 1 and 2), and similar effects occurred after correcting the subject's aberrations. Moreover, the strength of these after-

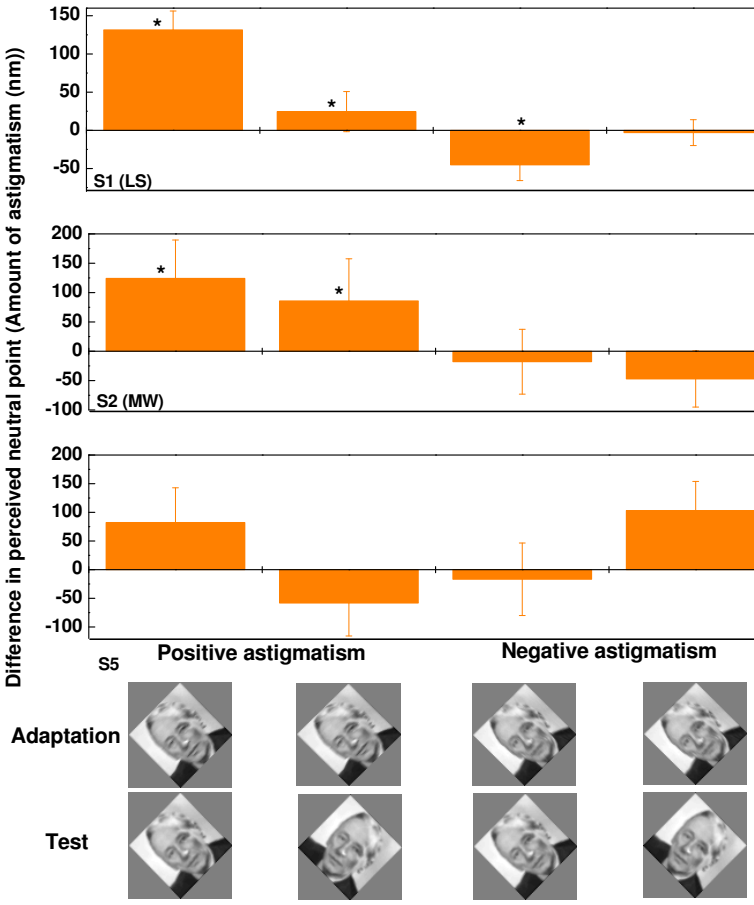

Figure 5.14: Adapting and test stimuli for comparing how astigmatic blur transfers across rotations in the image plane. Left: adaptation to positive astigmatism along the axis of the face and then tested at the same image orientation or rotated 90 deg. Right: adaptation to negative astigmatism along the image axis. The ordinate in the figure represents the difference in perceived neutral point in term of amount of astigmatism (in nm) necessary for the observers to perceive the test images as isotropically blurred, and is relative to the axis of the original image. Negative values mean that the observer shifted his neutral point to images more vertically oriented, and vice versa for positive values. * indicates significant ($p<0.05$) shift relative to the pre-adapt setting. (Reproduced from Sawides et al. [2010b]).

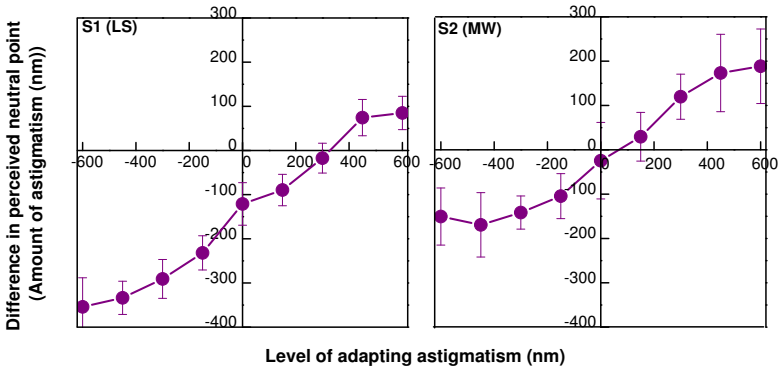

Figure 5.15: Perceived isotropic level as a function of the level of the adapting astigmatism for two subjects. (Reproduced from Sawides et al. [2010b]).

effects increased roughly monotonically with the strength of the adapting blur over the range tested (Experiment 5). These results suggest that individuals are thus probably routinely adapted to their astigmatism. This is important because uncorrected or under corrected levels of ocular astigmatism are highly prevalent. Astigmatism is a dominant aberration in uncorrected eyes [Porter et al., 2001], and remains a dominant aberration even in well-corrected eyes [Thibos et al., 2002]. Moreover, among contact lens wearers astigmatism is common yet often uncorrected [Tan et al., 2007].

To compensate for the variety of optical errors that exist in real eyes, processes like adaptation must be able to adjust to the different patterns of blur introduced by different aberrations. The adjustments we find for astigmatism complement and extend a number of studies that have explored adaptation to optical defocus, specifically to test for neural adjustments to myopia (e.g. Pesudovs and Brennan [1993]; Mon-Williams et al. [1998]; Rosenfield et al. [2004]; Vera-Diaz et al. [2004]; Rajeev and Metha [2010]), and suggest that the visual system can selectively adapt to different patterns of lower-order aberrations. An orientation-selective blur aftereffect is perhaps not surprising given the prominence of orientation tuning in visual coding and the prominent orientation and spatial-frequency selectivity of contrast adaptation [Blakemore and Campbell, 1969b; Bradley et al., 1988].

The pattern of aftereffects we observed is also important because it points to what is being adapted in blur adaptation. Studies of this adaptation have typically concentrated on attributes that limit visual resolution or that influence the perception of image focus. In the present study we instead tested for aftereffects across images that did not vary in the overall level of blur but rather in the form of the blur. These images appear to vary most clearly in the orientation of the blur, and we showed that adaptation to them correspondingly induces strong aftereffects in the orientation bias in images. The fact that these biases partially transfer across images with very different spatial structure (Experiment 2) sug-

gests that the adaptation is partly adjusting directly to the stimulus blur (though how this attribute is encoded by the visual system remains uncertain; [Georgeson et al., 2007; Field and Brady, 1997]). Such adjustments could include adaptation to basic properties such as the spatial frequency content of the image. However, the aftereffects also showed evidence of object-centric transfer across magnified or rotated images even though these changes strongly altered the retinocentric patterns of blur in the images (Experiments 3 and 4). Thus the aftereffects might also include processes that are common to conventional figural aftereffects [Kohler and Wallach, 1944]. Interestingly, clinicians often refrain from full correction of astigmatism because of their concerns about figural changes in the structure of the retinal images due to meridional magnification brought on by the spectacle lens magnification effect. It is generally felt that patients eventually become acclimated to these image distortions [Guyton, 1977], but it is also possible that the meridional adaptation that had developed prior to astigmatic correction slowly changes and thus the new post-correction PSF comes to appear isotropic. That is, even without spectacle magnification causing figural changes, meridian-specific defocus will introduce figural changes into images, and the rapid adaptation to these bares some of the trademarks of figural adaptation. A further implication is that - to the extent that blur can alter an attribute like perceived shape - visual processes that are normally recruited and adapted for encoding shape will be affected, so that a feature like blur that is often considered "low level" may trigger adaptation at many levels of the visual system.

5.5 Conclusions

Adaptation to images blurred by different axes of simulated astigmatism induces a strong orientation bias in the appearance of subsequently viewed images, and these biases show asymptotic increases with increasing blur strength. These aftereffects show that adaptation can be selective for different patterns of sphero-cylindrical errors and that perception is probably routinely adjusted through adaptation to the lower order aberrations characterizing an individual's optics.

The orientation-selective aftereffects induced by astigmatism share some characteristics with both contrast adaptation (in showing partial transfer of the blur across images with different content) and figural aftereffects (in showing partial transfer across images of the same objects at different sizes or orientations). Thus changes in optical blur may alter a number of attributes of the retinal image in addition to image sharpness, and may therefore invoke a number of distinct forms of adaptation.

The experiment performed with and without the AO-correction of subjects aberrations show that these adaptation effects occur consistently, minimally affected by the presence of other high order aberrations. Yet it remains important practically as an example of how this coding dimension can be calibrated to an important form of natural variation in the retinal image. It is less certain to

what extent adaptation can also adjust to higher-order aberrations. For example, if these aberrations produce more dimensions of variation in the PSF than the processes of adaptation can resolve, then there may be patterns of blur that are metameric for the adaptation (i.e. inducing equivalent adaptation effects) even if they lead to visually discriminable differences in blur. The next chapter will investigate short-term adaptation to blur produced by high order aberrations.

6

Short-term adaptation to blur produced by high order aberrations

The aberrations of the eye are routinely altered either in the course of pathology or aging, or artificially by ophthalmic, contact or intraocular lenses and corneal refractive surgery procedures. To fully understand how the visual system adapts to changes that can happen within the observer, we will investigate adaptation to blur produced by high order aberrations and scaled increases or decreases of subject's high order aberrations.

This chapter is based on the paper by Sawides et al. "Adapting to blur produced by high order aberrations" Journal of Vision, 2011. The co-authors of these studies are Pablo de Gracia, Carlos Dorronsoro, Michael A. Webster and Susana Marcos.

The author of this thesis implemented the experimental procedure, performed the measurement on human eye's, collected and analysed the data.

This work was also presented at the Association for Research in Vision and Ophthalmology (ARVO) annual meeting (May 2010) in Fort Lauderdale, Florida, USA, as an oral contribution.

6.1 Introduction

Understanding the potential role of adaptation to optical high order aberrations (HOA) is important because these aberrations can be and are routinely altered in a variety of ways. Certain treatments such as refractive surgery induce significant amounts of optical aberrations [Marcos, 2001], while optical aids such as progressive spectacles produce significant amounts of astigmatism and field distortions [Villegas et al., 2006]. Thus, how observers respond to these alterations in their aberrations patterns may depend importantly on how they are able to neuronally adapt to these optical changes. Moroever, several ocular pathologies also alter the natural wave aberration of the eye (for example, keratoconus, which produces a progressive deformation of the cornea and an increase in the HOA of the eye [Barbero et al., 2001]).

Pesudovs [2005] suggested that adaptation to surgically induced HOA occurs in patients after LASIK surgery. Artal et al. [2004a] showed that the stimuli seen through an individual's natural aberrations appear sharper than when seen through a rotated version of the same aberrations, suggesting that this may be a consequence of neural adaptation to the specific degradation produced by someone's High Order Aberrations. Chen et al. [2007b] also found that subjective image quality was best when the observer's HOA was not fully corrected, though the implied adaptation was only a small fraction ($\sim 12\,\%$) of the effect predicted by complete adaptation. Sabesan and Yoon [2009] reported that keratoconic eyes do not achieve the visual benefit expected by the optical improvement and suggested that long-term adaptation to poor retinal image quality may limit the visual improvement immediately following correction). Conversely they found better visual performance in real keratoconic eyes than normal eyes with a keratoconus wave aberration (simulated by Adaptive Optics), despite a similar optical degradation in both cases, which they attributed to adaptation to HOA in the keratoconic eyes [Sabesan and Yoon, 2010].

Alternatively, the ultimate goal of refractive correction is the elimination of HOA of the eye. Debate is ongoing whether patients adapt to their new pattern of optical aberrations so that vision is less compromised than the optical degradation of their retinal image quality would suggest, if aberrations have been induced, or conversely, whether they can take advantage of an improved image quality if aberrations have been corrected. For example, Rossi and Roorda [2010] showed in most cases an immediate improvement of visual acuity upon correction of high order aberrations that showed a minimal effect of short-term adaptation or perceptual learning. However, as noted by the authors, their study did not assess the potential effects of adaptation on subjective image quality, or on visual acuity or sensitivity to natural images. Thus the potential impact of adaptation on refractive corrections remains unknown. In addition, in chapter 4, we found in the subjective image sharpness assessment experiment that observers chose as "the sharpest image" 84 % on average of the images seen through a full correction of their HOA. The correction of HOA produces therefore a clear increase of the subjective impression

of sharpness. However, the question remains open whether the sharpest image actually appears "too sharp" to the subject because they are adapted so that they are adapted to compensate for their aberrations. In these prior studies adaptation to HOA was only implicitly tested by asking how perceived image quality or acuity changed with a change in the aberration pattern.

In the current chapter, we instead directly tested whether subjects can adapt to changes in the magnitude of HOA, by measuring the aftereffects of exposure to different levels of HOA on subjective image focus. We used a similar paradigm to that used by Webster et al. [2002] to study aftereffects following adaptation to blur or sharpened images. However, rather than artificial symmetric blur (introduced by filtering the image) we tested for potential aftereffects after adaptation to various levels of blur produced by actual HOA centered around the actual magnitudes of blur that the observers were normally exposed to (simulated in the image while subjects viewed the stimuli with their native HOA corrected with Adaptive Optics (AO)). Subjects were exposed to their own aberrations as well as other subject's aberrations. We also explored the dependence of the effect on the amount of blur in the adapting image, as well as the transfer of the effect across different adapting and test images.

6.2 Methods

6.2.1 Subjects

Four of the authors, aged 27 to 39 years, were tested in the experiment, with high order aberrations RMS error ranging from 0.18 to 0.39 μm (5 mm pupils).

6.2.2 Stimuli

The original images were acquired using a digital camera (Canon PowerShot) with a resolution of 4M pixels. The original was converted to grayscale and a resolution of 480,x 480 pixels, and then blurred by convolution with the PSF estimated from each subject's natural aberrations. Aberrations of the subject were measured using the AO-set-up, and fitted to 7^{th} order Zernike polynomials. Tilts, astigmatism and defocus were set to zero, except for a control experiment where defocus was optimized to maximize Strehl.

Different sets of images were generated for each subject's HOA. For each HOA pattern, a sequence of images was created by multiplying each Zernike coefficient by a factor (F) between 0 and 2 in 0.05 steps. Each set of testing images thus contained 41 different images ranging from diffraction-limited to double the amount of natural blur. For F=1, the simulated image represented the natural degradation imposed by the HOA. For adapting images, we used 5 different levels of blur (F=1, the native aberration; F=0 and F=0.5 for adaptation to sharper images; and F=1.5 and F=1.9 for adaptation to more blurred images). Multiplying the Zernike coefficients by these factors modified the amount of blur while preserving

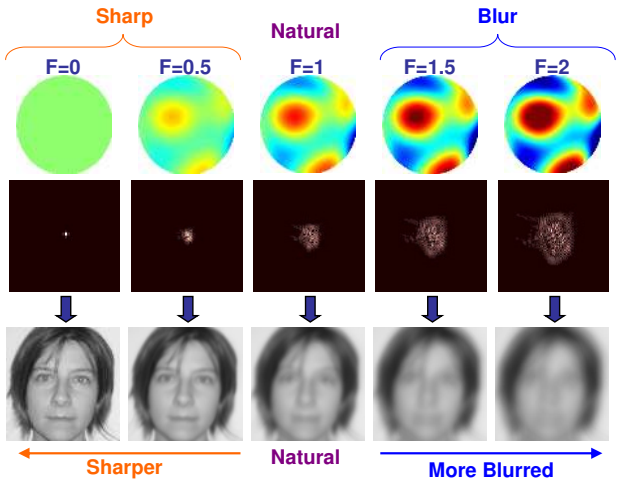

Figure 6.1: Illustration of the procedure to generate the sequences of testing and adapting images. The images are degraded by convolution with the PSF corresponding to an observer's natural wave aberrations. The sequence of images was achieved by scaling the wave aberration by different multiplicative factors F.

the relative shape of the PSF. Images were presented on the CRT monitor and subtended 1.98 deg. Figure 6.1 illustrates the image simulation procedure, for different scaling factors.

6.2.3 Experimental protocols

Measurements were done under natural viewing conditions in a darkened room for a 5 mm pupil diameter. Each experiment was conducted in a single session for each subject, lasting approximately four hours. All experiments were performed under full Adaptive-Optics corrected aberrations (astigmatism and high order aberrations with the deformable mirror) and best spherical refraction error correction (adjusted by the subject with the Badal system in the corrected state of the deformable mirror). .

6.2.4 Psychophysical paradigm and sequence

The psychophysical paradigm consisted of a two-alternative forced choice procedure (2AFC), where the subject had to respond whether the image was sharp or blurred. Test levels were chosen based on a quest algorithm in order to find the best perceived focus point for a given condition of adaptation.

Each subject performed the test for 6 different conditions: after neutral adaptation (to a gray screen) and after adaptation to 5 different levels of blur: 2 levels of sharper images (F=0; F=0.5), a natural aberration level (F=1) and 2 levels that were more blurred (F=1.5; F=1.9). Each subject was tested using the sequence of images generated with their own aberrations and with those generated using the

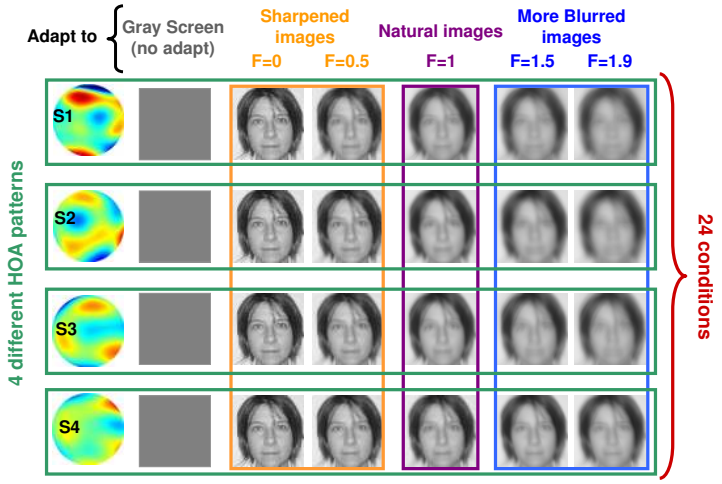

Figure 6.2: Wave aberration patterns of the 4 subjects and the 24 adapting conditions, tested in both experiments.

other three subject's aberrations.

In the first experiment, the test and adapting images were the same (an image of author LS's face). In the second experiment, observers again adapted to the image of LS but were tested on an image from a different face (author SM), in order to assess the transfer of the adaptation effect across images. A total of 24 conditions were tested in each experiment, as illustrated in Figure 6.2. The same sequence was tested on all 4 subjects (except S1, who did not perform the test with the S4 wavefront (WF) sequences, because of the larger natural amount of HOA for S1 which doubles the amount of natural HOA of S4).

A control experiment was performed on one observer (S4), similar to Experiment 1, where the subject adapted to his own aberrations and tested with 4 sequences of images generated with each subjects' aberrations, and alternatively, adapted to the other 3 subjects' aberrations and was then tested with the image sequence generated with his own aberrations. This experiment was designed to examine whether the perceived focus point was specific to the specific degradation produced by a certain pattern of aberrations, or rather to the overall level of blur, regardless the aberration pattern. In order to increase the range and resolution of the image sequence, the HOAs (for S4) were multiplied by a factor between 0 and 4 (instead of 0 and 2) and the generation of images was refined by setting the defocus to optimize the optical quality of the images (instead of setting it to 0).

In all cases, the sequence of the psychophysical experiment consisted of an initial 1 min adaptation to the adapting image after which a test image was presented for 1 sec to the subject who had to respond if the image was sharp or blurred. The adapting image was re-shown for 3 seconds in between each test presentation until the threshold was determined. Neutral settings (adaptation to gray field) were repeated three times in each subject. The standard deviation of those measurements

was used as an estimate of the typical measurement error. The other conditions were only performed once.

6.2.5 Data analysis

Aberrations

Wave aberrations were fitted by 7^{th} order Zernike polynomial expansions. Optical quality was evaluated in terms of RMS wavefront error (excluding tilts and defocus).

Best perceived focus point

The perceived focus point usually converges, in the 2AFC procedure, to the final value in less than 35 trials or 16 "reversals". At the end of each setting, the perceived focus point is checked to be stable over the last 8 reversals and the perceived focus point was obtained as the average of these 8 last reversals of the 2AFCP. The results were analysed in terms of the perceived focus point selected after adaptation to different levels of blur. Data were analysed as a function of factor F (relative blur) and RMS of the wave aberration used to degrade the image (absolute blur).

6.3 Results

6.3.1 Best corrected ocular aberrations

Figure 6.3 shows RMS wavefront error and wave aberrations (excluding tilts and defocus) for all subjects of the study before and after AO-correction of aberrations. Data are for 5 mm pupil diameters. Subject S1 performed the measurements wearing her soft contact lenses. On average, RMS (excluding tilts and defocus) decreased from 0.539±0.311 to 0.105±0.046 μm, with an average correction of 78±8 %.

6.3.2 Adaptation to blur produced by High Order Aberrations

Figure 6.4 shows the perceived neutral focus point of each subject after adaptation to images generated using each subject's own HOA, for the 6 levels of blur (gray field, sharpened, natural HOA, and blurred images). Again for this experiment a single face image was used for both adaptation and test. The blur level is represented in terms of factor F, i.e. the amount of blur relative to the natural aberration of each subject. After adapting to a sharper image, the subjective neutral focus point shifts to sharper levels and after adapting to a blurred image, the subjective neutral focus point shifts to more blurred levels. Typical errors (standard deviation of factor F) were 0.045 on average across subjects – from repeated

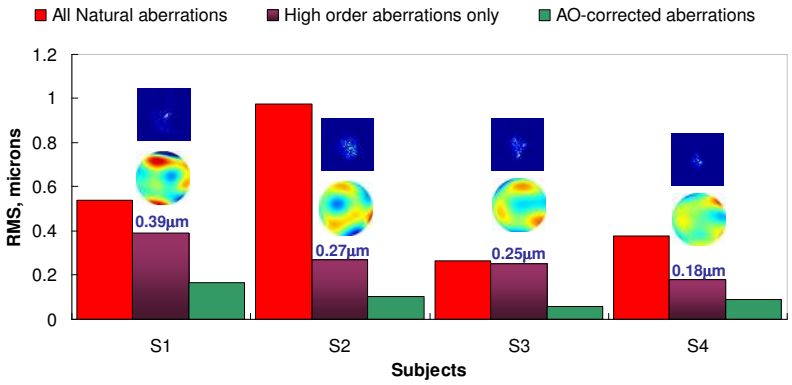

Figure 6.3: RMS wavefront error (excluding tilts and defocus, red), RMS for HOA (excluding tilts, defocus and astigmatism, purple) and AO-correction (correction of defocus, astigmatism and HOA, green). The corresponding RMS wave aberrations and PSF for the HOA of each subject are depicted above the purple bars. Measurements were for 5 mm-pupil diameters. (Reproduced from Sawides et al. [2011a]).

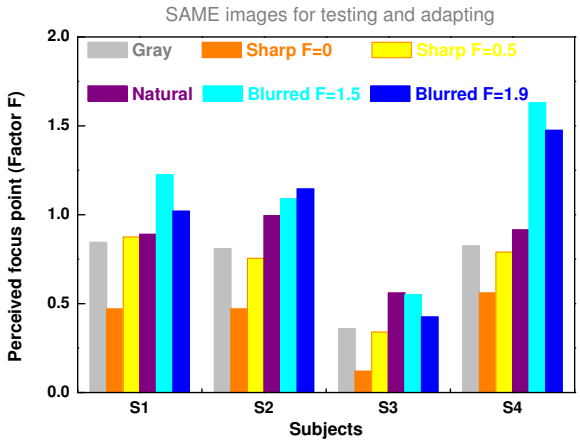

Figure 6.4: Perceived focus point for each subject when adapting to a gray field, and to images degraded using his/her own wave aberration (and scaled versions of it). The experiment was performed with the same images (LS) for testing and adapting. (Reproduced from Sawides et al. [2011a]).

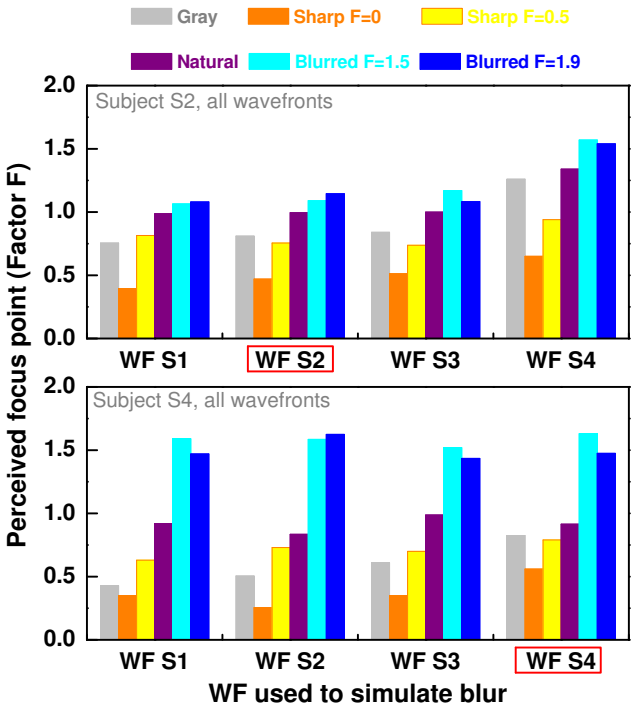

Figure 6.5: Perceived focus point for all conditions of adaptation. The case where adapting images were generated using the subject's own aberration is indicated by a red ellipse. The different colors represent the focus shift for different amounts of blur (F) relative to the natural aberrations. Results are for subjects S2 (upper panel) and S4 (lower panel). (Reproduced from Sawides et al. [2011a]).

measurements on the gray adaptation condition/test with their own HOA/LS face – which corresponded to less than 7 % error.

Figure 6.5 shows subjective neutral points for two of the 4 subjects, after adaptation to images generated using his/her own HOA and other subjects' HOA. The results were similar for all subjects. The shift (compared to the natural condition) in the subjective neutral focus occurs in all cases, regardless of the wave aberration pattern used to generate the image. Typical errors (standard deviation of factor F) were 0.080 on average, which corresponded to around 12 % error.

6.3.3 Adaptation as a function of the amount of blur in the adapting image

The data set of Experiment 1 allow us to assess whether the size of the aftereffect is proportional to the amount of blur in the adapting image, both within the images generated by scaling of a given wave aberration pattern, or within the range of blur produced by natural aberrations. Figure 6.6 shows the perceived neutral

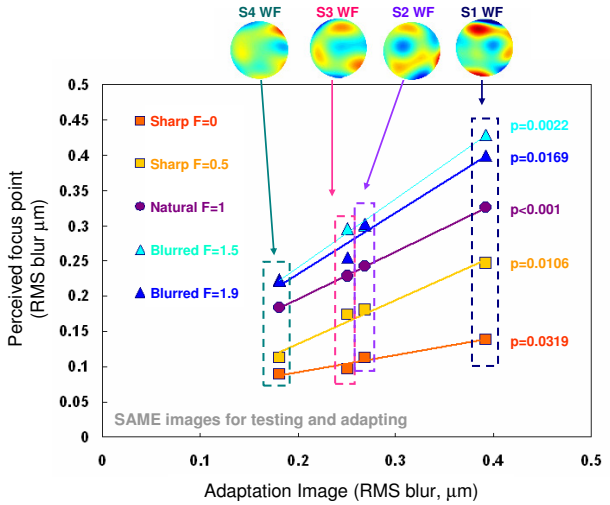

Figure 6.6: Perceived focus point in term of RMS (μm) when adapting to images blurred within the range of normal amounts of HOA, on average across subjects (Same images for testing and adapting). (Reproduced from Sawides et al. [2011a]).

focus point in terms of absolute RMS blur. Each point is the average setting across subjects. When adapting to images generated with low amounts of HOA, the perceived focus point is lower than when adapting to images generated with higher amounts of HOA, and this occurs at all adapting conditions. Therefore, the neutral point is proportional to the amount of adapting blur. Saturation occurs at the more blurred level in each sequence for all subjects. At all levels of blur in the adapting image there is a highly significant correlation between the perceived neutral focus point and the blur of the adapting image (in terms of RMS). Adaptation to a sharp image (F=0) shifted the perceived focus point toward sharper levels by -0.14±0.04 μm RMS on average, while adapting to a blurred image (F=1.5) shifted the neutral focus point to more blurred levels by 0.07±0.03 μm on average. The magnitude of the effect can be assessed by referring to the images Figure 6.2, where the image degradation for all subjects and different F factors is illustrated.

Figure 6.7 shows the results of the control experiment for one subject (S4), adapting to the other subjects' aberrations (and using the test image sequence generated with his own aberrations), or adapting to his own aberrations (and using test image sequences generated with the aberrations of the remaining subjects). As expected from experiment 1, when adapting to images with different amounts of blur (corresponding to the natural aberrations of the different subjects) the perceived focus point shifts proportionally to the amount of blur in the adapting image (Note this subject had the lowest RMS aberrations and thus was adapted to higher levels of blur when exposed to the aberrations of the other subjects). Interestingly, for a similar adapting image (his own aberrations), the perceived

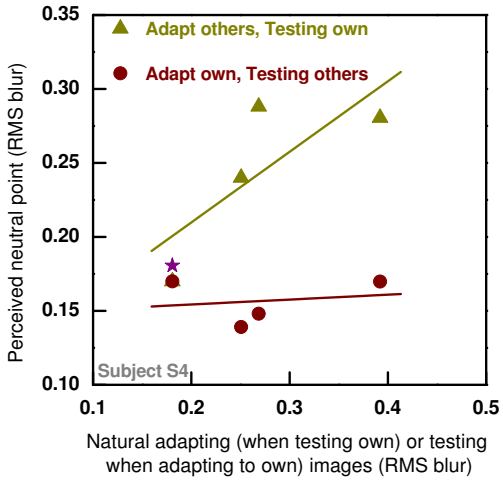

Figure 6.7: Perceived focus point in terms of RMS (μm) as a function of the blur of the adapting image (green triangles) or as a function of the aberrations of the central image test (F=1) of the sequence of test images (brown circles). The purple star represents the natural RMS of the subject. In the first case (green triangles), the test sequence was generated from the subject's own aberrations and the subject adapted to each subject's aberrations. In the second case (brown circles), the test sequences were generated from the other subjects' aberrations and the subject adapted to their own natural aberrations. Data are for subject S4 (Same images, LS, for testing and adapting). (Reproduced from Sawides et al. [2011a]).

focus point is rather constant, regardless of the specific pattern of degradation of the test image sequence.

6.3.4 Adaptation transfer across images

In the preceding experiments the test and adapt stimuli were drawn from the same image. In the next experiment we again adapted to the same image (of author LS), but then tested aftereffects by varying blur level in a different image (of author SM), again testing all subjects and the 6 conditions of adaptation. Typical errors (standard deviation of factor F) were 0.028 on average across subjects, which corresponded to less than 4 % error. The results are plotted in Figure 6.8. As in the first experiment, the subjective focus point shifts to sharper levels after adapting to a sharpened image, and to more blurred levels after adapting to a blurred image. The results therefore show that the adaptation effect transfers across different (albeit similar) images, consistent with the transfer found for artificial blur [Webster et al., 2002].

We again analysed the settings as a function of absolute RMS blur (as in Figure 6.6. Figure 6.9 revealed significant correlations and similar regressions between blur in the adapting image and blur level of the perceived focus point. The effects are

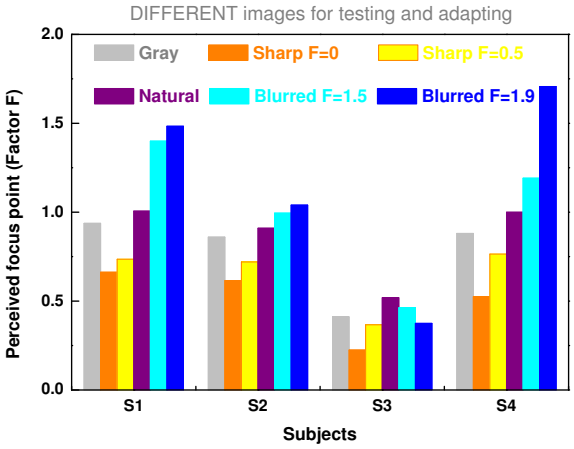

Figure 6.8: Perceived focus point for each subject when adapting to a gray field, and to images degraded using his/her own wave aberration and scaled versions of it (Different images for testing and adapting). (Reproduced from Sawides et al. [2011a]).

similar to those found in the previous experiment (same adapting and test images) except for the more blurred level, where we do not see the saturation effect when using different adapting and test images.

Finally, Figure 6.10 compares the perceived focus point obtained using the same or different images for testing and adapting, averaged across subjects. The results from both experiments are strongly correlated (p-value <0.001, $R=0.89$), suggesting that there was nearly complete transfer of the blur adaptation across the two different face images.

6.4 Discussion

Previous studies have shown that the perception of image blur can be strongly affected by adaptation to images that have been artificially blurred or sharpened [Webster et al., 2002], and that these aftereffects can also occur for the natural patterns of blur produced by low order aberrations of the eye's optics (chapter 5). The present results extend these findings by showing that adaptation also occurs for the patterns of natural blur produced by the high order aberrations of the eyes. The use of an Adaptive Optics system has allowed us to pre-compensate the natural aberrations of the eyes, and therefore expose all subjects to the same amounts and patterns of blur, ensuring that any difference across subjects will arise from their own neural processing or prior neural adaptation. As the measurements represent relative shifts, potential discrepancies in both in the adapting and test images, the use of convolved images to represent the retinal image quality should not affect the results. Furthermore, the fact that the blur level of the perceived

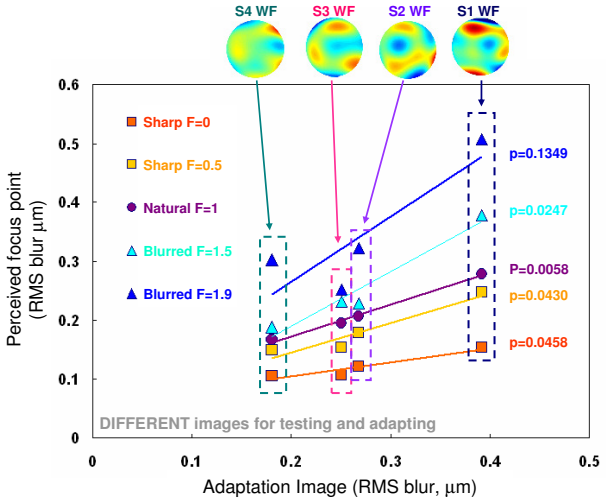

Figure 6.9: Perceived focus point in term of RMS (μm) when adapting to images blurred within the range of normal amount of HOA, on average across subjects (different images for testing and adapting). (Reproduced from Sawides et al. [2011a]).

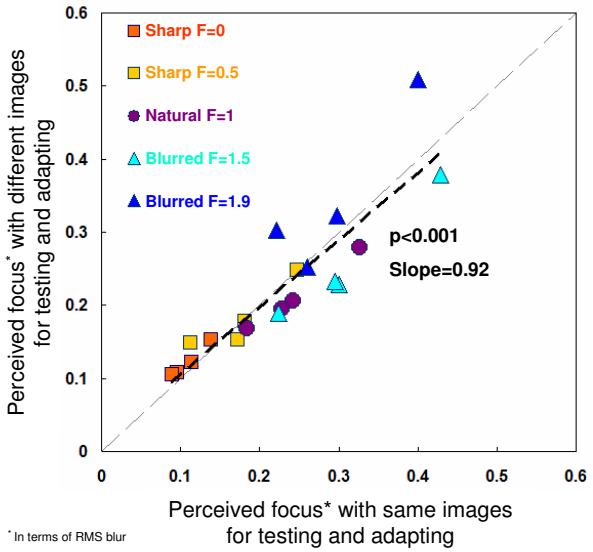

Figure 6.10: Perceived focus point (in terms of RMS blur) for same versus different adapt and test images. Data are averaged across subjects. (Reproduced from Sawides et al. [2011a]).

focus shift is similar under natural and gray adaptation supports the appropriate representation of blur in the simulated images.

For all subjects, there was a systematic shift of the perceived neutral focus after exposure to more blur when adapting to an image blurred by a scaled increase in the natural HOA (F>1), and to less blur when adapting to an image sharpened by a scaled decrease in the HOA (F<1). Interestingly, these adaptation effects occurred not only when subjects adapted to scaled versions of their own HOA, but also to the aberration pattern from other subjects. Moreover, we found that the shift of the neutral point after adaptation is proportional to the absolute amount of blur of the adapting image, regardless of whether the blur is produced by increasing the size of the PSF, or by natural aberrations found in different eyes. The results thus strongly suggest that changes in the magnitude of HOA – within the natural range characteristic of actual eyes – can strongly influence the state of blur adaptation in the visual system. (Notably, the perceived neutral point found after adapting to the natural HOA pattern was slightly lower than expected, (i.e. the factor F of the perceived neutral point is <1), which may be attributed to some residual defocus arising in the simulated degradation from setting defocus term to 0. A control experiment where the defocus term was set to optimize the optical quality of the simulated image produced an excellent correspondence between the blur level of the perceived neutral point and the amount of natural aberrations of a given eye.

However, it remains to be tested whether the adaptation is selective for different types of combinations of HOA, in the way it has been shown to be selective for differences in low order aberrations, and astigmatism in particular (chapter 5). The experiment in which the observer adapted to their own aberrations and then adjusted the perceived focus by varying the magnitude of a different observer's HOA or vice versa suggested that the adaptation effect is largely driven by the overall level of blur contained in the adapting images more than by the specific shape of the HOA pattern. This suggests that the aftereffects we measured depended largely on the global level of blur rather than local features associated with the asymmetric blur arising from particular HOA. However, our test stimuli did not in fact vary in ways that might capture aberration-selective aftereffects. The results of Artal et al. [2004a] showing variations in perceived image quality for rotated versions of the same HOA are consistent with an influence of the blur pattern on the adaptation.

Our present results also leave open the question of how selective the aftereffects are for changes in other properties of the images. We showed that there is almost complete transfer of the adaptation across different images of faces, suggesting that the adaptation is at least partly adjusting to the attribute of blur independently of the specific image structure. However, it remains to be seen to what extent this transfer occurs for more dissimilar images.

The fact that eyes can adapt to blur imposed by high order aberrations has important practical implications, as the aberrations of the eye are routinely altered either in the course of pathology or aging, or artificially by ophthalmic, contact or intraocular lenses and corneal refractive surgery procedures.

Although our data relate to changes in the perception of normal blur, and are not necessarily extrapolated to changes (or improvement) in visual function following adaptation, they suggest that patients can adapt perceptually to a change in the amount of these aberrations. In this sense, the perceptual changes in focus judgements following adaptation may be associated with the reported improvement of VA over time in patients following refractive surgery (which induced significant amount of aberrations) [Pesudovs, 2005], the relatively better VA in keratoconic eyes compared to normal eyes with similar induced aberrations [Sabesan and Yoon, 2010] or habitually non-corrected astigmats compared to normal eyes with induced astigmatism [de Gracia et al., 2011a; Vinas et al., 2012].

6.5 Conclusions

Adaptation occurs to changes in the natural levels of blur produced by high order aberrations. The perceived best focus is proportional to the amount of blur, produced both by changing the size of the blur (preserving its shape), or the amount and pattern of aberrations across different eyes. Moreover, adaptation to the fully corrected HOA produced aftereffects equivalent to a sharpened adapter, while adaptation to a more blurred image induce an aftereffect that was shifted toward the more blurred level of their natural HOA. These results demonstrate that the eye can adapt to the levels of blur produced by HOA and suggest that adaptation may be an important factor in understanding the perceptual changes that occur when HOA are altered by pathology or surgery.

The next chapters will discussed whether natural adaptation to subject's aberrations depends on the global level of blur and/or local features associated with the asymmetric blur arising from particular HOA

7

Adaptation to the natural level of blur produced by high order aberrations

Unlike spherical or cylindrical errors, high order aberrations (HOA) are not typically corrected, and thus individuals are each chronically exposed to different patterns of retinal blur. We examinated whether subject are naturally adapted to their own aberrations and blur level and whether spatial coding in the visual system is matched to the native blur level specific to an individual's HOA.

This chapter is based on the paper by Sawides et al. "Vision Is Adapted to the Natural Level of Blur Present in the Retinal Image" PLoS ONE, 2011. The co-authors of the study are Pablo de Gracia, Carlos Dorronsoro, Michael A. Webster and Susana Marcos.

The author of this thesis implemented the experimental procedure, performed the measurement on human eye's, collected and analysed the data.

This work was also presented at the Association for Research in Vision and Ophthalmology (ARVO) annual meeting (May 2011) in Fort Lauderdale, Florida, USA, as an oral contribution.

7.1 Introduction

Despite the fact that retinal images are blurred by low and high order aberrations, observers do not usually report that the world appears contrast attenuated, band-limited, nor phase altered ("blurred"), suggesting that the perception of image focus is somehow compensated for these aberrations. Individuals are each exposed to different long-term patterns of retinal blur. Yet it remains unknown to what extent and in what ways visual coding can adjust for the consequences of idiosyncratic variations in the optics.

In the previous chapter (6), we have shown that observers can adapt to the blur induced by HOA from scaled versions of their own aberrations, or those from other subjects. However, the extent to which observers are adapted to their own optical aberrations remains unresolved.

On the one hand, both short- and long-term adaptation can selectively adjust to the axis of astigmatic blur [de Gracia et al., 2010; Vinas et al., 2012], and visual performance is better in observers with optics strongly degraded by corneal pathology compared to normal subjects induced with similar amounts of HOA Sabesan and Yoon [2010]. Moreover, Artal et al. [2004a] found that stimuli seen through an individual's natural aberrations appear sharper than when seen through a rotated version of the same aberrations, and adaptation to surgically induced HOA has been suggested to occur in patients after LASIK surgery [Pesudovs, 2005]. These studies thus point to neural compensations for the wave aberrations characterizing the individual's eye.

Yet on the other hand, studies of visual acuity and subjective image quality have found immediate improvements after correcting HOAs, with only a small residual bias toward the observer's native HOA and little further improvement with training [Chen et al., 2007b; Rossi and Roorda, 2010]. These results have therefore suggested that there may instead be relatively little adaptation to HOA.

In this chapter, to directly test for this adaptation, we used the Adaptive Optics (AO) system to correct the natural aberrations of the eye. All observers were exposed to identical aberration patterns and therefore any difference in the visual response must be due to neural factors. We then manipulated retinal blur by projecting degraded images with known HOA. Subjective focus was measured with a 2-Alternative-Forced-Choice (2AFC) procedure in which the observer had to report whether the image displayed on the monitor appeared "too blurred" or "too sharp".

7.2 Methods

7.2.1 Subjects

Four experienced observers participated in the first experiment and 15 observers (3 of the authors and 12 naive observers) participated in experiment 2. All had normal vision, their natural Strehl Ratio at best focus varied from 0.097 to 0.356

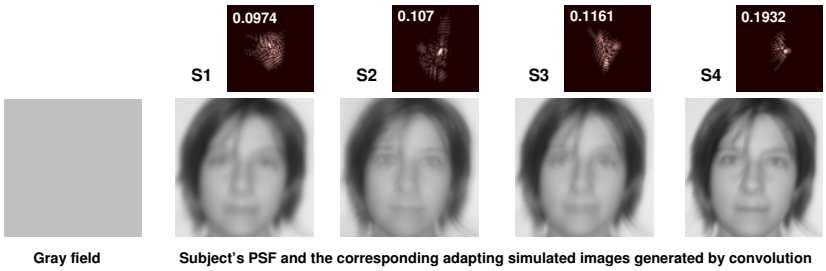

Figure 7.1: Testing scaled high order aberrations patterns. a) Adapting images in testing scaled high order aberrations patterns: Gray field and simulated adapting images generated by convolution with the PSFs (shown, with corresponding SR) obtained from 4 different subjects' HOA patterns. Tilt and astigmatism were set to zero whereas defocus was adjusted to maximize optical quality. Data are for 5 mm pupils.

(0.097 to 0.1932 in experiment 1 and 0.103 to 0.356 in experiment 2).

7.2.2 Generation of the optical blur

The original images (face) was acquired using a photographic digital camera with an original resolution of 4M pixels and converted to grayscale.

In a first experiment, testing scaled HOA patterns, we used the same stimuli as in chapter 6 (Face LS subtended 1.98^{o} viewed through a 5 mm pupil). The optical blur was generated using the same protocol as in chapter 6, "control experiment". Sequences of images were blurred by convolution with the corresponding point spread functions (PSFs) estimated from scaled versions of each observer's HOA patterns, ranging from diffraction limited (scale factor F=0) to double the amount of natural blur (F =2) in 0.05 steps. Aberrations of the subject were measured using the AO-set-up, and fitted by 7^{th} order Zernike polynomials. Tilts and astigmatism were set to zero whereas defocus was set to optimize SR and achieve best optical quality. Sequences of images were generated for each subjects' HOAs, by multiplying each Zernike coefficient by a factor F between 0 and 2 in 0.05 steps. In this experiment, SR was defined as the volume under the modulation transfer function (MTF). Each set of testing images contained 41 different test images ranging from diffraction-limited to double the amount of natural blur. See Figure 6.1 of chapter 6.

In the second experiment, testing 128 real complex HOA patterns, the optical blurred was generated by convolution with the PSF estimated from 128 different complex aberration patterns from real eyes. Again, tilts and astigmatism were set to zero and defocus was set to optimize Strehl Ratio. The optical quality ranged from high amounts of HOAs (from surgically altered eyes) to almost diffraction-limited (achieved with AO-correction measurements). The sequence of test images thus contains 128 images with Strehl Ratio ranging from 0.049 to 0.757 (5 mm pupils). Figure 7.2 shows a subset of PSFs used in the experiment and the cor-

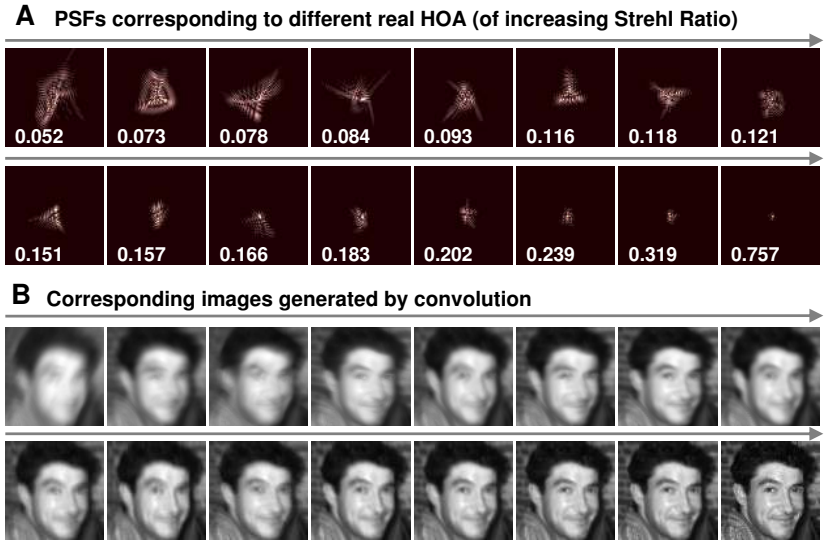

Figure 7.2: Testing 128 real complex high order aberration patterns. Subset of 16 PSFs estimated from HOA in real eyes (from a total of 128 used in the blur judgment experiment), with their corresponding SR. Tilt and astigmatism were set to zero whereas defocus was adjusted to maximize optical quality. Optical quality ranges from highly degraded from surgical eyes to almost diffraction-limited (from AO-correction). Data are for 5 mm pupil diameters. Test sequence images blurred by convolution with the corresponding PSFs above. The experiment used the complete sequence of 128 images.

recponding convolved images.

7.2.3 Experimental Procedure

Measurements were done under natural viewing conditions in a darkened room for a 5 mm pupil diameter. Psychophysical measurements were performed under full AO-correction of aberration (Astigmatism and high order aberrations achieved with the deformable mirror) and under best spherical refraction error correction (achieved with the Badal system), as described in chapter 2). On average, RMS (excluding tilts and defocus) decreased from $0.523 \pm 0.33\,\mu$m to $0.080 \pm 0.038\,\mu$m, with an average HOAs correction of $82.0 \pm 8.5\,\%$.

The images in the tests were presented on the CRT monitor and subtended 1.98 degrees. The psychophysical paradigm consisted of a 2AFC procedure, where the subject responded whether the image was sharp or blurred. Stimulus levels were varied with a quest algorithm in order to find the level of best perceived focus point for a given adaptation condition (neutral adaptation with a gray-field or adaptation to natural aberrations). In all cases, the sequence of the psychophysical experiment consisted of 1 min exposure to the adapting image after which a test image was presented to the subject who had to respond if the image was sharp or blurred. The subject re-adapted for 3 seconds between each test image. Adapting

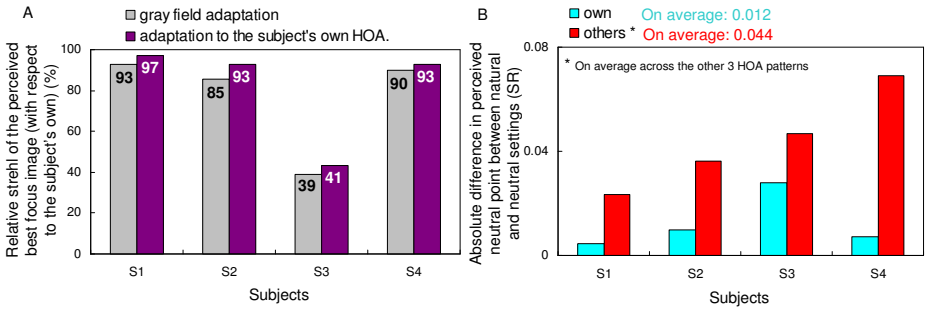

Figure 7.3: A. Testing scaled high order aberrations patterns. Relative Strehl Ratio of the perceived best focus image (with respect to the subject's native level) for gray field adaptation or adaptation to each subject's own HOAs. B. Difference in Strehl Ratio between gray and natural adaptation when subjects were adapted to their own HOAs (blue) and other subjects' HOAs (red), averaged across the other 3 HOA patterns. (Reproduced from Sawides et al. [2011b]).

images were spatially jittered in time to prevent local light adaptation.

In the first experiment, blur judgments were measured on 4 subjects (Strehl Ratio ranging from 0.094 to 0.1932 (5 mm pupils), after neutral adaptation (gray-field) and after adaptation to images blurred with the natural degradation imposed by each of the 4 subject's HOAs (F=1) as shown in Figure 7.1. In a second experiment, judgments of perceived blur were measured in 15 subjects to determine for each individual the physical blur level that appeared best focused under neutral adaptation (gray field). Typically 3 repeated settings were made for each observer. The results were analysed in terms of the SR of the perceived focus point.

7.3 Results

7.3.1 Testing scaled HOA patterns

The blur level selected as best focused was very close to the natural blur level for 3 of 4 observers, and for all observers remained very similar whether observers first adapted to a neutral gray field or to the image filtered by their own natural blur. The settings under neutral adaptation (gray field) were roughly 77 % of their HOA (89.3 % excluding Subject S3 who has a low tolerance to blur) and similar to the settings when they were adapted to their own HOA (82 %, and 94.3 % excluding S3) as shown in Figure 7.3 A. The neutral focus therefore was not perceived for fully corrected optics, and in general, occurred at a blur level near the subject's own aberrations. The low difference in the perceived neutral focus between neutral adaptation (gray field) and natural adaptation suggested that the subjects were "pre-adapted" to their own aberration level. The average difference in the perceived focus between the neutral and the natural adaptation conditions was 0.012 (in terms of strehl ratio, SR, defined as the normalized peak of the PSF). However, the perceived focus was biased from the blur level predicted by their HOAs (by

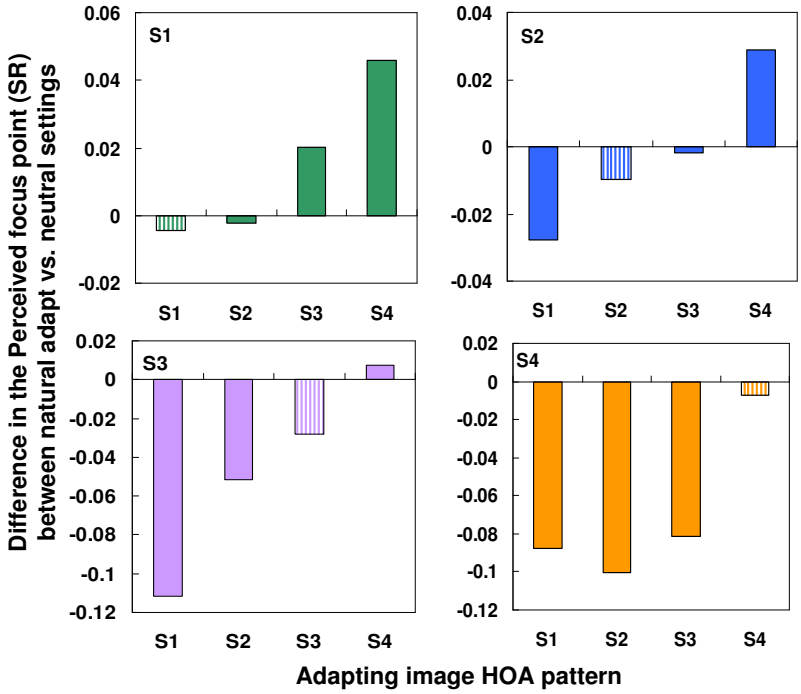

Figure 7.4: Testing scaled high order aberrations patterns. Difference in the perceived focus level (in terms of Strehl Ratio) between natural adaptation and the subject's neutral settings, when the subjects adapted to their own aberrations (striped bars) or to the aberrations for each remaining subject (solid bars). (Reproduced from Sawides et al. [2011b]).

0.044 in terms of SR, on average) when each observer was instead adapted to images blurred by other's HOA patterns, corresponding to the native blur of the other 3 participants (Figure 7.3 B). The pattern of after-effects was consistent with the adaptation predicted by the overall blur magnitude. Specifically, in individuals with lower Strehl Ratios (more native blur), adaptation to the blur from the less aberrated eyes caused their native focus level to appear too blurred (as expected if they were now adapted to images that were previously for them "too sharp" (Figure 7.4, observer S1). Conversely, observers with low levels of natural blur perceived their natural focus level as too sharp when adapted to the blur from more aberrated eyes (Figure 7.4, observer S4).

7.3.2 Testing 128 real complex HOA patterns

In a further experiment, we examined whether the internal norm for blur is set to a specific aberration pattern or to the overall blur, regardless of its form. Observers again judged whether images appeared too blurred or too sharp, but this time for an image sequence generated from a set of 128 different HOA patterns from real eyes. There was a close correspondence between the image quality perceived as

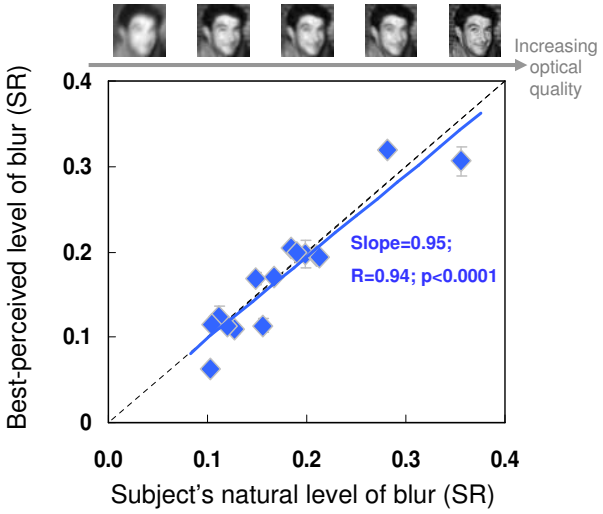

Figure 7.5: Testing 128 real complex high order aberration patterns: Strehl Ratio of the image perceived as best focused versus the natural Strehl Ratio for each of the 15 subjects. (Reproduced from Sawides et al. [2011b]).

neutral and the retinal image quality produced by the aberrations of the subject, with an average deviation of 0.014 (in terms of SR), and a strong correlation between the blur of the image perceived as neutral and the subject's own blur (Slope=0.95; R = 0.94; p<0.0001; Figure 7.5). For the majority of the subjects, the blur level perceived as best focused was well predicted from the magnitude of the native blur present in their eyes.

7.4 Discussion

Adaptive Optics, allowing to appropriately control the blur level of the retinal image, provided a powerful technique to directly test neural adaptation to the subjects' own blur level.

The innovative finding of the study is that subjects appear to be adapted to the blur level imposed by their own optical aberrations. Exposing observers to identical aberration patterns ensures that any difference across subjects will arise from their own neural processing and their prior neural adaptation.

Under these conditions, we found that an observer's focus settings remain largely unaffected when adapting to their own aberrations, but were significantly biased toward higher or lower blur levels when adapted to the aberrations from observers with more or less optical blur respectively. This demonstrates that the visual mechanisms mediating the perception of focus can differentially adapt to changes in image blur level resulting from HOAs. Moreover, the finding that after-effects were weakest near the level of the observer's natural blur (Figure 7.4, S1 and S4) further suggests that the individual's subjective neutral point corresponded to

the long-term adapted state induced by their optics. This in turn suggests that the blur level that appears correctly focused to an observer is not merely a learned criterion (e.g. so that all observers encode blur similarly but choose the blur level they are accustomed to seeing).

Specifically, if observers differed only in how they labelled the blur (and thus did not differ in the neural encoding) then they should all show the same aftereffects for a given adapting level, regardless of whether they described that level as too blurred or too sharp (since the adaptation would induce the same shifts in their neural sensitivity). Instead, direction of the blur aftereffect was specific to each observer's intrinsic blur level, revealing that the individual differences in perceived focus at least in part reflect differences in how their sensitivities are normalized to their ambient blur level [Webster and Leonard, 2008].

Our results also show that the close association between the coded norm for blur and the observer's aberrations holds over a very wide range of native blur levels (Fig 7.5). For the majority of subjects, the blur level that is perceived as best focused is very closely predicted from the magnitude of the native blur present in their eyes. Together with the observed adaptation effects, this finding strongly suggests that the perception of focus is calibrated for the specific blur levels present in each individual's retinal image. On the other hand, this normalization may depend largely on the overall level of the blur and not on the specific pattern of HOAs generating this level, for this close association held even though the stimuli were not matched to the observers in terms of the actual form of the HOAs. This raises the possibility that the processes of blur adaptation may be unable to resolve subtle differences in the patterns of blur specific to different HOAs, so that the adaptation state is instead largely controlled only by the blur magnitude. The fact that the overall amount of blur proved more critical than orientation is a further novel finding of the study. However, this does not preclude the possibility that the adaptation can also selectively adjust for some differences in the HOA pattern when blur magnitudes are equated [Artal et al., 2004a] analogous to the selectivity found for low order aberrations in chapter 5.

How can these results be reconciled with evidence for only weak adaptation to HOAs? A likely answer is that different studies have measured different perceptual judgments. Correcting HOAs leads to improvements in visual acuity as shown in chapter 3 and an increased subjective impression of sharpness as shown in chapter 4. Previous studies testing for adaptation after correction selected the sharpest image for best image quality, while our observers were instead required to choose the point of subjective focus at which the image appeared neither blurred nor sharp. Consistent with this difference, we scaled the PSF by factors ranging from 0 to 2, which ranged from sharper to blurrier than their natural HOA, whereas previous studies (e.g. Chen et al. [2007b]) instead used stimuli ranging from -1 to 1, and thus never increased the blur relative to the natural level. It is thus plausible that the much stronger implied adaptation we observed is because this adaptation is more conspicuous in how it affects judgments of perceived focus, which may correspond to the neural norm for blur perception [Elliott et al., 2011].

This norm is set by the observer's natural level of blur, yet as we have shown can be rapidly recalibrated when adapted to a different level of HOAs. Consequently spatial vision may be normalized to compensate for the optical imperfections of the eye in the same way that color vision is normalized to discount the spectral filtering of the lens [Delahunt et al., 2004].

7.5 Conclusions

The results provide strong evidence that spatial vision is calibrated for the specific blur levels present in each individual's retinal image and that this adaptation at least partly reflects how spatial sensitivity is normalized in the neural coding of blur.

To what extent judgments of perceived focus depend on the total magnitude as opposed to the specific pattern of blur introduced by the eye's high order aberrations (HOA) will be discussed in the following chapter.

8

Dependence of subjective image focus on the magnitude and pattern of high order aberrations

The image formed by the eye's optics is inherently blurred by aberrations specific to the individual's eyes. We examined to what extent judgments of perceived focus depend on the total magnitude as opposed to the specific pattern of blur introduced by the eye's high order aberrations.

This chapter is based on the paper by Sawides et al. " Dependence of subjective image focus on the magnitude and pattern of high order aberrations" Journal of Vision, 2012. The co-authors of these studies are Carlos Dorronsoro, Pablo de Gracia, Maria Viñas, Michael A. Webster and Susana Marcos.

The author of this thesis implemented the experimental procedure, performed the measurement on human eye's, collected and analysed the data.

This work was also presented at the Association for Research in Vision and Ophthalmology (ARVO) annual meeting (May 2012) in Fort Lauderdale, Florida, USA, as an oral contribution.

8.1 Introduction

In the previous chapter (7), we examined whether vision is adapted to the blur produced by the global level of blur produced by high order aberrations (HOA) of the individual's eyes by judging the best-perceived focus from a series of images blurred by HOA from real subjects with an extended range of blur. We found that, for most subjects, the blur level deemed as best focused was closely predicted from the magnitude of their native blur, even though the blur in the judged images was not matched to the subjects' blur in terms of the actual orientation of the HOA. This suggested that the codification of their internal blur might depend largely on the overall level of the blur and not on the specific features associated with the asymmetric blur arising from a particular HOA pattern. On the other hand, changes in the orientation of HOA have been found to significantly influence judgments of image quality. Artal et al. [2004a] showed that subjects considered images blurred with their own HOA as sharper than images blurred with rotating versions of their own HOA. Their results thus pointed to an adaptation that was selective for the specific pattern of HOA. Thus, the extent to which the overall magnitude of blur or the actual form of blur drives long-term adaptation to one's aberrations remains unresolved.

To directly answer whether the internal code for blur is biased by magnitude or by orientation, we examined the relative impact of the magnitude versus the pattern of HOA on blur adaptation in two experiments with stimuli that isolated the independent effects of blur level (with no orientation bias) and the effects of blur orientation (with an equal amount of blur) under full Adaptive Optics correction. In the first experiment, we measured the blur level perceived as best focused by subjects when images were blurred only by pure defocus, which allowed us to test the effect of blur magnitude when there were no differences in the orientational features of blur. In the second experiment, we instead held the overall level of blur constant, then compared the perceived focus of images, which varied only in the orientation of the HOA.

8.2 Methods

8.2.1 Subjects

Six subjects participated in the first experiment, and their natural Strehl Ratio at best focus varied from 0.103 to 0.356 (for 5 mm pupil diameters). Four experienced subjects participated in the second experiment, and their natural Strehl Ratio varied from 0.042 to 0.1233 (for 5 mm pupil diameters). All the subjects had normal vision as evaluated in clinical ophthalmological examination and were emmetropes or corrected ametropes. Their refractive error (without correction) was -1.5±2.4 D on average.

Figure 8.1: Images used in the experiments. The first image (face) was used in the first experiment. All 10 images were used in the second experiment.

8.2.2 Generation of optical blur

The original images in both experiments were acquired using a photographic digital camera with an original resolution of 4M pixels and converted to grayscale. The images showed a rich content of spatial frequencies and orientations with the typical power spectra of natural images. In the first experiment, one face image was used (the first image in Figure 8.1, in order to compare the results with those found in chapter 7). In the second experiment, the 10 images shown in Figure 8.1 were used. The images subtended 1.98 ^{o} on the retina.

As in the previous chapters, standard Fourier Optics techniques were used to calculate the Point Spread Function (PSF) corresponding to a given aberration pattern. Image convolutions were performed using routines in Matlab. All computations were performed for 5 mm pupils. Strehl Ratio (SR) was used as an image metric. Retinal-image- based metrics are preferred over wavefront-based metrics, such as root mean square (RMS) [Applegate et al., 2002, 2003a; Marsack et al., 2004], in relation to visual performance. For the purposes of this experiment, SR was defined as the volume under the modulation transfer function (MTF) (Experiment 1, to compare the results with those found in chapter 7) or PSF Maximum (Experiment 2).

In the first experiment, PSFs estimated from 128 levels of defocus (varying from 0.036 to 0.29 D with a 0.002 D step) were generated. This range of defocus was chosen to match a blur level (in terms of SR) similar to that of natural HOA of a group of 128 real wavefront aberrations used in chapter 7. The corresponding SR ranged from 0.049 to 0.844 (5 mm pupils). Figure 8.2 shows a subset of eight images from the 128 defocused images used in the experiment.

In the second experiment, images were convolved by the PSFs generated from 100 wave aberrations from real eyes. Tilts, astigmatism and defocus were set to zero. The original coefficients were scaled by a factor such that the resultant SR was similar across the 100 PSFs (within less than 2 % deviation) and matched the SR of the test subject. The experiment therefore maintained a similar level of blur in all images presented to a given subject but different orientations of the

Figure 8.2: Subset of images used in the first experiment (from a total of 128 images). Images are blurred by defocus (the corresponding Strehl Ratios are marked in white).

Figure 8.3: Subset of images (convolved with the corresponding PSFs shown in the upper-left corners) used in the second experiment (from a total of 100 images) for one subject (S1, SR=0.0625). PSFs were generated from HOA from real eyes, scaled to produce the same SR in all images, equal to the subject's natural SR. Simulations were for 5 mm pupil diameters.

blur. Four different series of images were generated, corresponding to the four subjects who participated in the second experiment, and for each of the images used in Figure 8.1 (i.e., 4 000 total images). Figure 8.3 illustrates a subset of images generated for the experiment by convolution with the corresponding subset of PSFs (upper-left image corner) for one of the subjects (S1).

The 100 wave aberration patterns, selected from a real subject database, presented a large diversity of orientation and aberration distribution. Correlation coefficients were used to quantify the similarity across patterns (keeping the blur level constant). Correlation coefficients between the subject's PSF and their rotated PSFs were 0.476 (S1), 0.387 (S2), 0.412 (S3), and 0.277 (S4) for each subject. Correlation coefficients ranged from 0.308 to 0.490 (between the subject's PSF and the other three subjects' PSFs), from 0.255 to 0.596 (between the subjects' PSFs and the 10 reference PSFs), and from 0.055 to 0.720 (between the subjects' PSFs and the test PSFs). The large range in the correlation coefficients indicated a wide distribution of orientations across aberration patterns.

8.2.3 Experimental procedure

Experiments were performed monocularly under natural viewing conditions (natural pupil and without cycloplegia), for 5 mm pupil diameter. We used the Adaptive

Optics (AO) system, described in the chapter 2, to measure and correct the natural aberrations of the subjects (with the deformable mirror (for astigmatism and high order aberrations correction) and the Badal system (for spherical refractive error correction)). On average, the RMS (excluding tilts and defocus) decreased from $0.361 \pm 0.124\,\mu$m to $0.081 \pm 0.050\,\mu$m with an average RMS error correction of 78 $\pm 9\,\%$. Subject S2 performed the measurements wearing her soft contact lenses.

In a first session, the aberrations of the participating subjects were measured to estimate their natural SR (which was needed to generate the set of images for the second experiment). This preliminary session and the test session for Experiment 2 were less than 1 month apart. Two psychophysical experiments were performed under full AO correction of the subject's aberrations: (1) Perceptual best focus from purely defocused images to investigate to what extent judgments of image focus might depend on the overall amount of their native blur (with no orientation) and (2) best focus from images with a similar blur level but different blur orientation to explore whether the focus judgments were also sensitive to the orientation of blur produced by HOA.

Experiment 1: Perceived best focus from images blurred with pure defocus

For six subjects, judgments of perceived blur were measured to determine the physical blur level that appeared best focused under neutral adaptation (to a gray field, which had a luminance level of $41\,\mathrm{cd/m^2}$, similar to the average of the test images). The psychophysical paradigm consisted of a 2AFC procedure (sharp/blurred). The sequence of the psychophysical experiment consisted of 1 min exposure to the gray field after which a test image was presented (1 s) to the subject, who had to respond if the image was sharp or blurred. The subject readapted for 3 seconds between each test image. Stimulus levels were varied with a Quest algorithm to find the best-perceived focus point. The perceived focus point usually converged, in the 2AFC procedure, to the final value in less than 35 trials or 16 reversals (if not, the measurement was discarded and repeated). Each subject repeated the experiment three times. Figure 8.4 shows a sequence of images presented in Experiment 1.

Experiment 2: Perceived best focus from images blurred with different HOA at the same blur level

Judgments of best focus from pairs of images with identical overall blur level (SR) and different blur orientation were obtained on four subjects. The psychophysical paradigm consisted of a 2AFC procedure where two images blurred with two different HOA patterns were presented sequentially (1.5 s each). The subject had to respond whether the first or second image appeared better focused. A 20-second adapting gray field was presented at the beginning of the experiment and for 3 seconds between trials.

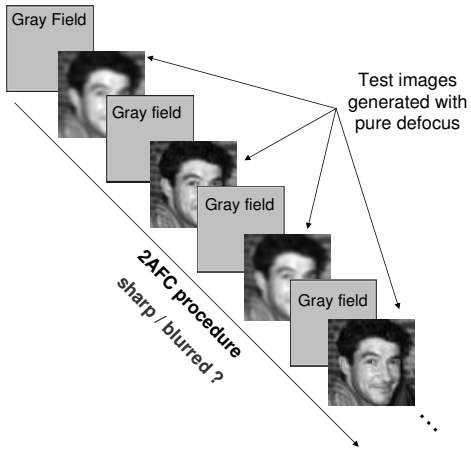

Figure 8.4: Subset of images (Sequence of images in the 2AFC procedure of Experiment 1 (perceived best focus from purely defocused images).

In each test, a series of 100 pairs of images (10 random repetitions of the 10 images of Figure 8.1) were presented to the subject. In all cases, one image in each pair was always blurred with a given reference PSF, while the other image was blurred by a PSF randomly selected among the 100 different PSFs (previously computed to match the subject's SR). Comparisons were performed between the images blurred by a reference pattern and a set of 100 other aberrations. The order of presentation of the images within a pair was random.

Each subject performed 11 tests for 11 different reference PSFs. The reference PSFs were: the PSF of the test subject (S#, condition 1); the 90 º rotated PSF of the subject (rotated S#, condition 2); and nine other PSFs, which included those corresponding to the other three participants of the study, as well as six additional patterns selected among the 100 PSFs (P#). Conditions 1 and 2 were tested three times in each subject, while the other nine conditions were tested once in each subject. Figure 8.5 shows an example of the image sequence in Experiment 2.

8.2.4 Data analysis

Experiment 1: Perceived best focus from images blurred by pure defocus

The blur level corresponding to the point of subjective best focus (perceptual blur) was obtained from the average of the last eight reverse responses in the QUEST sequence. The level was expressed in terms of SR (normalized volume under MTF) and compared to the SR of the natural retinal image blur for each subject (natural blur). Data were fitted by linear regression, and the correlation coefficient and significance were estimated.

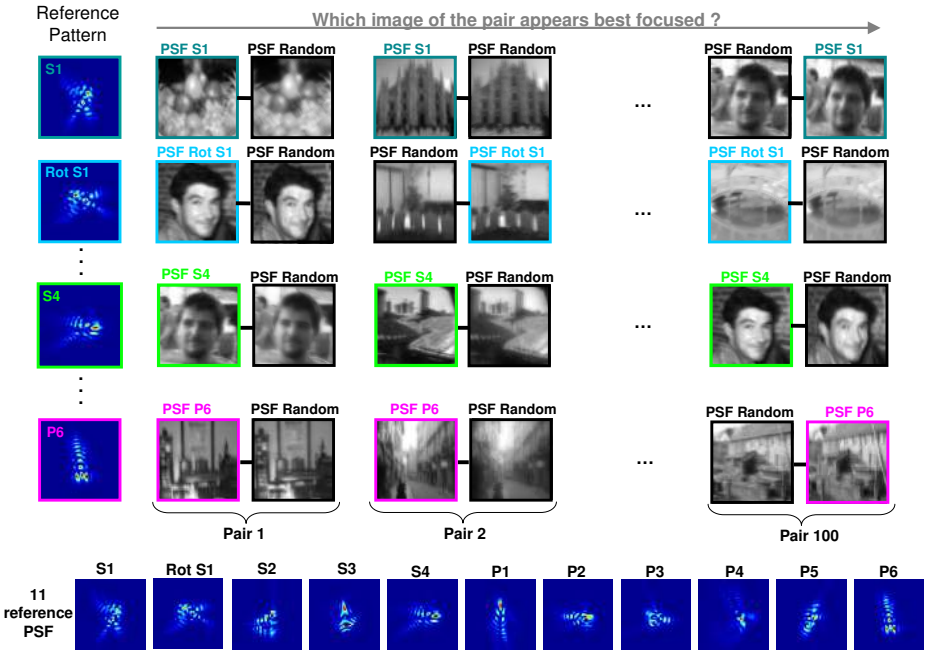

Figure 8.5: Sequence of images in the 2AFC procedure of Experiment 2 (in which images were blurred by different HOA but with the same SR as the subject's natural PSF, shown here for subject S1). In each pair, one of the images was always blurred with a constant reference PSF, while the other was blurred with a randomly selected PSF. The 11 reference PSFs corresponded to the PSF of the subject, a rotated version of their PSF, the PSFs for the three remaining subjects, and six other PSFs from the database. One-hundred image pairs were shown for each reference (corresponding to the 10 images in Figure 8.1, each shown 10 times in random order).

Experiment 2: Perceived best focus from images blurred with different HOA at the same blur level

For each image series, the percentage of times the image blurred with the reference PSF was perceived as better focused was recorded. The preferences were compared across conditions to assess whether the subject showed a bias for or against a particular HOA. The arcsine square root transformation was applied to all sets of percentage data to guarantee a normal distribution in the data set before the application of ANOVA and t-tests.

A one-way ANOVA (post-hoc: Tukey's b-test; $p<0.05$) was applied to the arcsine square root transformation to test for differences in the percentage across the 10 different references (all references except the rotated version) — with the reference pattern as the factor and the percentage preference for each image type as the dependent variable with separate responses — for every group of 10 image pairs (equal image, different blurring pattern). One-sample t-test was applied to test whether the percentage of preferred images blurred with the subject's PSF as reference was significantly different from 50 % and significantly higher than with other reference patterns. T-test as well as a mixed model analysis were also used to compare the percentage of images preferred when blurred with the subject's PSF or its rotated version. In the mixed model analysis, the fixed effect was the reference pattern (own/rotated); the random effect was the subject; and the repeated effect was the number of repeated measures (three in each condition [own/rotated]) associated with each reference pattern. The dependent variable was the arcsine square root transformation of the percentages. Statistical analysis was performed with SPSS software.

8.3 Results

8.3.1 Perceived best focus from purely defocused images

Figure 8.6 shows the correspondence between the level of physical defocus perceived as best focused and the subject's natural blur in terms of SR (blue points), along with a linear regression fit to the data. The correlation between the subject's natural blur and the defocus level identified as neutral is highly significant and nearly perfect ($R=0.999$; $p<0.0001$). Thus the differences in the focus percepts across subjects could be accounted for almost entirely by the differences in their overall levels of native blur, regardless of the individual HOA.

On the other hand, the negative offset of the regression line indicates that for the same amount of blur (Strehl defined by the normalized volume under MTF), pure defocus appears more blurred than the blur produced by their natural aberrations. Notably, this differs from the effects when images are blurred by the subject's actual HOA (shown by the gray points in the figure, from the previous chapter (7), for which SR accurately predicts the absolute levels of the subjective neutral points.

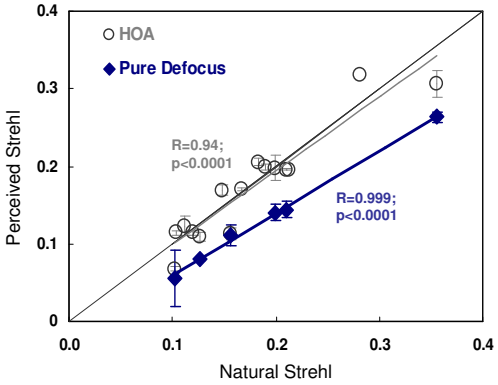

Figure 8.6: Strehl Ratio of the image perceived as best focused versus the natural Strehl Ratio of the subjects (defined as the volume under MTF) . Data in gray are the results reported in previous chapter 7 when blurring the sequence of images with different HOA patterns, tested for 15 subjects (y=0.952x + 0.0004; R=0.94; p<0.0001). The blue symbols are for the 6 subjects of the current study (a subset of the subjects from the previous study) when testing images blurred with only defocus (y=0.806x - 0.022; R=0.999; p<0.0001). (Reproduced from Sawides et al. [2012]).

We tested possible effects of the specific choice of image quality metric on the results of Figure 8.6. As shown in Figure 8.7, the strong correlation between the subject's natural blur and the perceived neutral blur was found regardless of the image quality metric (SR or Augmented VSOTF Visual SR, Iskander [2006]), in all cases (images blurred by HOA or pure defocus), with regression coefficients R ranging from 0.87 to 0.999 (p<0.05). The offset ranged from zero (HOA, all metrics) to negative (pure defocus, SR) and positive (pure defocus, Visual SR), because different metrics capture differently the effect of high spatial frequency content in purely defocused images.

8.3.2 Perceived best orientation from images with the same blur level

Figure 8.8 shows the percentage of images that were judged as better focused when filtered with a given HOA reference pattern. Each panel shows the settings for each subject, measured using as a reference his/her natural pattern (first bar), or a pattern corresponding to a different subject: the other three subjects of the study (bars 2-4) or six additional patterns (bars 5-10, denoted P1-6). (The remaining reference corresponding to a rotated version of the subject's own PSF is considered below and shown in Figure 8.9).

Figure 8.8 reveals that none of the patterns (the subject's own, in particular) is consistently chosen as best focused, or alternatively consistently rejected by all subjects. We assessed these preferences in a number of ways. First, if subjects

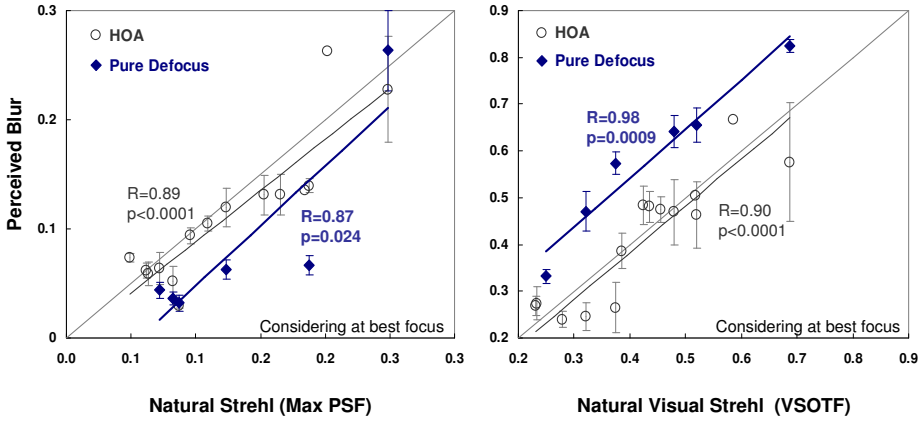

Figure 8.7: Strehl Ratio of the image perceived as best focused versus the natural Strehl Ratio of the subjects, defined as the maximum PSF or the visual strehl (VSOTF). As in Figure 8.6 data in gray are the results reported in previous chapter 7 when blurring the sequence of images with different HOA patterns but expressed with these new retinal metrics. tested for 15 subjects (y=0.9397x - 0.0057; R=0.89; p<0.0001 (Maximum PSF); y=1.0024x - 0.0184; R=0.90; p<0.0001 (VSOTF)). The blue symbols are for the 6 subjects of the current study when testing images blurred with only defocus (y=1.0990x - 0.0623; R=0.87; p=0.024 (Maximum PSF); y=1.0511x + 0.1216; R=0.98; p<0.001 (VSOTF)

were strongly adapted to the specific pattern of blur formed by their own HOA, then they should prefer images blurred with their HOA. However, the percentage of images judged as best focused was not systematically higher when filtered with the subject's own HOA pattern. For example, based on a conventional one-sample t-test applied to the arc sine square root transformation for the 300 pairs that included each subject's own HOA to test whether the percentages were different from 50 %, S2 did not show a significant preference (p=0.205), while S3 strongly preferred their own blur (p=0.001), and S1 and S4 instead showed a significant bias against their own blur (S1: p=0.015 and S4: p=0.046).

Second, if subjects were sensitive to their specific PSF, then the preferences for the remaining 9 reference PSFs should be lower on average, yet this was again found only for S3 (t-test, p<0.001). Finally, if the specific HOA pattern mattered at all for the blur judgments, then the preferences should show an effect of the reference HOA. To test this, we used a one-way ANOVA applied to the arc sine square root transformation to test for differences in the percentages across the different reference levels. The one-way ANOVA was performed for each individual subject for the 10 reference patterns (all patterns except the rotated version). Separate responses for every group of 10 image pairs (equal image, different blurring pattern) were analysed. The percentages of images judged as best focused for each pattern were compared. The analysis revealed that there was a statistically significant difference between the percentages of images perceived as best focused within the different PSF references, as determined by the one-way ANOVA for each subject:

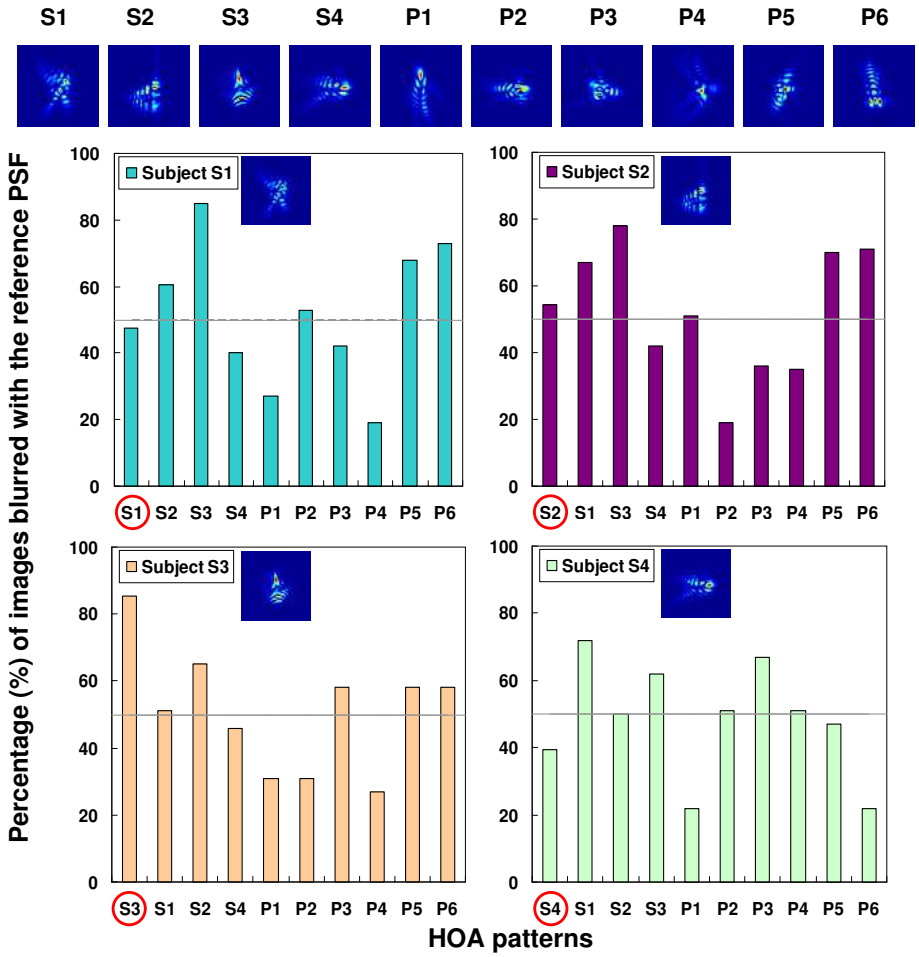

Figure 8.8: Percentage of images blurred with each reference pattern, which were judged as best focused. Data are for 10 different reference patterns (illustrated by the corresponding PSFs). Four reference patterns correspond to the HOA of the tested subjects (S1-S4) and the rest to additional HOA pattern selected among 100 PSFs (P1-P6). Each panel shows responses for each subject. The first bar in each panel represents the response for each subject's own PSF. (Reproduced from Sawides et al. [2012]).

for S1: ($F[9,90]=13.516$, $p<0.001$), for S2: ($F[9,90]=12.462$, $p<0.001$), for S3: ($F[9,90]=10.887$, $p<0.001$) and for S4: ($F[9,90]=11.614$, $p<0.001$). Together, these analyses suggest that subjects were sensitive to the specific pattern of HOA in their blur judgments, but were not biased toward preferring their own HOA for these judgments.

As a further test, we compared preferences when the reference blur corresponded to their own HOA or the same PSF rotated 90 deg (Figure 8.9). Comparisons were performed between the natural aberration condition (taken as a reference) and a set of 100 other aberrations, and between the rotated aberration condition (taken as a reference) and a set of 100 other aberrations. In this case, there was a clearer tendency to favor their own HOA. Specifically, with the rotated version, the percentage of images blurred by the reference PSF was systematically lower than that with the subject's natural pattern (averaging 45 % vs. 57 % across subjects). This difference was significant for each subject (t-test on the arc sine square root transformation; p-values displayed in Figure 8 for each subject). The mixed model analysis showed that the reference patterns had a significant effect on judgment of the perceived best focused images ($F=206.609$, $p<0.001$) and the percentages with their own PSF were significantly higher than the percentages with the rotated version of the subject's PSF ($t=14.374$, $p<0.001$, 95 % Confidence Interval for the difference is 0.0985 to 0.1427). These results thus point to a weak but consistent bias for the orientation of the subject's own HOA, an effect which is also hinted at by the pattern of results in Figure 8.8. Specifically, subjects with a vertically or horizontally oriented PSF tended to perceive as best focused those images blurred by PSFs with similar orientations. For example, for S2 (dominated by vertical coma) the percentages of images judged as better focused were higher when blurred by P1 or P6 (dominated by vertical coma) than when blurred by P2 and by P4 (dominated by horizontal coma). In contrast, for S4 (dominated by horizontal coma) the percentages of images judged as better focused when blurred by P2 and P4 were higher than those when blurred by P1 and P6. Moreover, Tukey's b-post hoc test revealed that for S4, both P2 and P4 belonged to the highest subset (for alpha=0.05) whereas both P1 and P6 belonged to the lowest subset. In contrast for S2, P2 was the only component of the lowest subset and P6 belonged to the highest subset.

8.3.3 Controlling for short term adaptation to the reference pattern

Finally, we explored the possibility that the judgments might be contaminated by adaptation to each reference PSF during the experiment, since this was shown repeatedly in each test pair. This adaptation might lead subjects to renormalize for the current reference HOA and thus mask a bias for their natural HOA. Short-term adaptation to the reference pattern blur would be expected to increase the percentage of selected reference pattern images over the course of the measurements. However, this effect was not found. We analysed the responses grouped in series of

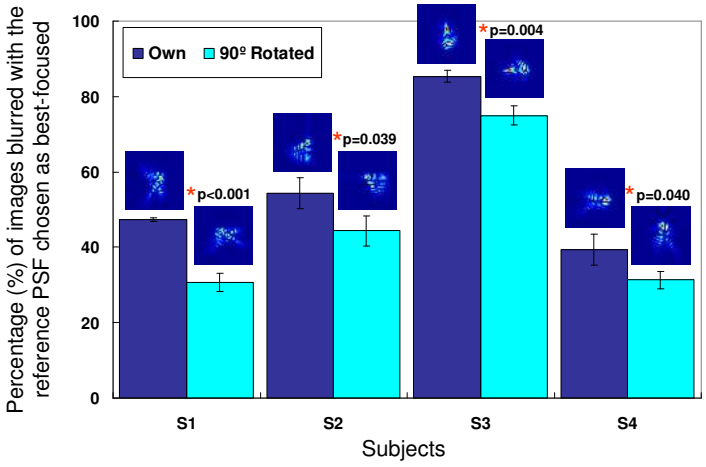

Figure 8.9: Percentage of images considered as best focused when the PSF reference corresponded to the subject's natural HOA pattern, or to a 90 º rotated version of subject's HOA pattern. (Reproduced from Sawides et al. [2012]).

10 image pairs. For none of the conditions was there an increase in the percentage of selected images over time.

8.4 Discussion

In previous chapters (5 and 6), we have examined the ability of subjects to dynamically adapt to new amounts and patterns of low and higher order aberrations. Also, we have examined how perception of focus is compensated for the retinal image blur produced by the eye's optics. These studies have shown that the point of subjective focus corresponds closely to the level of physical blur introduced by the high order aberrations of the individual's eye (as illustrated by the gray symbols in Figure 8.6, and chapter 7). Thus the judgments of focus appear to nearly completely discount the habitual uncorrected retinal blur from the observer's HOA so that perceived focus is tied to the properties of the stimulus rather than to the retinal image. Moreover, we also found that these focus judgments probably reflect an actual adaptation to the level of natural blur and are not simply a learned criterion for judging the blur. Specifically, the level of blur perceived as focused not only matched the observer's native blur, but was the level that did not produce a blur aftereffect. In contrast, when observers were exposed to images with higher or lower blur levels, their focus judgments were shifted to higher or lower levels because of short-term adaptation (chapter 7). Thus this suggests that the perceptual null for focus corresponded to an actual null in the neural mechanisms encoding focus, because it was the stimulus level - specific to each observer - that did not alter the relative responses within the spatial mechanisms mediating blurred or sharp percepts. This is similar to the finding in color vision that the stimulus

that appears white is compensated through adaptation for the specific spectral sensitivity of the observer [Webster and Leonard, 2008].

In the present study, we extended these results to directly assess how sensitive adaptation is to the specific pattern of blur resulting from the subject's HOA. To isolate the effects of the magnitude versus the orientation of blur, we tested blur judgments from purely defocused images with no orientation bias and blur judgments of images with a constant level of blur (matched to the subject's blur level) but different patterns. The first experiment restricted blurring to pure defocus and thus the only cue for focus judgments was the magnitude of the blur. Nevertheless, intersubject differences in the point of subjective focus could be very closely predicted from differences in the SR of their native blur. Again, this is similar to the effects we found in the chapter 7 when asking subjects to judge the perceived blur from images blurred by different natural HOA, which could also be closely predicted from the overall blur or SR. Together, these results suggest that overall blur level is a highly salient cue and likely the primary cue in the internal coding for blur, at least for HOA.

However, despite similar correlations between the subject's natural blur and the percepts of blur produced by pure defocus (current study) or actual HOAs (previous study), there were two differences in the results. First, unlike the previous experiment where there was a close absolute correspondence between the two measures (as shown by the gray regression line in Figure 8.6), the subject's natural SR overestimated the SR for subjective focus (i.e., images defocused by an amount equal to the subject's natural SR appeared too blurred as shown by the blue regression line in Figure 8.6). This negative offset for the purely defocused images suggests intrinsic differences to the blur nature of pure defocus versus HOA, likely as a result of the image quality metric used to describe the level of blur. In fact, analysing the data in terms of visual SR revealed a similar correlation of natural versus perceived blur, but a shift in the offset. Several studies suggest that subjects differently perceive blur from pure defocus or HOA, implying that the specific orientation of the blur in each subject's HOA does play a role in the judgment of best-perceived focus. The actual basis for this difference is not clear. Guo and Atchison [2010] also reported that subjective tolerance to blur produced by an oriented aberration (astigmatism) was greater than the tolerance to defocus, although the amounts varied with the experimental conditions. The relative effects of simple myopic defocus or myopic astigmatism on visual acuity appear however to be controversial in the literature [Sloan, 1951; Miller et al., 1997; Remón et al., 2006]. Also,while the relative effect of defocus and high order aberrations on vision have been reported in several studies [Applegate et al., 2002, 2003b; Atchison et al., 2009a; Atchison and Guo, 2010], in most cases comparisons are performed for similar Zernike coefficient weights or RMS (across orders or terms), which, unlike the current study, do not represent equal amounts of blur in terms of SR, so that direct comparisons are difficult.

A second difference between our current (using blur from pure defocus) and former (using blur produced by high order aberrations) measurements of the impact

of overall blur level on focus judgments is in the strength of the correlation. Specifically, variability in the predicted settings was higher when blur was introduced from actual HOA rather than from defocus. This difference may again indicate that subjects were sensitive to the actual HOA on the focus judgments. To directly evaluate this sensitivity, Experiment 2 was designed so that the overall amount of blur was kept constant, and only the shape of the PSF varied. This revealed a significant contribution of orientational aspects of the blur to the subject's judgments. In agreement with Artal et al. [2004a], images blurred by a 90 ^{o} rotated version of the subject's PSF were perceived consistently as less focused than images degraded by their natural PSF (a consistent effect across all subjects).

In the current study, the comparisons were not directly made between the HOA and its rotated pattern, but rather each was evaluated as a reference compared to 100 other aberrations. This again revealed a preference for the natural aberrations (57 % on average) in comparison with the rotated version (45 % on average). This bias was nevertheless surprisingly weak. In fact,only one of the four subjects judged their own blur as significantly better focused, suggesting that, in general, individuals may exhibit little preference for their own degradation pattern. Some subjects actually showed a higher bias for other aberration patterns than their own. The basis for these differences and how they depend on the subject's specific HOA is unclear and is a question we are currently investigating. However, the present findings strongly suggest that the perception of focus is primarily calibrated for the overall level of blur introduced by HOA and may be only weakly impacted by the local features associated with the asymmetric blur arising from a particular HOA, as other patterns are frequently identified as better focused than the native pattern.

8.5 Conclusions

The perceived best focus (from purely defocused images) is highly correlated with the overall amount of blur produced by the high order aberrations of the eye. The negative offset in that correlation suggests differences in the appearance or perception of blur produced by pure defocus from the blur produced by the natural aberrations of the eye, as measured by a global metric of blur like Strehl Ratio.

The fact that blur is discriminated across reference patterns as well as the higher preference for natural than rotated aberrations suggests some sensitivity to the orientation. However, the findings do not support a strong bias to prefer the individual's own HOA pattern.

The codification of internal blur thus seems to be highly driven by the overall amount of blur and only to a weak extent by blur orientation, as other patterns are frequently identified as better focused than the native pattern. In the next chapter, we designed a classification-images based psychophysical paradigm to systematically test he bias for the subject's own HOA pattern and estimate the subject's internal code for orientation.

9

Using pattern classification to measure adaptation to the orientation of high order aberrations

The preference for the individual overall amount of blurred appears strong. However, there is some evidence that the subject may also be adapted to specific features of blur, i.e. orientation. We used a version of the classification image paradigm - using a random assembly of human PSFs rather than spatial noise samples - to extract the PSF that best matched a subject's natural PSF.

This chapter is based on the paper by Sawides et al. " Using pattern classification to measure adaptation to the orientation of high order aberrations" submitted for review, 2013. The co-authors of these studies are Carlos Dorronsoro, Andrew M. Haun, Eli Peli and Susana Marcos.

The author of this thesis implemented the experimental procedure, performed the measurement on human eye's, collected and analysed the data.

This work was also presented at the 6^th European Optical Society (EOS) Topical Meeting on Visual and Physiological Optics (EMVPO) annual meeting (August 2012) in Dublin, Ireland, as an oral contribution.

9.1 Introduction

e have gained evidence that observers appear to be adapted to the blur produced by their own aberrations, as images blurred with similar magnitude of blur as the subject's own appear as best focused (unlike images blurred by lower or higher amounts of blur, which appear over sharpened or blurred, respectively (chapter 7). The preference for the individual overall amount of blurred appears strong. However, there is some evidence that the subject may also be adapted to specific features of blur, i.e. orientation. In the previous chapter (8), we showed that a subject's perceived normal is biased towards images blurred by their natural PSF as opposed to towards those with a 90 º rotation of their PSF, in agreement with a previous study showing that images blurred by the subject's Point Spread Function (PSF) were perceived as having better quality than those blurred with the same PSF but at different orientations [Artal et al., 2004a]. Similarly, in a test where subjects were presented with pairs of images randomly blurred by their own PSF or someone else's PSF (selected from a set of 10 other subjects, and scaled to match the subject's own overall blur level) there was some bias towards the natural PSF, but it was weak (53±21 % vs 51±19 %, on average). While prior experiments point to some role of the orientation of blur in the internal coding, they were not designed to identify the internally coded PSF.

In this study we employed a psychophysical experimental paradigm inspired by the Classification Image method. This method was first proposed by Ahumada and colleagues [Ahumada and Lovell, 1971; Ahumada and Marken, 1975] in audition to extract relevant features for tone detection, and more than 20 years later was applied to vision by the same authors in the study of vernier acuity tasks [Ahumada, 1996; Beard and Ahumada, 1998]. As typically employed, the technique involves the addition of random noise to a stimulus image so that all the information that can be potentially used by a subject to perform a given task is randomly perturbed from trial to trial. Subjects make a judgement about each stimulus, e.g. whether or not a target is present. The added noises are then averaged for each of the stimulus-response categories and differenced according to whether the observer made a correct or incorrect decision. These differenced sums of random noise samples yield a profile, called the Classification Image, which is assumed to describe how the observer weighted each pixel in the stimulus to reach their trial-by-trial decisions. This technique has been used extensively to study visual strategies in a variety of visual tasks [Eckstein and Ahumada, 2002]: visual detection and discrimination [Ahumada and Beard, 1999] [Watson and Rosenholtz, 1997][Murray et al., 2002], pattern recognition [Conrey and Gold, 2009], visual filtering [Solomon and Pelli, 1994], perceived contrast of natural images [Haun and Peli, 2011] and adaptation to different correlated noise textures [Abbey and Eckstein, 2007].

In this chapter, we used a variant of the classification image paradigm - using a pseudorandom assembly of human PSFs rather than spatial noise samples - to extract the PSF that best matched a subject's natural PSF.

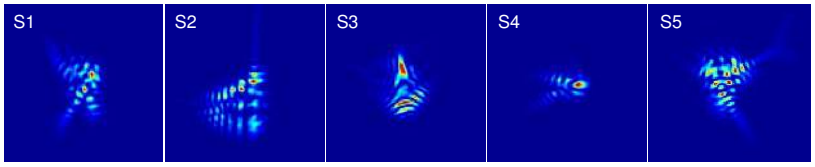

Figure 9.1: Point Spread Function (PSF) of the 5 subjects.

9.2 Methods

9.2.1 Subjects

Five observers with prior experience in visual psychophysical tasks participated in the experiments. All had normal vision according to a clinical ophthalmological evaluation and were emmetropes or corrected ametropes. Their refractive error (without correction) was -1.85±2.59 D on average. Subject S2 performed the measurements wearing her soft contact lenses. Their natural Strehl Ratio (defined as the PSF maximum relative to the diffraction-limited PSF maximum) varied from 0.040 to 0.1233.

9.2.2 Generation of the optical blur

An image of a face (1.98-deg angular subtend, 480 x 480 pixels) was blurred by convolution with the Point Spread Function (PSF) generated from 100 different wave aberrations obtained from real eyes where tilts, astigmatism and defocus were set to zero. To generate the simulated degraded images, the original Zernike coefficients of the 100 wave aberrations were scaled by a factor such that the corresponding Strehl Ratio (SR) was constant across all 100 PSFs, and matched the SR from the subject under test. The same protocol for generating the images was used in chapter 8. Five different series of 100 images were generated, corresponding to each of the 5 subjects participating in the experiment.

9.2.3 Experimental procedure

We used the Adaptive Optics system to fully correct the aberrations of the subject (astigmatism and high order aberrations (HOA) with the deformable mirror and spherical refractive error with the Badal system), while viewing the stimuli presented on the CRT monitor controlled by the psychophysical platform. The procedures for measuring and correcting the subject's aberrations are similar to those described in previous chapters. On average, the RMS error (Astigmatism and HOA) decreased from 0.516±0.275 μm to 0.108±0.021 μm, with an average RMS error correction of 76±8 %. Subject S2 performed the measurements wearing her soft contact lenses. Experiments were performed monocularly and under natural viewing conditions (no cyclopegia or pupil dilation) for 5 mm pupil diameter.

In a first session, the aberrations of the participating subjects were measured to estimate their natural Strehl Ratio (needed to generate the set of images). The

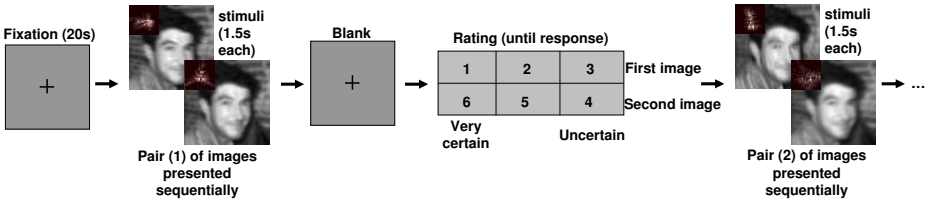

Figure 9.2: Illustration of the psychophysical experimental sequence (presentation of two pairs of blurred images out of a total of 500 pairs followed with a response on the 6 buttons box).

second session involved the Classification Images-based experiment. Subjects were presented sequentially with random pairs of images with similar overall blur level (identical PSF SR but different HOA patterns) and asked to judge which of the two images appeared better focused. The subjects used a 6-button box to respond and ranked their response with 6 choices according to their level of confidence in their judgment (from 1 meaning a high certainty that the first image presented was best-focused, and 6 meaning a high certainty that the second image of the pair was best-focused, 2 or 5 meaning moderate certainty, and 3 or 4 meaning low certainty for the first or second image, respectively). Figure 9.2 presents the sequence of the psychophysical experiment. Typically, the number of trials used in the Classification Image technique varies from hundreds to tens of thousands depending on the nature of the experiment. To balance this parameter with the experiment's duration, we used a total of 1000 blurred images (500 pairs, all random) presented in blocks of 50 pairs to the subject. In each pair, the images were blurred by two different HOA patterns randomly selected among the 100 different patterns. The sequence of the psychophysical test consisted of: (1) 20 seconds adaptation to a gray field; (2) Sequential presentation of 2 blurred images (1.5 s each); (3) Re-adaptation to gray field (blank), during which the subject responded. This sequence was repeated 10 times, with 50 pairs of images presented in each run, and breaks in between runs. Images blurred with the same HOA pattern were therefore presented 10 times during the experiment. The experimental session lasted typically around 3 hours in total.

9.2.4 Data analysis

The image in each pair that was judged as better focused was identified with a positive response, and the other with a negative response. The subject's PSF was compared with each PSF that resulted in a positive or negative response individually. Alternatively, the subject's PSF was compared with the average of PSFs resulting in positive or negative responses respectively. These analyses allowed extracting the features (orientation in particular) of the PSF set that best matched the subject's internal best optical blur code. The computations were carried considering either all responses, or only the 10 highest scored Positive and

Negative PSFs

For the assumed optical quality metric (Strehl Ratio), all images have identical optical degradation, and therefore a random response would be consistent with natural spatial adaptation unbiased by specific features of the natural PSF of the subject e.g., the orientation. On the other hand, a consistent bias of the Positive PSFs towards the natural PSF would indicate that the internally coded blur is driven by the specific features of the subject's natural aberrations. Furthermore, if adaptation is specific to the individual aberration pattern (and not only to the overall level of blur) the average Positive PSF should match more closely the natural aberration of the subject than the Negative PSF. The analyses are therefore carried in terms of: (1) correlation of the Positive and Negative PSF (both individually and on average) with the natural PSF of the subject; (2) Orientation of the Positive and Negative PSF, in comparison with the orientation of the natural PSF.

Correlations of Positive and Negative PSFs with subject's natural PSF

For each subject, the Positive PSFs were weighted with +10 (high certainty, corresponding to scores of 1 or 6), +5 (moderate certainty, corresponding to scores 2 or 5) and +1 (uncertain, corresponding to scores 3 or 4). The Negative PSFs (i.e. the image not identified as positive from the pair) were given the same weight than that given to the Positive PSF of the pair, but with negative sign. This scale allowed giving a strong weight to responses with high certainty. These weights were then added over the 10 presentation instances for each test image, yielding a total score that could range from +100 to -100 (if consistently ranked as positive or negative with the highest certainty). In addition, the average Positive and Negative PSFs were calculated, by registering the centers of mass of each individual PSF (an alternative analysis using maximum intensity did not modify the results). These calculations were performed either over the 10 highest positively and negatively ranked (according to their total scores) PSFs or over all 100 weighted PSFs. Pointwise spatial correlations between the individual (or average) Positive/Negative PSFs, and the natural PSFs were calculated, and the coefficients of correlation were used to evaluate the similarity of the subject's PSF to those identified as positive or negative (both individually and averaged).

Analysis of PSF orientation: Sampled PSF Classification Map and Orientation Plots

The subject's PSF and those identified as negative or positive were compared in terms of their orientation. To study orientations, the PSFs were sampled in 72 angular sectors (centered at the PSF center of mass, and 5 deg angles, from 0 degree centered in the first section). The analysis of PSF orientation is illustrated in Figure 9.3. The intensity of the PSF at a given orientation (mid-angle in each sector) was calculated as the integrated PSF intensity in each sector, and normalized to

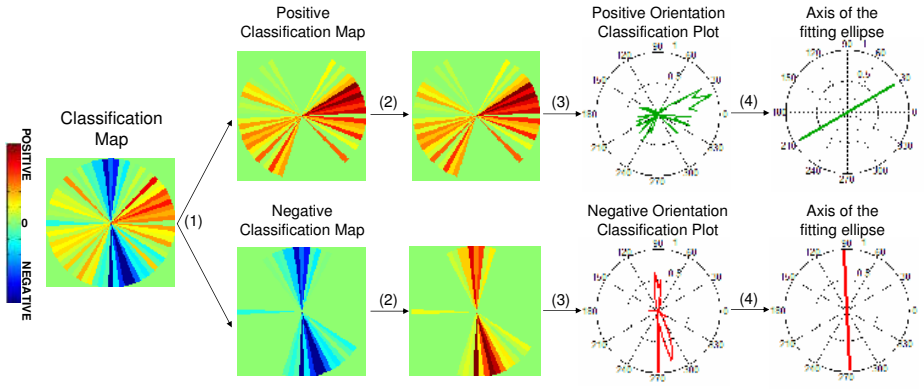

Figure 9.3: Illustration of the PSF orientation analysis: (a) Subject's PSF; (b) Sampled PSF Map in 72 angular sectors. The integrated intensity values are normalized to 1; (c) Corresponding polar plot of the Sampled PSF Map (Orientation Plot); (d) The orientation of the PSF is given by the axis of the fitting ellipse (where the angle represents the main axis of the ellipse and the line length the eccentricity e of the ellipse (e=0.98). Data are for S4).

1 (fig. 9.3 b), the values of the Sampled PSF plotted in polar plots (Orientation Plots, fig. 9.3 c). The orientation of the PSF is given by the main axis of the best fitting ellipse, with the length of the line representing the eccentricity e of the ellipse ranging from 0 (circle) to 1 (fig. 9.3 d).

PSF Classification Maps are built from the subject's responses, by averaging PSFs that were given the same score (1 or 6; 2 or 5; 3 or 4) and whether considered positive or negative. In these averages, the PSFs were weighted by the factors corresponding to the certainty (high/moderate/low) of the response (+10,+5,+1; -10,-5,-1 for positive and negative responses, respectively). Classification Maps were used to extract the PSF that best matched a subject's natural PSF. describing how the subject weighted each angular section of the Sampled PSF. Also, Positive and Negative Classification Maps were computed separately, as shown in Figure 9.4, from the Classification Map by separating the positive and negative weights. Positive and Negative PSF Classification Maps for each subject were represented in polar plots (Orientation Classification Plots), and ellipses were fitted to these. Classification Plots represent the average orientation perceived as best or worst by the subject, respectively.

Correlations were performed between the subject's PSF Orientation Plot and the Positive/Negative Orientation Classification Plots and used to evaluate the similarity of the subject's PSF and the Classification Maps.

The analyses rely on two assumptions: (1) The subjects' natural PSFs show a certain degree of anisotropy in orientation; (2) The 100 PSFs used in the experiment sample all orientations. The Orientation Plots of all PSFs of the sample revealed that 94 % of the fitting ellipse had a well defined orientation (eccentricity>0.6), 58 % had a strong orientation (eccentricity>0.9) ranging from 4 degrees to 179

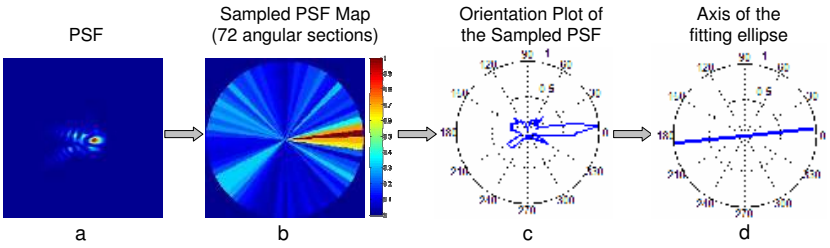

Figure 9.4: Construction of the Positive and Negative Classification Maps from the total Classification Map (1), considering absolute values (2), Polar plot representation of Positive and Negative Orientation Classification Plots (3), main axis of the fitting ellipse and eccentricities (e=0.88 for positive and 0.98 for negative) (4). Example is shown for subject S4.

degrees and 24 % of the ellipses had an orientation of the long axis between 85 and 95 degrees) which generated an averaged PSF (across all the 100 PSFs of the sample) with a slight vertical orientation (eccentricity=0.73, oriented at 85 degrees).

Correlation coefficients were used to quantify the similarity between the subject's PSF and Positive and Negative PSFs. We evaluated the sensitivity of this metric by calculating correlation coefficients of the subject PSFs with the individual PSFs of the sample, and also from the average correlation coefficients of 50 pairs of randomly selected PSFs (repeated 5 times). The Correlation coefficients between the subjects' PSFs and the 100 individual PSFs ranged from 0.055 to 0.720, and were on average for each subject: 0.462±0.093 (S1), 0.404±0.093 (S2), 0.465±0.110 (S3), 0.391±0.103 (S4), and 0.452±0.086 (S5). The large range of the correlation coefficients indicates a wide distribution of orientations across PSFs. The coefficients of correlation of 50 pairs of randomly selected PSFs from the sample were on average 0.442±0.100 (S1), r=0.424±0.101 (S2), 0.437±0.104 (S3), r=0.484±0.120 (S4) and r=0.408±0.097 (S5). These levels of correlations describe the distribution of sample means and represent the level of correlation that can be found by chance in this process.

Comparison with simulated responses

On the assumption that subjects would choose the image blurred with a more self-correlated PSF, we simulated the ideal responses of each observer to the task. The simulated observers gave positive responses for the image of each trial pair that was blurred with a PSF with a higher correlation with that of the observer's PSF. Similarly to the real experiment, we "presented" randomly 500 pairs of images, and the simulated responses were classified (and ranked) according to the correlation between the subject's PSF and the stimulus PSFs. A high certainty (1 or 6) response was given when the difference between the correlation of the PSF with one or the other image of the pair higher than 0.15, a mid certainty response (2 or

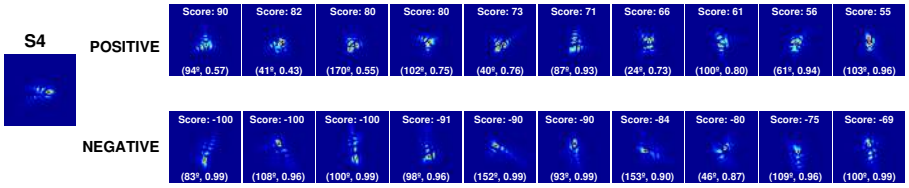

Figure 9.5: Example of the 10 top positively and negatively ranked PSFs for subject S4.The labels show the score and the parameters of the fitted ellipse (axis, eccentricity).

5) was given when this difference ranged between 0.15 and 0.05, and a low certainty response (3 or 4) when the difference was lower than 0.05. We performed the same analysis with the simulated data as with the human data, including weighted classification, correlation of Positive and Negative PSFs with the subject's PSF (on average and individually, and considering all responses or only the 10 top classified PSFs), and Classification Map and Orientation Plot analysis.

9.3 Results

The subjects identified the perceived best focus image in each of the 100 pairs. All subjects showed a clear bias towards a subset of PSFs. Each image was presented 10 times to the subject, and the score was generally very repetitive. Subjects ranked only 25 % of the images with a low certainty score (3 or 4), 36 % were mid-certainty (2 or 5), and 39 % were high-certainty (1 or 6).

9.3.1 Correlations of the natural PSF with the Positive and Negative PSFs (no orientation)

Figure 9.5 shows the natural PSF for one subject (S4) and 10 top positive (scored from 90 to 55) and 10 top negative PSFs (scored from -100 to -69). Qualitatively, the negative PSFs tend to be vertically oriented unlike the positive PSFs. Figure 9.6 shows the natural PSF of each subject, and the corresponding average positive and negative PSFs (average of the 10 highest scored PSFs), along with the corresponding coefficients of correlation.

The average Positive PSFs show a higher correlation with subject's natural PSF than the average Negative PSF. The average coefficients of correlation (across subjects) were r=0.62 for positive and r=0.54 for negative (see inset numbers in Figure 9.6, and Figure 9.7 a).

Although smaller, the difference between the coefficient of correlation for Positive or Negative PSFs is still present when all Positive and Negative PSFs are averaged (instead of the 10 highest ranked only) for 3 out of 5 subjects (Figure 9.7 b). The difference between Positive and Negative PSFs is more accentuated when the individual Positive and Negative PSFs are correlated with the subject's

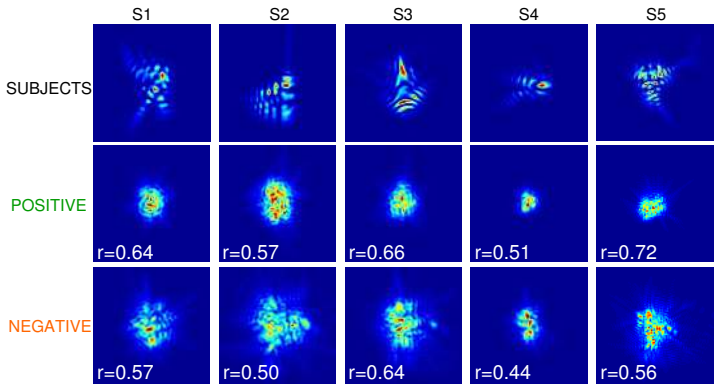

Figure 9.6: Subject's natural PSF (first row), averaged PSFs of the 10 best positive (middle row) and of the 10 best negative (last row) for each subject. The corresponding coefficients of correlation (r) between Subject's natural PSF and the Averaged Positive and Negative PSFs are shown in each panel.

PSF, showing average coefficients of correlation of r=0.47 for the positive PSFs and r=0.34 for the negative (highest ranked responses, Figure 9.7 c), and r=0.46 and r=0.41 for positive and negative (all responses, Figure 9.7 d). These differences are statistically significant: t-test, $p<0.016$ for highest ranked responses; and $p<0.031$ for all responses.

9.3.2 Analysis of PSF orientation: PSF Classification Maps and Orientation Plots

The subjects' Orientation Sampled PSFs were correlated with the PSF Classification Maps (Figure 9.8). The correlation was positive in 3 subjects out of 5.

Positive and Negative Classification Orientation Plots were compared to the subject's PSF Orientation Plots (Figure 9.9). Except for subjects S3 and S5, there is a high degree of overlapping of the natural and Positive Classification Orientation Plots, unlike the Negative Classification Orientation Plots. In subjects S1, S2 and S4 coefficients of correlation are positive for the Positive Classification Orientation Plots (r=0.40 (S1); r=0.24 (S2) and r=0.42 (S4)) and negative for the Negative Classification Orientation Plots (r=-0.35 (S1); r=-0.24 (S2) and r=-0.33 (S4)), but not for S3 (r=-0.31 and r=0.62 for positive and negative, respectively) and S5 (r=0.08 and r=0.19 for positive and negative, respectively).

The bias of the PSF Classification Orientation Plots towards the natural PSF is also revealed by the orientation of the fitting ellipses (Figure 9.9). For all subjects except S3, the orientation of natural PSF was within 21 ± 12 deg of the Positive Classification Orientation Plot but around 90 deg of the Negative (on average at 76 ± 10 deg). In contrast, for S3 there was a better alignment with the Negative PSF within 10 degrees (whereas it was within 41 degrees for Positive).

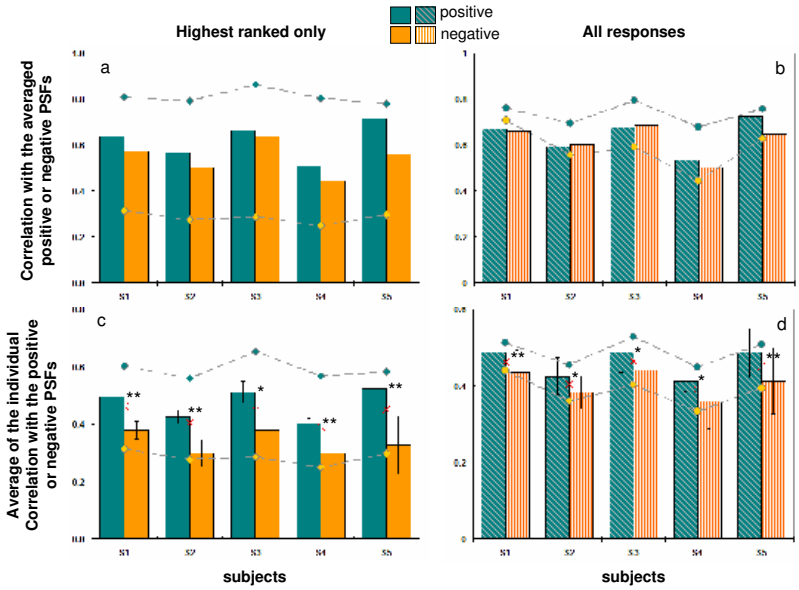

Figure 9.7: Upper row: Correlations of the averaged Positive or Negative PSFs with the subject's PSF a) for the highest ranked only and b) for all PSFs. Lower row: Correlations of the individual Positive or Negative PSFs with the subject's PSF c) for the highest ranked PSFs only and d) for all PSFs. The red crosses show the averaged of all the individual correlations of the 100 PSFs with the subject's natural PSF of the eye under test. Significant differences between Positive and Negative PSFs were found in all cases; * stands for significance at $p<0.05$; ** $p<0.005$ (t-test). Dashed lines and symbols correspond to the simulated ideal responses, based on correlations with the subject's PSF. Positive responses in blue, and negative responses in yellow.

9.3.3 Comparison with simulated responses

Theoretical simulations of the observer's response (assuming that the responses are based on correlations between the observers' PSF and the PSF blurring the images) showed an average correlation coefficient (across subjects) of 0.81 for positive responses and 0.44 for negative responses (considering the top ten responses) and 0.74 and 0.59 respectively (considering all responses). These values set a theoretical limit to performance in the task and show a good correspondence with the average correlation values in the human subjects, as shown in Figure 9.7. Note how the results are similarly modulated over individual subjects in both the ideal and human performance, representing different bounds set on performance by the match between each subject's own PSF and the total stimulus set.

The simulated responses were also analysed in terms of orientation, as with the actual responses from subjects. Figure 9.10 compares the orientation of the Positive and Negative Classification Orientation Plots computed from the simulated responses for each subject. The orientation of the Positive PSF computed from the simulated responses closely matches, within 19 °, the orientation of the

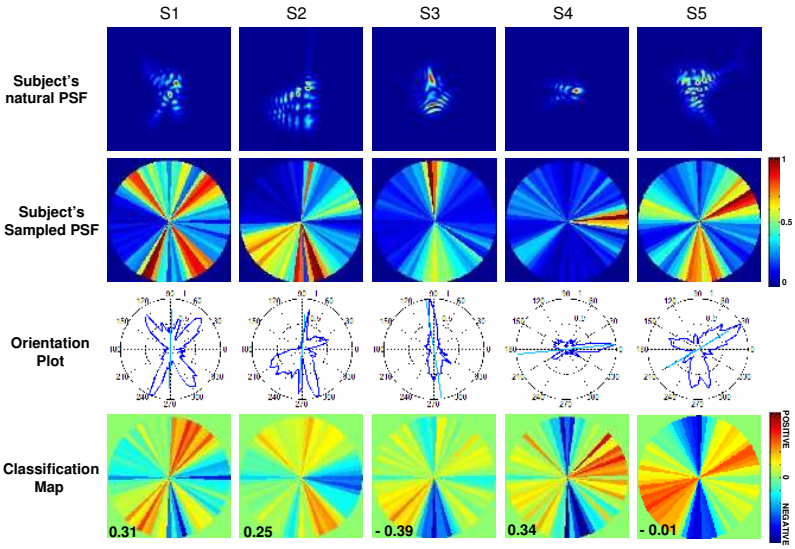

Figure 9.8: (1) Subjects' natural PSF; (2) Subject's Sampled PSF in angular sectors; (3) Corresponding PSF Orientation Plot (along with the axis of the fitted ellipses and eccentricities) and (4) the Classification Maps obtained from the subject's responses and all the 100 PSFs. Correlations between the Classification Map and the subject's Sampled PSF are shown in insets.

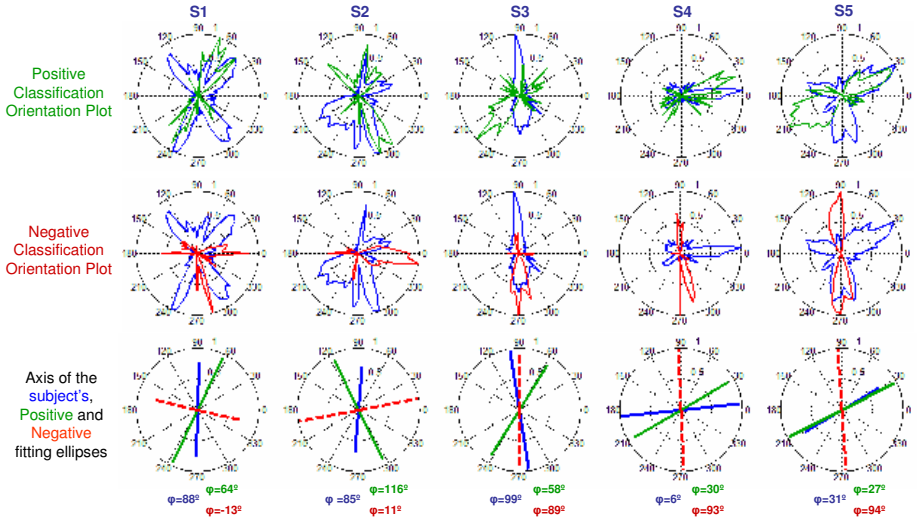

Figure 9.9: Positive (green) and Negative (red) Classification Orientation Plots, along with subject's natural PSF Orientation Plot (blue) for all subjects and the representation of the orientation of the fitting ellipses for the subject's PSF (blue), the positive internally coded PSF (green) and the negative internally coded PSF (dashed-red). The angle (ϕ) for each fitted ellipse is depicted in the corresponding graph.

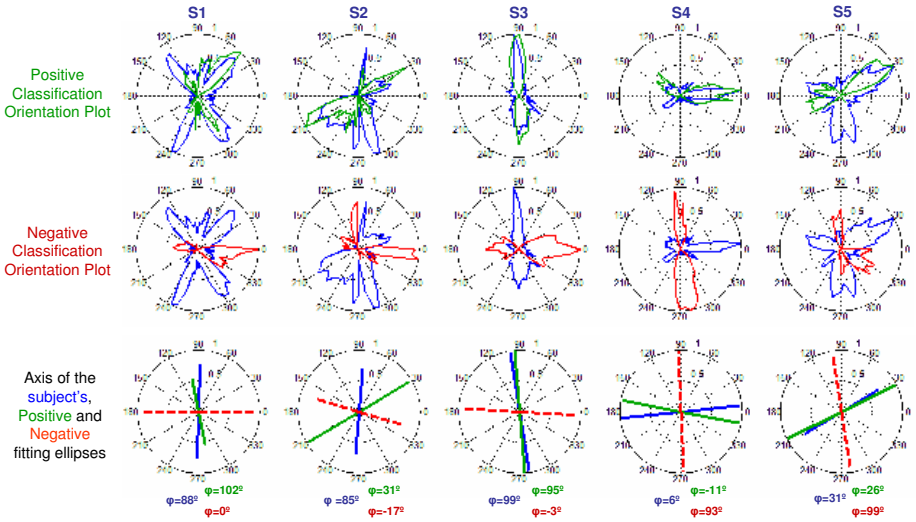

Figure 9.10: Ideal positive (green, upper row) and negative (red, mid row) Classification Orientation Plots computed from the simulated responses for each subject. The axis of the fitting ellipses and their corresponding angles ϕ are also shown (lower row, green for positive and dashed-red for negative). The subject's natural PSF Orientation Plot (blue) and axis are shown for reference.

subject's classification plot unlike the Negative PSF oriented at 80 °, on average across subjects. Figure 9.10 can be compared with the orientations of the measured Positive and Negative classification orientation plots in the subjects (last row in Figure 9.9). There is a high similarity between theoretically simulated and actual responses. The ideal and real response orientations fall within 40 ° on average for the Positive PSF, and 27 ° for the Negative PSF. The largest discrepancy (almost 90 °) occurs for S3 negative response. In subjects S4 and S5 the responses are within 12 ° on average.

9.4 Discussion

Chapter 7 showed that the internal code of blur was strongly driven by the overall blur level of the subject's HOA. The current study shows that this internal code of blur appears also to some extent to be adapted to the orientation of the natural aberrations. This confirms evidence from prior studies, which have investigated potential adaptation to the natural aberrations of the subject, using more restricted paradigms. Artal et al. [2004a] showed that images blurred by the natural aberrations of the subject were perceived as to have better quality than images blurred by rotating versions of the same aberration patterns. In chapter 8, where either images blurred with the subject's aberrations or a 90 ° rotated version of those were used as a constant reference against images blurred by aberrations from real subjects (but similar amount of blur) showed a bias towards the subject's natural

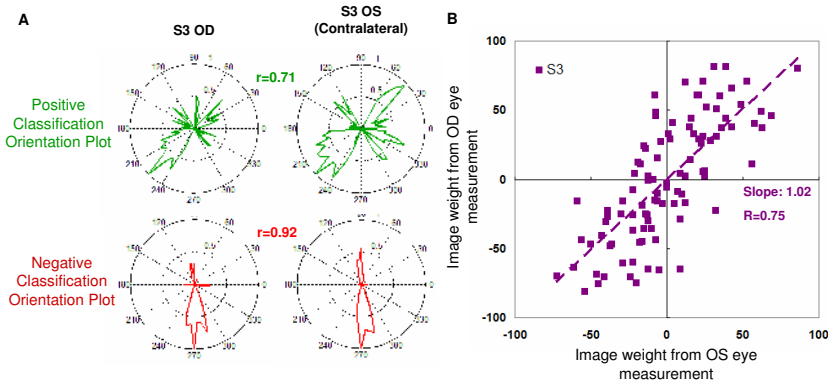

Figure 9.11: Comparison of the measurements of the internal code for blur (classification-images test) between eyes for S3. Classification Orientation plots for positive and negative responses and images ranking.

aberrations (averaging 45 % versus 57 % across subjects). In a companying experiment, where the aberrations of 10 subjects (including those of the subject's under test) were taken as a reference against images blurred by aberrations from real subjects (but similar amount of blur) we did not find a systematic bias towards the subject's own aberrations, with some subjects attributing higher image quality to images blurred by other subjects' aberrations (although in many cases those showed qualitatively similar orientation features than their own). The cumulative results pointed toward a weak bias toward orientation.

The current study used a classification-images inspired strategy to extract the orientation features of the PSF internally coded as producing best-perceived image quality. The fact that the internal code for blur exhibits an orientation bias indicates that not all orientations are perceived equally. In all subjects except one the orientation of the internally coded PSF matched that of the subject's own PSF (within 21 degrees, on average). In one subject, however, the orientation of the best-perceived PSF (obtained from averaging and weighting of the all subjects' responses) differed from the subject's natural aberrations (being almost perpendicular). As shown in figure 9.7, in this subject the correlation of the PSF averaged across all responses with the subject's natural PSF was higher for the negative than for the positive. However, the correlation between the natural PSF and the averaged PSF across the highest ranked PSFs was higher for the positive responses than for the negative. When the Positive and Negative Orientation Classification Plots were estimated only for the highest ranked responses we found that the Positive Classification Orientation Plot was in fact aligned with the subject's natural PSF (within 10 degrees) suggesting that in this subject, the perception of best-focused images was in fact very selective to her own blur orientation.

Alternatively, we tested the PSF orientation in the presence of small focus errors, and found that this particular subject experienced drastic changes in PSF orientation arising from combinations of the HOA and defocus. The internal code

for blur (considering all positive responses) better aligned (within 2 degrees) with the slightly defocused (0.5 D) PSF (and within 15 degrees for 0.4 D and 0.6 D). Although aberrations are correlated across eyes [Porter et al., 2001], they can be non-symmetric [Marcos and Burns, 2000]. In the quest for alternative reasons why the orientation for the internal code of blur and the natural's PSF of the subject disagreed in this subject (at 0 defocus/all responses), we evaluated the aberrations of the contralateral eye. To date, all previous studies addressing the extent to which subjects may be adapted to their own aberrations have investigated it from monocular measurements. However, a recent study by Kompaniez et al. [2013] suggested that transfer between eyes may occur in spatial visual adaptation to blur, particularly under contingent adaptation (conflicting blur magnitude or orientation in left and right eyes). Incidentally, the subject under test showed a discrepancy in the orientation of the PSFs of both right and left eyes, although a good similarity in the amount of blur in both eyes. Measurements of the internal code for blur (classification-images test) in the contralateral eye revealed Classification Orientation Plots for positive and negative responses strikingly similar in both eyes (slope=1.02, R=0.75, $p<0.05$; left/right eye coefficients of correlation 0.71 for the positive and 0.92 for the negative maps) (figure 9.11). Despite the fact of both eyes revealing the same internal code for blur, the alignment was better with the right eye PSF than the left eye PSF, suggesting that the effect may be driven by the dominant eye in this particular subject. The extent to which the optical blur amount and orientation contribute to the internal code of blur is an extremely interesting question and remains to be elucidated.

The great similarity between the theoretically simulated responses and the actual responses in most subjects strongly supports the hypothesis that images blurred with PSFs better correlated to the subject's own are consistently perceived as to have better quality. This shows that subjects do have some sensitivity to the internal structure of their own PSFs. More specifically, the orientation of the best perceived PSF (green lines, figure 9.10) of an "ideal observer" (which would use correlations with its own PSF as the rule to determine best quality) closely matches the orientation of the subject's Positive PSF (green lines, figure 9.9).

9.5 Conclusions

The classification-images inspired method is very powerful in identifying the internally coded blur of subjects. This pattern showed a defined orientation (generally well correlated to the subject's natural PSF), and was found to be consistent throughout time (repeated measurements in the same subject much apart) and across left and right eye of the same patient. The fact that the internal code of blur appears rather specific to each subject's high order aberrations reveals that the calibration mechanisms for normalizing blur operate using both contrast and phase/orientation cues.

10 Conclusions

In this thesis, a custom developed Adaptive Optics system was built and combined with psychophysical channels. We presented a series of psychophysical studies aiming at understanding the relationship between optical and visual quality and the role of neural adaptation in visual perception.

The novel results give new insight on the impact of optical aberrations on visual performance, and the extent to which subjects are adapted to their own aberrations, and can adapt to corrected or increased aberrations. These results are crucial in the development of new vision correction alternatives.

In this thesis we have accomplished the following achievements:

- We have developed an Adaptive Optics system, combined with psychophysical channels to measure, correct/ induce aberrations.

- We have implemented psychophysical paradigms to study visual performance and visual perception under controlled ocular aberrations – 4 alternative forced choice procedures, rating scale tasks and receiver operating characteristic curves, sequential images pairs comparisons, judgment of perceived blur and Classification-Image based tasks.

- We have explored the effect of aberrations on visual performance. In particular, we have tested visual acuity under a wide range of luminances and different contrast polarity. In addition, we have evaluated the effect of fully correcting the eye's optics on the subjective impression of sharpness and its benefit on the ability to recognize faces and facial expressions.

- Novel results allow to give new insight on understanding short and long-term adaptation to blur produced by ocular aberrations: the extent to which subjects are adapted to their own aberrations in terms of magnitude of blur and specific features of blur pattern (i.e. orientation) has been reported as well as the capability to adapt to new patterns of astigmatism and high order aberrations after brief exposure to blurred images.

The development of the Adaptive Optics (AO) combined with psychophysical channels and the experiment results allow us to conclude that:

1 Correcting aberrations produces an increase in high contrast visual acuity in normal eyes under a range of luminances and target contrast polarities, the effect being bigger in eyes with large amounts of natural aberrations. For Black targets on White background (BoW), there is a consistent increase in VA for both natural and AO corrected aberrations, and an improvement of VA at all luminances with the AO correction. For White targets on Black background (WoB), AO correction produces a significant increase of VA but only for low and intermediate luminances. Therefore the benefit at correcting the aberrations is largest for BoW than for WoB targets. For WoB the benefit of correcting HOA is reduced under undilated pupil conditions.

2 The subjective impression of sharpness of perceived natural images increases significantly when high order aberrations are corrected. In general, familiar face recognition improves when correcting high order aberrations but does not improve facial expression recognition

3 Adaptation to images blurred by different axes of simulated astigmatism induces a strong orientation bias in the appearance of subsequently viewed images towards the axis of astigmatism of the adapting image - and are minimally affected by the presence of other high order aberrations. These biases partially transfer across images with very different content and spatial structure, but also transfer across magnified or rotated images of the same objects. Moreover, adaptation aftereffects increase linearly with the level of astigmatic blur in the images, saturating for more extreme level of astigmatism.

4 Adaptation to increased or decreased levels of high order aberrations induces a shift in the best perceived focus of subsequently viewed images. The perceived best focus is proportional to the amount of blur in the adapting image.

5 The observer's focus settings remain largely unaffected when adapting to their own aberrations, but are significantly biased toward higher or lower blur levels when adapted to the aberrations from observers with more or less optical blur respectively. For the majority of subjects, the blur level that is perceived as best focused is very closely predicted from the magnitude of the native blur present in their eyes.

6 Differences in the appearance or perception of blur produced by pure de-

focus (symmetric blur) from the blur produced by high order aberrations (asymmetric blur) demonstrate that the codification of internal code of blur is sensitive to the specific features of blur. Isolating the effect of orientation from blur level reveals that this internal code of blur appears also to some extent to be adapted to the orientation of the natural aberrations.

7 The Classification-Images inspired method is very powerful in identifying the internally coded blur of subjects. The consistent bias of the best perceived PSFs (Positive) towards the natural PSF in most subjects indicates that the internal code of blur appears rather specific to each subject's high order aberrations and reveals that the calibration mechanisms for normalizing blur also operate using orientation cues.

Future Work

A direct follow-up of the study presented here includes the development of a second generation Adaptive Optics system aiming at studying the effect of polychromatic aberration on visual performance, the implementation of new psychophysical experiments on the current AO system to study interocular effect of blur adaptation and the adaptation to simultaneous vision and multifocal corrections. The author of this thesis is currently involved in these parts of the work.

1. New generation of Adaptive Optics instrument.

The studies presented here were performed with monochromatic light which does not provide a full representation of the polychromatic visual environment. A second generation Adaptive Optics system is being developed to fully understand the effect of chromatic aberrations on the retinal image quality and visual performance. This new AO system includes the Hartmann-Shack wavefront sensor, the magnetic deformable mirror as well as new features such as a supercontinuum laser source that allows to perform psychophysical experiment under a wide range of different wavelength from visible to far infrared (400-1100 nm) and a spatial light modulator that allows abrupt change in the phase pattern to test for new design of multifocal correction.

2. Interocular effects of blur adaptation.

Although aberrations, and specifically defocus and astigmatism, are correlated across the eyes, they can also be non-symmetric between eyes - for example different axis of astigmatism between eyes that do not follow either mirror or direct symmetry and interocular differences in refractive errors and blur level.

A first study, in collaboration with Prof. Michael. A. Webster and Elysse Kompaniez [Kompaniez et al., 2013], from the University of Nevada, Reno, USA, has been performed to investigate whether and how adaptation normalizes to differences in blur between the two eyes, which can routinely arise from differences in refractive errors. Answers to these questions are relevant for understanding the processes of adaptation to blur, and also have important clinical relevance for understanding how the visual system adapts to optimize coding for the weaker vs. stronger eye, or in monovision stategies for presbyopia correction.

Moreover, a direct follow-up of the classification Images based experiment has been planned in order to test for adaptation to the specific features that characterize individual's retinal blur (level, orientation, spatial frequencies bandwidth) and study the influence of interocular transfer of blur adaptation between eyes. Classification patterns will be performed in a larger number of observers with specific characteristics in their aberrations - Same amount of blur in both eyes but clear difference in the orientations patterns; Same orientation of blur pattern but different level of blur between eyes – allowing to investigate how the calibration mechanisms for normalizing blur operate at binocular levels.

3. Adaptation to simultaneous vision.

Simultaneous vision is an increasingly used solution for the correction of presbyopia. Simultaneous bifocal corrections (normally delivered in the form of contact or intraocular lenses) produce a sharp image overlapped to a defocused image. It is expected that the patient with such a correction adapts to simultaneous vision, although the mechanisms or even the extent to which this happens is not known. We investigate the visual aftereffects produced after adaptation to bifocal images (with different near additions, and different proportions of far and near vision) and measure the shifts in the best-perceived focus and in the perceived visual quality of bifocal images following brief periods of exposure to simultaneous vision images. Understanding the mechanisms of neural adaptation to multifocal solutions is essential to develop optimal simultaneous design for presbyopia correction.

4. Visual performance and adaptation to multifocal corrections.

Most of the multifocal corrections to correct presbyopia rely on expanding depth of focus by adding specific aberrations. How these aberrations interact with the natural optics of the eye, how they allow out-of-focus vision without compromising vision at best focus, and potential effects of neural adaptation to the correction are key to successful designs. Visual performance experiments with Adaptive Optics manipulated wave aberrations will allow to test the suitability of novel multifocal corrections and evaluate the effect of natural aberrations on their performance.

Summary of the chapters in Spanish

La calidad de las imágenes del mundo exterior que se proyectan en la retina está limitada por las imperfecciones del sistema visual conocidas como aberraciones ópticas. Éstas, provienen principalmente de la cornea, del cristalino y de sus descentramientos respectivos, que degradan el contraste y limitan el contenido de frecuencias espaciales de las imágenes proyectadas.

En los últimos años, se ha avanzado en la tecnología para la medida de las aberraciones oculares y la contribución de los distintos componentes oculares a la degradación de la calidad visual. Sin embargo, aunque existe una correlación entre calidad óptica y calidad visual, todavía no se comprende totalmente cómo afectan las aberraciones oculares a la visión. Esta información es esencial para entender los límites de la visión espacial humana y el diseño y optimización de nuevas alternativas de corrección ópticas.

El hecho de investigar el efecto de las aberraciones en la función visual - incluyendo la agudeza visual o otras tareas visuales cotidianas - permitirá no sólo avanzar más en la comprensión de los límites de la visión espacial, sino también avanzar en el desarrollo de correcciones individualizadas como la cirugía refractiva con patrones de ablación laser customizados o la implantación de lentes intraoculares o lentes de contacto personalizadas para ir más allá de la corrección de errores refractivos convencionales. La pregunta fundamental que queda pendiente es saber si la corrección de las aberraciones de alto orden produce una mejora relevante en la visión.

Citando a Von Helmholtz [1855] "nunca se perciben los objetos del mundo exterior directamente. Al contrario, sólo se perciben los efectos de estos objetos en nuestro sistema nervioso, esto siempre ha sido así desde el primer momento de nuestra vida". Algunos estudios han examinado los posibles factores neuronales

que limitan la función visual y otros han estudiado la adaptación a las aberraciones oculares. Estudios sobre adaptación han demostrado que cambios en el estado de adaptación tienen un efecto critico sobre la forma en que el mundo se percibe. Al corregir las aberraciones oculares de alto orden, la pregunta que surge es: ¿Cómo el sistema visual puede sacar el máximo provecho de la información que llega a la retina, cuando el cerebro nunca ha tenido que procesar información de imágenes tan perfectas? O alternativamente, si la calidad óptica está deteriorada por enfermedad y/o tratamiento, ¿será capaz el sistema visual de adaptarse a un nuevo emborronamiento óptico?

El objetivo de esta tesis doctoral es la comprensión de la relación entre la óptica de la imagen que se proyecta en la retina (en particular, la degradación impuesta por las aberraciones ópticas de alto orden) y la calidad visual. Se ha llevado a cabo el desarrollo de un nuevo sistema de Óptica Adaptativa implementando vías de psicofísica para la medida de la función visual y percepción neuronal bajo control de las aberraciones oculares mediante el espejo deformable. En esta tesis, se presenta una serie de estudios psicofísicos desarrollados para investigar el efecto de la aberraciones sobre la visión humana y la adaptación neuronal a las aberraciones oculares y también para demostrar la correlación entre la codificación interna del emborronamiento y el emborronamiento impuesto por las aberraciones de alto orden en términos de magnitud y orientación.

Capítulo 1: Introducción

En la introducción de esta tesis, se realiza una breve revisión del conocimiento sobre la calidad óptica del ojo. Se presentan las bases fundamentales de la Óptica Adaptativa y sus aplicaciones en ciencias de la visión. Y por último, se revisa el estado del arte de las medidas psicofísicas llevado a cabo para el estudio de la función visual y la adaptación neuronal.

Las imperfecciones oculares son principalmente el desenfoque (miopía, hipermetropía) y el astigmatismo, y suelen corregirse mediante gafas, lentes de contacto e incluso cirugía refractiva. Sin embargo, el ojo sufre de otras imperfecciones, las aberraciones de alto orden, que degradan la calidad óptica del ojo. Esas últimas no se toman en cuenta en la práctica clínica ni se corrigen mediante correcciones refractivas convencionales, pero sí provocan un emborronamiento de la imagen retiniana.

La calidad óptica de un ojo se mide mediante el cálculo de las desviaciones que sufren los rayos que entran en el ojo con respecto a las trayectorias ideales de un sistema óptico perfecto (solo limitado por difracción). La representación de las aberraciones de un sistema óptico se realiza en términos de las aberraciones del frente de onda (normal a las trayectorias de rayos), la aberración de onda. La aberración de onda se suele describir como suma de Polinomios de Zernike cuyos coeficientes se relacionan directamente con las aberraciones oculares: desenfoque, astigmatismo, coma, trefoil, etc. A partir de la aberración de onda se puede calcular la imagen de un punto en la retina (PSF, "Point Spread Function") y la función de transferencia de Modulación (MTF, "Modulation Transfer Function") a partir de las cuales se pueden calcular métricas de calidad visual (por ejemplo la razón de strehl).

En los últimos años, la tecnología desarrollada para la medidas de aberraciones de alto orden ha dado un paso adelante, abriendo la posibilidad de hacer correcciones de aberraciones personalizadas. Además, una nueva tecnología, cuyo origen proviene de la astronomía, facilita la corrección de las aberraciones del ojo, permitiendo estudios de la función visual con una calidad óptica perfecta: la Óptica Adaptativa.

La Óptica Adaptativa (OA) esta basada en dos componentes ópticos fundamentales para su desarrollo: un sensor de frente de onda – normalmente un Hartmann-Shack (HS)- que permite medir el frente de onda, y un modulador de fase - típicamente un espejo deformable que permite cambiar localmente la forma de su membrana reflectante y controlar la forma global de su superficie. Este elemento permite corregir y/o inducir cualquier patrón de aberraciones según las necesidades

del experimento. Estos dos elementos (sensor HS y espejo deformable) actúan en bucle cerrado controlado por ordenador, y permiten el control de las aberraciones oculares de forma dinámica.

La percepción visual resulta de una serie de transformaciones a 3 niveles diferentes: óptico (principalmente la cornea y el cristalino induciendo aberraciones), retiniano (muestreando la imagen con los fotoreceptores de la retina), y neuronal (transmitiendo la información a través del nervio óptico hasta llegar al cerebro y específicamente al córtex visual que procesa la información y la interpreta). Es muy común representar la calidad de la imagen retiniana mediante convolución con la PSF de un frente de onda aberrado. Sin embargo, la calidad subjetiva de una imagen (o percepción) depende también de factores neuronales y de la experiencia visual previa del observador.

Gracias a la teoría de la Psicofísica desarrollada por Fechner [1851] la percepción visual se puede medir de distintas maneras mediante tests de agudeza visual, de sensibilidad al contraste, de detección, de identificación, de reconocimiento de objetos, caras, de percepción de emborronamiento y adaptación.

Varios estudios han examinado el beneficio de la corrección de las aberraciones de alto orden bajo diversas condiciones: con y sin corrección de las aberraciones de alto orden, en función de la luminancia, en ojos emétropes o miopes, con distintos estímulos (blanco sobre fondo negro y viceversa), etc. De entre ellos, pocos han estudiado la función visual en un rango de condiciones extendido. En esta tesis, pretendemos ir más allá estudiando la función visual en un rango de condiciones amplio: en función de la luminancia, en función del contraste, con y sin dilatación de la pupila y con y sin corrección de las aberraciones oculares. (Capítulo 3).

Varios trabajos han evaluado los dispositivos para estudiar pacientes con baja visión usando imágenes naturales y reconocimiento de caras (familiares y expresiones faciales). La percepción de imágenes naturales (nítidas o emborronadas) se ha estudiado en otros campos como la radiología donde se utilizan técnicas de procesado de imágenes. Además, existe un gran debate sobre las tareas de reconocimiento de caras y el papel que juegan en ellas las frecuencias espaciales que limitan la función visual. En esta tesis, usamos el sistema de OA para compensar las aberraciones del sujeto y evaluar el beneficio visual al corregirlas en tareas cotidianas. La corrección de las aberraciones oculares de alto orden produce un aumento de contraste en la banda de frecuencia criítica. Esto permite estudiar la percepción de imágenes naturales y reconocimiento de caras liberándose del efecto de las aberraciones y del emborronamiento producido por ellas, asegurándose que la percepción bajo estas condiciones, será meramente dominada por factores neuronales (Capítulo 4).

El sistema visual se ajusta continuamente a los cambios que ocurren a su al-

rededor en el medio ambiente - cambios de color, de contraste, de luminancia, de emborronamiento – o dentro del propio observador – cambios debidos al envejecimiento, enfermedad, causados por un tratamiento o por correcciones oculares – para mantener una correspondencia entre la codificación interna y el entorno visual. Varios estudio han explorado el efecto de la adaptación al emborronamiento, al contraste o al color. Además, se ha estudiado la adaptación a la aberraciones propias del sujeto mediante Óptica Adaptativa en ojos normales o con enfermedades, e.g. Keratoconos. En esta tesis se presentan resultados sobre los efectos de la adaptación a corto plazo a aberraciones de bajo orden (astigmatismo + desenfoque) (Capítulo 5), de alto orden (Capítulo 6) y también se ha estudiado la adaptación a largo plazo al emborronamiento impuesto por las aberraciones naturales del ojo (Capítulos 7, 8 y 9), usando el sistema de Óptica Adaptativa para corregir las aberraciones y presentado imágenes degradadas por convolución. Al corregir las aberraciones oculares, todos los sujetos están expuestos a los mismos patrones de aberraciones y las diferencias que puedan surgir provendrían específicamente de factores neuronales.

Las grandes líneas de esta tesis doctoral se han orientado para responder a varias preguntas:

- **¿Produce la corrección de las aberraciones de alto orden una mejora relevante en la visión?** En particular, ¿existe un incremento de la Agudeza Visual (AV) al corregir las aberraciones oculares?, ¿varía este beneficio con la luminancia y el contraste?, ¿existe un beneficio visual al corregir las aberraciones a la hora de percibir las imágenes naturales y en el reconocimiento de caras?.

- **¿Cambia la percepción visual de imágenes naturales después de adaptarse a una imagen emborronada (por aberraciones de bajo o de alto orden)?** En particular, ¿la adaptación a corto plazo es especifica a una orientación dada?, ¿pueden los sujetos adaptarse a distintos patrones de aberraciones de alto orden?, ¿qué ocurre al adaptarse a patrones de aberraciones de otra persona?.

- **¿Está cada individuo adaptado a sus aberraciones naturales, en términos de magnitud y/o orientación del emborronamiento impuestos por las aberraciones de alto orden?** ¿Hasta qué punto la percepción de una imagen nítida (o enfocada) depende del nivel de emborronamiento, versus la orientación del patrón de aberraciones del individuo?

Capítulo 2: Métodos

En este capítulo se presentan las técnicas experimentales desarrolladas en esta tesis, especialmente se describe el sistema de Óptica Adaptativa junto a su calibración y validación para la medida y corrección de aberraciones en sujetos humanos. El sistema fue desarrollado para realizar medidas psicofísicas bajo control de aberraciones oculares e investigar de esta forma el impacto de las aberraciones sobre la visión y la adaptación neuronal a las aberraciones oculares. También se describen los experimentos de psicofísica que se han llevado a cabo durante la realización de esta tesis doctoral y se describe la metodología común a los distintos estudios.

El sistema de Óptica Adaptativa (OA) comprende 5 canales diferentes:
(1) Un canal de iluminación con un diodo súper luminiscente (λ=827 nm); (2) Un canal de control del sistema de OA que comprende un sensor de frente de onda, tipo Hartmann-Shack y un espejo magnético deformable que interactúan en bucle cerrado para el control de aberraciones. También existe en este canal un sistema de Badal para la corrección de errores refractivos del sujeto;
(3 y 4) Dos canales psicofísicos para la presentación del estimulo durante el experimento. Uno formado por un minidisplay, el otro por un monitor CRT controlado por una plataforma de psicofísica programable;
(5) Un canal de monitoreo de pupila para el control del centrado del sujeto y del tamaño de la pupila.

El sensor de Hartmann-Shack (HS) tiene una matriz de micro-lentes de 32 x 32, y un diámetro efectivo de 3.65 mm (HASO, Imagine Eyes, Paris Francia). El Espejo magnético deformable tiene 52 actuadores y un diámetro efectivo de 15 mm (MIRAO, Imagine Eyes, Paris France). Estos dos elementos tienen que estar conjugados de pupila con la pupila del sujeto, para medir, corregir y/o inducir adecuadamente las aberraciones oculares. Para medir una pupila de 7 mm, relés de lentes están necesarios para lograr un aumento de x 2 de la pupila al espejo (lentes de focales 50 mm y 100 mm) y un aumento de x 0.5 de la pupila al HS (con otras lentes de focales 200 mm y 50 mm) . Antes de medir a sujetos humanos, se calibró y validó el sistema se hicieron con dos ojos artificiales. El primero estaba compuesto por una lente (focal 35 mm) y un difusor rotativo (simulando la retina) y se utilizó principalmente para la calibración del sistema; El segundo ojo artificial fue encargado a la empresa Alcon, con aberraciones establecidas (desenfoque, astigmatismo, coma, aberración esférica) para la validación del sistema, comparando los valores medidos con los valores de fabrica.

El desarrollo del sistema comprende la implementación de los elementos ópticos y la calibración del sistema de Badal, del diodo superluminescente y del monitor. Además, una optimización y automatización de adquisición de datos dinámicos

(sincronización de diferentes ordenadores), han sido necesarias. Para ello, se han desarrollado programas en Matlab y Visual C++ para el manejo del sistema de OA y la presentación de los estímulos. Con estos programas, se han realizado diferentes experimentos psicofísicos para estudiar la función visual y la adaptación neuronal controlando las aberraciones y bajo diferentes condiciones experimentales incluyendo medidas de Agudeza Visual, percepción de imágenes naturales, reconocimiento de caras o percepción del emborronamiento producido por aberraciones de bajo y alto orden.

Capítulo 3: Agudeza visual en función de la luminancia y del contaste del estímulo

Con los avances en el desarrollo de la cirugía refractiva personalizada y la corrección de las aberraciones de alto orden en lentes intraoculares, de contacto o oftálmicas, se ha reabierto el debate sobre el beneficio visual logrado con una óptica perfecta.

En este capítulo, se evalúa el beneficio en la Agudeza Visual (AV) al corregir las aberraciones oculares en una amplia gama de condiciones, en función de la luminancia, del contraste del estímulo (Letras blancas sobre fondo negro (WoB) y letras negras sobre fondo blanco (BoW)) y en presencia y ausencia (mediante óptica adaptativa) de las aberraciones oculares para investigar si la corrección de las aberraciones de alto orden produce una mejora relevante en la calidad visual.

Este capítulo esta basado en el articulo de Marcos, Sawides et al. "Influence of adaptive-optics ocular aberration correction on visual acuity at different luminances and contrast polarities", Journal of Vision, 2008. Los coautores son Enrique Gambra y Carlos Dorronsoro.

Método. Se evalúa el beneficio visual al corregir el astigmatismo y las aberraciones de alto orden con el sistema de Óptica Adaptativa (OA) sobre la Agudeza Visual (AV) en siete sujetos. La agudeza visual ha sido medida con un test psicofísico de 4 elecciones forzadas (4AFC) con la letra E de Snellen ("Tumbling"[1] E) (programado en Matlbab con la psychtoolbox) en 42 condiciones diferentes:

Con 7 luminancias distintas : 0.8, 1.6, 2.5, 5, 16, 25 and 50 cd/m^2, empezando por la luminancia mas tenue;

Con dos tipos de estímulos: letras blancas sobre fondo negro y letras negras sobre fondo blanco, para este contraste, medidas con y sin dilatación de pupila (tropicamida, 1 %);

Bajo control de aberraciones, aleatoriamente con las aberraciones naturales del sujeto y con la corrección mediante OA.

Resultados. Para las letras negras sobre fondo blanco, la AV aumenta consistentemente con la luminancia, independientemente de la presencia o ausencia de aberraciones (con y sin OA-corrección). El beneficio al corregir las aberraciones se encuentra a todas las luminancias, en promedio la AV aumenta en un factor 1.29. En cambio, para las letras blancas sobre fondo negro, la AV aumenta con la luminancia pero disminuye para las luminancias mas altas (un comportamiento en forma de U invertida con la luminancia), volviéndose mas plana al aplicar la corrección de aberraciones (en los dos casos de pupila natural o dilatada). En este caso, la corrección de aberraciones mejora la AV en un factor 1.13 (en promedio),

[1] *Este anglicismo se usa para definir como se presenta la letra E de Snellen cayendo en diferentes orientaciones. Aquí la E se orienta hacia la derecha, izquierda, arriba o abajo.*

aunque no hay ningún beneficio para luminancias mas altas con la corrección.

Para las luminancias intermedias, la agudeza visual es más alta para letras blancas que para letras negras, aunque esa diferencia disminuye al aplicar la corrección. En los dos tipos de estímulos (letras blancas o letras negras) el mayor aumento de AV ocurre a la luminancia mas baja ($0.8 cd/m^2$). Para luminancias intermedias y altas, el beneficio de la corrección es mayor para letras negras sobre fondo blanco.

La mejora de agudeza visual (en promedio entre condiciones) esta significativamente correlacionado ($p=0.04$) con la cantidad de aberraciones corregidas por OA (en términos de razón de strehl).

Conclusión. La corrección de la aberraciones produce una mejora de la agudeza visual bajo un amplio rango de condiciones (luminancia y contraste del estimulo), especialmente en sujetos con altas cantidades de aberraciones naturales. Comparar el efecto de la corrección de aberraciones en función de la luminancia y del contraste permite investigar los limites de la visión espacial. Sin embargo, una pregunta importante a la hora de diseñar y optimizar lentes o cirugía refractivas individualizadas es saber si esos beneficios son relevantes en un entorno clínico -

Capítulo 4: Impacto de las aberraciones oculares en la percepción de imágenes naturales y en tareas cotidianas

Assumiendo que la corrección de las aberraciones de alto orden de relevancia clínica, es importante investigar si dicha corrección tiene un impacto positivo en las tareas de la vida cotidiana. En este capítulo, se estudia el impacto de las aberraciones (y el beneficio de su corrección) en la respuesta visual a tareas cotidianas. Para ello, se investiga el impacto de la corrección de aberraciones de alto orden en tres experimentos distinto: preferencia de calidad de imágenes naturales, reconocimiento de caras familiares y reconocimiento de expresiones faciales.

Este capítulo esta basado en el artículo de Sawides et al. "Visual performance with real-life tasks under Adaptive-Optics ocular aberration correction", Journal of Vision, 2009. Los coautores son Enrique Gambra, Daniel Pascual, Carlos Dorronsoro y Susana Marcos.

Métodos. 17 sujetos participaron en los tres experimentos – preferencia de la calidad de imágenes naturales, reconocimiento de caras familiares y reconocimiento de expresiones faciales. Se utilizó el sistema de Óptica Adaptativa (AO) para corregir las aberraciones (astigmatismo y aberraciones de alto orden mediante el espejo deformable, desenfoque mediante el sistema de Badal) y el canal psicofísico con el monitor CRT controlado por la plataforma psicofísica. La sincronización de 2 ordenadores, uno controlando el sistema de OA, el otro controlando la plataforma de psicofísica para la presentación de los estímulos psicofísicos (imágenes naturales y caras) fue específicamente necesaria para una presentación rápida de los estímulos bajo control de aberraciones (aberraciones naturales vs. aberraciones corregidas)

Test de preferencia de la calidad de imágenes naturales: 34 imágenes naturales fueron presentadas en el monitor CRT, alternativamente y de forma aleatoria,con las aberraciones naturales del sujeto y con su corrección. El sujeto tenía que responder cual de las dos imágenes (con/sin aberraciones) era mas nítida. Los resultados se analizaron en porcentaje de imágenes elegidas con la corrección de aberraciones.

Reconocimiento de caras familiares: 33 caras (de las cuales 15 de familiares) fueron presentadas al sujeto, con y sin corrección de aberraciones, aleatoriamente. El sujeto debía que proporcionar una respuesta de 1 a 6 según su grado de confianza al reconocer una cara familiar o no (1 con alta certeza de un cara familiar; 6 con alta certeza de cara no conocida; 2 y 5 con una certeza moderada en reconocer la cara; 3 y 4 estando inseguro al reconocer la cara).

Reconocimiento de expresiones faciales: 52 expresiones faciales (contento/enfadado)

fueron presentadas al sujeto, con y sin corrección de aberraciones, aleatoriamente. Como en el reconocimiento de caras familiares, el sujeto tenía que proporcionar una respuesta de 1 a 6 según su grado de confianza al reconocer una expresión contenta o enfadada.

Los resultados de las dos tareas de reconocimiento fueron analizadas en función de la área bajo las curvas ROC ("Receiver Operating Characteritic") con y sin corrección.

Resultados. En promedio, los sujetos consideran el 84±14 % de las imágenes mas nítidas cuando se aplicaba la corrección de aberraciones con OA. Este porcentaje está significativamente correlacionado con la cantidad de aberraciones corregidas. Para todos salvo uno de los sujetos, la corrección de aberraciones mejora la tarea de reconocimiento de caras familiares con un factor de x1.13±0.12 (promedio entre sujetos). Sin embargo, la corrección no produce una mejora sistemática en el reconocimiento de expresiones faciales (factor 1.01±0.11 en promedio).

Conclusión. Con la corrección de las aberraciones, se ha observado un alto porcentaje de imagenes naturales consideradas como nítidas (84 % de la imágenes están consideradas mas nítidas con la corrección), y una mejora en tareas de reconocimiento de caras familiares. La corrección de aberraciones no produce sin embargo en una mejora sistemática del reconocimiento de expresiones faciales. Este último resultado sugiere que la adaptación neuronal a las aberraciones juega un papel importante. Por ello, como se verá en los capítulos siguientes, extendimos el estudio a la investigación de la adaptación neuronal a la degradación retiniana impuesta por las aberraciones oculares, que vemos en los capítulos siguientes.

Capítulo 5: Adaptación neuronal a un emborronamiento astigmático a corto plazo

La adaptación a imágenes artificialmente mas emborronadas o mas nítidas produce un cambio de percepción de mejor foco en las imágenes visualizadas tras la adaptación. En este capítulo, examinamos si estos efectos de adaptación también ocurren tras adaptarse a un emborronamiento producido por errores refractivos (esfera y cilindro) explorando la adaptación al emborronamiento impuesto por astigmatismo e investigando la selectividad de la adaptación con la orientación.

Este capítulo esta basado en el articulo de Sawides et al. "Adaptation to astigmatic blur" Journal of Vision, 2010. Los co-autores son Susana Marcos, Sowmya Ravikumar, Larry Thibos, Arthur Bradley and Michael A. Webster. Este estudio se ha hecho en colaboración con el profesor M.A. Webster, de la Universidad de Nevada (Reno, Estados Unidos) y todos los experimentos han sido realizados en la Universidad de Nevada, excepto el experimento control, realizado en el Instituto de Óptica, en Madrid con el sistema de Óptica Adaptativa.

Métodos. Series de Imágenes naturales (imágenes de ruido, textura, escenas naturales y caras) fueron emborronadas, por convolución, con una combinación de aberraciones de bajo orden: astigmatismo ($\pm 0.3\,\mu$m ó $\pm 0.6\,\mu$m según el experimento) y desenfoque (manteniendo un nivel de emborronamiento constante). Los dos extremos de las series de imágenes aparecen por lo tanto emborronadas verticalmente (astigmatismo negativo -0.3 μm y desenfoque mínimo) o horizontalmente (astigmatismo positivo $+0.3\,\mu$m y desenfoque mínimo) mientras el centro de las series contienen imágenes emborronadas isotrópicamente (emborronadas solo con desenfoque, sin ningúna orientación). El protocolo experimental consistió en adaptarse a un emborronamiento astigmático (vertical o horizontal) durante 1 min (y durante 5 s ente imágenes test) . Un test psicofísico de 2 elecciones forzadas (2AFC staircase) fue llevado a cabo para evaluar la imagen percibida por el sujeto como isótropa (ni vertical, ni horizontal) en cinco experimentos diferentes:

Experimento 1 Selectividad de la adaptación con la orientación

Para evaluar si los sujetos pueden adaptarse a un emborronamiento astigmático y si se produce una selectividad de la adaptación con la orientación, la imagen de adaptación presentaba un astigmatismo extremo (vertical, -0.3 μm o horizontal $+0.3\,\mu$m). Las imágenes del test tenían el mismo contenido que la imagen de adaptación, es decir provenían de la misma serie de imágenes (ruido, textura, escenas naturales y cara). Un experimento control, desarrollado con el sistema de óptica adaptiva - corrigiendo las aberraciones del sujeto - permite evaluar el impacto de las aberraciones en la adaptación al astigmatismo.

Experimento 2: Transferencia de la adaptación entre imágenes

Para evaluar el grado de adaptación a las características específicas del emborronamiento independientemente de la imagen de adaptación se repitió el experimento 1 pero con imágenes de adaptación y de test de contenido distinto (por ejemplo, adaptación a una textura, test con una escena natural).

Experimento 3: "Aftereffects"[2] dependientes del emborronamiento local vs. la forma global

Para determinar si la adaptación al astigmatismo se transfiere entre imágenes de diferentes tamaños - considerando que el efecto del emborronamiento produce una diferencia en la forma global del emborronamiento percibido en imágenes de diferentes tamaños - imágenes de 2-grados versus 6-grados se utilizaron para imágenes de adaptación y/o en imágenes de test.

Experimento 4: Adaptación y orientación de la imagen

Para determinar si la adaptación al astigmatismo es especifico de la orientación del emborronamiento en retina o de la orientación de la propia imagen, se utilizó la imagen de la cara inclinada a -45 º para la adaptación mientras que en la sequencia del test se utilizaron imágenes inclinadas a -45 º y a +45 º.

Experimento 5: Adaptación y magnitud del emborronamiento

Para evaluar el efecto de la magnitud del emborronamiento en la imagen de adaptación, se procesaron imágenes emborronadas con un rango mas amplio de astigmatismo (de -0.6 μm a +0.6 μm). Se evaluaba la imagen isótropa después de adaptarse a diferentes magnitudes de astigmatismo.

Resultados. (1) La adaptación a una imagen emborronada horizontalmente provoca que un estímulo no-astigmático aparezca verticalmente orientado (y viseversa tras adaptar a un emborronamiento vertical), induciendo un desplazamiento de la imagen percibida como isótropa hacia una imagen emborronada con la misma orientación que la imagen de adaptación. Estos resultados no se ven afectados con la ausencia de las aberraciones naturales del sujeto (mediante corrección de aberraciones por óptica adaptativa). (2) "Aftereffects" similares aparecen para diferente tipo de imágenes. Una transferencia de la adaptación ocurre entre imágenes de diferente contenido, sin embargo el mayor efecto de adaptación ocurre cuando las imágenes de adaptación y de test provienen de la misma serie. También se ha demostrado transferencia parcial de la adaptación entre imágenes de diferente tamaño (3) y orientación (4). (5) Los "Aftereffects" aumentan linealmente con el nivel de emborronamiento en imagen de adaptación, aunque tienden a saturar para niveles extremos del emborronamiento.

[2] *El anglicismo "aftereffects" tendría como traducción literal "efectos a posteriori" y se utiliza para designar los cambios que ocurren después de una adaptación a una imagen.*

Conclusión. La adaptación al emborronamiento impuesto por el astigmatismo demuestra una selectividad de la adaptación con la orientación. Estos resultados son relevantes a la hora de evaluar la adaptación dinámica a la corrección del astigmatismo en sujetos astígmatas antes y después (medidas longitudinales) de una prescripción de lentes para la corrección del astigmatismo. Los resultados sugieren que al menos para aberraciones de bajo orden la visión espacial puede selectivamente adaptarse al emborronamiento inducido por la óptica del ojo. El capítulo siguiente examina la adaptación a un emborronamiento producido por aberraciones de alto orden.

Capítulo 6: Adaptación a un emborronamiento producido por aberraciones de alto orden a corto plazo

Las aberraciones del ojo son rutinariamente alteradas naturalmente por enfermedades (keratocono), por envejecimiento, o artificialmente debido a las correcciones refractivas como lentes intraoculares, lentes de contacto, lentes oftálmicas o cirugía corneal. Para entender cómo el sistema visual se adapta a los cambios que pueden ocurrir en el observador, investigamos, en este capítulo, la adaptación al emborronamiento producido por aberraciones oculares de alto orden y versiones re-escaladas de esas aberraciones.

Este capítulo esta basado en el articulo de Sawides et al. "Adapting to blur produced by high order aberrations", Journal of Vision, 2011. Los coautores son Pablo de Gracia, Carlos Dorronsoro, Michael Webster y Susana Marcos.

Métodos. En este experimento, el emborronamiento óptico fue generado por convolución de una imagen de una cara con la PSF correspondiente a 4 patrones de aberraciones de alto orden (de los 4 sujetos que participaron al estudio), cuyos coeficientes de Zernike (excluyendo tilt y desenfoque) fueron re-escalados por un factor (F) que variaba de F=0 (correspondiendo a une sistema óptico solo limitado por difracción) a F=2 (correspondiente a una cantidad doble de aberraciones naturales del sujeto) en pasos de 0.05.

En un test psicofísico de 2 elecciones forzadas (Emborronado/nítido, cuyo nivel de emborronamiento en la imagen test variaba según un algoritmo basado en QUEST[3]), el sujeto estimaba la imagen percibida como mejor enfocada ("Best Focused") antes (adaptándose a una pantalla gris: neutral) y después de adaptación a distintos niveles de emborronamiento producido por versiones re-escaladas de sus aberraciones de alto orden así como de los otros 3 sujetos del estudio. Para cada patrón de aberración, se utilizaron 5 niveles de emborronamiento correspondiente al nivel natural de emborronamiento (F=1); nivel mas nítido que el natural (F=0 y F=0.5) y niveles mas borrosos que el natural (F=1.5 y F=1.9). En total, fueron 24 condiciones de adaptación (incluyendo la neutra con pantalla gris).

Las imágenes se presentaron en un monitor CRT, vistas a través del sistema de Óptica Adaptativa que permitía la corrección de astigmatismo y aberraciones de alto orden (mediante el espejo deformable) y la corrección de errores refractivos (mediante el sistema de Badal). De esa manera, al corregir las aberraciones oculares, todos los sujetos fueron expuestos a los mismos patrones de aberraciones, por tanto, las diferencias deberían provenir específicamente de factores neuronales. El protocolo experimental consistía en adaptarse durante 1 minuto a una de las imágenes de adaptación (y durante 5s entre imagen test) y evaluar la cuantidad de

[3] *QUEST se refiere a "Quick Estimate by Sequential Testing", [Watson and Pelli, 1983]*

emborronamiento con el cual la imagen esta percibida como nítida : "Best Focused Point" (BFP). Los resultados se analizaron en términos de desplazamiento del BFP antes (pantalla gris) y después de la adaptación.

Resultados. Todos los sujetos se adaptan al los cambios de niveles de emborronamiento impuestos por aberraciones de alto orden, independientemente del patrón de aberraciones utilizado para generar el emborronamiento (el del propio sujeto, o de otro). La percepción de emborronamiento tras periodos de adaptación a imágenes emborronadas exhibe un cambio, reflejado en el desplazamiento del punto percibido como mas nítido (BFP) hacia el nivel de emborronamiento de la imagen de adaptación, proporcionalmente, en terminos de RMS.

Además, el desplazamiento, respeto al punto neutral (tras adaptar a una pantalla gris), de la imagen percibida como mas nítida tras adaptarse a un emborronamiento natural (F=1) era mínimo cuando se trataba de las propias aberraciones del sujeto, y mayor cuando la imagen se emborronaba con las aberraciones de otro sujeto.

Conclusión. Se demostró el efecto de adaptación a diferentes niveles de emborronamiento impuesto por aberraciones de alto orden. El nivel de emborronamiento percibido como neutral (i.e. mas nítido) esta proporcional al nivel de emborronamiento en la imagen de adaptación, impuesto tanto para un mismo patrón de aberraciones re-escalado (preservando la forma global del emborronamiento natural del patrón de aberraciones del sujeto) como para diferentes patrones de aberraciones (niveles y forma del emborronamiento entre sujetos). Esta adaptación puede ser relevante para entender los cambios perceptuales que surgen cuando las aberraciones de alto orden están alteradas por enfermedades o cirugías. Además, el hecho de que el efecto de la adaptación sea mínimo al adaptar al emborronamiento natural del sujeto (F=1) sugiere una adaptación previa (a largo plazo) a las aberraciones naturales del sujeto. Los siguientes capítulos tratan de demostrar esta hipótesis.

Capítulo 7: Adaptación al nivel de emborronamiento natural impuesto por las aberraciones naturales de alto orden - a largo plazo

Mientras las aberraciones de bajo orden (astigmatismo y desenfoque) se suelen corregir con gafas o lentes, no es muy usual corregir las aberraciones de alto orden por lo que los sujetos están crónicamente expuestos a diferentes patrones de emborronamiento retiniano. El grado de emborronamiento visual varía en cada persona y el concepto sobre lo que es demasiado borroso, demasiado nítido, o una imagen neutra, depende de la experiencia visual. Esto implica que el sistema visual humano, incluyendo el cerebro, que es el que interpreta las imágenes proporcionadas por el ojo, tiene la capacidad de adaptarse a un nuevo nivel de emborronamiento tras verse sometido a correcciones visuales, como el uso de gafas o la cirugía refractiva, o a enfermedades. En este capítulo, se evalúa la adaptación neuronal del sujeto a su propio nivel global de emborronamiento y se examina si la codificación espacial interna del sistema visual corresponde al nivel natural de emborronamiento específico impuesto por las aberraciones de alto orden de un individuo.

Este capítulo esta basado en el articulo de Sawides et al. " Vision Is Adapted to the Natural Level of Blur Present in the Retinal Image", PLoS One, 2011. Los coautores son Pablo de Gracia, Carlos Dorronsoro, Michael A. Webster y Susana Marcos.

Métodos. Cómo en los capítulos anteriores, las imágenes se presentaron en un monitor CRT, vistas a través del sistema de Óptica Adaptativa que permitía la corrección de astigmatismo y aberraciones de alto orden (mediante el espejo deformable) y la corrección de errores refractivos (mediante el sistema de Badal), exponiendo todos los sujetos a los mismos patrones de aberraciones.

Experimento 1: Versiones de patrón de aberración re-escaladas

Este experimento es la continuación directa del capítulo 6. El emborronamiento óptico se generó por convolución de una imagen de una cara con la PSF correspondiente a los 4 patrones de aberraciones de alto orden (de los 4 sujetos que participaron al estudio), cuyos coeficientes de Zernike (excluyendo tilt) e incluyendo un desenfoque optimizado para maximizar la calidad óptica (razón de strehl) fueron re-escalados por un factor (F) que variaba entre 0 y 2. Percepción del emborronamiento se evaluó en un test psicofísico de 2 elecciones forzadas (borroso/nítido) antes (adaptación neutral a una pantalla gris durante 20 s) y después de adaptación (1 minuto y 5 s entre imagen test) a una imagen natural (F=1, para los 4 patrones de aberraciones correspondientes a los 4 sujetos). Los resultados se analizaron en términos de desplazamiento de la imagen percibida como mas nítida, bajo adaptación neutral (pantalla gris) y natural (F=1).

Experimento 2: 128 patrones reales de aberraciones de alto orden

En este experimento, el emborronamiento óptico se genero por convolución de una imagen de una cara con la PSF correspondiente a 128 patrones de aberraciones de alto orden diferentes, de ojos reales. De la misma forma que el experimento anterior, el desenfoque fue optimizado para maximizar la calidad óptica (razón de strehl). La serie de imágenes contienen entonces 128 imágenes emborronadas con distintos niveles de emborronamiento (razón de strehl variando de 0.049 a 0.757) y distintas orientaciones. El protocolo experimental consiste en adaptare a una imagen neutral únicamente (pantalla gris) y evaluar la imagen percibida como mas nítida en un test psicofísico a dos elecciones forzadas (borroso/nítido, cuyo nivel de emborronamiento en la imagen test (Strehl de los 128 patrones) variaba según un algoritmo basado en QUEST[4])). Los resultados se analizaron en términos de razón de strehl de la imagen percibida como mas nítida, en comparación con la razón de strehl de las aberraciones naturales del sujeto.

Resultados. (1) La diferencia entre la imagen percibida como neutral (nítida) tras adaptación a una imagen emborronada con aberraciones naturales (F=1), y tras adaptación neutral (pantalla gris) es mínima cuando el sujeto se adapta a sus propias aberraciones (0.012 en promedio, en términos de razón de strehl). En cambio, esta diferencia aumenta cuando el sujeto se adapta a imágenes emborronadas por patrones de aberraciones de otros sujetos (0.044 en promedio entre los otros 3 patrones de aberraciones testeados). (2) Encontramos una estrecha correspondencia entre la calidad de la imagen percibida como neutral (nítida) y la calidad de la imagen retiniana degradada por las aberraciones del sujeto y una correlación alta entre el nivel de emborronamiento de la imagen percibida como neutral y el nivel de emborronamiento natural impuesto por las aberraciones de cada sujeto es (Slope=0.95; R = 0.94; $p<0.0001$).

Conclusión. Estos resultados proporcionan una prueba evidente de que la visión espacial está calibrada para los niveles específicos del emborronamiento presente en la retina de cada individuo. Esta adaptación natural refleja en parte cómo la sensibilidad espacial esta normalizada en la codificación neuronal del emborronamiento. La pregunta de si esta adaptación depende tanto del nivel global del emborronamiento cómo de la orientación especifica de cada patrón de aberración se discutirá en los siguientes capítulos.

[4] *QUEST se refiere a "Quick Estimate by Sequential Testing", [Watson and Pelli, 1983]*

Capítulo 8: Dependencia del mejor foco subjetivo con el nivel de emborronamiento vs. el patrón de aberraciones de alto orden

Las imágenes proyectadas en la retina están, de manera innata, emborronadas por las aberraciones oculares específicas de cada sujeto. En este capítulo, se investiga si la adaptación a las aberraciones naturales de cada individuo depende del nivel global o de la orientación específica del emborronamiento. Para ello, el nivel de emborronamiento y a la orientación del patrón de aberraciones se aíslan y se estudian de forma independiente.

Este capítulo esta basado en el articulo de Sawides et al. " Dependence of subjective image focus on the magnitude and pattern of high order aberrations", Journal of Vision, 2012. Los coautores son Carlos Dorronsoro, Pablo de Gracia, Maria Viñas, Michael A. Webster y Susana Marcos.

Métodos. De nuevo, las imágenes se presentaron en un monitor CRT, vistas a través del sistema de Óptica Adaptativa que permitía la corrección de las aberraciones del sujeto y la corrección de errores refractivos, exponiendo todos los sujetos a los mismos patrones de aberraciones.

Experimento 1: Percepción del mejor foco a partir de imágenes emborronadas con sólo desenfoque

Este experimento es la continuación directa del experimento 2 del capitulo 7 pero en vez de emborronar las imágenes con patrones reales de aberraciones de alto orden, se emborronaron con 128 niveles de desenfoque produciendo una serie de imágenes con una razón de strehl variando entre 0.049 y 0.844. De esta forma, el nivel de emborronamiento varía mientras la orientación es la misma.

6 sujetos (un subconjunto de los 15 sujetos que participaron en el experimento 2 del capítulo 7) participaron en este experimento. Se evaluó el nivel de emborronamiento percibido como neutral (produciendo una imagen nítida) y se comparó con el nivel de emborronamiento natural impuesto por las aberraciones oculares de cada sujeto (en términos de razón de strehl).

Experimento 2: Percepción del mejor foco a partir de imágenes emborronadas con el mismo nivel de emborronamiento pero con orientaciones distintas

En este experimento el emborronamiento óptico se generó por convolución de 10 imágenes naturales (incluyendo caras, escenas interiores, escenas exteriores) con la PSF correspondiente a 100 patrones de aberraciones de alto orden diferentes, de ojos reales, re-escalados para igualar la calidad óptica de cada sujeto en términos de razón de strehl. De esta forma, todos los patrones tienen el mismo nivel de emborronamiento pero con orientaciones distintas. 4 sujetos participaron (con

razón de strehl entre 0.042 y 0.1233) por lo tanto, para cada imagen natural, se generaron 4 series de imágenes.

El protocolo experimental consistió en presentar 100 pares de imágenes emborronadas con patrones distintos. En cada par, una imagen se emborronaba con un patrón de referencia, la otra con un patrón elegido dentro de los 100 patrones distintos, aleatoriamente. El sujeto debía elegir la imagen que le parecía mas nítida de las dos imágenes presentadas secuencialmente. Se testearon 11 patrones de referencia: el patrón natural del sujeto, el patrón del sujeto girado a 90 º, los patrones de los otros 3 sujetos haciendo el experimento, y otros 6 patrones distintos. El experimento estuvo compuesto por lo tanto de 11 medidas de comparación de 100 pares de imágenes. Se registraron los porcentajes de imágenes emborronadas con los patrones de referencia y percibidas como nítidas y se compararon entre ellos para evaluar si el sujeto demostraba una preferencia hacia su propio patrón de aberraciones o hacia patrones de orientación similar.

Resultados. (1) De la misma forma que la calidad de la imagen emborronada por aberraciones de alto orden podía ser perfectamente estimada a partir de la calidad de la imagen retiniana de cada sujeto (capítulo 7), encontramos una estrecha correspondencia (aunque con un offset) y una correlación alta, casi perfecta entre el desenfoque percibido como neutro y el nivel de emborronamiento natural del sujeto ($R=0.999$; $p<0.0001$).

(2) Aunque los patrones con orientación similares están percibidos de la misma manera por el sujeto, ningún patrón de aberraciones (y en particular el patrón de aberraciones naturales del mismo sujeto) es consistentemente considerado como mejor, tampoco es consistentemente rechazado por los sujetos. No obstante, si comparamos los porcentajes de imágenes consideradas mas nítidas cuando la referencia corresponde al patrón natural del sujeto o una versión girada a 90º, encontramos una clara tendencia a favor del patrón natural (57 %) frente al patrón girado (45 %).

Conclusión. El nivel de emborronamiento de la imagen percibida como mejor enfocada está altamente correlacionado con el nivel de emborronamiento global impuesto por las aberraciones de alto orden. El offset encontrado sugiere diferencias en la percepción del emborronamiento producido solamente por desenfoque o por aberraciones de alto orden.

No se ha demostrado una preferencia sistemática hacía el patrón natural del sujeto se ha demostrado aunque la alta preferencia por el patrón natural de emborronamiento frente al girado a 90º sugiere une sensibilidad a la orientación. El siguiente capítulo profundiza el estudio de la adaptación natural a la orientación de las aberraciones naturales del sujeto.

Capítulo 9: Clasificación de patrones para medir la adaptación a la orientación de las aberraciones de alto orden

Existen evidencias de que la visión espacial está calibrada para los niveles específicos del emborronamiento presente en la retina de cada individuo pero también, existen evidencias de que el sujeto podría estar adaptado a las características especificas de su patrón de aberraciones (i.e. orientación). En este capítulo, utilizamos una variante del método de "Clasificación de Imágenes" para extraer la PSF, neuralmente codificada, que mejor se ajuste al la PSF natural del sujeto y estudiar la adaptación a la orientación de las aberraciones de alto orden.

Este capítulo está basado en el estudio de Sawides et al. " Using pattern classification to measure adaptation to the orientation of high order aberrations", enviado para revisión a PLoS ONE, 2013. Los coautores son Carlos Dorronsoro, Andrew M. Haun, Eli Peli y Susana Marcos.

Métodos. Como en los capítulos anteriores, las imágenes se presentan en un monitor CRT, vistas a través del sistema de óptica adaptativa que permite la corrección de astigmatismo y aberraciones de alto orden (mediante el espejo deformable) y la corrección de errores refractivos (mediante el sistema de Badal).

Este experimento es la continuación directa del experimento 2 del capítulo 8, en el cual las imágenes estaban emborronadas por 100 patrones de aberraciones diferentes, re-escalados para igualar la calidad óptica (en términos de razón de strehl) del sujeto. En este experimento, se utilizan los mismos 100 patrones para emborronar solamente la imagen de la cara. De esta forma, tenemos une serie de 100 imágenes emborronadas, todas con un nivel de emborronamiento similar pero con distintas orientaciones. En este experimento, 5 sujetos participaron (razón de strehl variando entre 0.040 y 0.1233) y por lo tanto, se generaron 5 series de imágenes.

El test psicofísico utilizado en este experimento se basa en el método de "Clasificación de Imágenes" en el cual se presentaban al sujeto 500 pares de imágenes (10 veces 50 pares elegidas aleatoriamente dentro de las 100 imágenes emborronadas por un patrón elegido dentro de los 100 patrones). El sujeto tenía que elegir la imagen que le parecía mas nítida entre dos presentadas secuencialmente y puntuarla según su grado de seguridad en su respuesta (1) Muy seguro que la primera imagen del par era mas nítida; (6) muy seguro que la segunda imagen del par era mas nítida; (2 o 5) cuando el sujeto estaba casi seguro de su respuesta; (3 o 4) cuando no estaba seguro de su respuesta. Las imágenes consideradas como nítidas se califican de positivas, las otras de negativas.

Para clasificar, se atribuyen pesos positivos a las PSF positivas: $+10$ (alta seguridad en la respuesta (1 o 6)); $+5$ (media seguridad (2 o 5)); y $+1$ (baja seguridad (3 o 4)) y pesos negativos del mismo valor a las PSF negativas (-10; -5;

-1). A continuación, se calculan los coeficientes de correlación entre la PSF natural del sujeto con las PSFs positivas y negativas, en promedio e individualmente.

Para resaltar la orientación de la PSF, se muestrea la PSF en 72 secciones angulares (de 5 grados cada una); se administra un peso a cada sección correspondiente a la intensidad (integral) de la PSF en esta sección. Los valores de cada sección se dibujan en coordenadas polares y los datos se ajustan con una elipse cuyo eje principal y excentricidad se comparan con los resultados obtenidos. Se elabora el Mapa de clasificación a partir de todas las PSFs pesadas por las respuestas del sujeto promediadas y muestreadas para sacar mapas de clasificación positivo y negativo que contienen la información sobre las orientaciones que mejor definen la PSF codificada internamente (i.e. neuralmente.). Los ejes de la elipse (de ajuste) y excentricidad de los datos correspondientes a los mapas de clasificación positivo y negativo se comparan al de la PSF natural del sujeto.

Resultados. Las respuestas positivas se correlacionan mejor con la PSF natural del sujeto, sobre todo para las 10 mejores (con más puntos) PSFs ($r=0.47$ en promedio) que las respuestas negativas ($r=0.34$). Además la diferencia es significativa para todos los sujetos ($p<0.02$). El promedio de las PSF positivas también exhibe una correlación mas alta que el promedio de las PSF negativas.

En términos de orientación (con los Mapas de Clasificación y ajustes a elipses) encontramos que en 4 de los sujetos, la orientación del Mapa de Clasificación Positivo se aproxima a la orientación de la PSF natural del sujeto (dentro de 21 grados) mientras la orientación de las repuestas negativas es casi perpendicular a la orientación de la PSF natural del sujeto (a 76 grados en promedio).

Conclusión. El método de clasificación de imágenes es una herramienta poderosa para identificar el código interno del emborronamiento impuesto por las aberraciones naturales del sujeto. El sujeto tiende a preferir consistentemente PSF orientadas en la misma dirrección que su PSF natural.

La codificación interna del emborronamiento es específica a las características del emborronamiento impuesto por las aberraciones oculares de un individuo y los mecanismos de calibración del emborronamiento operan también según las características propias al contraste y orientación.

Translation of conclusions to Spanish

En esta tesis, se ha desarrollado un sistema de Óptica Adaptativa, en combinación con vías de psicofísicas para la presentación de distintos estímulos psicofísicos. Se presentaron una serie de experimentos psicofísicos desarrollados para estudiar la función visual y adaptación neuronal en diferentes condiciones experimentales, bajo control de las aberraciones mediante Óptica Adaptativa.

Esos resultados innovadores permiten entender mejor el impacto de la aberraciones ópticas en la función visual, en qué medida los sujetos están adaptados a sus propias aberraciones oculares y si pueden adaptarse a cambios inducidos en su patrón de aberraciones (corrección o aumento). Estos resultados son esenciales para entender los límites de la visión espacial humana y para el diseño y optimización de nuevas alternativas de corrección visual.

En esta tesis, reportamos los siguientes logros:

- Hemos desarrollado un sistema de Óptica Adaptativa junto con diferentes vías psicofísicas para medir, corregir y/o inducir aberraciones.

- Hemos implementado diferentes experimentos psicofísicos para estudiar la función y percepción visual bajo control de aberraciones – test psicofísico de elección forzada; tareas de clasificación del estímulo y "Receiver Operating Characteristic" ROC curves; tareas de percepción de imágenes, de percepción del emborronamiento y un test basado en el método de "Clasificación de Imágenes".

- Hemos explorado el impacto de las aberraciones oculares en la función visual. En particular hemos medido la agudeza visual en un amplio rango de luminancias y contraste del estímulo. Adicionalmente, hemos evaluado el beneficio al corregir las aberraciones sobre la percepción de la calidad de imágenes naturales y en tareas cotidianas como el reconocimiento de caras familiares y expresiones faciales.

- Los resultados permiten avanzar en la comprensión de los mecanismos de adaptación neuronal al emborronamiento impuesto por las aberraciones de alto orden. Hemos investigado la adaptación natural al emborronamiento impuesto por al óptica del ojo, en términos de nivel y orientación. Además, hemos evaluado la capacidad de un individuo para adaptarse a un nuevo patrón de aberraciones después de una breve exposición a una imagen emborronada por aberraciones de bajo y alto orden.

El desarrollo del sistema de Óptica adaptativa con vías de psicofísica y los experimentos llevado a cabo nos permiten concluir que:

1 La corrección de aberraciones produce una mejora de la agudeza visual (AV) en un amplio rango de condiciones (luminancia y contraste del estimulo), especialmente en sujetos con altas cantidades de aberraciones naturales. Para estímulo negro sobre fondo blanco, la AV aumenta consistentemente con la luminancia, independientemente de la presencia o ausencia de aberraciones y el beneficio al corregir las aberraciones ocurre para todas las luminancias. Para estímulo blanco sobre fondo negro, la corrección de aberraciones mejora la AV pero solo para luminancias bajas y intermedias. Por lo tanto, el beneficio de la corrección es mayor para estimulo negro sobre fondo blanco.

2 La impresión subjetiva de nitidez en imágenes naturales aumenta significativamente tras corrección de aberraciones. En general, el reconocimiento de caras familiares mejora al corregir las aberraciones pero la corrección no produce beneficio en el reconocimiento de expresiones faciales.

3 La adaptación a una imagen emborronada con astigmatismo a diferentes ejes induce un desplazamiento de la imagen percibida como isótropa hacia una imagen emborronada con la misma orientación que la imagen de adaptación. Estos resultados no se ven afectados por la ausencia de las aberraciones naturales del sujeto (mediante corrección de aberraciones por óptica adaptativa). hay una transferencia de la adaptación entre imágenes de diferente contenido y estructura espacial, pero también entre imágenes de mismo contenido pero de tamaño y orientación diferentes. Además, el efecto de la adaptación aumenta linealmente con el nivel de emborronamiento astigmático en la imagen de adaptación y tiende a saturar para niveles de astigmatismo extremos.

4 La adaptación a diferentes niveles de emborronamiento impuesto por aberraciones de alto orden (versiones re-escaladas de patrones) induce un desplazamiento del emborronamiento percibido como neutral (i.e. mas nítido) que es proporcional al nivel de emborronamiento en la imagen de adaptación, impuesto tanto para un mismo patrón de aberraciones re-escalado (preservando la forma global del emborronamiento) como para diferentes patrones de aberraciones (niveles y forma del emborronamiento entre sujetos).

5 La percepción de una imagen nítida no se ve afectada tras adaptarse a una imagen emborronada con las aberraciones naturales de un individuo. En cambio, se produce un desplazamiento significativo de la imagen percibida como nítida hacia niveles mas o menos emborronados, tras adaptación a imágenes emborronadas con patrones de aberraciones de otros sujetos. Para la mayoría de

los sujetos, existe una estrecha correspondencia entre la calidad de la imagen percibida como neutral (nítida) y la calidad de la imagen retiniana degradada por las aberraciones naturales del sujeto.

6 Las diferencias en la percepción del emborronamiento producido sólo por desenfoque (emborronamiento simétrico) frente al emborronamiento producido por aberraciones de alto orden (emborronamiento asimétrico) demuestran que la codificación interna del emborronamiento es sensible a las características del patrón de emborronamiento. Aislar el efecto de la orientación frente a la magnitud del emborronamiento, revela que la adaptación a las aberraciones naturales del sujeto depende de la orientación del patrón de aberraciones.

7 El método de clasificación de imágenes es una herramienta poderosa para identificar la codificación interna del emborronamiento impuesto por las aberraciones naturales del sujeto. El sujeto tiende a preferir consistentemente PSF orientadas como la su PSF natural. La codificación interna del emborronamiento es específica a las características del emborronamiento impuesto por las aberraciones oculares de un individuo y los mecanismos de calibración del emborronamiento operan también según las características propias al contraste y orientación.

Bibliography

Abbey, C. K. and Eckstein, M. P. (2007). Classification images for simple detection and discrimination tasks in correlated noise. *J Opt Soc Am A Opt Image Sci Vis*, 24(12):110–124.

Adams, W. J., Banks, M. S., and van Ee, R. (2001). Adaptation to three-dimensional distortions in human vision. *Nat Neurosci*, 4(11):1063–1064.

Ahissar, M. and Hochstein, S. (1996). Learning pop-out detection: specificities to stimulus characteristics. *Vision Res*, 36(21):3487–3500.

Ahissar, M. and Hochstein, S. (1997). Task difficulty and the specificity of perceptual learning. *Nature*, 387(6631):401–406.

Ahumada, A. J. (1996). Perceptual classification images from vernier acuity masked by noise. *Perception*, 26(Suppl. 18).

Ahumada, A. J. and Beard, B. L. (1999). Classification images for detection. *Invest. Ophthalmol. Visual Sci.*, 40, 3015.

Ahumada, A. J. and Lovell, J. (1971). Stimulus features in signal detection. *Journal of the Acoustical Society of America.*, 49:1751–1756.

Ahumada, A. J. and Marken, R. (1975). Time and frequency analyses of auditory signal detection. *J Acoust Soc Am.*, 57(2):385–390.

Anstis, S. (2002). Was el greco astigmatic? *Leonardo*, 35:p. 208.

Applegate, R. A. (2000). Limits to vision: can we do better than nature? *J Refract Surg*, 16(5):S547–S551.

Applegate, R. A., Ballentine, C., Gross, H., Sarver, E. J., and Sarver, C. A. (2003a). Visual acuity as a function of zernike mode and level of root mean square error. *Optom Vis Sci*, 80(2):97–105.

Applegate, R. A., Marsack, J. D., Ramos, R., and Sarver, E. J. (2003b). Interaction between aberrations to improve or reduce visual performance. *J Cataract Refract Surg*, 29(8):1487–1495.

Applegate, R. A., Marsack, J. D., and Thibos, L. N. (2006). Metrics of retinal image

quality predict visual performance in eyes with 20/17 or better visual acuity. *Optom Vis Sci*, 83(9):635–640.

Applegate, R. A., Sarver, E. J., and Khemsara, V. (2002). Are all aberrations equal? *J Refract Surg*, 18(5):S556–S562.

Applegate, R. A., Thibos, L. N., and Hilmantel, G. (2001). Optics of aberroscopy and super vision. *J Cataract Refract Surg*, 27(7):1093–1107.

Artal, P. (1990). Calculations of two-dimensional foveal retinal images in real eyes. *J Opt Soc Am A*, 7(8):1374–1381.

Artal, P. (2007). Neural adaptation to aberrations. the brain must adjust to a surgically altered visual system. *Cataract and Refractive Surgery Today.*, August:p. 76–77.

Artal, P., Chen, L., Fernández, E. J., Singer, B., Manzanera, S., and Williams, D. R. (2004a). Neural compensation for the eye's optical aberrations. *J Vis*, 4(4):281–287.

Artal, P., L. Chen, L., Manzanera, S., and William, D. (2004b). Temporal dependence of neural compensation for the eye's aberrations. *Invest Ophthalmol Vis Sci*, 45, E-Abstract 1077.

Atchison, D. A. and Guo, H. (2010). Subjective blur limits for higher order aberrations. *Optom Vis Sci*, 87(11):E890–E898.

Atchison, D. A., Guo, H., Charman, W. N., and Fisher, S. W. (2009a). Blur limits for defocus, astigmatism and trefoil. *Vision Res*, 49(19):2393–2403.

Atchison, D. A., Guo, H., and Fisher, S. W. (2009b). Limits of spherical blur determined with an adaptive optics mirror. *Ophthalmic Physiol Opt*, 29(3):300–311.

Atchison, D. A., Lucas, S. D., Ashman, R., Huynh, M. A., Schilt, D. W., and Ngo, P. Q. (2006). Refraction and aberration across the horizontal central 10 degrees of the visual field. *Optom Vis Sci*, 83(4):213–221.

Atchison, D. A., Marcos, S., and Scott, D. H. (2003a). The influence of the stiles-crawford peak location on visual performance. *Vision Res*, 43(6):659–668.

Atchison, D. A., Scott, D. H., and Charman, W. N. (2003b). Hartmann-shack technique and refraction across the horizontal visual field. *J Opt Soc Am A Opt Image Sci Vis*, 20(6):965–973.

Atchison, D. A. and Smith, G. (2000). *Optics of the Human Eye*. Oxford, Butterworth-Heinemann.

Atchison, D. A., Woods, R. L., and Bradley, A. (1998). Predicting the effects of optical defocus on human contrast sensitivity. *J Opt Soc Am A Opt Image Sci Vis*, 15(9):2536–2544.

Babcock, H. W. (1953). the possibility of compensating astronomical seeing. *Astronomical Society of the Pacific,*, 65(386).

Bailey, I. and Lovie, J. (1976). New design principles for visual acuity letter charts. *Am J Optom Physiol Opt*, 53(11):740–5.

Banks, M. S., Geisler, W. S., and Bennett, P. J. (1987). The physical limits of grating visibility. *Vision Res*, 27(11):1915–1924.

Barbero, S. (2006). Refractive power of a multilayer rotationally symmetric model of the human cornea and tear film. *J Opt Soc Am A Opt Image Sci Vis*, 23(7):1578–1585.

Barbero, S. and Marcos, S. (2007). Analytical tools for customized design of monofocal intraocular lenses. *Opt Express*, 15(14):8576–8591.

Barbero, S., Marcos, S., Martín, R., Llorente, L., Moreno-Barriuso, E., and Merayo-Lloves, J. (2001). Validating the calculation of corneal aberrations from corneal topography: a test on keratoconus and aphakic eyes. *Investigative Opthalmology and Visual Science*, 42 (Suppl.): 894.

Battaglia, P. W., Jacobs, R. A., and Aslin, R. N. (2004). Depth-dependent blur adaptation. *Vision Res*, 44(2):113–117.

Beard, B. L. and Ahumada, A. J. (1998). Technique to extract relevant image features for visual tasks. *Proceedings of SPIE, Human Vision & Electronic Imaging*, 3299:79–85.

Bilson, A. C., Mizokami, Y., and Webster, M. A. (2005). Visual adjustments to temporal blur. *J Opt Soc Am A Opt Image Sci Vis*, 22(10):2281–2288.

Blakemore, C. and Campbell, F. W. (1969a). Adaptation to spatial stimuli. *J Physiol*, 200(1):11P–13P.

Blakemore, C. and Campbell, F. W. (1969b). On the existence of neurones in the human visual system selectively sensitive to the orientation and size of retinal images. *J Physiol*, 203(1):237–260.

Bradley, A., Switkes, E., and De Valois, K. (1988). Orientation and spatial frequency selectivity of adaptation to color and luminance gratings. *Vision Res*, 28(7):841–856.

Brainard, D. H. (1997). The psychophysics toolbox. *Spat Vis*, 10(4):433–436.

Bruce, V. and Young, A. (1986). Understanding face recognition. *British Journal of Psychology*, 77:305–327.

Bullimore, M. A., Bailey, I. L., and Wacker, R. T. (1991). Face recognition in age-related maculopathy. *Invest Ophthalmol Vis Sci*, 32(7):2020–2029.

Burns, S. A., Marcos, S., Elsner, A. E., and Bara, S. (2002). Contrast improvement of confocal retinal imaging by use of phase-correcting plates. *Opt Lett*, 27(6):400–402.

Burns, S. A., Tumbar, R., Elsner, A. E., Ferguson, D., and Hammer, D. X. (2007). Large-field-of-view, modular, stabilized, adaptive-optics-based scanning laser ophthalmoscope. *J Opt Soc Am A Opt Image Sci Vis*, 24(5):1313–1326.

Burton, G. J. and Haig, N. D. (1984). Effects of the seidel aberrations on visual target discrimination. *J Opt Soc Am A*, 1(4):373–385.

Campbell, F. W. and Green, D. G. (1965). Optical and retinal factors affecting visual resolution. *J Physiol*, 181(3):576–593.

Campbell, F. W. and Gregory, A. H. (1960). Effect of size of pupil on visual acuity. *Nature*, 187:1121–1123.

Castejón-Mochón, J. F., López-Gil, N., Benito, A., and Artal, P. (2002). Ocular wave-front aberration statistics in a normal young population. *Vision Res*, 42(13):1611–1617.

Cavanagh, P. and Anstis, S. (1991). The contribution of color to motion in normal and color-deficient observers. *Vision Res*, 31(12):2109–2148.

Charman, W. N. (1991). Wavefront aberrations of the eye: A review. *Optometry and Vision Science*, 68:574–583.

Chen, D. C., Jones, S. M., Silva, D. A., and Olivier, S. S. (2007a). High-resolution adaptive

optics scanning laser ophthalmoscope with dual deformable mirrors. *J Opt Soc Am A Opt Image Sci Vis*, 24(5):1305–1312.

Chen, L., Artal, P., Gutierrez, D., and Williams, D. R. (2007b). Neural compensation for the best aberration correction. *J Vis*, 7(10):9.1–9.9.

Clifford, C. W. G., Webster, M. A., Stanley, G. B., Stocker, A. A., Kohn, A., Sharpee, T. O., and Schwartz, O. (2007). Visual adaptation: neural, psychological and computational aspects. *Vision Res*, 47(25):3125–3131.

Conrey, B. and Gold, J. M. (2009). Pattern recognition in correlated and uncorrelated noise. *J Opt Soc Am A Opt Image Sci Vis*, 26(11):94–109.

Costen, N. P., Parker, D. M., and Craw, I. (1996). Effects of high-pass and low-pass spatial filtering on face identification. *Percept Psychophys*, 58(4):602–612.

Dalcanton, J. J. (2009). 18 years of science with the hubble space telescope. *Nature*, 457(7225):41–50.

Dalimier, E., Dainty, C., and Barbur, J. (2008). Effects of higher-order aberrations on contrast acuity as a function of light level. *Journal of Modern Optics*, 55:791–803.

de Gracia, P., Dorronsoro, C., Gambra, E., Marin, G., Hernández, M., and Marcos, S. (2010). Combining coma with astigmatism can improve retinal image over astigmatism alone. *Vision Res*, 50(19):2008–2014.

de Gracia, P., Dorronsoro, C., Marin, G., Hernández, M., and Marcos, S. (2011a). Visual acuity under combined astigmatism and coma: optical and neural adaptation effects. *J Vis*, 11(2).

de Gracia, P., Dorronsoro, C., Sawides, L., Gambra, E., and Marcos, S. (2009). Experimental test of simulated retinal images using adaptive optics. *Proceedings : Adaptive Optics: Methods, Analysis and Applications, OSA Technical Digest (CD) (Optical Society of America)*, paper JWB4.

de Gracia, P., Marcos, S., Mathur, A., and Atchison, D. A. (2011b). Contrast sensitivity benefit of adaptive optics correction of ocular aberrations. *J Vis*, 11(12).

Delahunt, P. B., Webster, M. A., Ma, L., and Werner, J. S. (2004). Long-term renormalization of chromatic mechanisms following cataract surgery. *Vis Neurosci*, 21(3):301–307.

Delori, F. C., Webb, R. H., Sliney, D. H., and , A. N. S. I. (2007). Maximum permissible exposures for ocular safety (ansi 2000), with emphasis on ophthalmic devices. *J Opt Soc Am A Opt Image Sci Vis*, 24(5):1250–1265.

Dreher, A. W., Bille, J. F., and Weinreb, R. N. (1989). Active optical depth resolution improvement of the laser tomographic scanner. *Appl Opt*, 28(4):804–808.

Drexler, W. and Fujimoto, J. G. (2008). State-of-the-art retinal optical coherence tomography. *Prog Retin Eye Res*, 27(1):45–88.

Dubra, A., Sulai, Y., Norris, J. L., Cooper, R. F., Dubis, A. M., Williams, D. R., and Carroll, J. (2011). Noninvasive imaging of the human rod photoreceptor mosaic using a confocal adaptive optics scanning ophthalmoscope. *Biomed Opt Express*, 2(7):1864–1876.

Eckstein, M. P. and Ahumada, A. J. (2002). Classification images: a tool to analyze visual strategies. *Journal of Vision*, 2(1).

Elliott, S. L., Choi, S. S., Doble, N., Hardy, J. L., Evans, J. W., and Werner, J. S. (2009). Role of high-order aberrations in senescent changes in spatial vision. *J Vis*, 9(2):24.1–2416.

Elliott, S. L., Georgeson, M. A., and Webster, M. A. (2011). Response normalization and blur adaptation: data and multi-scale model. *J Vis*, 11(2).

Erickson, K. and Schulkin, J. (2003). Facial expressions of emotion: a cognitive neuroscience perspective. *Brain Cogn*, 52(1):52–60.

Fahle, M. and Morgan, M. (1996). No transfer of perceptual learning between similar stimuli in the same retinal position. *Curr Biol*, 6(3):292–297.

Fechner, G. (1851). *Elemente der Psychophysikin (translated to English in 1966, Elements of Psychophysics. Volume I)*. New York: Holt, Rinehart and Winston.

Fernandez, E. J., Vabre, L., Hermann, B., Unterhuber, A., Povazay, B., and Drexler, W. (2006). Adaptive optics with a magnetic deformable mirror: applications in the human eye. *Opt Express*, 14(20):8900–8917.

Ferree, C. and Rand, G. (1932). The effect of intensity of illumination on the acuity of the normal eye and eyes slightly defective as to refraction. *American Journal of Psychology*, 34:244–249.

Field, D. J. and Brady, N. (1997). Visual sensitivity, blur and the sources of variability in the amplitude spectra of natural scenes. *Vision Res*, 37(23):3367–3383.

Fine, I., Smallman, H. S., Doyle, P., and MacLeod, D. I. A. (2002). Visual function before and after the removal of bilateral congenital cataracts in adulthood. *Vision Res*, 42(2):191–210.

Fiorentini, A. and Berardi, N. (1980). Perceptual learning specific for orientation and spatial frequency. *Nature*, 287(5777):43–44.

Fischer (1952). Eidophor projector for tv theater. *Tele-Tech electronics devices-radio-television*, page 57.

Flamant, F. (1955). Etude de la répartition de lumière dans l'image rétinienne d'une fente. *Revue d'Optique*, 34:433 –459.

Gambra, E., Sawides, L., Dorronsoro, C., and Marcos, S. (2009). Accommodative lag and fluctuations when optical aberrations are manipulated. *J Vis*, 9(6):4.1–415.

Gehrz, R. D., Roellig, T. L., Werner, M. W., Fazio, G. G., Houck, J. R., Low, F. J., Rieke, G. H., Soifer, B. T., Levine, D. A., and Romana, E. A. (2007). The nasa spitzer space telescope. *Rev Sci Instrum*, 78(1):011302.

George, S. and Rosenfield, M. (2004). Blur adaptation and myopia. *Optom Vis Sci*, 81(7):543–547.

Georgeson, M. A., May, K. A., Freeman, T. C. A., and Hesse, G. S. (2007). From filters to features: scale-space analysis of edge and blur coding in human vision. *J Vis*, 7(13):7.1–721.

Georgeson, M. A. and Sullivan, G. D. (1975). Contrast constancy: deblurring in human vision by spatial frequency channels. *J Physiol*, 252(3):627–656.

Gibson, J. J. (1950). The perception of visual surfaces. *Am J Psychol*, 100(3-4):646–664.

Gold, J., Bennett, P. J., and Sekuler, A. B. (1999). Identification of band-pass filtered

letters and faces by human and ideal observers. *Vision Res*, 39(21):3537–3560.

Goodman, J. W. (1996). *Introduction to Fourier optics.* McGraw-Hill, New York., 2nd ed. edition.

Gregory, R. (1998). *Eye and brain, the psychology of seeing.* World university library, McGraw Hill book company, New York Toronto R.L, gregory first edition on 1966 edition.

Grieve, K., Tiruveedhula, P., Zhang, Y., and Roorda, A. (2006). Multi-wavelength imaging with the adaptive optics scanning laser ophthalmoscope. *Opt Express*, 14(25):12230–12242.

Grossmann, T. and Vaish, A. (2008). Reading faces in infancy: Developing a multi-level analysis of a social stimulus. *Social cognition: Development, neuroscience and autism. Blackwell*, In T. Striano & V. Reid (Eds.),.

Guirao, A. and Williams, D. R. (2003). A method to predict refractive errors from wave aberration data. *Optom Vis Sci*, 80(1):36–42.

Guo, H. and Atchison, D. A. (2010). Subjective blur limits for cylinder. *Optom Vis Sci*, 87(8):E549–E559.

Guo, H., Atchison, D. A., and Birt, B. J. (2008). Changes in through-focus spatial visual performance with adaptive optics correction of monochromatic aberrations. *Vision Res*, 48(17):1804–1811.

Gur, D., Rubin, D. A., Kart, B. H., Peterson, A. M., Fuhrman, C. R., Rockette, H. E., and King, J. L. (1997). Forced choice and ordinal discrete rating assessment of image quality: a comparison. *J Digit Imaging*, 10(3):103–107.

Guyton, D. L. (1977). Prescribing cylinders: the problem of distortion. *Surv Ophthalmol*, 22(3):177–188.

Halit, H., de Haan, M., Schyns, P. G., and Johnson, M. H. (2006). Is high-spatial frequency information used in the early stages of face detection? *Brain Research*, 1117:154–161.

Hammer, D. X., Ferguson, R. D., Bigelow, C. E., Iftimia, N. V., Ustun, T. E., and Burns, S. A. (2006). Adaptive optics scanning laser ophthalmoscope for stabilized retinal imaging. *Opt Express*, 14(8):3354–3367.

Hampson, K. M. (2008). Adaptive optics and vision. *Journal of Modern Optics*, 55:3425–3467.

Hanley, J. A. (1988). Alternative approach to receiver operating characteristic analyses. *Radiology*, 168:568–570.

Hanley, J. A. and McNeil, B. J. (1982). The meaning and use of the area under a receiver operating characteristic (roc) curve. *Radiology*, 143:29–36.

Hanley, J. A. and McNeil, B. J. (1983). A method of comparing the areas under receiver operating characteristic curves derived from the same case. *Radiology*, 148:839–843.

Hardy, J. W., Lefebvre, J. E., and Koliopoulos, C. L. (1977). Real-time atmospheric compensation. *JOSA*, 67(3,):360–369.

Harris, C. S. (1965). Perceptual adaptation to inverted, reversed, and displaced vision. *Psychol Rev*, 72(6):419–444.

Hartwig, A. and Atchison, D. A. (2012). Analysis of higher-order aberrations in a large

clinical population. *Invest Ophthalmol Vis Sci*, 53(12):7862–7870.

Haun, A. M. and Peli, E. (2011). Measuring the perceived contrast of natural images. *SID 11 DIGEST*, pages 302–304.

Hecht, S., Shlaer, S., and Pirenne, M. H. (1942). Energy, quanta, and vision. *J Gen Physiol*, 25(6):819–840.

Hermann, B., Fernández, E. J., Unterhuber, A., Sattmann, H., Fercher, A. F., Drexler, W., Prieto, P. M., and Artal, P. (2004). Adaptive-optics ultrahigh-resolution optical coherence tomography. *Opt Lett*, 29(18):2142–2144.

Hofer, H., Artal, P., Singer, B., Aragón, J. L., and Williams, D. R. (2001). Dynamics of the eye's wave aberration. *J Opt Soc Am A Opt Image Sci Vis*, 18(3):497–506.

Hubel, D. H. (1963). The visual cortex of the brain. *Sci Am*, 209:54–62.

Iskander, D. R. (2006). Computational aspects of the visual strehl ratio. *Optom Vis Sci*, 83(1):57–59.

Jimenez, J. R., Ortiz, C., Hita, E., and Soler, M. (2008). Correlation between image quality and visual performance. *Journal of Modern Optics*, 55:783–790.

Karni, A. and Sagi, D. (1991). Where practice makes perfect in texture discrimination: evidence for primary visual cortex plasticity. *Proc Natl Acad Sci U S A*, 88(11):4966–4970.

Kohler, W. and Wallach, H. (1944). Figural aftereffects: An investigation of visual processes. *Proceedings of the American Philosophical Society*, 88:269–357.

Kompaniez, E., Sawides, L., Marcos, S., and Webster, M. A. (2013). Adaptation to interocular differences in blur. *JOV, in press*, (11).

Legras, R., Chateau, N., and Charman, W. N. (2004). Assessment of just-noticeable differences for refractive errors and spherical aberration using visual simulation. *Optom Vis Sci*, 81(9):718–728.

Legras, R. and Rouger, H. (2008a). Calculations and measurements of the visual benefit of correcting the higher-order aberrations using adaptive optics technology. *J Optom*, 01:22–9.

Legras, R. and Rouger, H. (2008b). Just-noticeable levels of aberration correction. *J Optom*, 1:71–77.

Levy, Y., Segal, O., Avni, I., and Zadok, D. (2005). Ocular higher-order aberrations in eyes with supernormal vision. *Am J Ophthalmol*, 139(2):225–228.

Liang, J., Grimm, B., Goelz, S., and Bille, J. F. (1994). Objective measurement of wave aberrations of the human eye with the use of a hartmann-shack wave-front sensor. *J Opt Soc Am A Opt Image Sci Vis*, 11(7):1949–1957.

Liang, J., Williams, D. R., and Miller, D. T. (1997). Supernormal vision and high-resolution retinal imaging through adaptive optics. *J Opt Soc Am A Opt Image Sci Vis*, 14(11):2884–2892.

Linden, D. E., Kallenbach, U., Heinecke, A., Singer, W., and Goebel, R. (1999). The myth of upright vision. a psychophysical and functional imaging study of adaptation to inverting spectacles. *Perception*, 28(4):469–481.

Llorente, L., Diaz-Santana, L., Lara-Saucedo, D., and Marcos, S. (2003). Aberrations of

the human eye in visible and near infrared illumination. *Optom Vis Sci*, 80(1):26–35.

Losada, M. A., Navarro, R., and Santamaría, J. (1993). Relative contributions of optical and neural limitations to human contrast sensitivity at different luminance levels. *Vision Res*, 33(16):2321–2336.

Lu, Z.-L., Hua, T., Huang, C.-B., Zhou, Y., and Dosher, B. A. (2011). Visual perceptual learning. *Neurobiol Learn Mem*, 95(2):145–151.

MacRae, S. M. (2000). Supernormal vision, hypervision, and customized corneal ablation. *J Cataract Refract Surg*, 26(2):154–157.

MacRae, S. M., Schwiegerling, J., and Snyder, R. (2000). Customized corneal ablation and super vision. *Journal of Refractive Surgery*, 16:230–235.

Manzanera, S., Prieto, P. M., Ayala, D. B., Lindacher, J. M., and Artal, P. (2007). Liquid crystal adaptive optics visual simulator: Application to testing and design of ophthalmic optical elements. *Opt Express*, 15(24):16177–16188.

Marcos, S. (2001). Aberrations and visual performance following standard laser vision correction. *J Refract Surg*, 17(5):S596–S601.

Marcos, S. (2005). Calidad de imagen retiniana. *Investigación y Ciencia*, 34(6674).

Marcos, S. and Burns, S. A. (2000). On the symmetry between eyes of wavefront aberration and cone directionality. *Vision Res*, 40(18):2437–2447.

Marcos, S., Burns, S. A., Moreno-Barriusop, E., and Navarro, R. (1999). A new approach to the study of ocular chromatic aberrations. *Vision Res*, 39(26):4309–4323.

Marcos, S. and Navarro, R. (1997). Determination of the foveal cone spacing by ocular speckle interferometry: limiting factors and acuity predictions. *Journal of the Optical Society of America A*, 14:731–740.

Marcos, S., Sawides, L., Gambra, E., and Dorronsoro, C. (2008). Influence of adaptive-optics ocular aberration correction on visual acuity at different luminances and contrast polarities. *J Vis*, 8(13):1.1–112.

Marsack, J. D., Thibos, L. N., and Applegate, R. A. (2004). Metrics of optical quality derived from wave aberrations predict visual performance. *J Vis*, 4(4):322–328.

McCollough-Howard, C. and Webster, M. A. (2011). Mccollough effect. *Scholarpedia,*, 6, 8175.

McGovern, D. P., Roach, N. W., and Webb, B. S. (2012a). Perceptual learning reconfigures the effects of visual adaptation. *J Neurosci*, 32(39):13621–13629.

McGovern, D. P., Webb, B. S., and Peirce, J. W. (2012b). Transfer of perceptual learning between different visual tasks. *J Vis*, 12(11):4.

McLellan, J. S., Prieto, P. M., Marcos, S., and Burns, S. A. (2006). Effects of interactions among wave aberrations on optical image quality. *Vision Res*, 46(18):3009–3016.

Metz, C. E. (1978). Basic principles of roc analysis. *Semin Nucl Med*, 8(4):283–298.

Metz, C. E. (1986). Roc methodology in radiologic imaging. *Invest Radiol*, 21(9):720–733.

Metz, C. E. (2006). Receiver operating characteristic analysis: a tool for the quantitative evaluation of observer performance and imaging systems. *J Am Coll Radiol*, 3(6):413–422.

Metz, C. E. (2008). Roc analysis in medical imaging: a tutorial review of the literature. *Radiol Phys Technol*, 1(1):2–12.

Metz, C. E., Wang, P. L., and Kronman, H. B. (1984). A new approach for testing the significance of differences between roc curves measured from correlated data. *Information Processing in Medical Imaging (Amsterdam, Nijhoff)*, pages 432–445.

Miller, A. D., Kris, M. J., and Griffiths, A. C. (1997). Effect of small focal errors on vision. *Optom Vis Sci*, 74(7):521–526.

Miller, D. T., Kocaoglu, O. P., Wang, Q., and Lee, S. (2011). Adaptive optics and the eye (super resolution oct). *Eye (Lond)*, 25(3):321–330.

Miller, D. T., Qu, J., Jonnal, R. S., and Thorn, K. E. (2003). Coherence gating and adaptive optics in the eye. *Proceedings of SPIE.*, 4956:65–72.

Miller, W. H. and Bernard, G. D. (1983). Averaging over the foveal receptor aperture curtails aliasing. *Vision Res*, 23(12):1365–1369.

Mizokami, Y., Paras, C., and Webster, M. A. (2004). Chromatic and contrast selectivity in color contrast adaptation. *Vis Neurosci*, 21(3):359–363.

Mon-Williams, M., Tresilian, J. R., Strang, N. C., Kochhar, P., and Wann, J. P. (1998). Improving vision: neural compensation for optical defocus. *Proc Biol Sci*, 265(1390):71–77.

Murray, R. F., Bennett, P. J., and Sekuler, A. B. (2002). Classification images predict absolute efficiency. *J. Vision*, 5:139–149.

Navarro, R., Moreno-Barriuso, E., Bará, S., and Mancebo, T. (2000). Phase plates for wave-aberration compensation in the human eye. *Opt Lett*, 25(4):236–238.

Nelson, C. A. (2001). Infant and child development. *The development and neural bases of face recognition*, 10:3–18.

Näsänen, R. (1999). Spatial frequency bandwidth used in the recognition of facial images. *Vision Res*, 39(23):3824–3833.

Ohlendorf, A., Tabernero, J., and Schaeffel, F. (2011). Visual acuity with simulated and real astigmatic defocus. *Optom Vis Sci*, 88(5):562–569.

Ostergerb, G. (1935). Topography of the layers of rods and cones in the human retina. *Acta Ophthal (Suppl.)*, 6:1–103.

Owen, D. H. (1978). *The psychophysics of prior experience.* Edited by Ohio State University Press.

Owsley, C. and Sloane, M. E. (1987). Contrast sensitivity, acuity, and the perception of 'real-world' targets. *Br J Ophthalmol*, 71(10):791–796.

Pallikaris, A., Williams, D. R., and Hofer, H. (2003). The reflectance of single cones in the living human eye. *Invest Ophthalmol Vis Sci*, 44(10):4580–4592.

Peli, E., Goldstein, R. B., Young, G. M., Trempe, C. L., and Buzney, S. M. (1991). Image enhancement for the visually impaired. simulations and experimental results. *Invest Ophthalmol Vis Sci*, 32(8):2337–2350.

Peli, E. and Lang, A. (2001). Appearance of images through a multifocal intraocular lens. *J Opt Soc Am A Opt Image Sci Vis*, 18(2):302–309.

Peli, E., Lee, E., Trempe, C. L., and Buzney, S. (1994). Image enhancement for the

visually impaired: the effects of enhancement on face recognition. *J Opt Soc Am A Opt Image Sci Vis*, 11(7):1929–1939.

Pelli, D. and Farell, B. (1995). *Handbook of Optics. Volume I. Fundamentals, Techniques and design.*, volume I. McGraw-Hill, second edition edition.

Pelli, D. G. (1997). The videotoolbox software for visual psychophysics: transforming numbers into movies. *Spat Vis*, 10(4):437–442.

Pesudovs, K. (2005). Involvement of neural adaptation in the recovery of vision after laser refractive surgery. *J Refract Surg*, 21(2):144–147.

Pesudovs, K. and Brennan, N. A. (1993). Decreased uncorrected vision after a period of distance fixation with spectacle wear. *Optom Vis Sci*, 70(7):528–531.

Piers, P. A., Manzanera, S., Prieto, P. M., Gorceix, N., and Artal, P. (2007). Use of adaptive optics to determine the optimal ocular spherical aberration. *J Cataract Refract Surg*, 33(10):1721–1726.

Plainis, S. and Pallikaris, I. (2008). Ocular monochromatic aberration statistics in a large emmetropic population. *Journal of Modern Optics*, 55,(4–5,):759–772.

Poggio, T., Fahle, M., and Edelman, S. (1992). Fast perceptual learning in visual hyperacuity. *Science*, 256(5059):1018–1021.

Pointer, J. S. (2001). The influence of level and polarity of figure-ground contrast on vision. *Acta Ophthalmol Scand*, 79(4):422–425.

Poonja, S., Patel, S., Henry, L., and Roorda, A. (2005). Dynamic visual stimulus presentation in an adaptive optics scanning laser ophthalmoscope. *J Refract Surg*, 21(5):S575–S580.

Porter, J., Guirao, A., Cox, I. G., and Williams, D. R. (2001). Monochromatic aberrations of the human eye in a large population. *J Opt Soc Am A Opt Image Sci Vis*, 18(8):1793–1803.

Posamentier, M. T. and Abdi, H. (2003). Processing faces and facial expressions. *Neuropsychol Rev*, 13(3):113–143.

Poulere, E., Moschandreas, J., Kontadakis, G. A., Pallikaris, I. G., and Plainis, S. (2013). Effect of blur and subsequent adaptation on visual acuity using letter and landolt c charts: differences between emmetropes and myopes. *Ophthalmic Physiol Opt*, 33(2):130–137.

Raasch, T. W. (1995). Spherocylindrical refractive errors and visual acuity. *Optom Vis Sci*, 72(4):272–275.

Rajeev, N. and Metha, A. (2010). Enhanced contrast sensitivity confirms active compensation in blur adaptation. *Invest Ophthalmol Vis Sci*, 51(2):1242–1246.

Ravin, J. G. (1985). Monet's cataracts. *JAMA*, 254(3):394–399.

Remón, L., Tornel, M., and Furlan, W. D. (2006). Visual acuity in simple myopic astigmatism: influence of cylinder axis. *Optom Vis Sci*, 83(5):311–315.

Riggs, L. A. and Graham, C. H. (1965). Visual acuity (chap. vision and visual perception). *New York: John Wiley and Sons.*

Roorda, A., Romero-Borja, F., Donnelly Iii, W., Queener, H., Hebert, T., and Campbell, M. (2002). Adaptive optics scanning laser ophthalmoscopy. *Opt Express*, 10(9):405–412.

Roorda, A. and Williams, D. R. (1999). The arrangement of the three cone classes in the living human eye. *Nature*, 397(6719):520–522.

Roorda, A. and Williams, D. R. (2002). Optical fiber properties of individual human cones. *J Vis*, 2(5):404–412.

Rosenfield, M., Hong, S. E., and George, S. (2004). Blur adaptation in myopes. *Optom Vis Sci*, 81(9):657–662.

Rossi, E. A. and Roorda, A. (2010). Is visual resolution after adaptive optics correction susceptible to perceptual learning? *J Vis*, 10(12):11.

Rossi, E. A., Weiser, P., Tarrant, J., and Roorda, A. (2007). Visual performance in emmetropia and low myopia after correction of high-order aberrations. *J Vis*, 7(8):14.

Ruiz-Soler, M. and Beltran, F. S. (2006). Face perception: an integrative review of the role of spatial frequencies. *Psychol Res*, 70(4):273–292.

Sabesan, R., Jeong, T. M., Carvalho, L., Cox, I. G., Williams, D. R., and Yoon, G. (2007). Vision improvement by correcting higher-order aberrations with customized soft contact lenses in keratoconic eyes. *Opt Lett*, 32(8):1000–1002.

Sabesan, R. and Yoon, G. (2009). Visual performance after correcting higher order aberrations in keratoconic eyes. *J Vis*, 9(5):6.1–610.

Sabesan, R. and Yoon, G. (2010). Neural compensation for long-term asymmetric optical blur to improve visual performance in keratoconic eyes. *Invest Ophthalmol Vis Sci*, 51(7):3835–3839.

Sawides, L., de Gracia, P., Dorronsoro, C., Webster, M., and Marcos, S. (2011a). Adapting to blur produced by ocular high-order aberrations. *J Vis*, 11(7).

Sawides, L., de Gracia, P., Dorronsoro, C., Webster, M. A., and Marcos, S. (2011b). Vision is adapted to the natural level of blur present in the retinal image. *PLoS One*, 6(11):e27031.

Sawides, L., Dorronsoro, C., de Gracia, P., Vinas, M., Webster, M., and Marcos, S. (2012). Dependence of subjective image focus on the magnitude and pattern of high order aberrations. *J Vis*, 12(8):4.

Sawides, L., Gambra, E., Pascual, D., Dorronsoro, C., and Marcos, S. (2010a). Visual performance with real-life tasks under adaptive-optics ocular aberration correction. *J Vis*, 10(5):19.

Sawides, L., Marcos, S., Ravikumar, S., Thibos, L., Bradley, A., and Webster, M. (2010b). Adaptation to astigmatic blur. *J Vis*, 10(12):22.

Schwendeman, F., Ogden, B., Horner, D., and Thibos, L. (1997). Effect of sphero-cylinder blur on visual acuity. *Optometry and Vision Science*, 74/12S:180.

Schwiegerling, J. and Snyder, R. W. (2000). Corneal ablation patterns to correct for spherical aberration in photorefractive keratectomy. *J Cataract Refract Surg*, 26(2):214–221.

Shack, R. and Platt, B. (1971). Production and use of a lenticular hartmann screen'. *J.Opt. Soc. Am.*, 61:656.

Sloan, L. L. (1951). Measurement of visual acuity; a critical review. *AMA Arch Ophthalmol*, 45(6):704–725.

Sloan, L. L. (1968). The photopic acuity-luminance function with special reference to parafoveal vision. *Vision Res*, 8(7):901–911.

Slone, R. M., Foos, D. H., Whiting, B. R., Muka, E., Rubin, D. A., Pilgram, T. K., Kohm, K. S., Young, S. S., Ho, P., and Hendrickson, D. D. (2000). Assessment of visually lossless irreversible image compression: comparison of three methods by using an image-comparison workstation. *Radiology*, 215(2):543–553.

Solomon, J. A. and Pelli, D. G. (1994). The visual filter mediating letter identification. *Nature*, 369(6479):395–397.

Stiles, W. S. and Crawford, B. H. (1933). The luminous efficiency of rays entering the eye pupil at different points. *Proc. Roy. Soc.*, 112:428–450.

Stratton, G. (1896). Some preliminary experiments on vision without inversion of the retinal image. *Psychological Review*, 3:611–617.

Stratton, G. (1897). Upright vision and the retinal image. *Psychological Review*, 4:182–187.

Tan, J., Papas, E., Carnt, N., Jalbert, I., Skotnitsky, C., Shiobara, M., Lum, E., and Holden, B. (2007). Performance standards for toric soft contact lenses. *Optom Vis Sci*, 84(5):422–428.

Thibos, L. N. and Bradley, A. (1995). *Vision Models for Target Detection and Recognition. Modeling off-axis vision — II: the effect of spatial filtering and sampling by retinal neurons.*, volume 2. Singapore: World Scientific Press.

Thibos, L. N., Hong, X., Bradley, A., and Applegate, R. A. (2004). Accuracy and precision of objective refraction from wavefront aberrations. *J Vis*, 4(4):329–351.

Thibos, L. N., Hong, X., Bradley, A., and Cheng, X. (2002). Statistical variation of aberration structure and image quality in a normal population of healthy eyes. *J Opt Soc Am A Opt Image Sci Vis*, 19(12):2329–2348.

Thibos, L. N., Wheeler, W., and Horner, D. (1997). Power vectors: an application of fourier analysis to the description and statistical analysis of refractive error. *Optom Vis Sci*, 74(6):367–375.

Vera-Diaz, F. A., Gwiazda, J., Thorn, F., and Held, R. (2004). Increased accommodation following adaptation to image blur in myopes. *J Vis*, 4(12):1111–1119.

Vera-Diaz, F. A., Woods, R. L., and Peli, E. (2010). Shape and individual variability of the blur adaptation curve. *Vision Res*, 50(15):1452–1461.

Villegas, E. A., Alcon, E., and Artal, P. (2006). The effect of correcting small astigmatisms on visual acuity. *Investigative . Ophthalmology & Visual Sciences,*, 47, E-Abstract, 1173.

Vinas, M., de Gracia, P., Dorronsoro, C., Sawides, L., Marin, G., Hernandez, M., and Marcos, S. (2013). Visual performance under natural, corrected and adaptive optics induced astigmatism: meridional and adaptational effects. In *Association for Research in Vision and Phthalmology (ARVO). Abstract ID: 1281.*

Vinas, M., Sawides, L., de Gracia, P., and Marcos, S. (2012). Perceptual adaptation to the correction of natural astigmatism. *PLoS One*, 7(9):e46361.

Von Helmholtz, H. (1855). Ueber das sehen des menschen. In *(lecture, 27 february 1855, Königsberg) Leipzig:Voss.*

Von Helmholtz, H. (1881). Popular lectures on scientific subjects: Second series. In *London: Longmans, Green*.

Vuilleumier, P., Armony, J. L., Driver, J., and Dolan, R. J. (2003). Distinct spatial frequency sensitivities for processing faces and emotional expressions. *Nat Neurosci*, 6(6):624–631.

Waldrop, M. M. (1990). Hubble space telescope takes aim at the stars. *Science*, 247(4950):1546–1547.

Walls, G. L. (1943). Factors in human visual resolution. *Journal of the Optical Society of America*, 33:487–505.

Walsh, G., Charman, W. N., and Howland, H. C. (1984). Objective technique for the determination of monochromatic aberrations of the human eye. *J Opt Soc Am A*, 1(9):987–992.

Watson, A. B. and Ahumada, A. J. (2008). Predicting visual acuity from wavefront aberrations. *J Vis*, 8(4):1–19.

Watson, A. B. and Pelli, D. G. (1983). Quest: a bayesian adaptive psychometric method. *Percept Psychophys*, 33(2):113–120.

Watson, A. B. and Rosenholtz, R. (1997). A rorschach test for visual classification strategies. *Investigative Ophthalmology and Visual Science*, 38, pp. S1 (abstract).

Watson, T. L. and Clifford, C. W. G. (2003). Pulling faces: an investigation of the face-distortion aftereffect. *Perception*, 32(9):1109–1116.

Webster, M., Webster, S., MacDonald, J., and Bharadwadj, S. (2001). Adaptation to blur. *In Rogowitz, B.E. and Pappas, T.N. (Eds.),in Human Vision and Electronic Imaging, SPIE*, 4299:69–78.

Webster, M. A. (2011). Adaptation and visual coding. *J Vis*, 11(5).

Webster, M. A., Georgeson, M. A., and Webster, S. M. (2002). Neural adjustments to image blur. *Nat Neurosci*, 5(9):839–840.

Webster, M. A., Juricevic, I., and McDermott, K. C. (2010). Simulations of adaptation and color appearance in observers with varying spectral sensitivity. *Ophthalmic Physiol Opt*, 30(5):602–610.

Webster, M. A. and Leonard, D. (2008). Adaptation and perceptual norms in color vision. *J Opt Soc Am A Opt Image Sci Vis*, 25(11):2817–2825.

Webster, M. A. and MacLeod, D. I. A. (2011). Visual adaptation and face perception. *Philos Trans R Soc Lond B Biol Sci*, 366(1571):1702–1725.

Webster, M. A. and Maclin, O. (1999). Figural after-effects in the perception of faces. *Psychonomic Bulletin and Review*, 6:647–653.

Webster, M. A. and Miyahara, E. (1997). Contrast adaptation and the spatial structure of natural images. *J Opt Soc Am A Opt Image Sci Vis*, 14(9):2355–2366.

Webster, M. A., Mizokami, Y., Svec, L. A., and Elliott, S. L. (2006). Neural adjustments to chromatic blur. *Spat Vis*, 19(2-4):111–132.

Webster, M. A. and Mollon, J. D. (1995). Colour constancy influenced by contrast adaptation. *Nature*, 373(6516):694–698.

Webster, M. A. and Mollon, J. D. (1997). Adaptation and the color statistics of natural

images. *Vision Res*, 37(23):3283–3298.

Webster, M. A., Werner, J. S., and Field, D. J. (2005). *Fitting the Mind to the World. Adaptation and After-Effects in High-Level Vision. Ch.9 Adaptation and the phenomenology of perception.*

Werner, J. S. (1997). *Aging through the eyes of Monet.*

Werner, J. S. and Schefrin, B. E. (1993). Loci of achromatic points throughout the life span. *J Opt Soc Am A*, 10(7):1509–1516.

Westheimer, G. (2003). Visual acuity with reversed-contrast charts: I. theoretical and psychophysical investigations. *Optom Vis Sci*, 80(11):745–748.

Westheimer, G. and Campbell, F. W. (1962). Light distribution in the image formed by the living human eye. *J Opt Soc Am*, 52:1040–1045.

Westheimer, G., Chu, P., Huang, W., Tran, T., and Dister, R. (2003). Visual acuity with reversed-contrast charts: Ii. clinical investigation. *Optom Vis Sci*, 80(11):749–752.

Wilcox, W. W. (1932). The basis of the dependence of visual acuity on illumination. *Proc Natl Acad Sci U S A*, 18(1):47–56.

Williams, D. R. (2011). Imaging single cells in the living retina. *Vision Res*, 51(13):1379–1396.

Yehezkel, O., Belkin, M., Sagi, D., and Polat, U. (2005). Adaptation to astigmatic lens: effects on lateral interactions. *Journal of Vision*, 5(8).

Yehezkel, O., Sagi, D., Sterkin, A., Belkin, M., and Polat, U. (2010). Learning to adapt: Dynamics of readaptation to geometrical distortions. *Vision Res*, 50(16):1550–1558.

Yellott, Jr, J. (1982). Spectral analysis of spatial sampling by photoreceptors: topological disorder prevents aliasing. *Vision Res*, 22(9):1205–1210.

Yoon, G., Jeong, T. M., Cox, I. G., and Williams, D. R. (2004). Vision improvement by correcting higher-order aberrations with phase plates in normal eyes. *J Refract Surg*, 20(5):S523–S527.

Yoon, G.-Y. and Williams, D. R. (2002). Visual performance after correcting the monochromatic and chromatic aberrations of the eye. *J Opt Soc Am A Opt Image Sci Vis*, 19(2):266–275.

Young, A. W., McWeeny, K. H., Hay, D. C., and Ellis, A. W. (1986). Matching familiar and unfamiliar faces on identity and expression. *Psychol Res*, 48(2):63–68.

Young, T. (1802). On the theory of light and colours. *Phil. Trans. R. Soc*, 92:12–48.

Zawadzki, R. J., Choi, S. S., Jones, S. M., Oliver, S. S., and Werner, J. S. (2007). Adaptive optics-optical coherence tomography: optimizing visualization of microscopic retinal structures in three dimensions. *J Opt Soc Am A Opt Image Sci Vis*, 24(5):1373–1383.

Zernike, F. (1934). Physica. page 1:689.

Zhang, Y., Rha, J., Jonnal, R., and Miller, D. (2005). Adaptive optics parallel spectral domain optical coherence tomography for imaging the living retina. *Opt Express*, 13(12):4792–4811.

Zhao, L. and Chubb, C. (2001). The size-tuning of the face-distortion after-effect. *Vision Res*, 41(23):2979–2994.

Zhong, Z., Petrig, B. L., Qi, X., and Burns, S. A. (2008). In vivo measurement of erythrocyte velocity and retinal blood flow using adaptive optics scanning laser ophthalmoscopy. *Opt Express*, 16(17):12746–12756.

Publications during this research

SCIENTIFIC PAPERS ASSOCIATED WITH THIS THESIS

1. S. Marcos, L. Sawides, E. Gambra & C. Dorronsoro. "Influence of adaptive-optics aberration correction on visual acuity at different luminances and contrast polarities". *Journal of Vision*, 8 (13):1-12, 2008.
2. L. Sawides, E. Gambra, D. Pascual, C. Dorronsoro & S. Marcos. "Visual performance with real-life tasks under Adaptive-Optics ocular aberration correction". *Journal of Vision*, 10(5): 1-12, 2010.
3. L. Sawides, S. Marcos, S. Ravikumar, L. Thibos, A. Bradley & M. A. Webster. "Adaptation to astigmatic Blur". *Journal of Vision*, 10(12): 1-15, 2010.
4. L. Sawides, P. de Gracia, C. Dorronsoro, M.A. Webster & S. Marcos. "Adapting to the blur produced by high order aberrations". *Journal of Vision*, 11(7):1-11, 2011.
5. L. Sawides, P. de Gracia, C. Dorronsoro, M.A. Webster & S. Marcos. "Vision is adapted to the natural level of blur present in the retinal image". *PLoS One*, 6(11), e27031, p. 1-6, 2011.
6. L. Sawides, C. Dorronsoro, P. de Gracia, M. Vinas, M.A. Webster & S. Marcos. "Dependence of subjective image focus on the magnitude and pattern of High Order Aberrations". *Journal of Vision*, 12(8): 1-12, 2012.
7. L. Sawides, C. Dorronsoro, A.M. Haun, E. Peli & S. Marcos. "Using Pattern Classification to Measure Adaptation to the Orientation of High Order Aberrations". *PLoS One*, under review, 2013.

OTHER PUBLICATIONS

1. E. Gambra, L. Sawides, C. Dorronsoro & S. Marcos. "Accommodative lag and fluctuations when optical aberrations are manipulated". *Journal of Vision*, 9(6):1-15, 2009.
2. A. Perez-Escudero, C. Dorronsoro, L. Sawides, L. Remon, J. Merayo-Lloves & S. Marcos. "Minor influence of myopic laser in situ keratomileusis on the posterior corneal surface". *IOVS*, 50, p. 4146- 154, 2009.

3. M. Vinas, L. Sawides, P. de Gracia & S. Marcos. "Perceptual Adaptation to the Correction of Natural Astigmatism". *PLoS One*, 7(9), e46361, p. 1-10, 2012.
4. P. de Gracia, C. Dorronsoro, A. Sanchez-Gonzalez, L. Sawides & S. Marcos. "Experimental simulation of simultaneous vision". *IOVS*, 54(1):415-22, 2013.
5. E. Kompaniez, L. Sawides, S. Marcos & M. A. Webster. "Adaptation to interocular differences in blur". *Journal of Vision*, in press, 2013.
6. M. Vinas, P. de Gracia, C. Dorronsoro, L. Sawides, G. Marin, M. Hernandez & S. Marcos. "Astigmatism impact on visual performance: meridional & adaptational effects". *OVS*, under review 2013.

INTERNATIONAL CONGRESS CONTRIBUTIONS

Personally presented

1. L. Sawides, C. Dorronsoro, E. Gambra & S. Marcos. "Effect of Adaptive-Optics-Corrected Ocular Aberrations on Visual Acuity as a Function of Luminance and Polarity". Association for Research in Vision and Ophthalmology's Annual Meeting oral presentation, Fort Lauderdale, FL, USA, 2008.
2. L. Sawides, C. Dorronsoro, E. Gambra & S. Marcos. "Visual performance after adaptive-optics correction of ocular aberrations: visual acuity, subjective quality preference of natural images and recognition of faces and facial expressions". Fall Vision Meeting, poster presentation, Rochester, NY, USA, 2008.
3. L. Sawides, E. Gambra, c. Dorronsoro & S. Marcos. "Adaptive Optics to improve vision". IONS-5 (5^{th} meeting of the International OSA Network of Students), oral presentation, Barcelona, Spain, 2009.
4. L. Sawides, E. Gambra, C. Dorronsoro & S. Marcos. "Visual Performance With Real-Life Tasks Under Adaptive-Optics Ocular Aberration Correction". Association for Research in Vision and Ophthalmology's Annual Meeting, oral presentation, Fort Lauderdale, FL, USA, 2009
5. L. Sawides, P. de Gracia, C. Dorronsoro, E. Gambra, M. Webster & S. Marcos. "Adapting to Blur Produced by Ocular High Order Aberrations". Association for Research in Vision and Ophthalmology's Annual Meeting, oral presentation, Fort Lauderdale, FL, USA, 2010.
6. L. Sawides, P. de Gracia, C. Dorronsoro, M.A. Webster & S. Marcos. "The eye is adapted to the blur level imposed by its optical aberrations". Association for Research in Vision and Ophthalmology's Annual Meeting, oral presentation, Fort Lauderdale, FL, USA, 2011.
7. L. Sawides, P. de Gracia, M. Vinas, C. Dorronsoro, M. Webster & S. Marcos. "Adaptive Optics to test Adaptation to the eye's optics". IONS-11 (11^{th} meeting of the International OSA Network of Students), oral presentation, Paris, France, 2012.
8. L. Sawides, P. de Gracia, C. Dorronsoro, M. Webster, A.M. Haun, E. Peli & S. Marcos. "Neural Adaptation to the orientation of high Order Aberrations". Association for Research in Vision and Ophthalmology's Annual Meeting,

oral presentation, Fort Lauderdale, FL, USA, 2012.

9. L. Sawides, C. Dorronsoro, P. de Gracia, M. Vinas, A.M. Haun, E. Peli & S. Marcos. "Classification method to test natural adaptation to the high order aberrations of the eye". 6^{th} European Meeting on Visual and Physiological Optics (EMVPO), oral presentation, Dublin, Ireland, 2012.

Presented by collaborators

1. E. Gambra, L. Sawides, C. Dorronsoro, L. Llorente & S. Marcos. "Development, calibration and performance of an electromagnetic-based adaptive optics mirror for visual optics". The 6^{th} International Workshop on. Adaptive Optics for Industry and Medicine, oral presentation, Galway, Irlande, 2007
2. E. Gambra, L. Sawides& S. Marcos. "Accommodation Dynamics With Adaptive-Optics-Corrected Ocular Aberrations". Association for Research in Vision and Ophthalmology's Annual Meeting, poster presentation, Fort Lauderdale, FL, USA, 2008.
3. E. Odlund, F. Harms, J. Charton & L. Sawides. "A novel stroboscopic technique for assessing a deformable mirror's ability to perform in ophthalmic applications". Association for Research in Vision and Ophthalmology's Annual Meeting, poster presentation, Fort Lauderdale, FL, USA, 2008.
4. S. Marcos, L. Sawides, E. Gambra & C. Dorronsoro. "Effect of correcting high-order aberration on vision with different luminance, accommodative demands and targets". 4^{th} European Meeting on Visual and Physiological Optics (EMVPO), oral presentation, Heraklion, Greece, 2008.
5. M.A. Webster, L. Sawides, S. Ravikumar, L.N. Thibos, A. Bradley & S. Marcos. "Adapting to Astigmatism". Visual Sciences Society's Annual Meeting, oral presentation, Naples, FL, USA, 2009.
6. P. de Gracia, C. Dorronsoro, L. Sawides, E. Gambra & S. Marcos. "Experimental test of simulated retinal images using adaptive optics". Frontiers in Optics, oral presentation, San Jose, CA, USA, 2009.
7. S. Marcos, L. Sawides, P. de Gracia, C. Dorronsoro, E. Gambra & M. Webster. "Using adaptive optics to test spatial neural adaptation to Blur". 11^{th} International Congress of Wavefront & Presbyopic Refractive Corrections, oral presentation, San Francisco, CA, USA, 2010.
8. E. Gambra, L. Sawides, C. Dorronsoro & S. Marcos. "Influence of high order aberrations on the accommodative response". 13^{th} International Myopia Conference, oral presentation, Tubingen, Germany, 2010.
9. S. Marcos, L. Sawides, P. de Gracia, C. Dorronsoro & M. Webster. "Subjects are naturally adapted to their own optical aberrations". 5^{th} European Meeting on Visual and Physiological Optics (EMVPO), oral presentation, Stockholm, Sweden, 2010.
10. E. Kompaniez, A. Dye, L. Sawides, S. Marcos & M. Webster. "Adaptation to interocular effects in blur". Visual Sciences Society's Annual Meeting, oral presentation, Naples, FL, USA, 2011.

11. M. Vinas, L. Sawides, P. de Gracia & S. Marcos. "Adaptive Optics as a tool to study changes in the perceived neutral point after correction of astigmatism". 8^{th} International Workshop on Adaptive Optics for Industry and Medicine, poster presentation, Murcia, Spain, 2011.
12. M. Vinas, L. Sawides,, P. de Gracia & S. Marcos. "Shift of the neutral perceived focus after correction of astigmatism: evidence using adaptive optics". Engineering the Eye III, oral presentation, Benasque, Spain, 2011.
13. S. Marcos, L. Sawides, P. de Gracia, M. Vinas, M. Webster & C. Dorronsoro. "Adaptation to the aberrations and daily tasks". Engineering the Eye III, oral presentation, Benasque, Spain, 2011.
14. M. Vinas, L. Sawides, P. de Gracia & S. Marcos. "Adaptive Optics as a tool to study changes in neural adaptation to astigmatism". IONS-11 (11^{th} meeting of the International OSA Network of Students), poster presentation, Paris, France, 2012.
15. M. Vinas, L. Sawides, P. de Gracia & S. Marcos. "Longitudinal Changes In Perceptual Judgment Of Astigmatic Blur". Association for Research in Vision and Ophthalmology's Annual Meeting, oral presentation, Fort Lauderdale, FL, USA, 2012.
16. P. de Gracia, C. Dorronsoro, A. Sanchez-Gonzalez, L. Sawides & S. Marcos. "Visual Performance Under Pure Simultaneous Vision". Association for Research in Vision and Ophthalmology's Annual Meeting, oral presentation, Fort Lauderdale, FL, USA, 2012.
17. M. Vinas, P. de Gracia, C. Dorronsoro, L. Sawides & S. Marcos. "Testing the effect of astigmatism on vision with Adaptive Optics". IONS-13 (11^{th} meeting of the International OSA Network of Students), Oral presentation, Zurich, Switzerland, 2013.
18. M. Vinas, P. de Gracia, C. Dorronsoro,L. Sawides, G. Marin, M. Hernandez & S. Marcos. "Visual performance under natural, corrected and Adaptive Optics induced astigmatism: meridional and adaptational effects". Association for Research in Vision and Ophthalmology's Annual Meeting, oral presentation, Seattle, WA, USA, 2013.
19. C. Dorronsoro, A. Radhakrishnan, L. Sawides & S. Marcos. "Optical quality and subjective judgments of blur under pure simultaneous vision". Association for Research in Vision and Ophthalmology's Annual Meeting, oral presentation, Seattle, WA, USA, 2013.

PUBLICATIONS IN PROCEEDINGS

1. E. Gambra, L. Sawides, C. Dorronsoro, L. Llorente & S. Marcos. "Development, calibration and performance of an electromagnetic mirror based adaptive optics system for visual optics". Proceedings of the 6^{th} International Workshop on Adaptive Optics for Industry and Medicine.pp. 322 - 328.In C. Dainty (Ed.), London: Imperial College Press.,2008.
2. P. de Gracia, C. Dorronsoro, L. Sawides, E. Gambra & S. Marcos. "Experimental tests of simulated retinal images using Adaptive Optics". Proceedings

Adaptive Optics: Methods, Analysis and Applications, OSA Technical Digest (CD) (Optical Society of America, 2009), paper JWB4,2009.

Acknowledgments

After all these years in the Institute of Optics that bring into existence this doctoral thesis, I thank all the people who helped me, supported me and gave me the strength, in one way or another, to persevere and go through this long but fulfilling road, making this stage an unforgettable experience.

My first thank go undeniably to Susana Marcos, who welcomed me in her group just for a 6-months internship then for some years more, giving me the opportunity to complete the PhD... I have really enjoyed being part of this incredible group with so much optimistic mood. Your hard work, your fruitful discussion and perseverance constitute the model to follow and a way to know that every challenge is possible. Thank you so much.

Of course, I have to deeply thank all the members of the laboratory of Visual Optics and Biophotonics who helped me from the very beginning. First, Patricia (who took care of me when landing to Spain), Lourdes, Alberto and Elena who helped me in the first steps in the lab and who were, at my arrival, the people that formed, along with Susana, the group which has been growing progressively.

The work performed in the Adaptive Optics' lab has been possible with the help of many people: Carlos Dorronsoro who gave me so much fruitful advices and help me in the VA measurements (and big thank also for the camera objective...), Enrique Gambra with whom I shared the lab during years, for his patience, for his calm, for his constant work on the set-up phase of the system and the programs of the AO interface, Lourdes Llorente for the multiple checking comparisons of the aberrations measurements with the LRT (and the big headaches!), Jose Requejo for his advices for the system alignment, Daniel Pascual for his help in programming the synchronization of computers and his help for all the electronic "stuff", Pablo de Gracia for his help in the PSF generation and convolution, Daniel Cortés for all the informatic "stuff" and the programming of the new AO interface. Alberto de

Castro for dissolving all my doubts in Matlab programming, and, of course, María Viñas for the infinite and crazy hours in the lab aligning the system, for her friendly talk and hey energy to cheer-up in the big moments of stress. I would like to thank Enrique Bustos for his help in all the administrative paperwork (which has been many in the last year!). I would also like to thank Laura Barrios from CTI (Centro Técnico de Informática) for her support and her patience in explaining all the different aspects of statistics. I want to thank Laurent Vabre, from Imagine Eyes in Paris, for his help and support when having some trouble with the deformable mirror. I would like to thank Eli Peli and Andrew M. Haun, from the Schepens Eye Research Institute in Boston, for their suggestions and fruitful discussions that allow the last chapter of this thesis to emerge. And finally, I want to thank Eloy, Chary and Encarnita in the Institute of Optics for always having a kind word and a smile.

During my stayings abroad, I would like to deeply thank Prof. Michael Webster from the University of Nevada in Reno, for his warm welcome in his lab, for the concepts and tools he provided me to work on Neural Adaptation, which is a big part of this doctoral thesis and would not have been possible without his help and fruitful discussions. I also want to sincerely thank Prof. Stephen Burns from the University of Indiana in Bloomington, for his warm welcome in his lab, to give me the opportunity to work on the retinal imaging AO set-up. Even if the project didn't come to an end, I really enjoyed to work (briefly) there and learn so much.

I also want to thank Igor (the post doc who helped me with all my doubts in the lab), Maria and Fallon for their friendship in Reno, Hongxin for his patience and his help with the AO-set-up in Bloomington along with Weiyao, Gary, Zhangyi, Xiaofeng, Jamie and Tristan.

I could not complete this work without the friends I met during all this years and the colleagues who fill my daily hours in the lab, in the office (thanks to all (!) my "office mates"), during the coffee (and "piti") breaks, sharing knowledge or just making some jokes (which I never understood, sorry Daniel Pascual) and who became invaluable friends and even more ...

Specially, for sharing so greats moments, I want to mention Vincenzo and Hector (gambiteros), Dani Puerto for my first "Feria de la Tapa", Andrés for teaching me all the "Clásicos", María for her constant joy for Madrid's nights, Pablo Pérez for his constant optimism, Dani Cortés for sharing some french words after some beers, Giorgio for the culinary events when raining, Judith for her non-stop good mood and laugh, Carlos for keeping his young spirit and the road trip in Florida along with Alberto, Enrique and Alfonso, Antonio for appreciating "los juegos de mesa", Laura for her constant optimism and her famous "refranes" and Lourdes for being so friendly from the very beginning and of course, both of you for sharing so great moments during the painting sessions of the 3L, Patricia for the trip to Canada, Sergio Barbero for his famous memorable excursions, Rafa and his radio, Ana and her doubts about "ce soir o ce soir", Ainara, Noemí, Jorge, Miriam, Ser-

gio (O.), all the members of the IOSA for sharing so greats moments in organizing Optics events, and specially Sara for her energy to make all happen, Pablo (de G.) for his never-ending crazy stories, Damian, Nandor, Stéphanie and Aiswaryah for sharing typical gastronomic food, Elena for the cultural events, Sabine for the accordion classes, Alberto for so many things (and of course "le réveilleur magique"). I am grateful for the time spent with all of you and for our memorable trips to Marruecos, Marseille, Toulouse and La Selve (of course), Huesca, Biescas, Sevilla, Alicante, Valencia, Galicia, Milan, Barcelona, Paris, Zurich, Malasia... and for the ones to come.

I cannot forget my friends from France, specially those who I met in Lannion and in Paris. A big thank to Lucie Labat (for every time I came back to Toulouse, and ... don't worry I'll come back one day), Eloise and Daphné. Big thank for your Neutral, Happy and Angry expressions in the pictures I took for my experiment, you three were the first.

Et finalement j'aimerais remercier toute ma famille. Suite aux éternelles questions "Bon alors, tu finis quand?" le moment tant attendu arrive enfin! Un grand merci à Maman et à mes "hermanitos" Sylvain et Victor (cherchez bien, vous vous retrouverez tous les 3, tout au long de la these, héhé). Maman, merci pour toute ton inventivité creative que tu m'as transmise et pour la couverture de cette thèse. Et aussi, je n'oublie pas Marion, ma véritable Prima Hermana (!) pour toutes ces longues conversations autour d'un thé ou d'un bon petit repas (¿calabacín hoy? siii!!), pendant un an, ici, à Madrid. Y también, agradezco muchísimo a Rosa, Ángel e Inés, mi "familia española" y por supuesto a Alberto... (porque es así!)

Σε όλη την οικογένειά μου.